Interface Shear Transfer of Lightweight Aggregate Concretes with Different Lightweight Aggregates

by

Lesley H. Sneed
Samantha Wermager
Kristian Krc

Department of Civil, Architectural & Environmental Engineering
Missouri University of Science and Technology

Final report submitted to
Precast/Prestressed Concrete Institute

May 2016

Interface Shear Transfer of Lightweight Aggregate Concretes with Different Lightweight Aggregates

Final Report

Submitted to:
Precast/Prestressed Concrete Institute
200 W. Adams St. #2100, Chicago, IL 60606

Funded by:
Precast/Prestressed Concrete Institute

Co-funded by:
ACI Foundation Concrete Research Council

Principal Investigator: Dr. Lesley H. Sneed

Graduate Research Assistants: Samantha Wermager
Kristian Krc

PCI Industry Advisory Committee: Neal Anderson, Simpson Gumphertz & Heger Inc.
Roger Becker, PCI
Dr. Reid Castrodale, Castrodale Engineering Consultants PC
Harry Gleich, Metromont Precast
Dr. Neil Hawkins
Dr. Donald Meinheit, Wiss, Janney, Elstner
Dr. Larbi Sennour, Consulting Engineering Group, Inc.

ABSTRACT

This report presents the results from the second phase of an ongoing investigation of the direct shear transfer across an interface of lightweight aggregate concretes. The lightweight concretes were made with different lightweight aggregate materials (expanded shale, expanded slate, and expanded clay). The second phase of the experimental investigation included 52 push-off specimens. Test variables included concrete type (normalweight, sand-lightweight, or all-lightweight), lightweight aggregate materials, surface preparation of the shear interface, reinforcement ratio, and crack interface condition. Applied shear force-slip relations are presented and discussed. Peak shear strengths are also compared. Current shear-friction design provisions in the ACI 318 code and the PCI Design Handbook are examined. Shear strengths computed using the coefficient of friction μ-approach by the PCI Design Handbook (Equation 5-32a) and the ACI 318 code (Equation 22.9.4.2) and the effective coefficient of friction μ_e-approach in the PCI Design Handbook (Equation 5-32b) are found to be conservative for the sand-lightweight and all-lightweight monolithic and cold joint specimens in this study.

This report also presents a database of shear-friction test results collected from the literature that is analyzed for the effective coefficient of friction μ_e-approach used in the PCI Design Handbook (Equation 5-32b), and the coefficient of friction μ-approach used in the PCI Design Handbook (Equation 5-32a) and the ACI 318 code (Equation 22.9.4.2). The database is limited to pushoff specimens subjected to monotonic loading and without external normal forces. The data are categorized in terms of concrete type, interface condition, compressive strength of concrete, clamping stress, and area of shear interface to help identify gaps in the literature. It is envisioned that this database will be expanded in the future to further examine shear-friction models and design provisions in various codes/standards. Analysis of the current database shows that PCI Equation 5-32b is more accurate and has a lower coefficient of variation than both PCI Equation 5-32a and ACI Equation 22.9.4.2 for normalweight, sand-lightweight, and all-lightweight concrete with monolithic uncracked, monolithic pre-cracked, and cold joint roughened interface conditions.

Based on the results of the experimental program conducted and analysis of the database developed, revisions to the PCI Design Handbook and ACI 318 code are proposed for shear-friction design provisions of a smooth interface condition. For the cold joint smooth interface condition, the authors recommend removing the term λ in the coefficient of friction μ to provide more accurate and economical designs.

ACKNOWLEDGMENTS

This research was conducted with the sponsorship of the Precast/Prestressed Concrete Institute (PCI) and the American Concrete Institute (ACI) Concrete Research Council (CRC). Lightweight aggregates were donated by Buildex, Inc., STALITE, and Trinity Lightweight. Longitudinal reinforcing steel bars used in this work were provided by Ambassador Steel Corporation. The authors wish to thank Neal Anderson of Simpson Gumphertz & Heger Inc., Roger Becker of PCI, Reid Castrodale of Castrodale Engineering Consultants PC, Harry Gleich of Metromont Precast, Dr. Neil Hawkins, Dr. Donald Meinheit of Wiss, Janney, Elstner, and Dr. Larbi Sennour of Consulting Engineering Group, Inc. who served as advisors to this project; their assistance and input are greatly appreciated. Additionally, the authors gratefully acknowledge the assistance provided by Metromont Precast.

TABLE OF CONTENTS

Page

LIST OF FIGURES

Page

LIST OF TABLES

NOMENCLATURE

Symbol	Description
A_c	area of concrete shear interface (ACI 318 code), in^2
A_{cr}	area of concrete shear interface (PCI Design Handbook), in^2
A_{vf}	area of shear reinforcement across shear plane, in^2
f'_c	28-day concrete compressive strength, lb/in^2
f_{ct}	tensile strength of concrete, measured by splitting tensile strength, lb/in^2
f_y	yield stress of reinforcement, lb/in^2
P_c	permanent net compressive force normal to the shear plane; if force is tensile, P_c = 0.0, kip
V	applied shear force, lb
v	applied shear stress, lb/in^2
V_{calc}	calculated shear strength, lb
V_{cr}	interfacial cracking force, lb
v_{cr}	interfacial cracking stress, lb/in^2
$v_{cr,avg}$	average interfacial cracking stress, lb/in^2
V_n	nominal shear strength, lb
$V_{n,max}$	nominal shear strength, lb
v_n	nominal shear stress, lb/in^2
V_u	ultimate shear strength, lb
v_u	ultimate shear stress, lb/in^2
$v_{u,avg}$	average ultimate shear stress, lb/in^2
V_{ur}	residual shear strength, lb
v_{ur}	residual shear stress, lb/in^2
$v_{ur,avg}$	average residual shear stress, lb/in^2
α	angle defining the orientation of reinforcement
λ	modification factor reflecting the reduced mechanical properties of lightweight concrete, relative to normalweight concrete of the same compressive strength
τ	shear stress
σ	normal stress
μ	coefficient of friction
μ_e	effective coefficient of friction
$\mu_{e,max}$	maximum value of effective coefficient of friction
μ_{test}	effective coefficient of friction associated with the measured shear strength
ρ	shear-friction reinforcement ratio, A_v/A_{cr}
ϕ	capacity reduction factor
AASHTO	American Association of State Highway and Transportation Officials
ACI	American Concrete Institute
ASTM	American Society for Testing and Materials
Avg	average
COV	coefficient of variation
DC-LVDT	direct current - linear voltage displacement transducer
PCI	Precast/Prestressed Concrete Institute

1. INTRODUCTION

1.1. PROBLEM DEFINITION

The shear-friction design provisions presented in the PCI Design Handbook: Precast and Prestressed Concrete (7th edition) (2010) and American Concrete Institute's (ACI's) Building Code Requirements for Structural Concrete (ACI 318-14) and Commentary (ACI 318R-14) are based on physical test data, although most published test data pertain to concrete that is normalweight. Lightweight aggregate concretes are often considered for use when it is desirable to reduce member weight, such as in precast concrete construction to reduce transportation costs and enhance fire resistance. Precast concrete elements commonly incorporate connections that are designed based on the shear-friction concept to transfer forces across an interface. According to this method, shear transfer strength is a function of the interface conditions listed in Table 1.1.

Table 1.1 Shear Interface Conditions – PCI Design Handbook (2010)

Case	Interface Condition
1	Concrete to concrete, cast monolithically
2	Concrete to hardened concrete, with roughened surface[1]
3	Concrete placed against hardened concrete not intentionally roughened
4	Concrete to steel

[1]The PCI Design Handbook (2010) and ACI 318 code (2014) shear-friction design provisions specify an intentionally roughened surface to have an average amplitude of 0.25 in.

Previous studies on shear-friction have shown that interface condition, reinforcement ratio, concrete strength, and concrete type (normalweight, sand-lightweight, or all-lightweight) influence the shear transfer strength (Anderson 1960; Hofbeck et al. 1969; Mattock and Hawkins 1972; Mattock 1976; Mattock et al. 1976; Walraven and Stroband 1994; Kahn and Mitchell 2002). However, few studies have investigated the direct shear transfer of structural lightweight aggregate concretes, especially for conditions in which concretes are cast at different times, that is, cold joint conditions. Lightweight aggregates commonly used in the production of structural lightweight concretes include expanded shale, expanded slate, and expanded clay. These aggregates can have different unit weights and mechanical properties depending on the aggregate source and production process.

The study presented in this report was the second phase of an ongoing investigation of the direct shear transfer across an interface of lightweight aggregate concretes. Results from the first phase of the study were presented in the report by Sneed and Shaw (2013), who studied the shear transfer strength of lightweight aggregate concretes made with expanded shale lightweight aggregate and a cold joint interface condition. In the second phase of the study, the shear transfer strength of lightweight aggregate concretes made with different structural lightweight aggregates was investigated. Lightweight aggregate concretes were made with different lightweight aggregate materials (expanded shale, expanded slate, or expanded clay), different interface conditions (monolithic or cold joint), and different reinforcement ratios.

1.2. GOAL AND OBJECTIVES

The overarching goal of this project was to study the effect of structural lightweight aggregate on the direct shear transfer across a given plane in structural concrete. Specific objectives of the second phase of the project were to:

1. Determine whether structural lightweight aggregate material plays a role in the direct shear transfer across a cold joint interface (Case 2 or 3 from Table 1.1);
2. Determine the appropriate modification factor λ for lightweight aggregate concretes (relative to normalweight concrete) for use in current PCI Design Handbook (2010) and ACI 318 code (2014) shear-friction design provisions for the cases of concrete placed monolithically (Case 1 from Table 1.1) and concrete placed against hardened concrete (Case 2 or 3 from Table 1.1); and
3. Determine whether the shear transfer strength of lightweight aggregate concrete with a cold joint interface increases with increasing reinforcement ratio.

1.3. PROJECT SCOPE

The scope of this study contained the following tasks to accomplish the objectives set forth in Section 1.2:

1. Design, construct, and test a matrix of test specimens where the variables included concrete type designated by aggregate composition (normalweight, sand-lightweight, all-lightweight); lightweight aggregate material (expanded shale, expanded slate, expanded clay); interface condition (monolithic uncracked, monolithic pre-cracked, cold joint – roughened, cold joint – smooth), and reinforcement ratio (ρ = 0.009, 0.013, 0.017, 0.022).
2. Analyze the above mentioned variables and their influence on shear transfer strength.
3. Analyze the effective coefficient of friction μ_e and its applicability for use in the PCI Design Handbook shear-friction design provisions.
4. Study the need for the lightweight aggregate modification factor λ and recommend any necessary changes to the shear-friction design provisions in the PCI Design Handbook (2010) and ACI 318 code (2014).

The experimental work in the second phase of the study, summarized in this report, was designed to address items 1 and 2 above and included 52 push-off specimens. The test matrix is shown in Table 1.2, which also includes the specimens from the first phase of the study to illustrate the relation between the specimens in both phases. In Table 1.2, specimens shown in normal text were constructed for the second phase of the study, while specimens shown in *italics* were tested in the first phase summarized by Sneed and Shaw (2013). Parameters held constant in the second phase of the study were shear plane area (49.5 in^2) and target compressive strength of concrete (5000 psi).

For items 3 and 4 above, a comprehensive database including results from this study and the literature was developed and analyzed. It is envisioned that this database will be expanded in the future to further examine shear-friction models and design provisions in various codes/standards.

1.4. SUMMARY OF REPORT CONTENT

The problem definition, goal, objectives, and scope of this project are defined in Section 1 of this report. A summary of current shear-friction design provisions in the PCI Design Handbook (2010)

and ACI 318 code (2014) is presented in Section 2. Section 3 describes the experimental program in terms of materials, specimen design and fabrication, test set-up, and a summary of the test results. Section 4 analyzes and discusses results of the experiments conducted in this study. Section 5 presents a database of shear-friction test results collected from the literature that was analyzed for the effective coefficient of friction μ_e-approach used in the PCI Design Handbook (2010) and the coefficient of friction μ-approach used in the PCI Design Handbook (Equation 5-32a) and the ACI 318 code (2014) (Equation 22.9.4.2). Finally, Section 6 contains a summary, conclusions, and recommendations for design equations as well as suggestions for future work. Comprehensive results of each of specimen series are presented in Appendix A. The database of test results used for analysis within this report is included in Appendix B. References are provided after Appendix B.

Table 1.2 Combined Test Matrix for Phases 1 and 2

Concrete Type	**Lightweight Aggregate Material**	**Interface Condition[1]**	**Reinforcement Ratio[1]**	**Number of Specimens[1]**
Normalweight	N/A	Monolithic – Uncracked	0.013	2
		Monolithic – Precracked	0.013	2
		Cold joint - Roughened	*0.013*	*3*
		Cold joint – Smooth	*0.013*	*3*
Sand-Lightweight	Shale	Monolithic – Uncracked	0.013	2
		Monolithic – Precracked	0.013	2
		Cold joint - Roughened	*0.013*	*3*
		Cold joint – Smooth	*0.013*	*3*
	Slate	Cold joint - Roughened	0.009/0.013/0.017/0.022	2/2/2/2
		Cold joint – Smooth	0.009/0.013/0.017/0.022	2/2/2/2
	Clay	Cold joint - Roughened	0.009/0.013/0.017/0.022	2/2/2/2
		Cold joint – Smooth	0.009/0.013/0.017/0.022	2/2/2/2
All-Lightweight	Shale	Monolithic – Uncracked	0.013	2
		Monolithic – Precracked	0.013	2
		Cold joint - Roughened	*0.013*	*3*
		Cold joint – Smooth	*0.013*	*3*
	Slate	Cold joint - Roughened	0.013	2
		Cold joint – Smooth	0.013	2
	Clay	Cold joint - Roughened	0.013	2
		Cold joint – Smooth	0.013	2

[1]Specimens shown in normal text were constructed for the second phase of the study; specimens shown in *italics* were tested in the first phase summarized by Sneed and Shaw (2013).

2. BACKGROUND INFORMATION

2.1. INTRODUCTION

Due to the non-ductile material behavior of concrete, the design of connections in reinforced concrete structures is of great concern when there is little redundancy or high levels of shear forces involved. One way to design these types of connections is by the shear-friction method, which was pioneered in the 1960s by Birkeland and Birkeland (1966), Mast (1968), and Hofbeck et al. (1969). Particularly with the development and widespread use of precast reinforced concrete members, the design of connections has become increasingly complex. The transfer of shear forces across an interface is discussed in Section 2.2. The development and the current (as of 2016) shear-friction design provisions according to the PCI Design Handbook and the ACI 318 code are described in Section 2.3. A comprehensive literature review on shear-friction research is included in the report from the first phase of this project (Sneed and Shaw 2013; Shaw 2013).

2.2. INTERFACE SHEAR-FRICTION

2.2.1. Shear-friction

The shear-friction theory was initially developed to describe the transfer of shear forces across the interface of a precast concrete element to a cast-in-place concrete element. It has been extended to include shear transfer across monolithic interfaces as well. One of the principal assumptions of the shear-friction theory is that a crack or discontinuous interface exists. The shear force causes the two surfaces to slip relative to each other. The mechanisms of aggregate interlock, interface shear-friction, dowel action of the reinforcement, and cohesion of the two surfaces work in unison to resist shear forces. These mechanisms are further described in Section 2.2.2.

While the shear-friction concept is applied to the design of uncracked elements, cracked elements generally correspond to lower ultimate shear transfer strengths. In order to simulate the worst-case condition, it is assumed that a crack has formed in the element in the most undesirable location. This crack could be due to temperature and/or shrinkage cracking, accidental dropping of the specimen, unintended impact forces during transportation or placement of a precast specimen, etc. Thus, many previous studies have included both uncracked and pre-cracked monolithic specimens to compare their shear transfer strengths.

Several factors have been found to influence the shear transfer strength including the interface condition, the amount of reinforcement crossing the shear plane, the yield strength of the reinforcement, the compressive strength of the concrete, the density of the concrete, the presence of an externally applied tension or compression force, etc. Concretes with higher compressive strengths have the potential for higher shear capacities for normalweight concrete as noted by Mattock (2001) and Kahn and Mitchell (2002). Cyclic or sustained loading has been shown by Walraven et al. (1987) to have little effect on the shear transfer capacity; thus, it is typical for shear-friction specimens to be tested by monotonic loading. Hsu et al. (1987) warned of the potential influence of large amounts of steel reinforcement parallel to the shear plane on the ultimate shear strength of connections.

Several researchers (Mattock, et al. 1976; Hoff 1993; Sneed and Shaw 2013) have investigated the effect on shear transfer when lightweight concrete is used. Their results reveal that the bond

between the mortar and aggregate particles is stronger than the tensile strength of the aggregate alone, and cracks may propagate directly through the aggregate particles. This causes a smoother crack surface that reduces the ultimate shear capacity when compared to that of normalweight concrete. Typically, in normalweight concrete the cracks propagate around the aggregate since the aggregate's tensile strength is higher than the bond between the mortar and aggregate particles (Mattock et al. 1976). This phenomenon produces a rougher surface that aids in aggregate interlock resulting in higher surface separation for a given amount of slip.

Previous studies (Mattock and Hawkins 1972; Mattock et al. 1975) have concluded that tension or compression that is externally applied normal to the shear plane can either hinder or aid in, respectively, the resistance of shear forces and must be included in shear-friction provisions.

2.2.2. Shear-friction Mechanisms

When shear forces are applied in a cracked region of concrete, slip will occur along the crack. If the surface of the shear plane is jagged (in the direction normal to the shear plane), the two faces of concrete resist slipping through the mechanism of 'aggregate interlock.' These rough surfaces must first separate to overcome small ridges before slip can occur. Steel reinforcement normal to the shear plane is strained when there is separation of the concrete surfaces. Tension forces are induced in the steel which in turn create equal and opposite compression forces between the concrete faces. These compression forces correspond to the 'normal' forces of the basic friction equation, which is discussed below. The combination of this steel clamping force and the inherent friction along the crack surface is referred to as the mechanism of interface shear-friction. The shear-friction principle is graphically demonstrated in Figure 2.1.

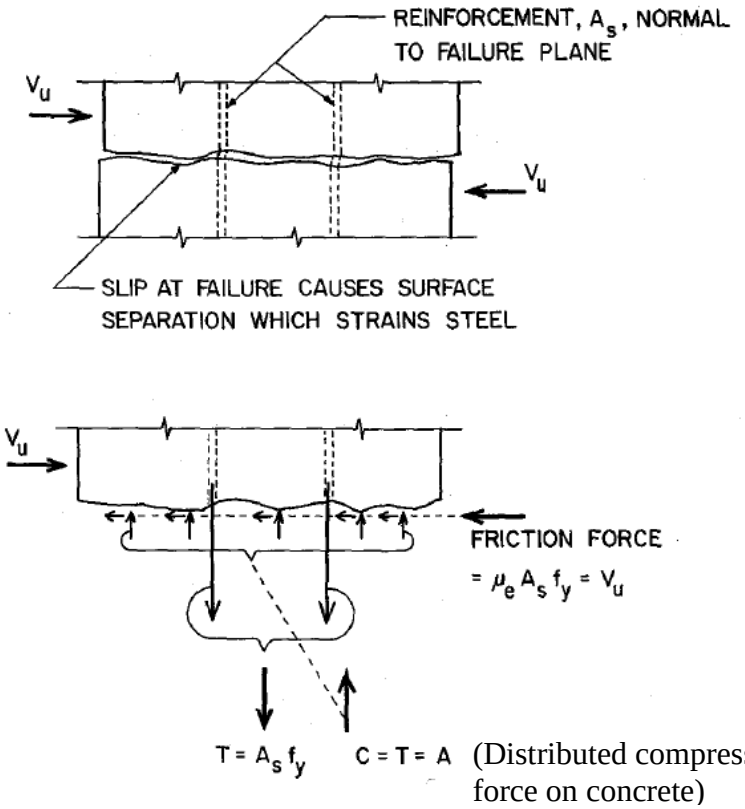

Figure 2.1 Schematic diagram of shear-friction principle (Shaikh 1978)

The shear-friction factor μ can be defined as the ratio of shear stress τ to the normal stress σ across the shear interface (Equation 2.1), which can be manipulated by representing the normal force as equivalent to the tensile force in the steel $A_{vf}f_s$ combined with an external clamping force P_c that may or may not be present. In this equation, V is the shear applied along the interface, and A_{cv} is the area of the shear interface.

$$\mu = \frac{\tau}{\sigma} = \frac{V/A_{cv}}{\left(A_{vf}f_s + P_c\right)/A_{cv}} = \frac{V}{A_{vf}f_s + P_c} \tag{2.1}$$

The classical equation from basic physics for the force due to friction F_f (Equation 2.2) is simply the coefficient of friction μ multiplied by the normal force N. In the case of shear-friction design, this coefficient of friction does not represent the true roughness of the shear interface. Instead, researchers have modified it in the development of empirical equations. The coefficient of friction in modern design codes has become an all-inclusive parameter that also accounts for the effects of aggregate interlock and cohesion (Harries et al. 2012). These design code provisions are further discussed in Section 2.3.

$$F_f = \mu N \tag{2.2}$$

Another contributor to the resistance to shear forces along an interface is dowel action of reinforcement crossing the interface. For steel reinforcing bars, Paulay et al. (1974) separated dowel action into three different mechanisms (Figure 2.2) that include flexure, shear, and kinking of the steel bar. Since significant levels of slip and crushing of the concrete are required to engage reinforcing bars in these manners, dowel action alone cannot be relied upon as a principle shear force resistance mechanism. Large levels of slip can cause deflection issues, and large, unsightly cracks in a reinforced concrete structure are likely to be a major concern to its tenants. For typical levels of load and slip, Paulay et al. state that only 15% of the shear-friction capacity is attributed to dowel action.

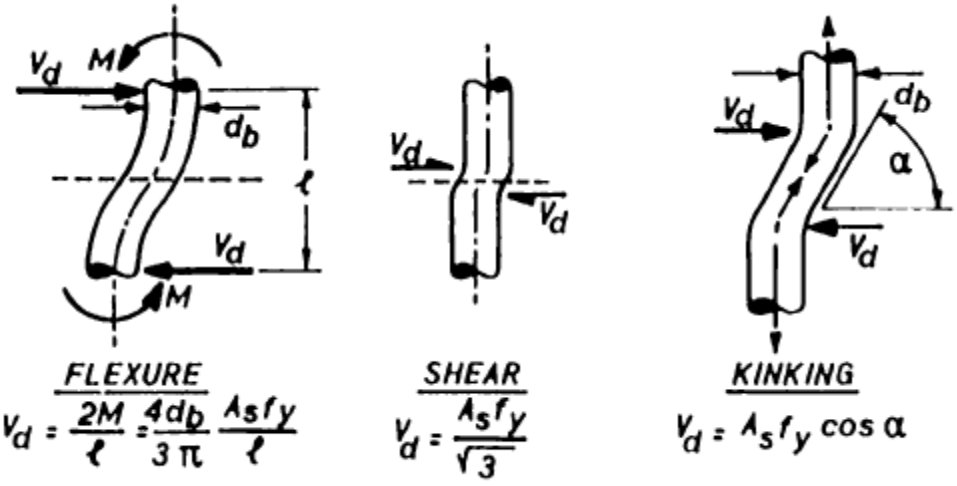

Figure 2.2 Mechanisms of dowel action (Paulay et al. 1974)

Another component of shear-friction resistance is bond of the two opposing concrete faces, also referred to as cohesion. It has been suggested by Kahn and Mitchell (2002) that concretes with higher compressive strengths have higher shear strengths in monolithic and cold joint specimens due to the contribution of cohesion. These researchers included a term in their proposed shear-friction equation to account for bond and asperity shear. The literature does not clearly define the term asperity shear, but the context suggests that asperity shear is the additional shear strength attributed to resistance by the projections (asperities) on the crack interface that did not previously interact with rough areas on the opposite face as slip progresses along the shear plane.

2.3. SHEAR-FRICTION DESIGN PROVISIONS

In the fundamental equation (Equation 2.1) for the coefficient of friction μ, the term P_c accounts for an external normal force. It is conservative to neglect this external force if it is compressive. Yet, if an external tensile force is applied across the shear plane, extra reinforcement must be provided to account for this force, and it shall be separate from the reinforcement required by shear-friction provisions. Such a tension force may be caused by restraining the movement of members due to temperature or shrinkage expansion/contraction. If P_c is neglected in Equation 2.1, this equation can be rearranged in terms of nominal shear strength, V_n (Equation 2.3). Here, V_u is the applied factored shear force parallel to the assumed crack, ϕ is the strength reduction factor, A_{vf} is the area of shear reinforcement, f_y is the yield strength of the reinforcement, and μ is the coefficient of friction.

$$V_n = \frac{V_u}{\phi} = A_{vf} f_y \mu \tag{2.3}$$

This fundamental equation (Equation 2.3) forms the basis of shear-friction design in the PCI Design Handbook and the ACI 318 code. Their specific provisions are detailed in Sections 2.3.1 and 2.3.2, respectively. Within these provisions, a modification factor λ is used to account for the reduced tensile strength (and thus, reduced shear strength and friction capacity) of lightweight aggregate concrete. In the current editions of the PCI Design Handbook (2010) and the ACI 318 code (2014), a value of λ = 1.0 corresponds to normalweight concrete, λ is taken as 0.75 for all-lightweight concrete, and λ may be taken as 0.85 for sand-lightweight concrete. Alternatively, if lightweight concrete is used and the splitting tensile strength f_{ct} is known, ACI and PCI design provisions allow the lightweight modification factor λ to be determined by Equation 2.4. Note that the maximum value of λ allowed by this equation is 1.0.

$$\lambda = \frac{f_{ct}}{\left(6.7\sqrt{f_c'}\right)} \leq 1.0 \tag{2.4}$$

2.3.1. PCI Design Handbook

The Precast/Prestressed Concrete Institute has been developing the body of knowledge surrounding precast and prestressed concrete since the 1950s. The current PCI Design Handbook (2010) includes two approaches for shear-friction design. The first approach, which has existed since the 2nd edition of the handbook (1978), uses the effective coefficient of friction μ_e, and the second uses the coefficient of friction μ. Use of the effective coefficient of friction μ_e is based on work summarized by Shaikh (1978), who proposed revisions to the traditional shear-friction design

concept by Mast (1968) used in the ACI 318 code to produce designs that were more economical. Shaikh evaluated equations for μ_e proposed by Mattock (1974), Birkeland (1969), and Raths (1977) against the experimental test data available at that time. Equations for μ_e proposed by Birkeland and Raths took on a parabolic form relating the shear strength and a friction term and is the form of the equations for μ_e in the PCI Design Handbook discussed in the sections that follow. On the other hand, the equation proposed by Mattock was the summation of a friction term and a cohesion term and is the form of shear-friction design provisions in the current AASHTO (2014) provisions.

The equation used to compute μ_e has been modified in the past several editions of the PCI Design Handbook due to several mathematical anomalies identified by Tanner (2008) including revisions to the load and strength reduction factors and the inclusion of the modification factor for lightweight concrete. While the method proposed by Shaikh (1978) was applicable to the four crack interface conditions in Table 1.1, revisions to the current edition of the PCI Design Handbook (2010) have excluded its use for certain crack interface conditions, namely Cases 3 and 4 in Table 1.1 (concrete placed against hardened concrete not intentionally roughened, and concrete to steel, respectively).

2.3.1.1 PCI Design Handbook 6th Edition (2004)

Shear-friction provisions of the 6th Edition of the PCI Design Handbook (2004) are based on the μ_e-approach and require an amount of shear reinforcement normal to the crack A_{vf} as given by Equation 4.3.6.1 in the PCI Design Handbook, where, ϕ = 0.75, V_u is the applied factored shear force parallel to the assumed crack plane (lb), f_y is the yield strength of the steel reinforcement (less than or equal to 60 ksi), and μ_e according to Equation 4.3.6.2.

$$A_{vf} = \frac{V_u}{\phi f_y \mu_e} \qquad \text{(PCI Design Handbook 6th ed. 4.3.6.1)}$$

$$\mu_e = \frac{1000 \lambda A_{cr} \mu}{V_u} \qquad \text{(PCI Design Handbook 6th ed. 4.3.6.2)}$$

A different value of μ is recommended for each of the four different crack interface conditions (Table 2.1) and is a function of the value of λ, which is a modification factor to account for the use of lightweight aggregate. The lightweight modification factor is given in Section 2.3. Table 2.1 also shows suggested maximum values of the effective coefficient of friction μ_e and maximum values of the nominal shear strength V_n for each interface condition.

Table 2.1 Shear-friction Coefficients for PCI Design Handbook 6th Edition (2004)

Case	Crack Interface Condition	μ	Max μ_e	Max $V_u = \phi V_n$
1	Concrete to concrete, cast monolithically	1.4λ	3.4	$0.30\lambda^2 f'_c A_{cr} \leq 1000\lambda^2 A_{cr}$
2	Concrete to hardened concrete, with roughened surface	1.0λ	2.9	$0.25\lambda^2 f'_c A_{cr} \leq 1000\lambda^2 A_{cr}$
3	Concrete placed against hardened concrete not intentionally roughened	0.6λ	2.2	$0.20\lambda^2 f'_c A_{cr} \leq 800\lambda^2 A_{cr}$
4	Concrete to steel	0.7λ	2.4	$0.20\lambda^2 f'_c A_{cr} \leq 800\lambda^2 A_{cr}$

2.3.1.2 PCI Design Handbook 7th Edition (2010)

The 7th Edition of the PCI Design Handbook (2010) states that the shear-friction method is applicable to reinforced concrete bearing, corbels, daps, composite sections, connections of shear walls to foundations, shear connections in precast concrete diaphragms, and other applications. From the 6th to the 7th edition, there were a few modifications. First, Table 2.2 shows that μ_e became inapplicable for the case of concrete to concrete not intentionally roughened (Case 3), as well as the case of the concrete to steel interface condition (Case 4). Instead, Equation 5-32a (μ-approach) in the PCI Design Handbook (2010) is used for these two cases, where μ is used in place of μ_e. Equation 5-32a may also be used for Case 1 and Case 2 interface conditions. Alternatively, Equation 5-32b (μ_e-approach) may be used for Case 1 and Case 2 interface conditions, which corresponds to Equation 4.3.6.1 of the 6th Edition of the PCI Design Handbook (2004) (see Section 2.3.1.1) with values of μ_e according to Equation 5-33. The second change in the 7th Edition is the addition of ϕ to Equation 5-33, as compared to Equation 4.3.6.2 of the 6th Edition of the PCI Design Handbook (2004) (see Section 2.3.1.1) . This change was made to reflect the fact that μ_e is not a function of V_u, but rather it is a function of $V_n = V_u/\phi$. The third major change of this edition is shown in Table 2.2, where the reduction factor λ is no longer squared in the limits for $V_{n,max}$.

$$A_{vf} = \frac{V_u}{\phi f_y \mu} \qquad \text{(PCI Design Handbook 7th ed. 5-32a)}$$

$$A_{vf} = \frac{V_u}{\phi f_y \mu_e} \qquad \text{(PCI Design Handbook 7th ed. 5-32b)}$$

$$\mu_e = \frac{\phi 1000 \lambda A_{cr} \mu}{V_u} \qquad \text{(PCI Design Handbook 7th ed. 5-33)}$$

Table 2.2 Shear-friction Coefficients for PCI Design Handbook 7th Edition (2010)

Case	Crack Interface Condition	μ	Max μ_e	Max $V_u = \phi V_n$
1	Concrete to concrete, cast monolithically	1.4λ	3.4	$0.30\lambda f'_c A_{cr} \leq 1000\lambda A_{cr}$
2	Concrete to hardened concrete, with roughened surface	1.0λ	2.9	$0.25\lambda f'_c A_{cr} \leq 1000\lambda A_{cr}$
3	Concrete placed against hardened concrete not intentionally roughened	0.6λ	N/A	$0.20\lambda f'_c A_{cr} \leq 800\lambda A_{cr}$
4	Concrete to steel	0.7λ	N/A	$0.20\lambda f'_c A_{cr} \leq 800\lambda A_{cr}$

2.3.2. ACI 318 Code (2014)

Unlike the PCI Design Handbook (Section 2.3.1), the current ACI 318 code (2014) does not include the use of an effective coefficient of friction μ_e; instead, μ is used for all interface conditions. The nominal shear strength for the case of reinforcement perpendicular to the shear plane is given by Equation 22.9.4.2 of the ACI 318 code (2014). When the shear-friction reinforcement is inclined at an angle α from the shear plane, Equation 22.9.4.3 is used.

$$V_n = \mu A_{vf} f_y \qquad \text{(ACI 318-14 22.9.4.2)}$$

$$V_n = A_{vf} f_y (\mu \sin\alpha + \cos\alpha) \qquad \text{(ACI 318-14 22.9.4.3)}$$

Table 2.3 Shear-friction Coefficients for ACI 318 (2014)

Case	Crack Interface Condition	μ	$V_{n,max} = V_u / \phi$
1	Concrete to concrete, cast monolithically	1.4λ	For normalweight concrete (monolithic or roughened), $V_{n,max}$ equals least of: $0.2f'_c A_c$ $(480 + 0.08f'_c)A_c$ or $1600A_c$ For all other cases, $V_{n,max}$ equals lesser of: $0.2f'_c A_c$ or $800A_c$
2	Concrete to hardened concrete, with roughened surface	1.0λ	
3	Concrete placed against hardened concrete not intentionally roughened	0.6λ	
4	Concrete anchored to as-rolled structural steel by headed studs or by reinforcing bars	0.7λ	

In Equations 22.9.4.2 and 22.9.4.3, the yield strength of reinforcement f_y has an upper limit of 60,000 psi. The ACI 318 code values for μ are a function of crack interface condition given in Table 2.3 and are the same as those in the PCI Design Handbook 6th and 7th editions (Section 2.3.1); however, the limitations on $V_{n,max}$ are slightly different (Table 2.3). The value of μ is also a function of the lightweight modification factor λ discussed in Section 2.3. If the average splitting tensile strength of the lightweight concrete f_{ct} is known, the lightweight modification factor λ may be calculated according to Equation 2.4, which is also specified in the PCI Design Handbook. However, unlike the PCI Design Handbook, the ACI 318 code also allows λ to be modified based

on volumetric fractions of normalweight and lightweight coarse and fine aggregates. When lightweight coarse aggregate is used with a mix of lightweight and normalweight fine aggregate, the ACI 318 code allows linear interpolation between the values of 0.75 and 0.85 based on the volumetric fraction of lightweight fine aggregate that is replaced with normalweight fine aggregate. Also, when normalweight fines are used with a blend of normalweight and lightweight coarse aggregate, the ACI 318 code allows λ to be interpolated by volumetric fraction (with λ ranging between 0.85 and 1.0).

3. EXPERIMENTAL PROGRAM

3.1. INTRODUCTION

This section describes the experimental program conducted in this study (second phase) and includes materials, specimen design, specimen assembly, test setup, and test results. The laboratory work was completed by two graduate students, Mr. Kristian Krc and Ms. Samantha Wermager, and portions of the data were used in separate analyses and are summarized in separate theses (Krc 2015; Wermager 2015). This section summarizes the combined work and includes a concise summary of results. Comprehensive test results are presented in terms of shear strength, shear stress, slip of shear plane, dilation of shear plane, and strain in the reinforcing bars crossing the shear plane are summarized in Appendix A of this report. Analysis and discussion of the combined results and the results from the first phase are presented in Section 4 of this report.

3.2. SPECIMEN DESIGN

As discussed in Section 1.3, a total of 52 push-off type specimens were constructed and tested for the second phase of the study. The specimens were designed similar to previous research studies to allow the direct comparison of test results. The test variables included concrete type (normalweight, sand-lightweight, or all-lightweight), lightweight aggregate material (expanded shale, expanded slate, or expanded clay), casting procedure (monolithic or cold joint), interface condition (uncracked, pre-cracked, roughened, or smooth), and reinforcement ratio ρ.

Specimen designation notation is explained in Figure 3.1, and the test matrix for this phase of the study is summarized in Table 3.1. The normalweight concrete and shale lightweight aggregate concrete specimens were cast monolithically. Monolithic specimens were either uncracked or pre-cracked. The slate and clay lightweight aggregate specimens were constructed of sand-lightweight or all-lightweight concrete and had a cold joint interface that was either roughened to a 0.25 in. amplitude or troweled smooth. Slate and clay sand-lightweight specimens were constructed with varying reinforcement ratios. For a shear plane area of 49.5 in^2, and either 2, 3, 4, or 5 No. 3 double-legged stirrups crossing the shear plane, associated reinforcement ratios were 0.009, 0.013, 0.017, and 0.022, respectively. All other specimens had a constant reinforcement ratio of 0.013. All specimens had the same target compressive strength of concrete (5000 psi). Actual concrete compressive strengths varied between 4380 psi and 5570 psi.

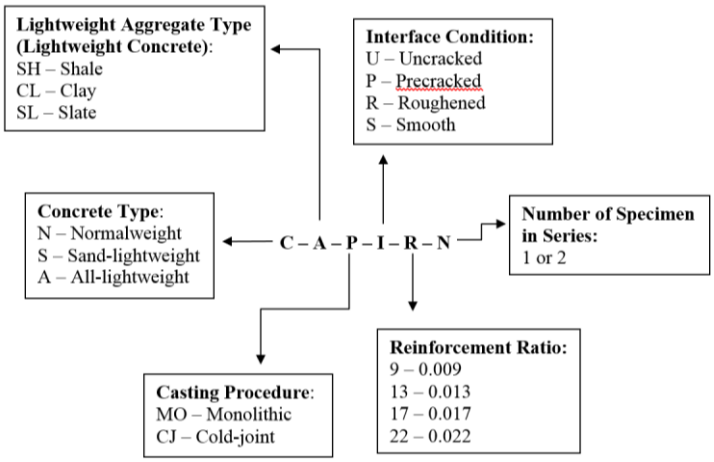

Figure 3.1 Specimen designation notation

Table 3.1 Specimen Test Matrix

Concrete Type	Lightweight Aggregate Type	Casting Procedure and Condition	Series Designation	Reinforcement Ratio	Number of Specimens
Normalweight	N/A	Monolithic – Uncracked	N-MO-U-13	0.013	2
		Monolithic – Pre-cracked	N-MO-P-13	0.013	2
Sand-Lightweight	Shale	Monolithic – Uncracked	S-SH-MO-U-13	0.013	2
		Monolithic – Pre-cracked	S-SH-MO-P-13	0.013	2
	Slate	Cold Joint – Roughened	S-SL-CJ-R-9	0.009	2
		Cold Joint – Smooth	S-SL-CJ-S-9	0.009	2
		Cold Joint – Roughened	S-SL-CJ-R-13	0.013	2
		Cold Joint – Smooth	S-SL-CJ-S-13	0.013	2
		Cold Joint – Roughened	S-SL-CJ-R-17	0.017	2
		Cold Joint – Smooth	S-SL-CJ-S-17	0.017	2
		Cold Joint – Roughened	S-SL-CJ-R-22	0.022	2
		Cold Joint – Smooth	S-SL-CJ-S-22	0.022	2
	Clay	Cold Joint – Roughened	S-CL-CJ-R-9	0.009	2
		Cold Joint – Smooth	S-CL-CJ-S-9	0.009	2
		Cold Joint – Roughened	S-CL-CJ-R-13	0.013	2
		Cold Joint – Smooth	S-CL-CJ-S-13	0.013	2
		Cold Joint – Roughened	S-CL-CJ-R-17	0.017	2
		Cold Joint – Smooth	S-CL-CJ-S-17	0.017	2
		Cold Joint – Roughened	S-CL-CJ-R-22	0.022	2
		Cold Joint – Smooth	S-CL-CJ-S-22	0.022	2
All-Lightweight	Shale	Monolithic – Uncracked	A-SH-MO-U-13	0.013	2
		Monolithic – Pre-cracked	A-SH-MO-P-13	0.013	2
	Slate	Cold Joint – Roughened	A-SL-CJ-R-13	0.013	2
		Cold Joint – Smooth	A-SL-CJ-S-13	0.013	2
	Clay	Cold Joint – Roughened	A-CL-CJ-R-13	0.013	2
		Cold Joint – Smooth	A-CL-CJ-S-13	0.013	2

3.3. MATERIALS

The main materials used for this research were concrete and reinforcing steel. Three general types of concrete were used including normalweight concrete, sand-lightweight concrete, and all-lightweight concrete defined by their designated aggregate composition. Aggregates used to achieve these types of concrete are described in Section 3.3.1. Concrete mixture designs used to achieve the target compressive strength of 5000 psi are summarized in Section 3.3.2. Lastly, information about the reinforcing steel used in this study is presented in Section 3.3.3.

3.3.1. Aggregates

3.3.1.1 Normalweight aggregates

Normalweight coarse aggregate used was crushed dolomite from the Jefferson City formation readily available in Missouri. Natural river sand was used as fines. Both aggregates conformed to ASTM C33. Properties of the aggregates are summarized in Table 3.2.

The coarse aggregate gradation used was 100% passing the 1 in. sieve and less than 5% passing the No. 8 sieve. The fine aggregate gradation used was 100% passing No. 4 sieve and less than 1% retained on No. 200 sieve.

Table 3.2 Description of Aggregates

Aggregate	Origin	Density[1] (lbs/ft^3)	Specific Gravity[2]	Size
Normalweight – Coarse	Capital Quarry, Rolla, MO	99	2.63	3/4 in. to No. 8
Normalweight – Fine	Capital Sand, Jefferson City, MO	110	2.55	No. 8 to 0
Shale – Coarse	Buildex, New Market, MO	44	1.35	3/8 in. to No. 8
Shale – Coarse/Fine Premix	Buildex, New Market, MO	54	1.69	3/8 in. to 0
Slate – Coarse	STALITE, Gold Hill, NC	52	1.60	3/8 in. to No. 16
Slate – Fine	STALITE, Gold Hill, NC	60	1.75	No. 4 to 0
Clay – Coarse	Trinity Lightweight, Livingston, AL	33	1.30	3/8 in. to No. 8
Clay – Fine	Trinity Lightweight, Livingston, AL	40	1.42	No. 8 to 0

1 ft = 0.305 m; 1 lb = 0.454 kg

[1]Loose Bulk Density, ASTM C29 (2009)

[2] Bulk Specific Gravity SSD, ASTM C127/C128 (2015/2015)

3.3.1.2 Lightweight aggregates

Expanded shale, expanded slate, and expanded clay aggregates were used for the lightweight concrete mixtures. Expanded shale was produced by Buildex in New Market, Missouri. Expanded slate was manufactured by STALITE in Gold Hill, North Carolina. Expanded clay was produced by Trinity Lightweight in Livingston, Alabama. Properties of the aggregates are summarized in Table 3.2. Figure 3.2 shows a photo of the expanded shale, expanded slate, and expanded clay aggregates. Aggregates used for the sand-lightweight concrete are shown in the top row of the figure. The expanded shale provided was pre-mixed (blend of coarse and fine aggregates produced by Buildex) in the case of aggregate used to achieve the all-lightweight concrete (bottom left). The

expanded clay aggregate was the lightest of the aggregates used in this research. In fact, it was observed that some of the saturated clay aggregates floated in water.

Figure 3.2 From left to right: expanded shale, expanded slate, expanded clay aggregates. Coarse aggregates top row, fine aggregates bottom row

For the sand-lightweight and all-lightweight concrete mixtures, a goal of the mixture proportioning was to obtain a consistent aggregate gradation of the combined lightweight aggregates for direct comparison of the results. The expanded shale gradations were used as the control since they were used in the first phase of this study (Sneed and Shaw 2013). It should be noted that the relative proportions of coarse and fine aggregates used in this study for the slate and clay lightweight concretes might not be typical, and that mixtures designed in this study may have slightly different densities than those that would have been achieved otherwise.

The expanded shale coarse aggregate gradation used in the production of the sand-lightweight concrete mixture was 3/8 in. x No. 8 sieve. The all-lightweight aggregate gradation was 3/8 in. x No. 0. These gradations are summarized in Table 3.3.

Table 3.3 Expanded Shale Aggregate Gradations (Buildex)

Sieve Designation	3/8 in. x No. 8 Gradation	3/8 in. x No. 0 Gradation
	Percent Passing	Percent Passing
1/2 in.	100	100
3/8 in.	99	100
No. 4	18	87
No. 8	1	51
No. 16	1	33
No. 30	-	21
No. 50	-	14
No. 100	-	7

The expanded slate coarse and fine aggregates had gradations shown in Table 3.4. For the sand-lightweight concrete mixture, only the coarse aggregate was used. For the all-lightweight concrete mixture, it was determined that a mixture of 30% coarse and 70% MS16 Fines would produce a gradation similar to that of the expanded shale gradation.

Table 3.4 Expanded Slate Gradations (STALITE)

	3/8 in.	MS16 Fines (#4-0)
Sieve Designation	Percent Passing	Percent Passing
1/2 in	100	100
3/8 in	98.5	100
No. 4	3.6	100
No. 8	1.3	84.5
No. 16	1.3	32.6
No. 30	1.2	2.3
No. 50	0.8	0.5
No. 100	0.5	0.3

The expanded clay coarse and fine aggregates had a gradation shown in Table 3.5. For the sand-lightweight concrete mixture, only the coarse aggregate was used. For the all-lightweight concrete mixture, a mixture consisting of 55% of coarse aggregate by weight and 45% of fine aggregate by weight was used so that it was similar to the expanded shale pre-mixed gradation.

Table 3.5 Expanded Clay Aggregate Gradations (Trinity Lightweight)

	Coarse Aggregate	Fine Aggregate
Sieve Designation	**Percent Passing**	**Percent passing**
1/2 in.	100	100
3/8 in.	99.9	100
No. 4	41.8	100
No. 8	7.9	90.8
No. 16	2.0	69.3
No. 30	1.6	45.9
No. 50	1.1	30.2
No. 100	0.9	19.6

3.3.2. Concrete Mixtures

3.3.2.1 Mixture Designs

The concrete mixtures were designed and verified by several trial batches to achieve the target plastic and hardened properties. The lightweight concrete mixtures were designed with guidance from the lightweight aggregate manufacturers. The target compressive strength of 5000 psi was desirable, but concretes within approximately 500 psi of the target compressive strength were accepted. Low slump (~2 in.) was desired due to the nature of a "step-like" placement in the formwork for specimens with a cold joint interface condition.

All concrete mixtures were composed of portland cement (Type I/II), water, coarse aggregates, and fine aggregates. No chemical additives were used in the concrete mixtures. Normalweight concrete was made with normalweight coarse and fine aggregates described in Section 3.3.1.1. Sand-lightweight concretes were made with lightweight coarse aggregates described in Section 3.3.1.2 and normalweight fine aggregates described in Section 3.3.1.1. All-lightweight concretes were made with lightweight coarse and fine aggregates described in Section 3.3.1.2.

Final mixture proportions for each concrete mixture are summarized in Table 3.6. The normalweight concrete mixture met the ASTM C33 (2013) specification requirements. All of the lightweight concrete mixtures met the requirements set forth by the ASTM C330 (2014) specification.

Table 3.6 Concrete Mixture Proportions

Concrete Type	Lightweight Aggregate Type	Mixture Design Quantities (lb/yd^3)				
		Coarse Aggregate	Fine Aggregate	Water	Cement[5]	w/c
Normalweight[1]	N/A	1728	1302	305	517	0.59
Sand-lightweight[2]	Shale	834	1498	281	535	0.53
	Slate	975	1125	265	530	0.50
	Clay	692	1251	263	612	0.43
All-lightweight[3]	Shale[4]	1885		260	610	0.43
	Slate	528	1233	378	801	0.47
	Clay	692	556	263	796	0.46

[1] Normalweight concrete coarse and fine aggregates satisfied ASTM C33 (2013)
[2] Sand-lightweight concrete coarse aggregates were ASTM C330, fine aggregates were ASTM C33 (2013)
[3] All-lightweight concrete coarse and fine aggregates satisfied ASTM C330 (2014)
[4] All-lightweight expanded shale aggregate was premixed by the manufacturer
[5] Type I/II cement

3.3.2.2 Batching Procedure

Lightweight aggregates are capable of high water absorption. This is due to the manufacturing process of being heated to high temperatures during which the aggregates expand and create a complex capillary void structure. Due to this phenomenon it is necessary to saturate lightweight aggregates prior to batching. It is usually most desirable to bring the aggregate to a wetted surface-dry (WSD) condition, which is analogous to the saturated surface-dry condition (SSD) for normalweight aggregates. This, however, is difficult to achieve on a large scale. Instead, it is common practice for batching plants to soak lightweight aggregate with soaker hoses for a period of time prior to batching.

To achieve adequate and uniform saturation in this experimental work, a saturation tank was created by cutting off the top of a 1000 lb liquid storage tank with a valve near the bottom. A strainer was used to catch any particles larger than 1/16 in. by gluing a piece of metal mesh over the valve opening. The tank is shown in Figure 3.3. Two days prior to batching, the tank was filled with the required amount of lightweight aggregate. Then it was filled with water until the water level was about 2 in. above the aggregate. This was to provide a water level sufficient to cover all aggregate for the duration of soaking. The tank was then allowed to sit undisturbed for 48 hours. After the 48 hour period the tank was drained using the built-in valve. The outflow of the tank was passed over a No. 100 and No. 200 sieve to retain all fines. These fines were then returned back to the tank. The saturating procedure was identical for all lightweight aggregates.

Figure 3.3 Tank used for lightweight aggregate saturation

All concrete mixtures were batched, mixed, and placed in the Concrete Materials Laboratory in Butler-Carlton Hall at Missouri S&T. Mixing was performed using a 6-cubic foot rotary drum mixer shown in Figure 3.4.

Figure 3.4 Six cubic foot rotary drum mixer

3.3.2.3 Plastic Concrete Properties

The plastic concrete properties of the mixtures used for specimen casting are summarized in Table 3.7. Slump of concrete mixtures was determined following steps of ASTM C143 (2015). Density and air content of the concrete mixtures were measured according to ASTM C138 (2014). Unit weight of fresh concrete mixtures was measured and reported. Due to the capillary nature of lightweight aggregate, using pressure air meter is not recommended. To determine the air content of lightweight concrete mixtures, the ASTM C173 (2014) – volumetric method was used. Figure 3.5 shows the equipment used to determine the air content.

Table 3.7 Plastic Concrete Properties

Concrete Type	**Lightweight Aggregate Material**	**Density[1] (lb/ft^3)**	**Air[2] (%)**	**Slump[3] (in.)**
Normalweight	N/A	148	2.5	5.5
Sand-lightweight	Shale	117	2.0	4.25
	Slate (S-SL-CJ-XX-09 series)	117	1.5	2.0
	Slate (S-SL-CJ-XX-13 series)	117	2.5	0.75
	Slate (S-SL-CJ-XX-17 series)	117	2.0	2.25
	Slate (S-SL-CJ-XX-22 series)	118	2.5	2.0
	Clay (S-CL-CJ-XX-09 series)	105	2.5	1.25
	Clay (S-CL-CJ-XX-13 series)	105	2.5	1.25
	Clay (S-CL-CJ-XX-17 series)	104	2.0	1.5
	Clay (S-CL-CJ-XX-22 series)	106	2.5	1.5
All-lightweight	Shale	108	3.0	2.5
	Slate	106	2.8	6.5
	Clay	88	2.5	0.5

[1] Density of freshly mixed concrete; ASTM C138 (2014)
[2] Gravimetric method used for normalweight concrete, ASTM C138 (2014); volumetric method used for lightweight concrete, ASTM C173 (2014)
[3] ASTM C143 (2015)

(a) (b) (c)

Figure 3.5 a) Modulus of elasticity yoke, b) brass volumetric meter, c) pressure meter

(a) (b)

Figure 3.6 a) Cylinder compressive strength test, b) splitting tensile strength test

3.3.2.4 Hardened Concrete Properties

Hardened concrete properties are summarized in Table 3.8. The concrete compressive strength of each batch was measured at 3, 7, 14, 21, and 28 days. Compressive strength, splitting tensile strength, and modulus of elasticity were determined at test day, which for this research was 28 days after casting the specimen. The compressive strength was determined according to ASTM C39 (2015) using a minimum of three 4 in. by 8 in. cylinders. The splitting tensile strength was determined using a minimum of one cylinder according to ASTM C496 (2011). Figure 3.5 and Figure 3.6 show the equipment used for determining the above mentioned properties.

Table 3.8 Hardened Concrete Properties

Specimen Series	**Target f'_c (psi)**	**f'_c [1] (psi)**	**f'_c at test day[1] (psi)**	**f_{ct} [2] (psi)**	**$\sqrt{f'_c}$**	**E_c [3] (psi)**
N-MO-XX-13	5000	4840	4840	420	6.0	3900000
S-SH-MO-XX-13	5000	4770	4770	460	6.7	3300000
A-SH-MO-XX-13	5000	4700	4700	515	7.5	2650000
S-SL-CJ-XX-09	5000	5380	5380	595	8.1	3300000
S-SL-CJ-XX-13	5000	5570	5570	570	7.6	3500000
S-SL-CJ-XX-17	5000	4950	4950	670	9.5	3050000
S-SL-CJ-XX-22	5000	5000	5000	445	6.3	3450000
A-SL-CJ-XX-13	5000	4380	4380	420	6.3	2450000
S-CL-CJ-XX-09	5000	4770	4770	340	4.9	2500000
S-CL-CJ-XX-13	5000	4640	4640	360	5.3	2650000
S-CL-CJ-XX-17	5000	4550	4550	410	6.1	2600000
S-CL-CJ-XX-22	5000	4790	4790	485	7.0	2700000
A-CL-CJ-XX-13	5000	4460	4460	405	6.1	1700000

[1] Values reported are the average of three cylinder tests, ASTM C1231 (2014)
[2] ASTM C496 (2011)
[3] ASTM C469 (2014)

It is interesting to note that values of tensile strength for the sand-lightweight concrete and all-lightweight concretes, particularly those with shale and slate aggregates, are similar to that of normalweight concrete. Also, the measured values of E_c for the all-lightweight concrete with shale and slate aggregates are similar to that of the sand-lightweight clay concrete, and E_c appears to be dependent on concrete density rather than concrete type.

3.3.3. Reinforcing Steel Bars

Deformed reinforcing steel bars were provided for this research by Ambassador Steel Corporation. The bars were ASTM A615 Grade 60. All bars of the same size used in this study were supplied from the same heat.

Mill certifications were provided upon shipment for quality assurance purposes. The mill certifications stated that the yield stress was 73,865 psi for the No. 3 bars and 65,818 psi for the No. 5 bars. Properties reported by the manufacturer were verified by conducting tensile tests according to ASTM A370 (2015). Strain was measured using strain gages described in Section 3.5.5.2. The strain readings were also verified using an 8 in. extensometer that was removed from the tensile coupon upon yielding. The average yield stress of the No. 3 and No. 5 bars were 72,185 psi and 70,695 psi, respectively. The average ultimate stress of the No. 3 bars was 101,055 psi, while the average ultimate stress of the No. 5 bars was 102,390 psi. Representative stress-strain curves for the No. 3 and No. 5 bars are shown in Figure 3.7. A summary of the tensile test results is presented in Table 3.9. It should be noted that for Specimen 3-1, the extensometer slipped upon loading and damaged the strain gage as well. Therefore only the peak stress was obtained for this specimen.

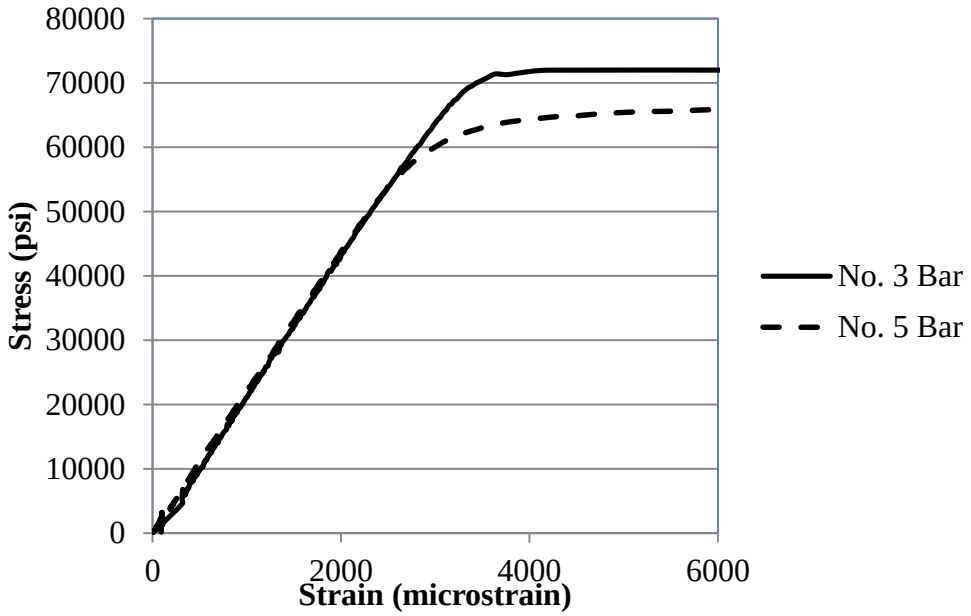

Figure 3.7 Representative stress vs. strain plots for steel reinforcing bars used in this study

Table 3.9 Measured Reinforcing Steel Bar Properties

Tensile Specimen ID	Bar Size	Yield Stress (psi)	Peak Stress (psi)	Modulus of Elasticity (psi)
3-1	No. 3	ND[1]	100,870	ND[1]
3-2	No. 3	72,200	101,110	32,040,000
3-3	No. 3	72,165	100,995	28,466,000
Average		**72,185**	**101,055**	**30,253,000**
5-1	No. 5	70,700	102,750	27,437,000
5-2	No. 5	70,470	102,555	28,021,000
5-3	No. 5	70,915	101,870	28,871,000
Average		**70,695**	**102,390**	**28,110,000**

[1]Values denoted ND as indicate no data

3.4. SPECIMEN FABRICATION

Specimens were fabricated during the spring of 2015. Casting dates are summarized in Table 3.10. A total of 54 specimens were constructed and tested including 52 specimens summarized herein and two trial specimens – one with a cold joint interface, and one with a monolithic interface. Section 3.4.1 discusses the preparation of the reinforcing bar cages. Formwork assembly is presented in Section 3.4.2. Concrete placement and shear interface preparation is described in Section 3.4.3. Lastly, Section 3.4.4 discusses the concrete curing procedure.

Table 3.10 Specimen Casting and Testing Dates

Specimen Series	Casting Date	Test Date	Age at Test Date (days)	Number of Tests
N-MO-13	1/23/2015	2/20/15	28	4
S-SH-MO-13	1/28/2015	2/25/15	28	4
S-SL-CJ-9	3/2/15	3/30/15	28	4
S-SL-CJ-13	1/30/15	2/27/15	28	4
S-SL-CJ-17	3/9/15	4/6/15	28	4
S-SL-CJ-22	2/11/15	3/11/15	28	4
S-CL-CJ-9	4/1/15	4/29/15	28	4
S-CL-CJ-13	4/8/15	5/6/15	28	4
S-CL-CJ-17	4/15/15	5/13/15	28	4
S-CL-CJ-22	4/24/15	5/22/15	28	4
A-SH-MO-13	2/6/2015	3/6/15	28	4
A-SL-CJ-13	4/27/2015	5/25/15	28	4
A-CL-CJ-13	3/16/2015	4/13/15	28	4

3.4.1. Reinforcing Steel Bar Cage Preparation

Each reinforcing cage was constructed of ASTM A615 Grade 60 steel, as described in Section 3.3.3. Reinforcing steel bars were bent and the cages were assembled in the High Bay Structural Engineering Research Laboratory at Missouri S&T. Specimens presented in this report were based

on the design used in the first phase of the study described in Sneed and Shaw (2013), which had reinforcement ratio of 0.013. This corresponds to three No. 3 closed stirrups orthogonal to the shear plane as shown in Figure 3.8. Reinforcing bars located parallel to the shear plane were four No. 5 bars that were bent into an "L" shape. These No. 5 bars were confined by No. 3 closed stirrups inside the flanges. Concrete cover was 0.75 in. throughout the specimen except at the shear plane where the concrete cover was 0.25 in. (see Figure 3.8 cross section).

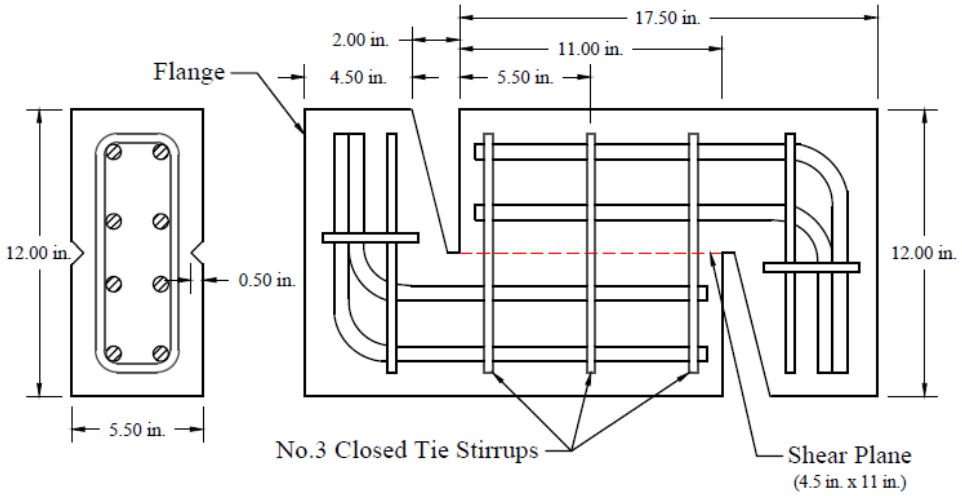

Figure 3.8 Reinforcement detail (dimensions shown in the figure are measured to the nearest 0.25 in.). Note: Details shown are for a specimen with ρ=0.013. For specimens with reinforcement ratios of 0.009, 0.017, and 0.022, the number of No. 3 closed tie stirrups crossing the shear plane is 2, 4, and 5, respectively, and they are distributed uniformly across the 11 in. long shear plane

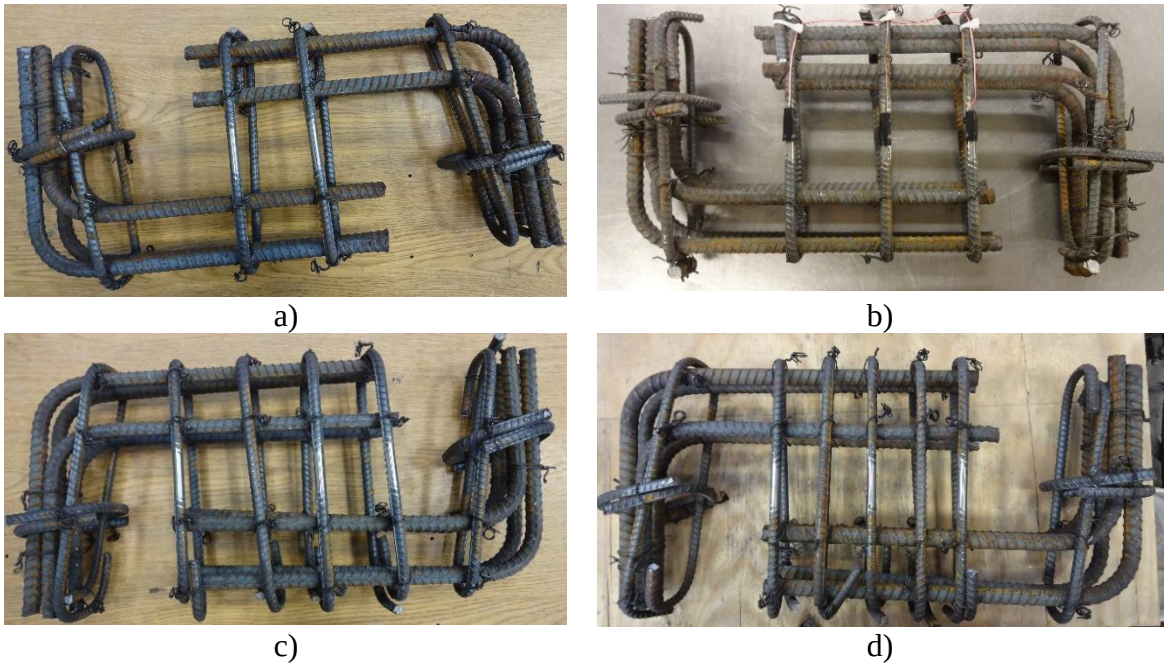

a) b)

c) d)

Figure 3.9 Reinforcement cages of each reinforcement ratio a) 0.009, b) 0.013, c) 0.017, d) 0.022

In order to achieve four different reinforcement ratios among the slate sand-lightweight and clay sand-lightweight test specimens, four different reinforcing cage configurations were used (Figure 3.9). The No. 3 stirrups that served as the shear reinforcement were distributed evenly across the shear plane. As shown in Figure 3.8, the shear plane measured 11 in. x 4.5 in. to equal a total shear plane area of 49.5 in^2. Either two, three, four, or five double-legged stirrups were used as shear reinforcement for the slate sand-lightweight and clay sand-lightweight test specimens to create reinforcement ratios of 0.009, 0.013, 0.017, or 0.022, respectively. No. 3 bars were also used in the flanges to confine the L-shapes and to provide extra reinforcement of the flanges.

3.4.2. Formwork and Assembly

Specimens constructed for this study required two types of formwork, one for specimens with a monolithic interface, and one for specimens with a cold joint interface. Specimens with a monolithic interface were cast on their side using formwork shown in Figure 3.10. This formwork allowed for easy placement and consolidation of concrete. The formwork was built using 0.75 in. thick untreated plywood and 2 in. by 6 in. untreated boards. Steel void formers used by Sneed and Shaw (2013) were modified for this formwork. The void formers can be seen in Figure 3.10. The overall inside dimensions were 12 in. by 24 in. by 5.5 in. This size provided a shear plane of 49.5 in^2. The shape of the specimens was designed based on previous research conducted by Mattock and Hawkins (1972). Indentations along the shear plane in the cross section view of Figure 3.8 were achieved by a 0.5 in. chamfer on the bottom and by inserting an identical 11 in. long piece into the finished top surface.

Specimens with a cold joint interface were to be cast in two stages to achieve the non-monolithic condition along the shear plane. Formwork shown in Figure 3.11 was used for this type of casting. By casting specimens this way, the shear plane was fully exposed to allow for preparation of its surface. The materials and dimensions used were identical to those of the monolithic formwork.

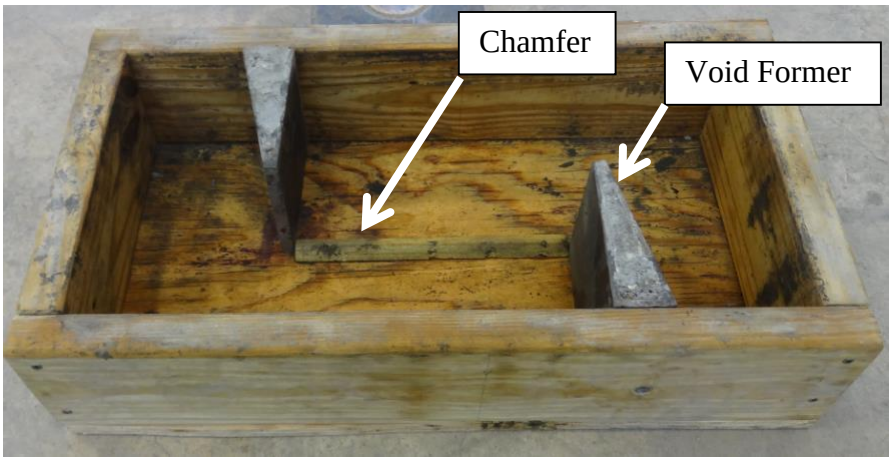

Figure 3.10 Formwork for specimens with a monolithic interface

Figure 3.11 Formwork for specimens with a cold joint interface

3.4.3. Concrete Placement and Shear Interface Preparation

All specimens were cast in the Concrete Materials Laboratory in the Butler-Carlton Hall at Missouri S&T. Concrete placement of the monolithic specimens was conducted in one lift without any shear interface preparation. The monolithic specimens were cast from the same concrete batch in groups of four: two were to have an uncracked interface, and two were to have a pre-cracked interface (described in Section 3.5.4).

For the cold joint specimens the concrete was placed in two lifts with a minimum of eight hours between casting each lift to achieve the cold joint condition. The cold joint specimens were cast from the same concrete batch in groups of four: two with a smooth and two with a roughened interface. After the first lift was placed, the shear plane of the smooth interface specimens was troweled smooth. The roughened interface specimens were left alone for approximately 4 hours. After initial setting of concrete, the shear plane of the roughened interface specimens was roughened to amplitude of approximately 0.25 in. as specified by the ACI 318 code (2014) and PCI Design Handbook (2010). This was achieved using the tool shown in Figure 3.12. The depth of scoring was controlled by inserting one quarter of the 1 in. hook of the scoring tool. The shear plane was scored in the direction perpendicular to the direction of loading across the entire width of the shear plane. After scoring was completed, the shear plane was cleaned using compressed air. The depth of roughening was then measured and verified at several random locations using a digital caliper as shown in Figure 3.13.

Figure 3.12 Roughening tool

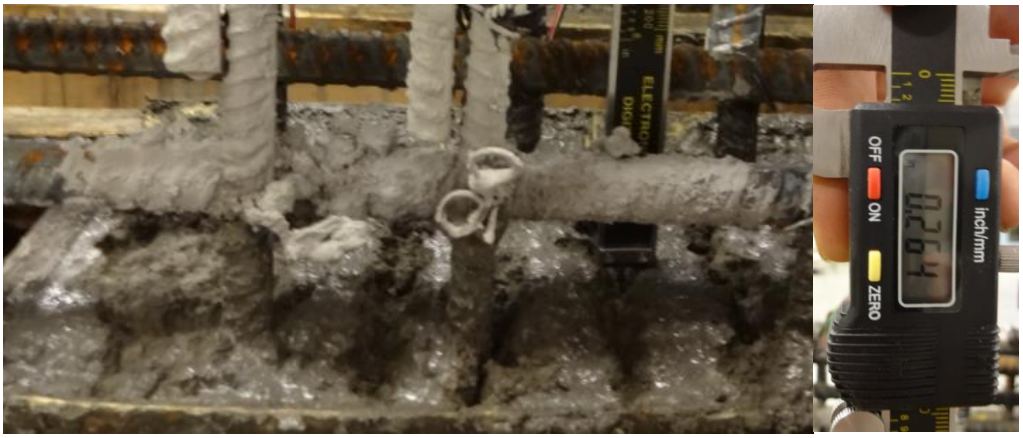

Figure 3.13 Example of roughened surface and measuring of roughness

3.4.4. Concrete Curing

The specimens along with cylinders were covered with plastic immediately after casting the concrete. After a 24-hour period, the specimens and cylinders were de-molded and placed inside the moist-cure room located in the Concrete Materials Laboratory in the Butler-Carlton Hall at Missouri S&T. This room is maintained at 70 degrees Fahrenheit and 100 percent humidity. The specimens and cylinders were kept in the moist-cure room until the day before testing. The night before testing, the specimens and cylinders were removed from the moist-cure room and allowed to dry off in order to be tested the next day. Casting and test dates are summarized in Table 3.11.

3.5. TEST SETUP

This research expanded on the previous research conducted in the first phase of this study by Sneed and Shaw (2013). Therefore, this research utilized a similar test setup. Two trial specimens were constructed to confirm the test setup used previously and to test the data acquisition system. This section describes the test setup including the support conditions, loading protocol, pre-cracking procedure (where applicable), and flange confinement. Data acquisition and instrumentation used to collect electronic data are discussed in this section as well.

3.5.1. Support Conditions

After thorough evaluation of previous research conducted, it was determined to follow the final support conditions used by Sneed and Shaw (2013). This was done for two reasons: it was proven to work for the testing at Missouri S&T, and it was already available for this research. It was determined to not use the roller system used previously by Hofbeck (1969) due to minimal lateral translation of the specimen during testing observed by Sneed and Shaw (2013). The support conditions for testing of specimens are shown in Figure 3.14. A hemispherical bearing head was used on top of the specimen to transfer the load from the crosshead of the Tinius Olsen universal testing machine to the specimen. The specimen was supported on the bottom by the steel platen of the testing machine. Neoprene pads were placed between the specimen flanges and the steel plates used on the top and bottom to help distribute the load evenly.

Figure 3.14 Typical support conditions for testing

3.5.2. Flange Prestressing/Confinement Systems

Based on the research conducted by Sneed and Shaw (2013) it was determined that primary and secondary confinement of the flanges would be used was used to avoid premature flange failure. The primary confinement system consisted of two steel plates and four all-thread rods around each flange as shown in Figure 3.15 and was intended to provide active confinement to the flange. The all-thread rods with nuts were tightened to 50 lb-ft. This corresponds to approximately 325 psi of compression to each flange. The effect of prestressing was monitored using the strain gages mounted on the reinforcing bars crossing the shear plane. No effect outside of the noise levels of strain gages was seen during the primary prestressing.

The secondary prestressing system shown in Figure 3.15 consisted of four 0.5 in. plates. On the back of the specimen they were held in place with two structural steel angles. On the front of the

specimen the plates were pushed against the flange using four bolts per plate as seen in Figure 3.15. This confinement was intended to provide passive support in the event of flange failure out of plane. It should be noted that no premature flange failures were observed in any of the tests included in this study.

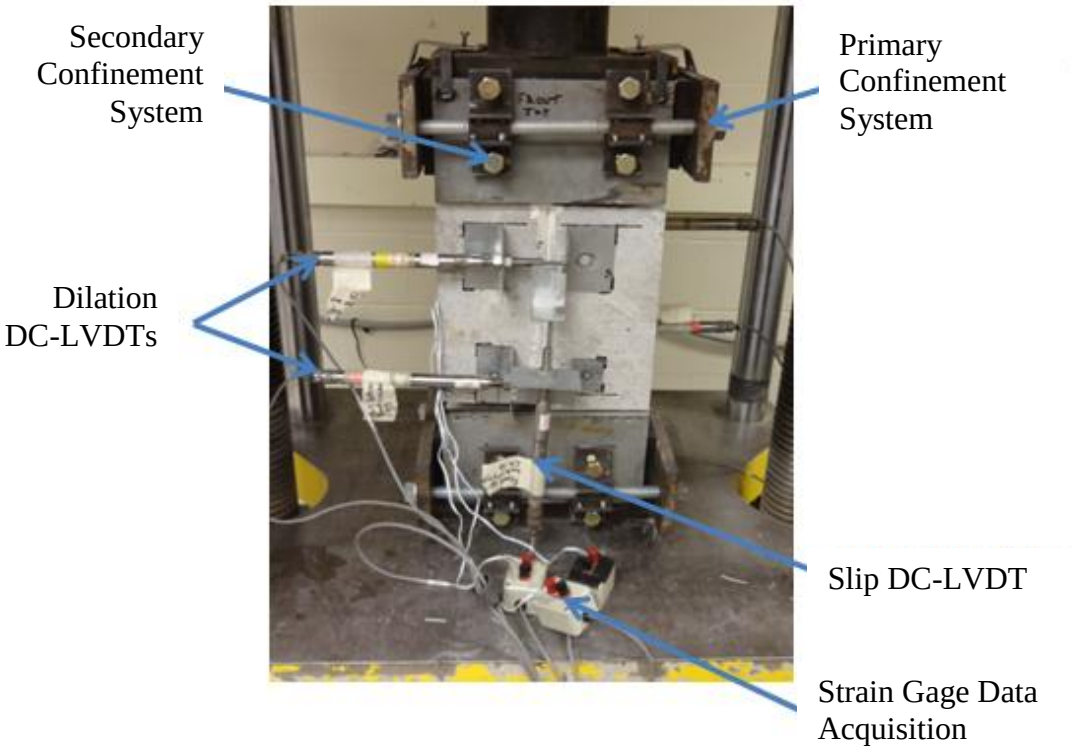

Figure 3.15 Primary and secondary flange confinement systems

3.5.3. Loading Protocol

As mentioned in Section 3.5.1, a Tinius Olsen universal testing machine with 200-kip capacity was used to apply the load to the test specimens. The load frame is located in the Jones Structural Materials Testing Laboratory in Butler-Carlton Hall at Missouri S&T. For this study, all specimens were tested under displacement controlled loading by controlling the stroke of the testing machine at a rate of 0.015 in. per minute. The specimens were tested until one of the following conditions occurred: a target slip of 0.3 in. was reached, or 60 percent of the ultimate strength was reached (after the ultimate strength was reached).

3.5.4. Pre-cracking of Monolithic Specimens

During the review of previously conducted research involving pre-cracking of monolithic specimens, it was discovered that different researchers used different methods to accomplish this task. The Mattock and Hawkins' (1972) approach was modified and used in this study. Prior to pre-cracking, the shear plane was painted white on both sides of the specimen. A crack was produced along the shear plane by applying a line load to both sides of the specimen using an in-house developed splitting tool shown in Figure 3.16. The specimen was placed on its side, and the pre-cracking tool edge was placed into the chamfers used to create the shear plane as shown in

Figure 3.17. Loading was gradually increased until a significant drop in load occurred. At this point, the load was paused, and the specimen was examined visually for hairline cracks.

Figure 3.16 Pre-cracking tool

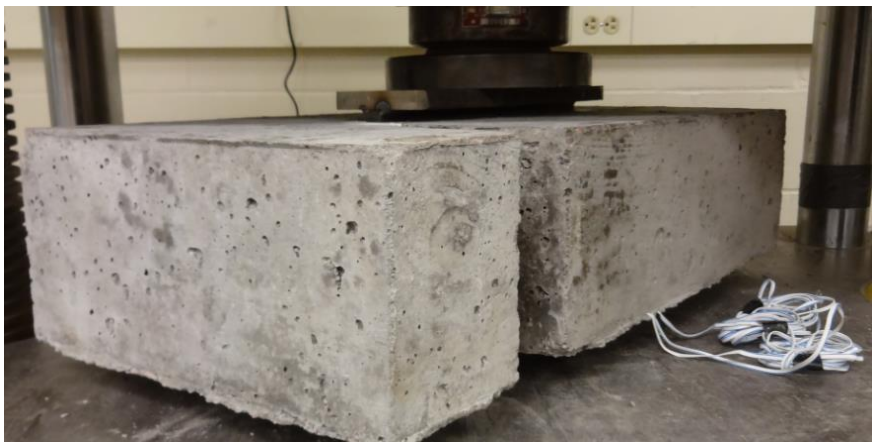

Figure 3.17 Pre-cracking setup

3.5.5. Instrumentation and Data Acquisition

Eleven data channels were used to monitor each test. Six data channels were displacements measured with direct current-linear variable differential transducers (DC-LVDTs). Three channels recorded strains measured using uniaxial strain gages. The last two data channels were used to measure the load and global displacement (stroke) of the testing machine. Both of these measurements were acquired from the on board load cell and transducer on the bottom platen of the Tinius Olsen testing machine. The specimen instrumentation is shown in Figure 3.15 (except for the load and global displacement). All channels were observed in real time throughout the test to ensure proper functioning of each data channel.

3.5.5.1 Direct current – LVDTs

Two DC-LVDTs were used to measure slip along the shear interface, and four DC-LVDTs were used to measure dilation of the shear interface. Three DC-LVDTs were mounted on the front face of the specimen, and an identical configuration was used on the back face of each specimen. The DC-LVDTs used to measure the dilation (horizontal separation) had ±1.0 in. stroke, while the DC-LVDTs measuring slip had ±0.5 in. stroke. These were sufficient to measure the displacements experienced by each specimen. The DC-LVDTs were mounted to the aluminum brackets that were

mounted on specimens using a hot-glue gun with a slow setting glue readily available at the local hardware store. This method was recommended by HILTI Test Lab staff from Tulsa, Oklahoma.

3.5.5.2 Strain Gages

Two sets of strain gages were mounted on the reinforcing steel used in this study. The first set of strain gages used were uniaxial electronic resistance strain gages (CEA-06-125UN-120) manufactured by Vishay Micro-measurements. The second set was type EA-06-250BG-120/LE by Vishay Micro-measurements ordered at a later date.

Three strain gages per specimen were attached to the exterior face of the reinforcing bars crossing the shear plane. The strain gages were positioned so that they would be at the location of shear plane crack as shown in Figure 3.18. During the bar preparation (i.e. removing the lugs), special care was taken to not reduce the bar cross-sectional area more than necessary. The manufacturer's instructions were followed to attach the strain gages. After the strain gage was attached, a protective covering – butyl rubber patch (Vishay Barrier E) was placed over the strain gage as shown in Figure 3.19. When the reinforcement cage was placed in the form, it was checked to ensure that strain gages were crossing the shear plane. All strain gages were checked for operation before the placement of concrete.

During testing, it was observed that a large amount of noise was present in the strain gage readings. It took the research team several testing sessions to determine that the power supply on the strain gage data acquisition system was malfunctioning. However, this noise was later removed in the strain data.

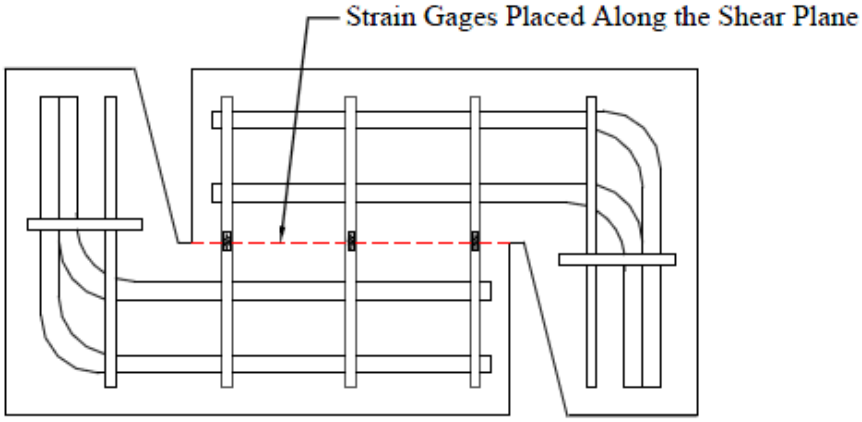

Figure 3.18 Location of strain gages

Figure 3.19 Strain gages attached to shear reinforcement

3.6. TEST RESULTS

This section summarizes the salient results from the second phase of the experimental program. Comprehensive test results are presented in terms of shear strength, shear stress, slip of shear plane, dilation of shear plane, and strain in the reinforcing bars crossing the shear plane in Appendix A.

3.6.1. Failure Mode and Cracking Behavior

The failure mode of each test specimen is summarized in Table 3.11. Failure of most specimens was associated with shear failure of the shear interface. Figure 3.20 shows a photo of a typical failure along the shear plane.

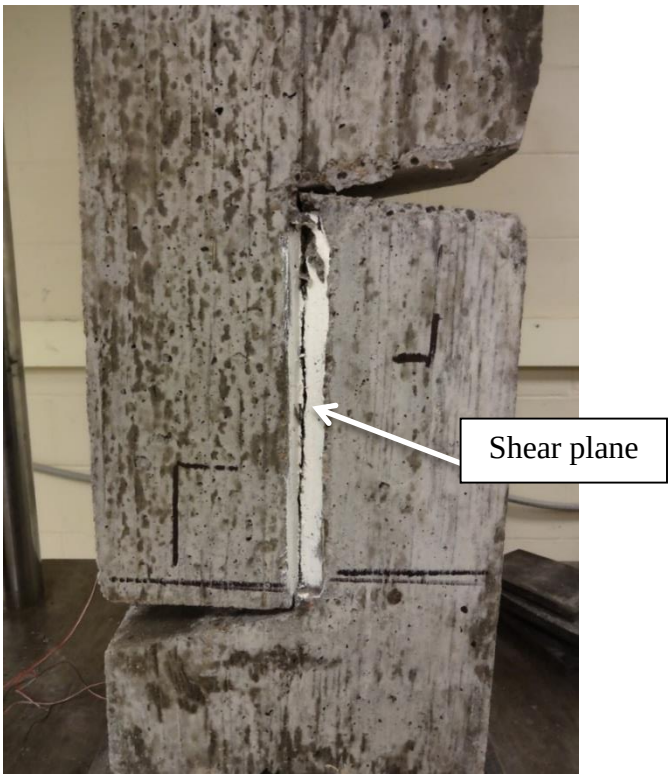

Figure 3.20 Typical specimen failed in shear along the intended shear plane

Specimens S-CL-CJ-R-17-1, S-CL-CJ-R-17-2, S-CL-CJ-R-22-1, S-CL-CJ-R-22-2, S-CL-CJ-S-22-1, and S-CL-CJ-S-22-2, each of which had expanded clay aggregates and reinforcement ratio ρ=0.017 or 0.022, failed due to concrete splitting (ACI Committee 408 2003) prior to shear failure. Figures 3.21 and 3.22 show photographs of specimens that failed due to concrete splitting of the longitudinal and auxiliary reinforcement. It is worth noting that the concrete with expanded clay aggregates had the lowest splitting tensile strength and elastic modulus of all sand-lightweight concrete mixtures in this study (Table 3.8). Specimens S-SL-CJ-R-22-1, S-SL-CJ-R-22-2, S-SL-CJ-S-22-1, and S-SL-CJ-S-22-2, which had expanded slate aggregates and ρ=0.022, failed in shear but also exhibited several splitting cracks. Additional discussion on splitting failure observed in these specimens in included in Wermager (2015).

Table 3.11 Summary of Test Results

Specimen ID	f'_c at test day (psi)	V_u (lbs)	v_u[1] (psi)	$v_{u,avg}$ (psi)	Slip at V_u (in.)	Dilation at V_u (in.)	V_{ur}[2,3] (lbs)	v_{ur}[1,3] (psi)	$v_{ur,avg}$ (psi)	$(v_u/v_{ur})_{avg}$	Failure Mode
N-MO-U-13-1	4840	63410	1281	1269	0.019	0.014	40729	823	823	1.54	Shear
N-MO-U-13-2		62203	1257		0.017	0.015	ND	ND			Shear
N-MO-P-13-1		61071	1234	1192	0.017	0.011	45537	920	1011	1.18	Shear
N-MO-P-13-2		56973	1151		0.023	0.012	54598	1103			Shear
S-SH-MO-U-13-1	4770	55434	1120	1132	0.011	0.009	40773	824	801	1.41	Shear
S-SH-MO-U-13-2		56588	1143		0.010	0.010	38501	778			Shear
S-SH-MO-P-13-1		50593	1022	1035	0.013	0.007	39068	789	830	1.25	Shear
S-SH-MO-P-13-2		51884	1048		0.020	0.009	43098	871			Shear
A-SH-MO-U-13-1	4700	52032	1051	1056	0.016	0.009	32821	663	707	1.49	Shear
A-SH-MO-U-13-2		52549	1062		0.013	0.009	37162	751			Shear
A-SH-MO-P-13-1		46120	932	998	0.038	0.009	41332	835	906	1.10	Shear
A-SH-MO-P-13-2		52692	1064		0.026	0.007	48352	977			Shear
S-SL-CJ-R-9-1	5380	49340	1000	1010	0.009	0.007	30560	617	617	1.63	Shear
S-SL-CJ-R-9-2		50475	1020		0.007	0.006	ND	ND			Shear
S-SL-CJ-S-9-1		26945	540	600	0.021	0.007	23040	465	529	1.14	Shear
S-SL-CJ-S-9-2		32500	660		0.012	0.006	29300	592			Shear
S-SL-CJ-R-13-1	5570	63167	1276	1238	0.013	0.008	ND	ND	735	1.68	Shear
S-SL-CJ-R-13-2		59370	1199		0.013	0.009	36363	735			Shear
S-SL-CJ-S-13-1		39487	798	891	0.017	0.007	30508	616	700	1.27	Shear
S-SL-CJ-S-13-2		48767	985		0.016	0.008	38771	783			Shear
S-SL-CJ-R-17-1	4950	62385	1260	1290	0.012	0.008	ND	ND	ND	ND	Shear
S-SL-CJ-R-17-2		65150	1320		0.009	0.007	ND	ND			Shear
S-SL-CJ-S-17-1		47640	960	955	0.018	0.007	ND	ND	694	1.38	Shear
S-SL-CJ-S-17-2		47120	950		0.019	0.007	34330	694			Shear
S-SL-CJ-R-22-1	5000	64455	1300	1230	0.011	0.006	39640	801	801	1.54	Shear
S-SL-CJ-R-22-2		57590	1160		0.006	0.007	ND	ND			Shear
S-SL-CJ-S-22-1		49810	1010	1075	0.018	0.006	32600	659	694	1.55	Shear
S-SL-CJ-S-22-2		56535	1140		0.016	0.006	36130	730			Shear
A-SL-CJ-R-13-1	4380	46525	940	944	0.012	0.006	30148	609	645	1.46	Shear
A-SL-CJ-R-13-2		46925	948		0.005	0.005	33741	682			Shear
A-SL-CJ-S-13-1		37842	764	774	0.019	0.007	30810	622	671	1.15	Shear
A-SL-CJ-S-13-2		38751	783		0.024	0.007	35575	719			Shear
S-CL-CJ-R-9-1	4770	37060	750	810	0.012	0.007	ND	ND	ND	ND	Shear
S-CL-CJ-R-9-2		42910	870		0.008	0.005	ND	ND			Shear
S-CL-CJ-S-9-1		31920	650	710	0.012	0.005	23610	477	519	1.36	Shear
S-CL-CJ-S-9-2		37960	770		0.009	0.005	27730	560			Shear
S-CL-CJ-R-13-1	4640	50785	1026	986	0.007	0.006	31310	633	651	1.51	Shear
S-CL-CJ-R-13-2		46885	947		0.015	0.005	33178	670			Shear
S-CL-CJ-S-13-1		41006	828	822	0.015	0.006	31025	627	600	1.37	Shear
S-CL-CJ-S-13-2		40436	817		0.018	0.007	28402	574			Shear
S-CL-CJ-R-17-1	4550	51240	1040	1095	0.004	0.004	37420	756	751	1.45	Splitting
S-CL-CJ-R-17-2		56660	1150		0.009	0.005	36920	746			Splitting
S-CL-CJ-S-17-1		43140	870	930	0.012	0.005	ND	ND	667	1.39	Shear
S-CL-CJ-S-17-2		48930	990		0.013	0.006	33040	667			Shear
S-CL-CJ-R-22-1	4790	56720	1146	1111	0.008	0.003	ND	ND	670	1.66	Splitting
S-CL-CJ-R-22-2		53225	1075		0.017	0.006	33250	672			Splitting
S-CL-CJ-S-22-1		52405	1059	1061	0.01	0.004	40300	814	815	1.30	Splitting
S-CL-CJ-S-22-2		52590	1062		0.005	0.003	ND	ND			Splitting
A-CL-CJ-R-13-1	4460	41858	846	865	0.009	0.006	ND	ND	534	1.62	Shear
A-CL-CJ-R-13-2		43816	885		0.011	0.006	26451	534			Shear
A-CL-CJ-S-13-1		36966	747	750	0.008	0.005	ND	ND	501	1.50	Shear
A-CL-CJ-S-13-2		37324	754		0.015	0.006	24795	501			Shear

[1] v_u and v_{ur} are defined as the peak and residual applied shear force respectively, divided by the area of the shear plane

[2] Residual shear force V_{ur} is defined as the load at 0.15 in. of slip

[3] Some values for V_{ur} and v_{ur} are denoted as ND (no data) because the slip did not reach a value of 0.15 in. before the test was concluded.

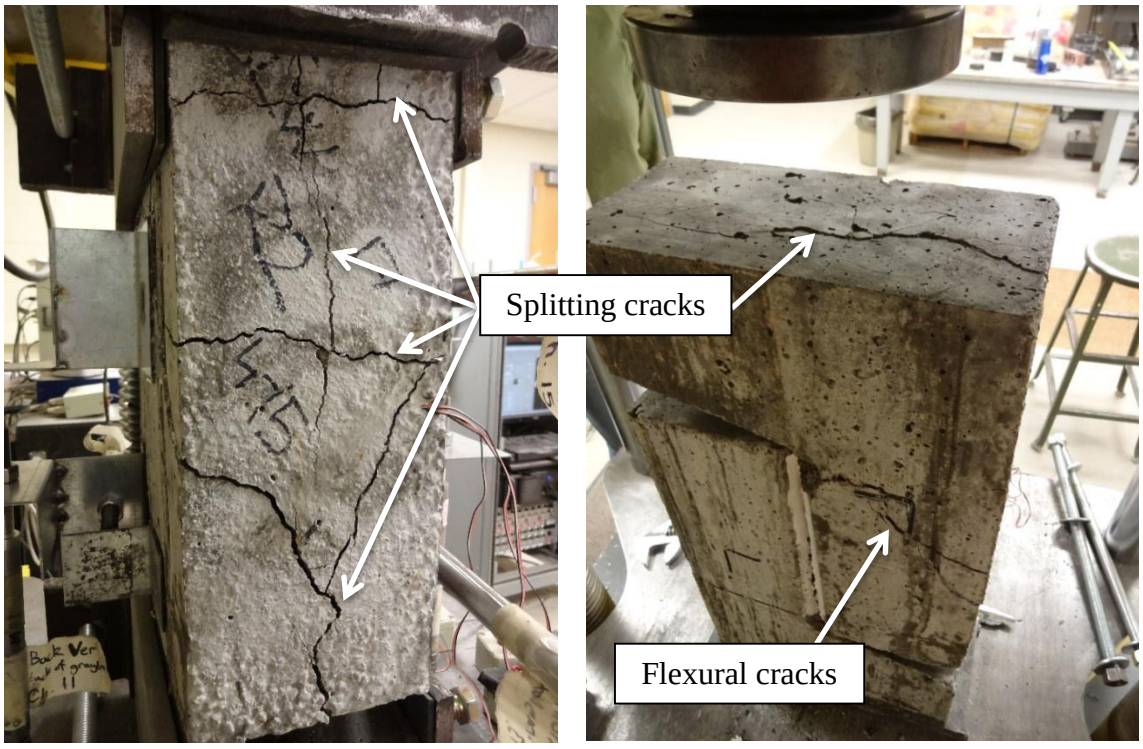

(a) (b)

Figure 3.21 Typical cracking due to splitting failure: a) side face, b) top/back face; specimen S-CL-CJ-R-17-2 shown

Figure 3.22 Specimen S-CL-CJ-R-17-2 with loose concrete removed, confirming that cracks extend to surface of longitudinal reinforcement bar (splitting failure)

Typical shear plane cracks for monolithic normalweight and monolithic lightweight concrete specimens are shown in Figure 3.23. Dilation of the shear-plane crack at the peak applied shear force was the most significant for normalweight concrete specimens, which is likely the result of the use of a larger maximum aggregate size (i.e. 3/4 in.). This larger aggregate creates greater dilation as described by the saw-tooth analogy by Birkeland and Birkeland (1966). This dilation ranges from 0.011 in. to 0.015 in. at the peak applied shear force (Table 3.11). For sand-lightweight concrete and all-lightweight concrete the maximum aggregate size was 3/8 in. causing the shear crack dilation at the peak applied shear force to range from 0.003 in. to 0.010 in. (Table 3.11).

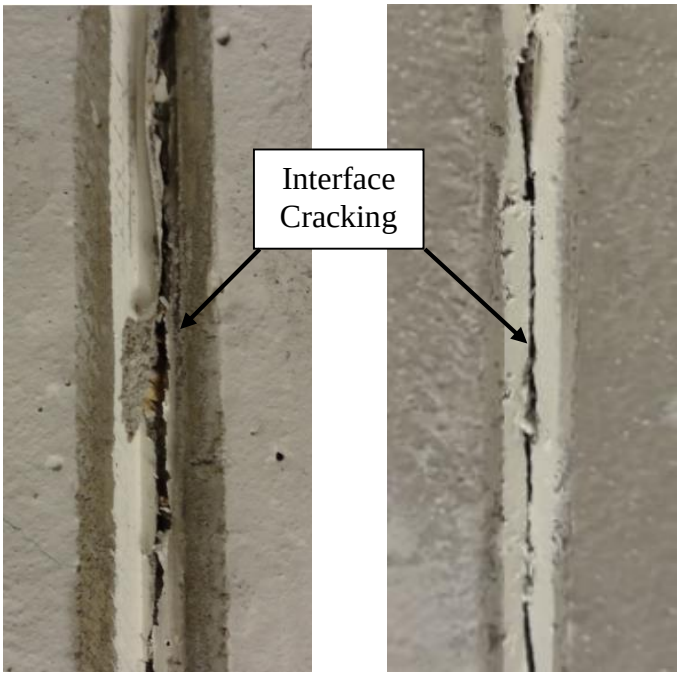

(a) (b)

Figure 3.23 Typical shear plane crack a) normalweight concrete monolithic interface, b) shale sand-lightweight concrete monolithic interface

Examples of interface cracking observed at peak load in specimens with the different cold joint interface conditions are shown in Figure 3.24. The dilation of the crack along the shear plane was larger for specimens with a roughened interface than for corresponding specimens with a smooth interface (Table 3.11), and the cracks along the shear plane of the roughened specimens appeared jagged when compared to smooth interface specimens at the conclusion of testing (Figure 3.24). For cold joint specimens, the cracking behaviors of specimens with lower reinforcement ratios (ρ = 0.009 and ρ = 0.013) differed from that of the specimens with higher reinforcement ratios (ρ = 0.017 and ρ = 0.022). As shown in Figure 3.24, most of the specimens with lower reinforcement ratios had clearly defined cracks along the shear plane with smaller flexural cracks horizontally across the front face of the specimen and small splitting cracks inside the cavity beneath the top flange. The flexural and splitting cracks are not associated with the shear failure, and the applied shear force, slip, strain, and dilation responses as well as the real-time plots from Wermager (2015) indicate that these specimens failed predominately due to shear along the intended shear plane, not flexure or splitting. Specimens with higher reinforcement ratios had more splitting and flexural

cracks that were significantly wider than those of the specimens with smaller reinforcement ratios, but most of these specimens failed in shear (Figure 3.25).

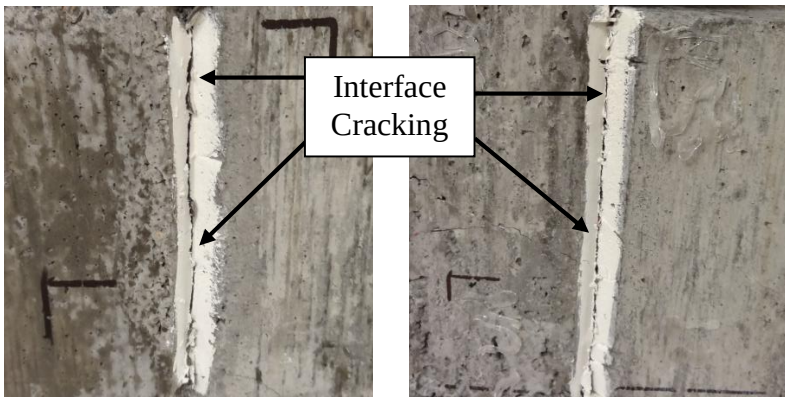

(a) (b)

Figure 3.24 Typical shear crack of a) specimens with a roughened interface, specimen S-CL-CJ-R-13-1 shown, and b) specimens with smooth interface, specimen S-SL-CJ-S-22-S shown

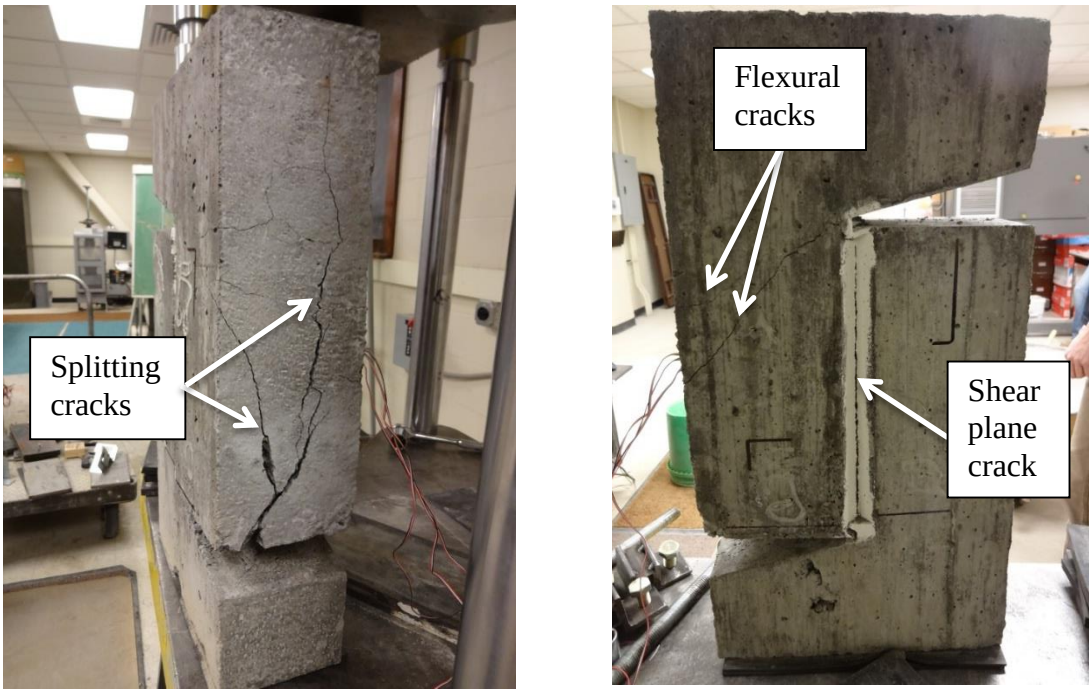

Figure 3.25 Typical cracking of cold joint specimens with higher reinforcement ratio that failed in shear along the shear plane; specimen S-SL-CJ-R-22-1 shown

Spalling of concrete cover occurred for some specimens, particularly those that failed due to concrete splitting. In some instances, this spalling caused detachment of the aluminum brackets that held the LVDTs.

Previous studies discuss diagonal tension cracks forming across the shear plane at angles between 15 to 50 degrees, and ranging from 1 to 3 in. long. The reinforcement ratio used in these studies ranged from ρ = 0.003 to ρ = 0.019 (Mattock and Hawkins 1972), or ρ = 0.000 to ρ = 0.026

(Mattock et al. 1976), or ρ = 0.004 to ρ = 0.015 (Kahn and Mitchell 2002). A vertical crack eventually formed along the shear plane that connected these diagonal cracks. This behavior was noted by Mattock and Hawkins (1972) as well as Mattock et al. (1976) for uncracked monolithic specimens. Kahn and Mitchell (2002) also described this behavior occurring for both uncracked monolithic and cold joint specimens. These diagonal tension cracks were not observed for any specimens in this study.

3.6.2. Applied Shear Force *V*-slip Relations

Applied shear force *V*-slip relations for the normalweight, sand-lightweight, and all-lightweight series specimens with a reinforcement ratio ρ=0.013 are shown in Figures 3.26 to 3.32. Monolithic interface specimens are presented in Section 3.6.2.1, and cold joint interface specimens are presented in Section 3.6.2.2.

In summary, the applied shear force versus slip relations in Figures 3.26 to 3.32 follow a general trend of an elastic region, then a softening behavior up to a peak in applied shear force, followed by a gentle decline in applied shear force until it levels off to a constant value in which slip continues to increase. The elastic region is approximately linear, and its slope appears to be unaffected by shear plane interface condition. The peak applied shear force, however, tends to be higher for specimens with a roughened interface as compared to specimens of similar aggregate type and reinforcement ratio having a smooth interface. The peak applied shear force occurred at levels of slip ranging from 0.004 in. to 0.021 in. (Comparison of the peak applied shear forces in terms of the test variables and values determined by the PCI Design Handbook and ACI 318 code shear friction design provisions is presented in Section 4.) After the peak shear force is achieved, the roughened specimens also have a steeper drop-off in applied shear force as compared to smooth specimens. This quasi-brittle behavior was also noted in Sneed and Shaw (2013). As a general trend, the roughened specimens had residual shear strengths similar to those of the specimens with a smooth interface, where residual shear strength is defined in this study as the shear force that corresponds to slip of 0.15 in.

3.6.2.1 Monolithic Interface Specimens

From Figure 3.26, it can be seen that the normalweight monolithic interface specimens exhibit roughly the same stiffness prior to the peak applied shear force. The peak applied shear force is not significantly affected by pre-cracking. After the peak shear force was achieved, the applied shear force reduced with increasing slip until a nearly constant value of applied shear force was reached for all specimens in a given series. The uncracked specimens behaved in a more quasi-brittle manner than the corresponding pre-cracked specimens, that is, after the peak shear force was achieved, the shear force decreased rapidly with increasing slip.

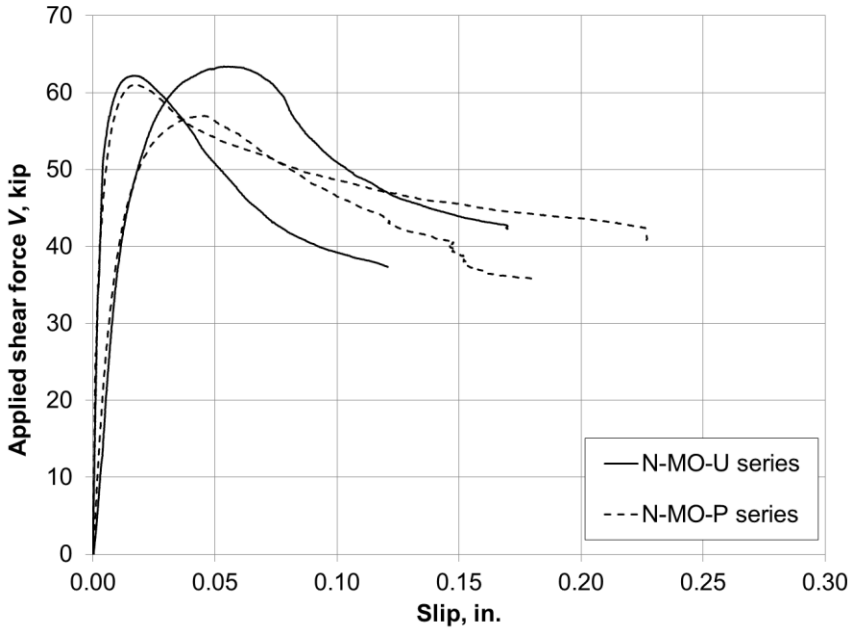

Figure 3.26 Applied shear force *V*-slip relations for normalweight concrete specimens with ρ=0.013 and monolithic interface

Figure 3.27 shows that the shale sand-lightweight concrete monolithic specimens with an uncracked or pre-cracked interface exhibited similar initial stiffness. The peak shear force was larger for the uncracked specimens (solid lines in the figure) than the pre-cracked specimens (dashed lines in the figure). Quasi-brittle, post-peak behavior was observed with uncracked specimens.

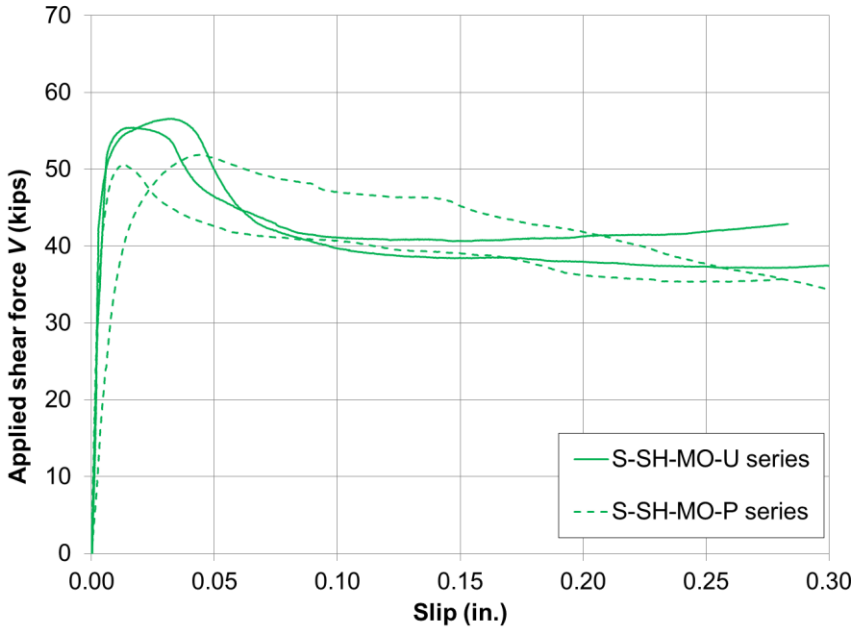

Figure 3.27 Applied shear force *V* slip relations for sand-lightweight concrete specimens with ρ=0.013 and monolithic interface

Figure 3.28 shows that the shale all-lightweight concrete monolithic specimens with an uncracked or pre-cracked interface had similar initial stiffness. The peak applied shear force did not appear to be influenced by pre-cracking of the specimens. However, the uncracked specimens (solid lines in the figure) exhibited more quasi-brittle, post-peak behavior compared to the pre-cracked specimens (dashed lines in the figure).

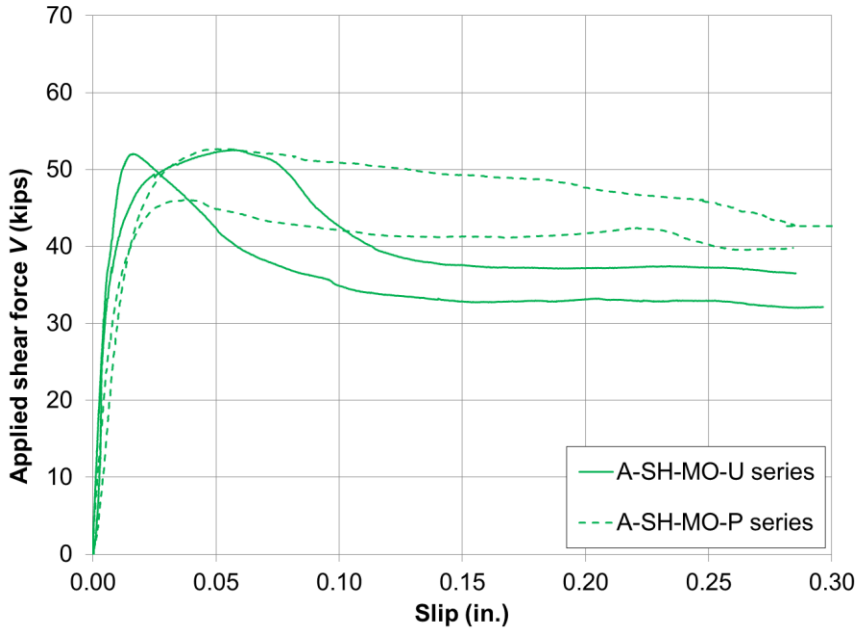

Figure 3.28 Applied shear force *V*-slip relations for all-lightweight concrete specimens with ρ =0.013 and monolithic interface

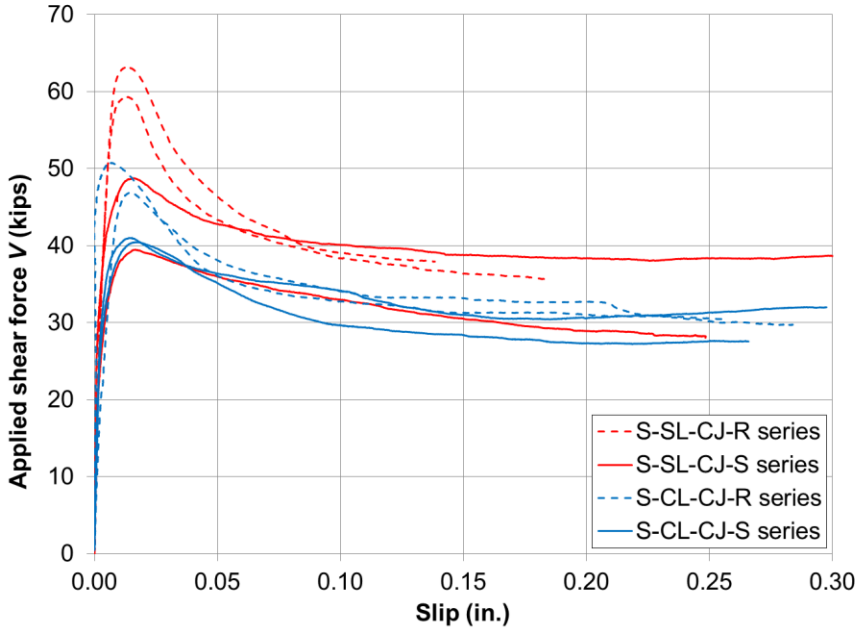

Figure 3.29 Applied shear force *V* slip relations for sand-lightweight concrete specimens with ρ=0.013 and cold joint interface

For the slate and clay sand-lightweight concrete cold joint interface specimens, Figure 3.29 shows that the initial stiffness of the smooth (solid lines in the figure) and roughened (dashed lines in the figure) interface specimens was similar. The peak values correspond to a slip of about 0.015 in. A significantly higher peak shear force is achieved with the roughened interface specimens compared to smooth interface specimens. Specimens with a roughened interface behaved in a more brittle manner than the corresponding smooth interface specimens in that applied load dropped off sharply after the peak load was achieved, although the residual shear force was similar to that of the corresponding specimens with a smooth interface.

3.6.2.2 Cold Joint Interface Specimens

The slate and clay all-lightweight concrete cold joint interface specimens shown in Fig. 3.30 also exhibited similar initial stiffness. The peak values correspond to a slip of 0.015 in. to 0.020 in. A larger peak shear force was observed in the specimens with a roughened interface (dashed lines in the figure) than the corresponding smooth interface specimens (solid lines in the figure). This higher peak shear force was accompanied by quasi-brittle, post-peak behavior. The residual shear force did not appear to be affected by the shear plane surface preparation.

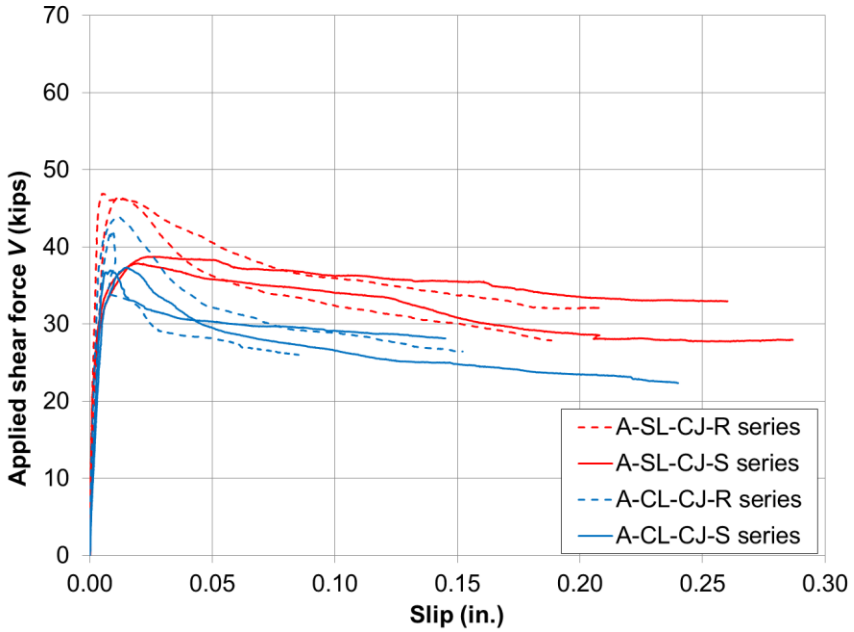

Figure 3.30 Applied shear force *V*-slip relations for all-lightweight concrete specimens with ρ =0.013 and cold joint interface

Figure 3.31 plots representative applied shear force *V*-slip relations for the slate sand-lightweight concrete specimens with varying reinforcement ratios ρ. As shown in Fig. 3.31, the slate sand-lightweight specimens with a roughened interface had larger peak shear force than corresponding specimens with a smooth interface and the same ρ, and specimens with higher reinforcement ratios achieved larger peak shear forces.

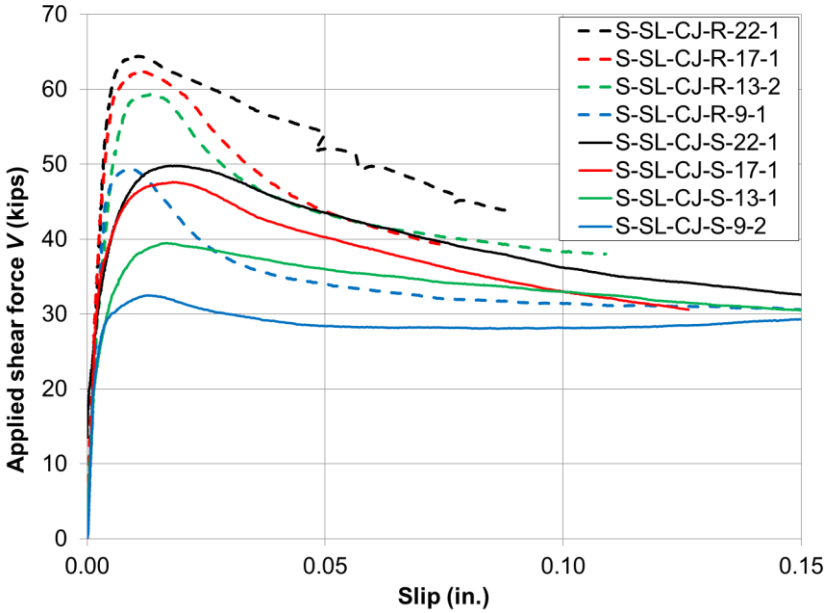

Figure 3.31 Applied shear force *V*-slip relations for representative sand-lightweight concrete specimens with expanded slate aggregate and a cold joint interface

The same trends were observed for the clay sand-lightweight specimens in Fig. 3.32, although the difference in shear force between corresponding roughened and smooth interface specimens is more pronounced for the slate aggregate specimens than the clay aggregate specimens. As a general trend, the slate sand-lightweight concrete specimens had a larger peak shear force than corresponding clay sand-lightweight specimens with similar interface condition and ρ with two exceptions (S-CL-CJ-S-13-2; S-CL-CJ-S-22-1).

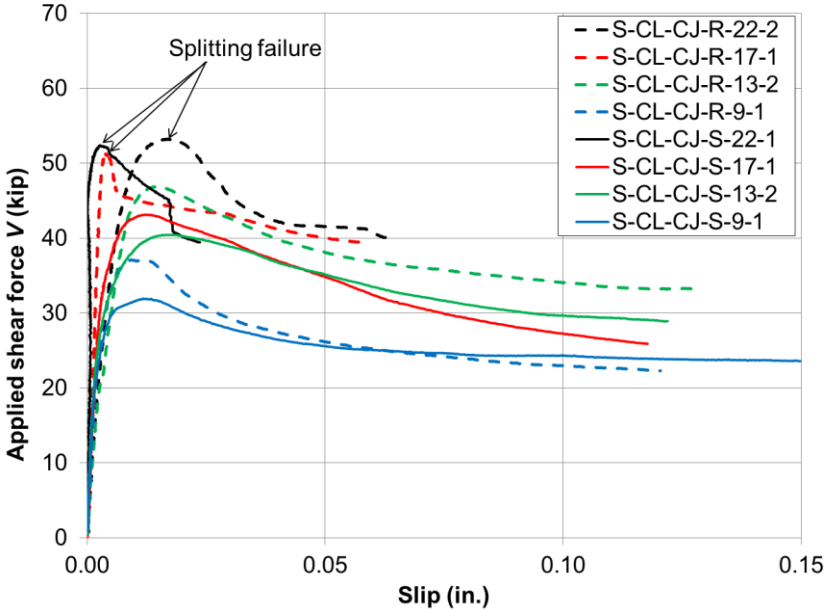

Figure 3.32 Applied shear force *V*-slip relations for representative sand-lightweight concrete specimens with expanded clay aggregate and a cold joint interface and

As mentioned in Section 3.6.1, six of the clay sand-lightweight specimens failed due to concrete splitting and loss of bond instead of shear failure along the intended shear plane. This behavior is observed in Figure 3.32, which shows a sharp drop-off in applied shear force after the peak shear force is achieved for specimens S-CL-CJ-R-17-1 and S-CL-CJ-S-22-1.

3.6.3. Interfacial Cracking Stress

The applied shear force versus interface steel strain plots for each specimen are presented in Appendix A. Each of the plots was generated using the data from one strain gage, even if all three gages from a specimen were in working order. This ensured that multiple yield plateaus were not exhibited on a single graph as would occur if all three stain gage readings had been averaged.

When the shear crack forms, the shear reinforcement engages, which can be detected from the strain measurements as a sudden increase in strain. This cracking is associated with a "plateau" on the applied shear stress v ($v=V/A_{cr}$) versus interface reinforcement strain plot. A typical example of this response is shown in Figure 3.33.

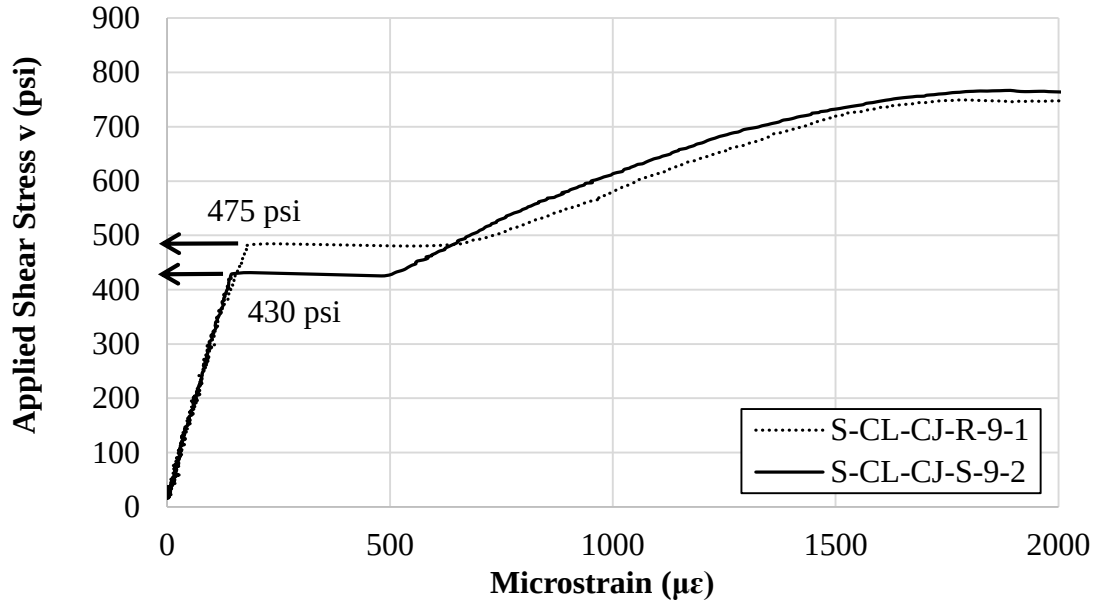

Figure 3.33 Typical shear stress-interface reinforcement strain plots for the determination of interface cracking stress (Specimens S-CL-CJ-R-9-1 and S-CL-CJ-S-9-2 shown)

Values of shear stress associated with the interfacial crack formation v_{cr} for all monolithic uncracked, roughened, and smooth interface specimens are summarized Table 3.12. The monolithic pre-cracked specimens are not included in this table because the crack was initiated prior to testing. The values of v_{cr} in Table 3.12 are the average determined from each of the shear force – strain relations for all properly functioning strain gages of the corresponding specimens. Values are reported to the nearest 25 psi. Average values of v_{cr} for each series are reported as $v_{cr,avg}$. It should be noted that the values for series N-MO-U in Table 3.12 are not the averaged values because cracking was not detected by the strain readings in specimen N-MO-U-13-1.

Table 3.12 Summary of Interface Cracking Stresses v_{cr} Determined From Strain Measurements

Specimen ID	Interface Condition	ρ	v_{cr} (psi)	$v_{cr,avg}$ (psi)	STD $v_{cr,avg}$ (psi)	Ratio Roughened / Smooth
N-MO-U-13-1	Uncracked	0.013	ND[1]	700	N/A	N/A
N-MO-U-13-2	Uncracked	0.013	700			
S-SH-MO-U-13-1	Uncracked	0.013	625	538	87.5	N/A
S-SH-MO-U-13-2	Uncracked	0.013	450			
A-SH-MO-U-13-1	Uncracked	0.013	750	525	225	N/A
A-SH-MO-U-13-2	Uncracked	0.013	300			
S-SL-CJ-R-9-1	Roughened	0.009	625	650	25	2.08
S-SL-CJ-R-9-2	Roughened	0.009	675			
S-SL-CJ-S-9-1	Smooth	0.009	275	313	38	
S-SL-CJ-S-9-2	Smooth	0.009	350			
S-SL-CJ-R-13-1	Roughened	0.013	625	625	0	2.08
S-SL-CJ-R-13-2	Roughened	0.013	625			
S-SL-CJ-S-13-1	Smooth	0.013	300	300	0	
S-SL-CJ-S-13-2	Smooth	0.013	300			
S-SL-CJ-R-17-1	Roughened	0.017	625	688	63	2.04
S-SL-CJ-R-17-2	Roughened	0.017	750			
S-SL-CJ-S-17-1	Smooth	0.017	375	338	38	
S-SL-CJ-S-17-2	Smooth	0.017	300			
S-SL-CJ-R-22-1	Roughened	0.022	625	563	63	1.45
S-SL-CJ-R-22-2	Roughened	0.022	500			
S-SL-CJ-S-22-1	Smooth	0.022	400	388	13	
S-SL-CJ-S-22-2	Smooth	0.022	375			
A-SL-CJ-R-13-1	Roughened	0.013	550	550	0	1.91
A-SL-CJ-R-13-2	Roughened	0.013	550			
A-SL-CJ-S-13-1	Smooth	0.013	300	288	13	
A-SL-CJ-S-13-2	Smooth	0.013	275			
S-CL-CJ-R-9-1	Roughened	0.009	475	500	25	1.29
S-CL-CJ-R-9-2	Roughened	0.009	525			
S-CL-CJ-S-9-1	Smooth	0.009	350	388	38	
S-CL-CJ-S-9-2	Smooth	0.009	425			
S-CL-CJ-R-13-1	Roughened	0.013	525	500	25	1.60
S-CL-CJ-R-13-2	Roughened	0.013	475			
S-CL-CJ-S-13-1	Smooth	0.013	325	313	13	
S-CL-CJ-S-13-2	Smooth	0.013	300			
S-CL-CJ-R-17-1	Roughened	0.017	650	650[2]	0[2]	1.73
S-CL-CJ-R-17-2	Roughened	0.017	650			
S-CL-CJ-S-17-1	Smooth	0.017	350	375	25	
S-CL-CJ-S-17-2	Smooth	0.017	400			
S-CL-CJ-R-22-1	Roughened	0.022	800	713[2]	88[2]	1.14
S-CL-CJ-R-22-2	Roughened	0.022	625			
S-CL-CJ-S-22-1	Smooth	0.022	575	625[2]	50[2]	
S-CL-CJ-S-22-2	Smooth	0.022	675			
A-CL-CJ-R-13-1	Roughened	0.013	550	538	13	1.10
A-CL-CJ-R-13-2	Roughened	0.013	525			
A-CL-CJ-S-13-1	Smooth	0.013	475	488	13	
A-CL-CJ-S-13-2	Smooth	0.013	500			

[1]ND denotes no data - cracking was not detected from strain measurements

[2]Specimens in this series failed predominantly due to concrete splitting

Considering the specimens that failed in shear, values of v_{cr} for specimens with a monolithic uncracked interface were between 300 psi and 750 psi, with larger values for normalweight concrete than those with sand-lightweight and all-lightweight concrete. Values of v_{cr} for specimens with a roughened interface condition were between 475 psi and 750 psi. Values of v_{cr} for specimens with a smooth interface condition were between 275 psi and 425 psi.

Figure 3.34 shows the average value of interface cracking stress $v_{cr,avg}$ and standard deviation for each series with ρ = 0.013. Series with a monolithic or roughened interface condition had similar values of $v_{cr,avg}$. As expected, series with a smooth interface condition had the lowest values of $v_{cr,avg}$. No trends are apparent with respect to lightweight aggregate material.

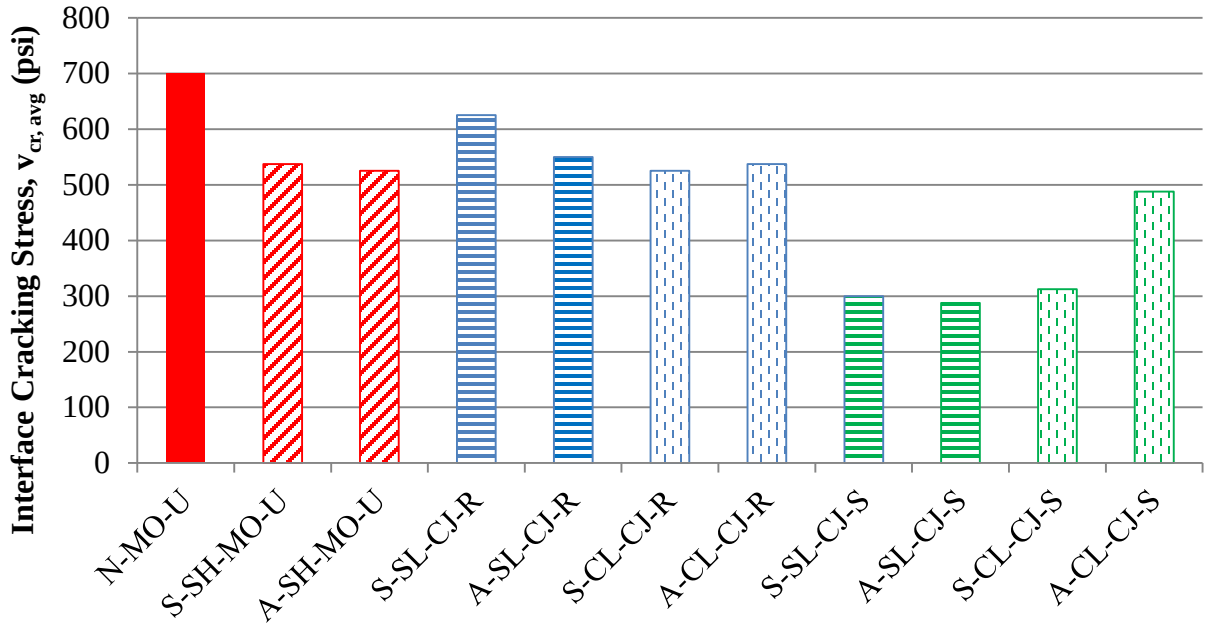

Figure 3.34 Average value of stress associated with interface cracking $v_{cr,avg}$ determined from strain measurements for specimens with ρ = 0.013

Figure 3.35 shows the values of $v_{cr,avg}$ for the sand-lightweight cold joint specimens with varying reinforcement ratios. Figure 3.35 shows these values averaged for each series $v_{cr,avg}$, including those specimens that failed due to splitting. Each series shown in Figure 3.35 has higher $v_{cr,avg}$ values for roughened interface specimens versus smooth interface specimens of the same aggregate type and reinforcement ratio.

It is worth noting in Figure 3.35 that the specimens with concrete splitting failures had some of the highest values of average interface cracking stresses v_{cr}. Since these values represent cracking of the interface rather than cracking in other areas of the specimen, it is possible that the first cracks to form on these specimens were splitting cracks, rather than interfacial shear cracks. Because of the redistribution of stress that occurs after splitting, it is possible that the interfacial shear cracks formed on the intended shear plane at higher levels of applied shear force than would normally occur if the specimen were free of splitting cracks.

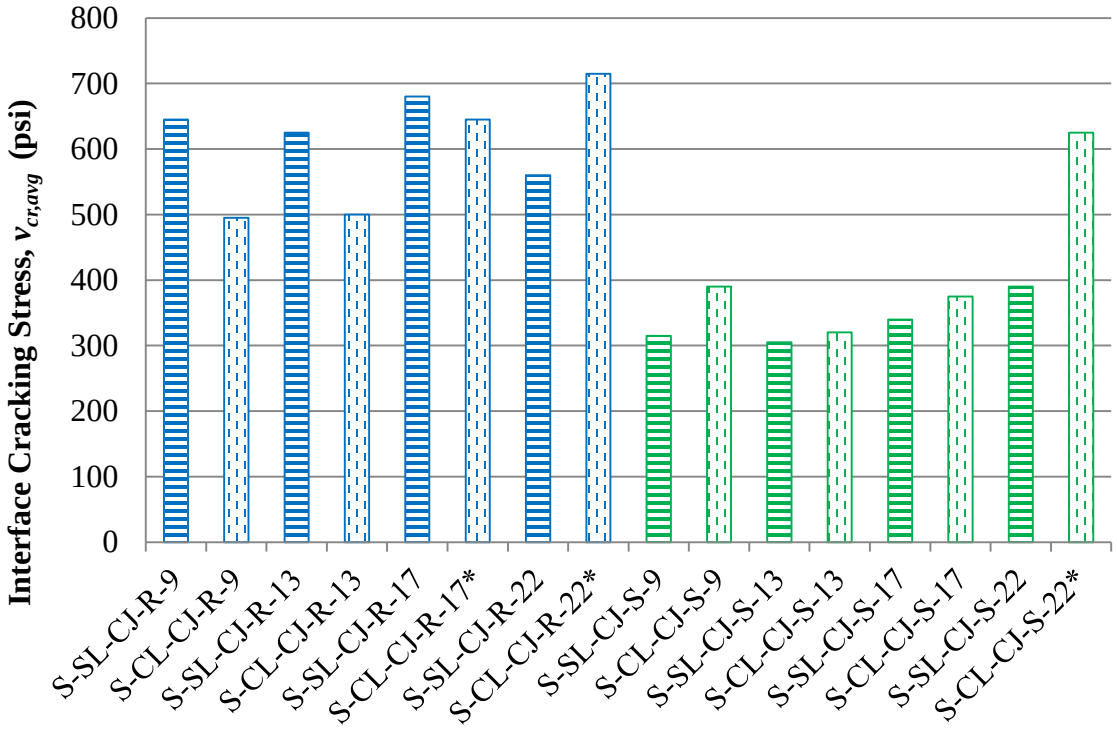

*Specimens in this series failed predominantly due to concrete splitting

Figure 3.35 Average interface cracking stress, $v_{cr,avg}$ for all sand-lightweight concrete series with varying reinforcement ratio

3.6.4. Summary of Test Results

Table 3.11 summarizes key values from the experiments. The Specimen ID follows the naming convention that is shown in Section 3.2. The compressive strength f'_c at test day has been rounded to the nearest 10 psi. Other data presented in the table include the peak (ultimate) applied shear force V_u, peak applied shear stress v_u ($v_u=V_u/A_{cr}$), slip at V_u, dilation at V_u, residual force V_{ur}, and residual stress v_{ur} ($v_{ur}=V_{ur}/A_{cr}$). The residual force V_{ur} corresponds to the strength of the joint after a complete fracture (Mattock et al. 1976; Kahn and Mitchell 2002) and is defined in this study as the load corresponding to a slip of 0.15 in. For the calculation of stresses v_u and v_{ur} the area used was the cross-sectional area of the shear plane equal to 49.5 in^2. Average values of stresses v_u and v_{ur}, for each series are shown as $v_{u,avg}$ and $v_{ur,avg}$, respectively. Finally, the average values for peak-to-residual shear stress ratio (v_u/v_{ur}) are also presented in Table 3.11 for each series. Values of ND listed in Table 3.11 indicate that the specimen reached 60% of its ultimate shear strength (post-peak) before reaching the slip of 0.15 that is used to define the residual shear strength, v_{ur}. However, these values can be estimated from the applied shear force versus slip plots.

4. ANALYSIS AND DISCUSSION

4.1. INTRODUCTION

This section analyzes and discusses results of the experiments conducted in both the first and second phases this study. Results from the first phase of this study are presented in Sneed and Shaw (2013) with a summary in Shaw and Sneed (2014), and results from the second phase are presented in Section 3.6.

In the sections that follow, the influence of the test variables is examined in terms of peak shear strength and residual shear strength in Section 4.2. In Section 4.3, results are compared to the current editions of the PCI Design Handbook (2010) and the ACI 318 code (2014). Concluding remarks from the analysis in this section are summarized in Section 4.4.

4.2. ANALYSIS OF TEST VARIABLES

This section analyzes the experimental results from this study to determine the influence of the test variables included in this study. The studied test variables include concrete type, lightweight aggregate material, shear interface preparation, and reinforcement ratio.

4.2.1. Concrete Type

In this study, three types of concrete were used (normalweight, sand-lightweight, and all-lightweight concrete) where each type was designated by its aggregate composition. The unit weight (measured on fresh concrete) ranged from 88 lb/ft^3 for all-lightweight concrete to 148 lb/ft^3 for normalweight concrete (see Table 3.7). In this section, the shear transfer strength specimens with a constant reinforcement ratio, ρ=0.013, and different concrete types is analyzed in terms of unit weight. Monolithic interface specimens and cold joint interface specimens are compared separately.

Figures 4.1 and 4.2 plot the peak (ultimate) shear stress v_u and residual shear stress v_{ur} versus concrete unit weight for specimens with a monolithic interface condition and reinforcement ratio ρ=0.013. Figure 4.1 shows the relation of the peak (ultimate) shear stress v_u versus concrete unit weight. Trendlines are plotted in the graph for the uncracked and pre-cracked specimens, maintaining the distinction between the different interface conditions. The trends show that for specimens with a monolithic interface, the peak shear stress increases with increasing unit weight. This is true for both uncracked and pre-cracked specimens. The slopes of the trendlines are similar suggesting that the increase in peak shear stress with increasing concrete unit weight is similar with or without a pre-existing crack. It should be noted, however, that the normalweight concrete specimens had a larger maximum aggregate size (3/4 in.) than the sand-lightweight and all-lightweight concrete specimens (3/8 in.).

Figure 4.2 plots the residual shear stress v_{ur} versus concrete unit weight. The residual shear stress values have slightly greater deviation between the specimens of each series compared to the peak shear stress values from Figure 4.1. The slopes of the trendlines suggest increasing residual shear stress with increasing concrete unit weight.

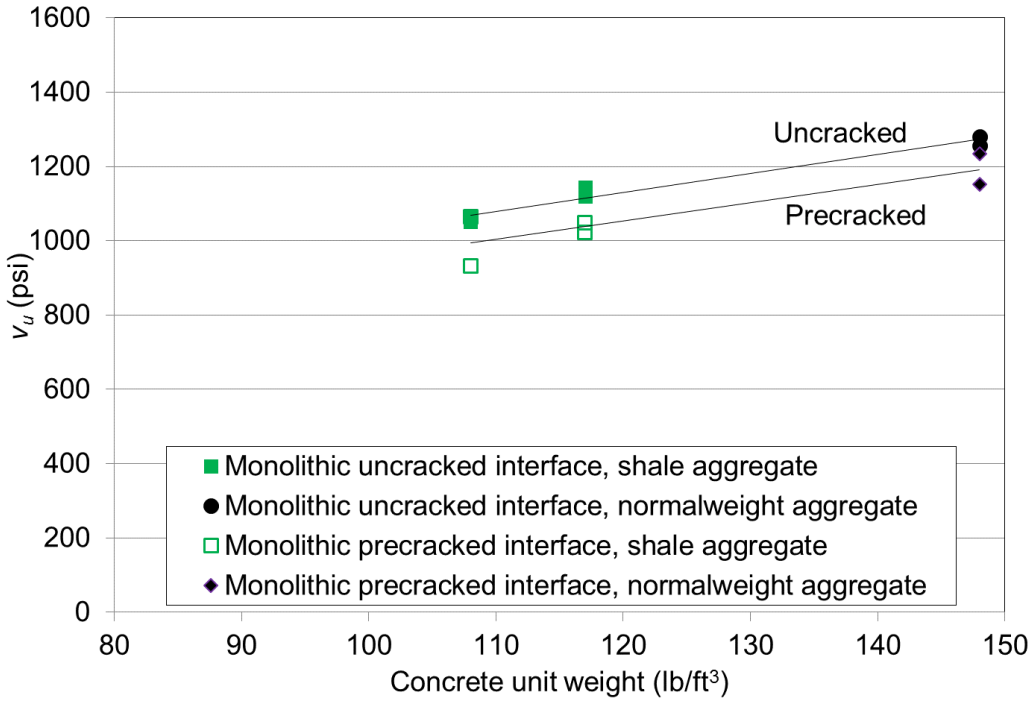

Figure 4.1 Peak shear stress v_u vs. concrete unit weight for monolithic interface specimens with ρ=0.013

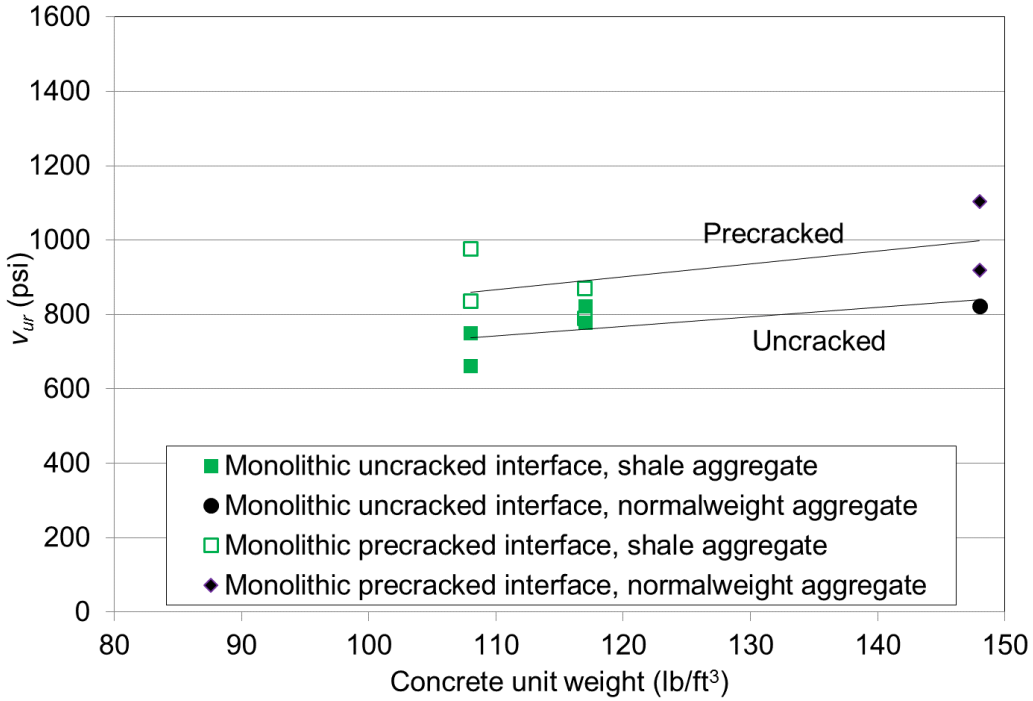

Figure 4.2 Residual shear stress v_{ur} vs. concrete unit weight for monolithic interface specimens with ρ=0.013

Figures 4.3 and 4.4 compare the peak shear stress v_u and residual shear stress v_{ur} to concrete unit weight for the cold joint interface specimens in this study with ρ=0.013. The data are supplemented with data from the N-5, S-5, and A-5 series from the first phase of this study reported by Sneed and Shaw (2013), which had a reinforcement ratio ρ =0.013 and the same nominal compressive strength as those in this phase of the study (f'_c≈5000 psi). Figure 4.3 plots the peak shear stress v_u versus concrete unit weight for the cold joint specimens, along with trendlines, maintaining the distinction between roughened and smooth interface specimens. For specimens with a roughened interface condition, the trendlines show that the peak shear stress increases with increasing unit weight. For specimens with a smooth interface condition, trendlines have a slightly negative slope. It should be noted that values of shear strength are not normalized, and the compressive (and tensile) strength of the different concretes has some slight variations, which may explain the negative slope. In general, the trendlines for the specimens with a smooth cold joint interface condition show that specimens with the same concrete compressive strength had nearly the same peak shear stress v_u (approximately 800 psi) irrespective of concrete unit weight (concrete type) and lightweight aggregate material. This suggests that aggregate material does not play a role in the shear-transfer strength across a smooth interface, where the shear transfer may be attributed to cohesion and dowel action of the reinforcement. These results are supported by those from Sneed and Shaw (2013), which showed that the shear transfer strength across a smooth interface was not influenced by concrete unit weight. However, Sneed and Shaw (2013) also showed that shear strength increases with increasing concrete strength, where a higher compressive strength is associated with a higher cementitious materials content resulting in increased cohesion. Figure 4.3 also shows that the difference in peak shear stress values between roughened and smooth interface specimens tends to decrease with decreasing unit weight. It is possible that roughened interface specimens with a lower unit weight were more likely to shear off across the grooves in the intentional roughness than those with a higher unit weight.

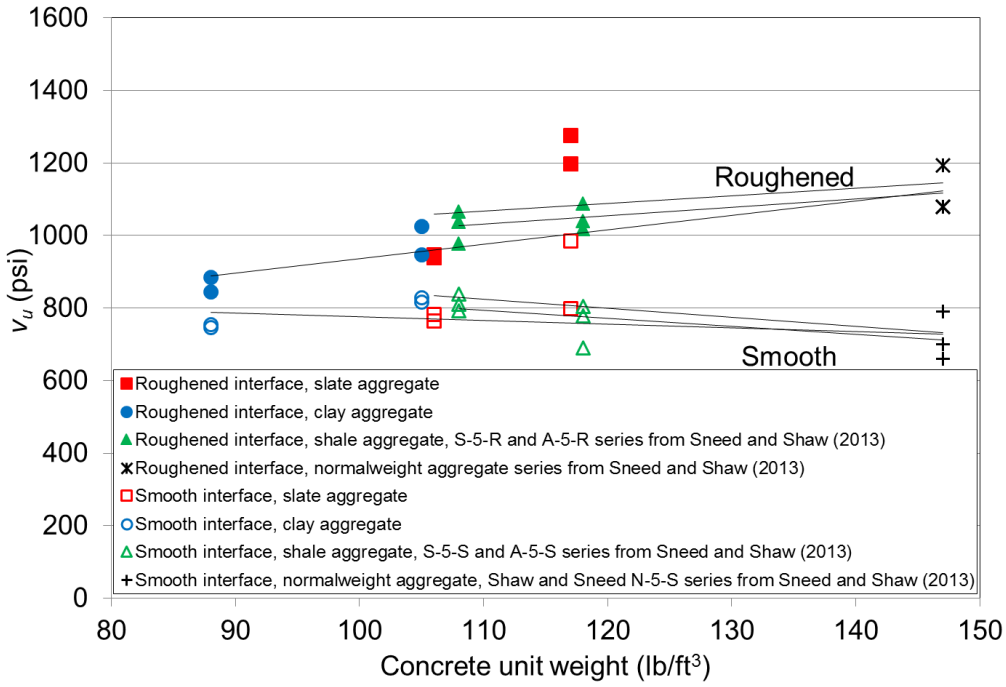

Figure 4.3 Peak shear stress v_u vs. concrete unit weight for cold joint specimens with ρ=0.013

Figure 4.4 plots the residual shear stress v_{ur} versus unit weight of concrete. The trendlines suggest a slight increase in residual shear strength with increasing concrete unit weight.

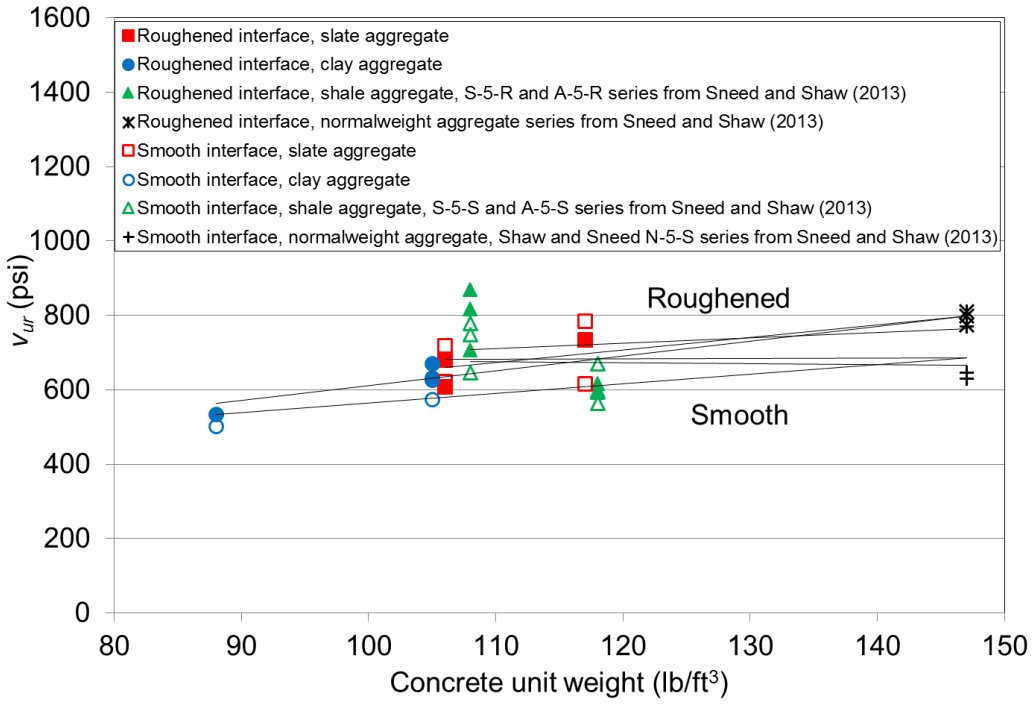

Figure 4.4 Residual shear stress v_{ur} vs. concrete unit weight for cold joint specimens with ρ=0.013

4.2.2. Lightweight Aggregate Material

Three lightweight aggregate materials (expanded shale, expanded slate, and expanded clay) were included in this study. This section examines the effect of lightweight aggregate material on the shear transfer strength of specimens with a cold joint interface. (Lightweight aggregate material was not varied for specimens with a monolithic interface condition, so the monolithic interface condition is not included in this section.)

In Figure 4.3, the peak shear stress v_u is plotted versus concrete unit weight for the specimens with ρ =0.013 and a cold joint interface. Distinction is maintained between specimens with different interface conditions and different lightweight aggregates. The concrete compressive strength for each series is nominally the same (f'_c≈5000 psi). The data are supplemented with data from the N-5, S-5, and A-5 series from the first phase of this study reported by Sneed and Shaw (2013), which had a reinforcement ratio ρ =0.013, expanded shale lightweight aggregates from the same producer, and the same nominal compressive strength of concrete as the specimens in the present study. Trendlines are also plotted for each lightweight aggregate material and including data for the normalweight concrete specimens from the N-5 series by Sneed and Shaw (2013).

For the roughened interface condition, the trendlines in Figure 4.3 show an increase in the shear strength with increasing unit weight for concretes with each lightweight aggregate material. In

general, shear strength values for the expanded clay aggregate specimens were slightly lower than those of specimens with expanded shale and expanded slate.

For the smooth interface condition, the trendlines have a slightly negative slope. As noted in Section 4.2.1, the values of shear strength are not normalized, and the compressive (and tensile) strength of the different concretes has some slight variations, which may explain the negative slope. In general, the trendlines for the specimens with a smooth cold joint interface condition show that specimens with the same concrete compressive strength had nearly the same peak shear stress v_u (approximately 800 psi) irrespective of concrete unit weight (concrete type) and lightweight aggregate material. This suggests that aggregate material does not play a role in the shear-transfer strength across a smooth interface, where the shear transfer may be attributed to cohesion and dowel action of the reinforcement.

4.2.3. Shear Interface Preparation

Specimens used to evaluate the influence of shear interface preparation include those with a monolithic and non-monolithic (cold joint) interface.

4.2.3.1 Monolithic Interface

Specimens with a monolithic interface were either uncracked or pre-cracked prior to testing. To examine the influence of interface preparation, specimens with the same reinforcement ratio (ρ = 0.013), same concrete type (unit weight), and same lightweight aggregate material are compared. The concrete compressive strength for each series is nominally the same ($f'_c \approx 5000$ psi). Figure 4.1 shows that the average values of peak shear stress v_u for specimens with a monolithic uncracked interface are slightly larger than those with a monolithic pre-cracked interface for the same concrete compressive strength, lightweight aggregate material, and unit weight, which suggests that the pre-cracking of the interface has a slight influence on the peak shear stress. On the other hand, Figure 4.2 shows that the average values of residual shear stress v_{ur} for specimens with a pre-cracked interface are slightly larger than those with an uncracked interface for the same concrete compressive strength, lightweight aggregate material, and unit weight.

Table 4.1 summarizes and compares the average peak shear stress $v_{u,avg}$ and average residual shear stress $v_{ur,avg}$ for the monolithic uncracked and pre-cracked specimen series in this study. Values of $v_{u,avg}$ for the uncracked specimens were 1.06 to 1.09 times those of the corresponding pre-cracked specimens. Values $v_{ur,avg}$ for the uncracked specimens were 0.78 to 0.97 times those of the corresponding pre-cracked specimens.

Table 4.1 Effect of Monolithic Interface Preparation on the Peak Shear Stress and Residual Shear Stress for Specimens with ρ = 0.013

Specimen Series	Average Peak Shear Stress $v_{u,avg}$ (psi)			Average Residual Shear Stress $v_{ur,avg}$ (psi)		
	Interface Preparation		Ratio Uncracked / Pre-cracked	Interface Preparation		Ratio Uncracked / Pre-cracked
	Pre-cracked	Uncracked		Pre-cracked	Uncracked	
N-MO-XX-13	1192	1269	1.06	1011	823	0.81
S-SH-MO-XX-13	1035	1132	1.09	830	801	0.97
A-SH-MO-XX-13	998	1056	1.06	906	707	0.78

It is possible that the procedure used to pre-crack the monolithic specimens induces some residual effects that may influence the results. As noted in Section 3.5.4, different researchers have used different methods to induce a crack in monolithic specimen. For example, Figure 4.5 shows a schematic of one such method that involves applying a line load (this method was used in this study). This method induces force components parallel and perpendicular to the shear plane. The residual effects of this procedure have not been studied.

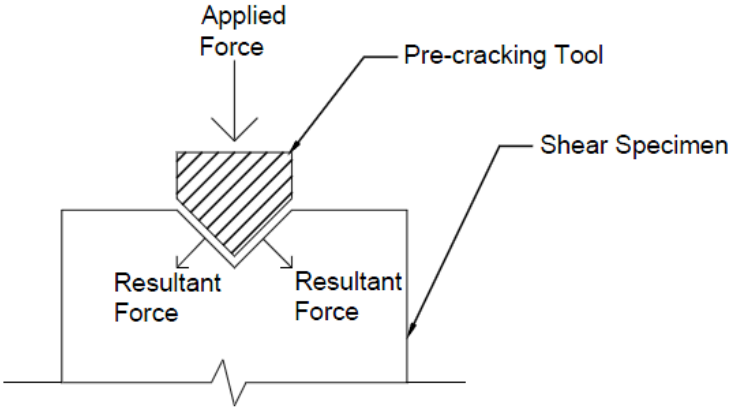

Figure 4.5 Applying a line load during pre-cracking

4.2.3.2 Cold Joint Interface

Specimens with a cold joint interface were either troweled smooth or roughened to average amplitude of 1/4 in. To examine the influence of the interface preparation, specimens constructed using the same concrete type (unit weight), same lightweight aggregate material, and same reinforcement ratio (ρ = 0.013) are compared. The concrete compressive strength for each series is nominally the same ($f'_c \approx 5000$ psi).

As expected, Figure 4.3 shows that the average values of v_u for specimens with a roughened interface are larger than those with a smooth interface for the same concrete compressive strength, lightweight aggregate material, and unit weight. The increase in shear strength for specimens with a roughened interface is attributed to increased surface interaction resulting from the irregular profile and the separation (dilation) that must be achieved to overcome the interlock of the shear interface.

Table 4.2 compares the average peak shear stress for the cold joint interface specimens studied in this project. The data are supplemented with data from the S-5 and A-5 series from the first phase of this study reported by Sneed and Shaw (2013), which had a reinforcement ratio ρ =0.013, expanded shale lightweight aggregates, and the same nominal compressive strength of concrete as the specimens in the present study. In all cases, specimens with roughened interface achieved a higher peak shear force than the specimens with smooth interface. This phenomenon can be explained on basis of aggregate interlock. The specimens with smooth interface rely solely on cohesion and dowel action before cracking along the shear plane and reaching their peak applied shear force. For the smooth specimens there is no contribution from interlocking of one roughened interface with the other. Once the initial crack has been formed, the smoothness of the interface allows for easier relative motion of the planes. Values of $v_{u,avg}$ for the roughened interface specimens were 1.15 to 1.48 times those of the corresponding smooth interface specimens.

Table 4.2 Effect of Cold Joint Interface Preparation on the Peak Shear Stress and Residual Shear Stress for Specimens with $\rho = 0.013$

Specimen Series	Average Peak Shear Stress $v_{u,avg}$ (psi)			Average Residual Shear Stress $v_{ur,avg}$ (psi)		
	Interface Preparation		Ratio Roughened / Smooth	Interface Preparation		Ratio Roughened / Smooth
	Smooth	Roughened		Smooth	Roughened	
S-SL-CJ-XX-13	891	1238	1.39	700	735	1.05
A-SL-CJ-XX-13	774	944	1.22	671	645	0.96
S-CL-CJ-XX-13	822	986	1.20	600	651	1.09
A-CL-CJ-XX-13	750	865	1.15	501	534	1.07
S-5[1]	757	1117	1.48	610	603	0.99
A-5[1]	813	1030	1.27	727	800	1.10

[1]Specimens from Sneed and Shaw (2013)

From the cracking stress values v_{cr} in Table 3.12 it can also be seen that in general, the cracking stress is lower for smooth interface specimens than corresponding roughened interface specimens. It should also be noted that the smooth specimens have smaller interface surface area compared to the roughened interface specimens, where the 1/4 in. grooves used to roughen the surface add to the surface area. This increase in area increases the area over which cohesion is acting, and therefore increases the cracking stress.

Figure 4.4 and Table 4.2 show that the residual shear stress for the sand-lightweight and all-lightweight concrete specimens is roughly the same regardless of the interface preparation (i.e., ratios are close to 1.0). Therefore the interface preparation does not appear to influence the residual shear stress of specimens with a cold joint interface.

4.2.4. Reinforcement Ratio

Within this study, four reinforcement ratios ρ were tested (0.009, 0.013, 0.017, and 0.022) in two series of sand-lightweight concrete specimens with a cold joint interface condition (series S-SL-CJ and S-CL-CJ). These reinforcement ratios correspond to the use of 2, 3, 4, or 5 double-legged No. 3 stirrups across the shear plane, which had an area of $A_{cr} = 49.5$ in^2. This section summarizes the effect of varied reinforcement ratios on shear transfer strength of the specimens in this study. To isolate this parameter, specimens with the same aggregate materials and interface condition were compared. The concrete compressive strength for each series is nominally the same ($f'_c \approx 5000$ psi).

The peak shear stress v_u of the sand-lightweight concrete specimens in this study with different reinforcement ratios are plotted versus ρf_y in Figure 4.6. The data are supplemented with the S-5 series from the first phase of this study by Sneed and Shaw (2013) with the same expanded shale aggregate and nominal compressive strength of concrete as the specimens in the present study. Distinction is maintained between different lightweight aggregates and interface condition.

Specimens that failed in splitting are identified in the figure. For each smooth interface series plotted, Figure 4.5 shows an increase in shear strength with increasing ρf_y. For the roughened interface specimens in Figure 4.5, there is also an increase in shear strength with increasing ρf_y, yet the shear strength values level off at high values of ρf_y (after approximately 1200 psi). As mentioned previously, all four clay aggregate sand-lightweight specimens with ρ=0.022, as well as the two clay sand-lightweight roughened specimens with ρ=0.017, failed due to splitting rather than shear. For the specimens with slate aggregate and a roughened interface, Fig. 4.6 also shows that the shear strength values tend to level off at the largest values of ρf_y. Again, these specimens exhibited some small flexure and splitting cracks, but the main mechanism of failure was shear along the shear plane. This figure also shows the recurring trend of the series with a roughened interface condition (solid markers in the figure) having larger values of shear strength v_u than corresponding specimens with a smooth interface condition (hollow markers in the figure).

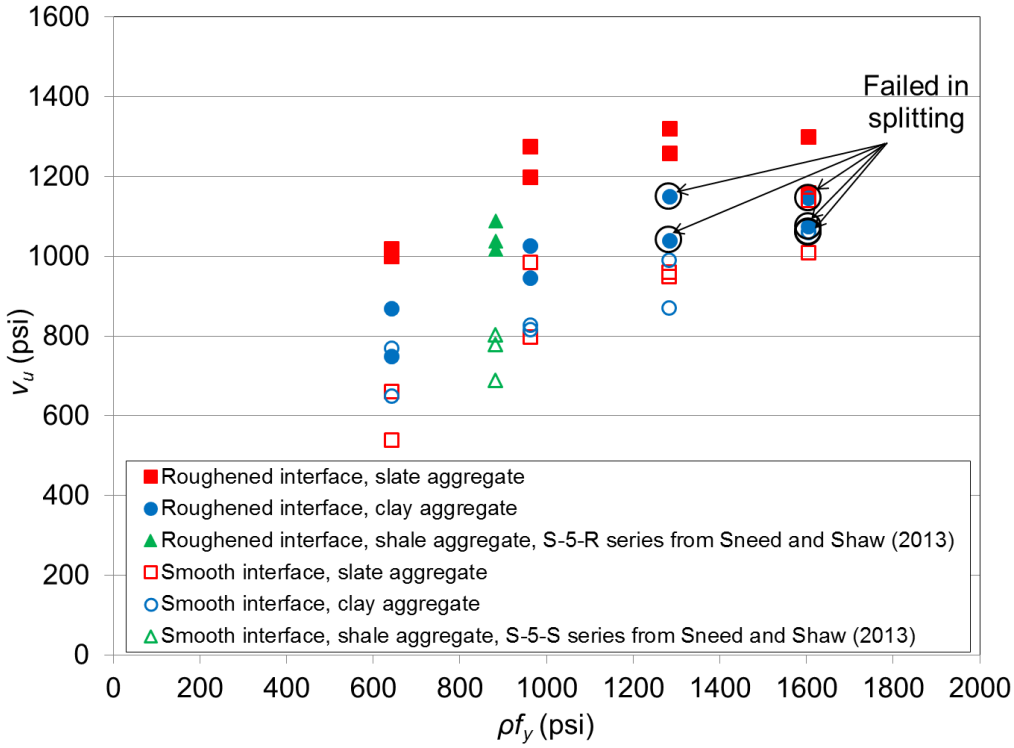

Figure 4.6 Comparison of shear strength v_u versus ρf_y for sand-lightweight concrete specimens with different interface conditions

Residual shear stress v_{ur} is analyzed in Figure 4.7 in a similar manner. Residual shear stress is defined in this study as the stress corresponding to a slip of 0.15 in. Figure 4.7 shows a plot of the residual shear stress v_{ur} versus reinforcement ratio, along with associated trendlines.

As previously discussed, all specimens in this program were tested under displacement control until one of the following conditions occurred: a target slip of 0.3 in. was reached, or the applied load dropped to 60% of the peak capacity. In several instances, the applied load dropped to 60% of the peak capacity before the slip reached 0.15 in. This occurred for the following specimens: S-CL-CJ-R-9-1, S-CL-CJ-R-9-2, S-CL-CJ-S-17-1, S-SL-CJ-R-9-2, S-SL-CJ-R-13-1, S-SL-CJ-R-17-1, S-SL-CJ-R-17-2, and S-SL-CJ-S-17-1. For these eight specimens, the residual shear stress

was estimated as the applied shear stress at the last recorded value of slip, which happened to lie between 0.10 in. and 0.14 in. This was considered to be a valid range of slip for recording v_{ur} because it represents the initiation of the plateau in which applied shear stress remains constant as slip continues to increase. For two specimens, S-CL-CJ-R-22-1 and S-SL-CJ-R-22-2, the residual shear stress was not recorded due to the low levels of final recorded slip (0.08 in. or less). Thus, values of v_{ur} for these specimens are not shown in Figure 4.7. The trendlines in Figure 4.7 indicate that overall, an increase in residual shear strength is associated with an increase in reinforcement ratio.

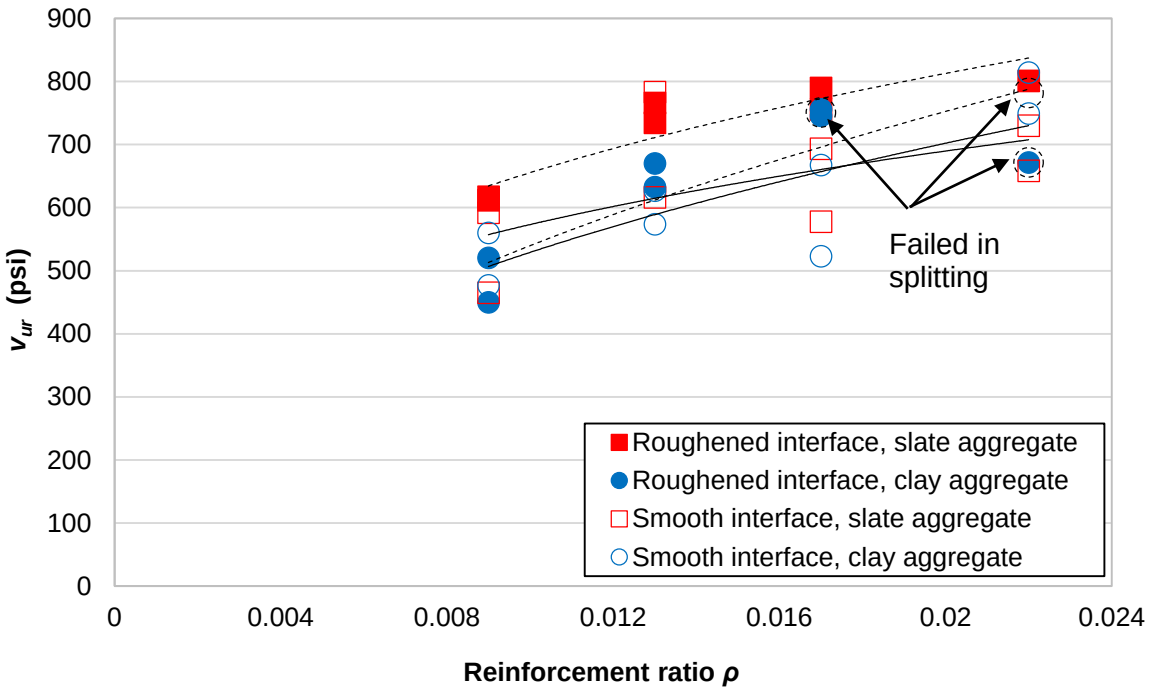

Figure 4.7 Residual shear strength v_{ur} versus reinforcement ratio ρ for each series

4.3. COMPARISON TO DESIGN PROVISIONS

This section assesses how well the results of this study correlate to current shear-friction design provisions. Section 4.4.1 summarizes the equations and limits used for this analysis from the current editions of the PCI Design Handbook (2010) and the ACI 318 code (2014). Section 4.4.2 compares the test results to design provisions in terms of the effective coefficient of friction μ_e. In Section 4.4.3, results of the specimens in this study are compared to design provisions in terms of nominal shear strength V_n (or $v_n = V_n/A_{cr}$).

4.3.1. Shear-friction Design Provisions

This section describes the equations and limits used in the comparison of test results to current editions of the PCI Design Handbook (2010) and the ACI 318 code (2014). The shear-friction provisions of these codes/specifications are thoroughly described in Section 2.3. Tables 4.3 through 4.5 summarize the code/specification limits for V_u (or V_n), as well as recommended values for μ, μ_e, and λ.

Table 4.3 Limits for Applied Shear of Shear-friction Elements

Case	PCI Design Handbook (2010) Max $V_u = \phi V_n$	ACI 318-14 Max $V_n = V_u/\phi$	
		NWC	Other
1	$0.30\lambda f'_c A_{cr} \leq 1000\lambda A_{cr}$	$0.2f'_c A_c$ <$(480+0.08f'_c)A_c$ < $1600A_c$	$0.2f'_c A_c$ <$800A_c$
2	$0.25\lambda f'_c A_{cr} \leq 1000\lambda A_{cr}$		
3	$0.20\lambda f'_c A_{cr} \leq 800\lambda A_{cr}$	$0.2f'_c A_c$ <$800A_c$	
4	$0.20\lambda f'_c A_{cr} \leq 800\lambda A_{cr}$		

Table 4.4 PCI and ACI Recommended Values for μ and λ with Respect to Concrete Type and Crack Interface Condition

Factor	Normalweight		Sand-lightweight		All-Lightweight	
	Smooth	Rough	Smooth	Rough	Smooth	Rough
μ	0.60	1.00	0.51	0.85	0.45	0.75
λ	1.00	1.00	0.85	0.85	0.75	0.75

Table 4.5 PCI Design Handbook (2010) and ACI 318 Code (2014) Shear-friction Design Coefficients

Case	Crack Interface Condition	PCI 7th Edition		ACI 318-14
		μ	Max μ_e	μ
1	Concrete to concrete, cast monolithically	1.4λ	3.4	1.4λ
2	Concrete to hardened concrete, with roughened surface	1.0λ	2.9	1.0λ
3	Concrete placed against hardened concrete not intentionally roughened	0.6λ	N/A	0.6λ
4	Concrete to steel	0.7λ	N/A	0.7λ

4.3.1.1 PCI Design Handbook 7th Edition (2010)

The 7th Edition of the PCI Design Handbook contains a major change from the previous edition in that μ_e is no longer considered applicable for crack interface condition Cases 3 and 4: smooth interface and concrete to steel, respectively. Instead, shear-friction design for these two cases is governed by Equation 5-32a, as explained in Section 2.3.1.2.

$$A_{vf} = \frac{V_u}{\phi f_y \mu} \qquad \text{(PCI Design Handbook 7th ed. 5-32a)}$$

When the term V_n is substituted for V_u/ϕ, and V_n/A_{cr} is then replaced with v_n, with ρ used in place of A_{vf}/A_{cr}, Equation 5-32a can be rearranged as shown in Equation 4.1. Equation 4.1 can also be expressed in terms of μ as shown in Equation 4.2:

$$v_n = \rho f_y \mu \tag{4.1}$$

$$\mu = \frac{v_n}{\rho\, f_y} \tag{4.2}$$

For cases where load reversal does not occur, and the interface is either monolithic or roughened (Cases 1 or 2), Equation 5-32b may be used to design the amount of reinforcement crossing the shear plane perpendicularly:

$$A_{vf} = \frac{V_u}{\phi f_y \mu_e} \qquad \text{(PCI Design Handbook 7th ed. 5-32b)}$$

The value for μ_e in Equation 5-32b is computed using Equation 5-33:

$$\mu_e = \frac{\phi 1000 \lambda A_{cr} \mu}{V_u} \qquad \text{(PCI Design Handbook 7th ed. 5-33)}$$

When the term V_n is substituted for V_u/ϕ, and V_n/A_{cr} is then replaced with v_n, with ρ used in place of A_{vf}/A_{cr}, Equations 5-32b and 5-33 can be rearranged and combined as shown in Equation 4.3:

$$v_n = 31.62 \sqrt{\rho f_y \lambda \mu} \tag{4.3}$$

Also, as done before, Equation 5-32b can be solved for μ_e as shown in Equation 4.4:

$$\mu_e = \frac{v_n}{\rho f_y} \tag{4.4}$$

The provisions of the 7th Edition of the PCI Design Handbook restrict the design value of f_y to a maximum of 60 ksi as discussed in Section 2.3.1.2. Maximum values for V_u are listed in Table 4.3 for all interface conditions, Cases 1-4; values for μ and $\mu_{e,max}$ are listed in Table 4.5; and corresponding values for μ and λ are summarized in Table 4.4 for all concrete types and interface conditions.

4.3.1.2 ACI 318-14

The design equations in ACI 318-14 do not include an effective coefficient of friction. Rather, a similar shear-friction design approach is used as for the smooth interface and concrete to steel conditions in the 7th Edition of the PCI Handbook. The nominal shear strength V_n is calculated according to Equation 22.9.4.2:

$$V_n = \mu A_v f_y \qquad \text{(ACI 318-14 22.9.4.2)}$$

When the term V_n/A_{cr} is replaced with v_n, with ρ used in place of A_{vf}/A_{cr}, Equation 22.9.4.2 can be rearranged as shown in Equations 4.1 and 4.2 in Section 4.3.1.1.

The provisions of ACI 318-14 restrict the design value of f_y to a maximum of 60 ksi as discussed in Section 2.3.2. Maximum values for V_n are listed in Table 4.3 for all interface conditions, Cases 1-4; values for μ are listed in Table 4.5; and corresponding values for μ and λ are summarized in Table 4.4 for all concrete types and interface conditions.

4.3.2. Shear Strength

Figures 4.8, 4.9, and 4.10 compare the peak shear stress v_u of the sand-lightweight and all-lightweight concrete specimens with Equation 4.1 (μ-approach) and Equation 4.3 (μ_e-approach) and the design provisions in the PCI Design Handbook (2010) and ACI 318 code (2014) for a monolithic interface condition, roughened interface condition, and smooth interface condition, respectively. In comparisons with Equations 4.1 and 4.3, the strength reduction factor ϕ was taken as 1.0 since the loads and material properties were known. For a monolithic interface condition, Equations 4.1 and 4.3 are limited to 800 psi in the ACI 318 code and to 1000λ psi in the PCI Design Handbook as shown in Table 4.3. For a roughened interface condition (¼ in. amplitude) corresponding to Case 2, Equations 4.1 and 4.3 are limited to 800 psi in the ACI 318 code and to 1000λ psi in the PCI Design Handbook. For an interface that is not intentionally roughened, corresponding to Case 3, Equation 4.1 is limited to 800 psi in the ACI 318 code and to 800λ psi in the PCI Design Handbook (Equation 4.3 is not applicable for Case 3 interface conditions). In Figures 4.14, 4.15, and 4.16, values of λ were taken as 0.85 and 0.75 for sand-lightweight and all-lightweight concrete, respectively. Values of f_y were the measured values. Specimens that failed in splitting are identified in the figures.

Figure 4.8 shows that the measured shear strength of each sand-lightweight and all-lightweight concrete specimen with a monolithic interface condition (Case 1 in Table 4.5) is larger than the value computed using Equation 4.1 (μ-approach) for both the ACI 318 code (2014) and the PCI Design Handbook (2010). Similarly, Figure 4.9 shows that the measured shear strength of each sand-lightweight and all-lightweight specimen with a roughened interface (Case 2 in Table 4.5) was larger than the value computed by Equation 4.1 (μ-approach) for both the ACI 318 code and the PCI Design Handbook. Figure 4.10 shows that the measured shear strength of each sand-lightweight and all-lightweight specimen with a smooth interface (Case 3 in Table 4.5) was larger than the value computed by Equation 4.1 (μ-approach) for both the ACI 318 code and the PCI Design Handbook. Therefore the μ-approach shear-friction design provisions in the ACI 318 code and the PCI Design Handbook for Case 1, 2, and 3 interface conditions in Table 4.5 are conservative for the sand-lightweight and all-lightweight specimens in this study, even using the measured values of f_y. (If the maximum specified value of 60,000 psi for f_y are used instead, the points shift slightly to the left in each graph, which would yield even more conservative results with respect to Equation 4.6). These results are significant since they are among the first in the literature that can be used to validate, with physical test data, shear-friction design provisions for sand-lightweight and all-lightweight concrete with a non-monolithic interface condition.

With regard to the μ□-approach in the PCI Design Handbook, Figure 4.8 shows that the measured shear strength of each sand-lightweight and all-lightweight concrete specimen with a monolithic interface condition (Case 1 in Table 4.5) is larger than the value computed using Equation 4.3 Equation 4.3 (μ_e-approach). Similarly, Figure 4.9 shows that the measured shear strength of each sand-lightweight and all-lightweight specimen with a roughened interface (Case 2 in Table 4.5) was larger than the value computed by Equation 4.3 (μ_e-approach) from the PCI Design Handbook.

Again, these results are significant since they are among the first in the literature that can be used to validate, with physical test data, shear-friction design provisions for sand-lightweight and all-lightweight concrete with a non-monolithic interface condition.

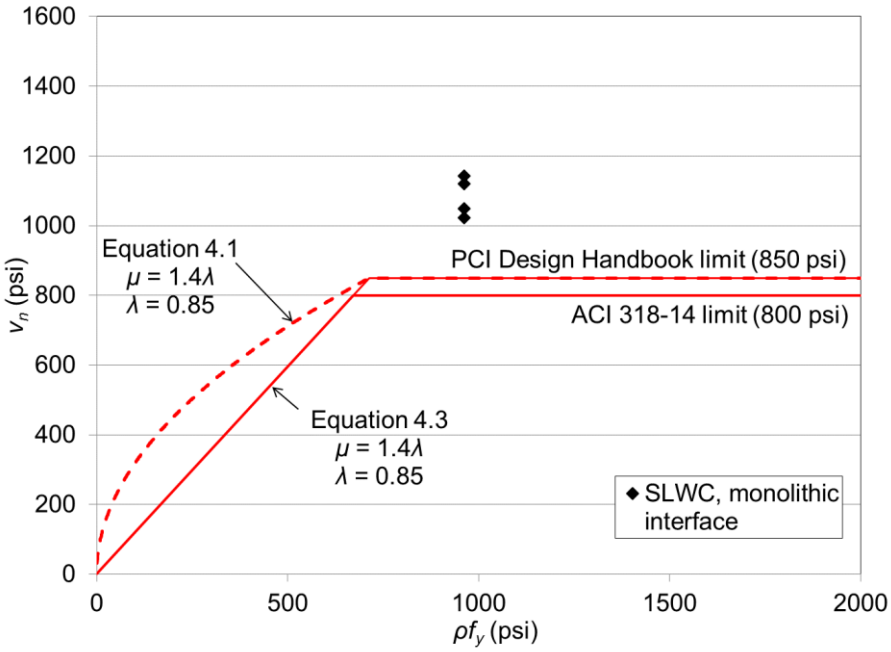

(a)

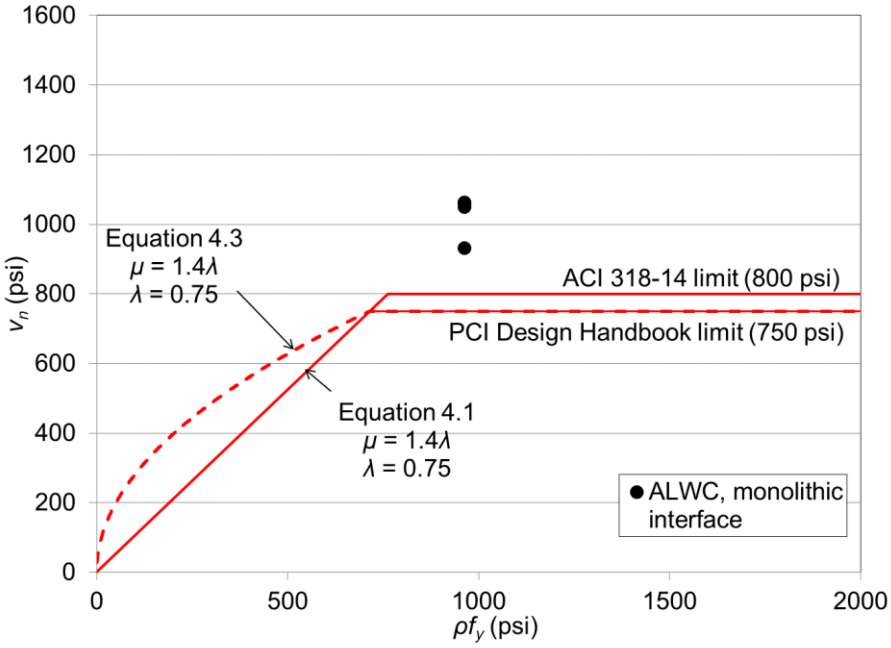

(b)

Figure 4.8 Comparison of peak shear stress v_u with Equation 4.1 (μ-approach) and Equation 4.3 (μ_e-approach) for specimens with a monolithic uncracked or pre-cracked interface a) sand-lightweight concrete specimens b) all-lightweight concrete specimens

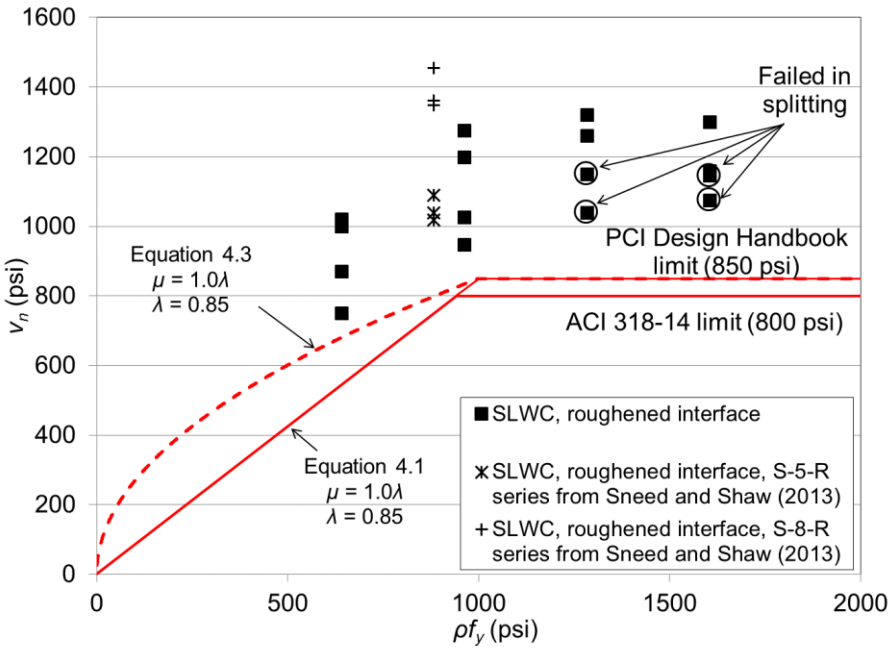

(a)

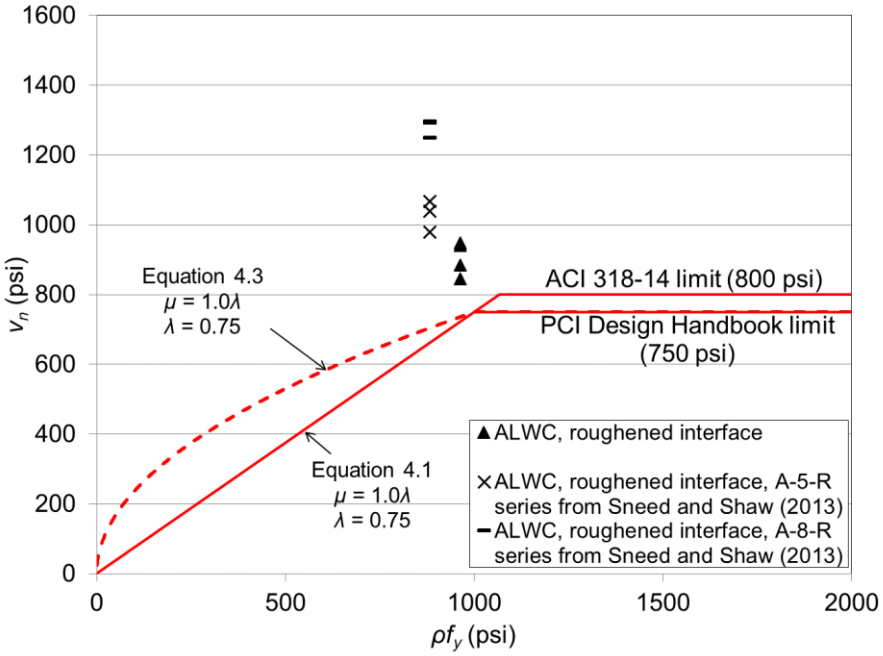

(b)

Figure 4.9 Comparison of peak shear stress v_u with Equation 4.1 (μ-approach) and Equation 4.3 (μ_e-approach) for specimens with a roughened interface a) sand-lightweight concrete specimens b) all-lightweight concrete

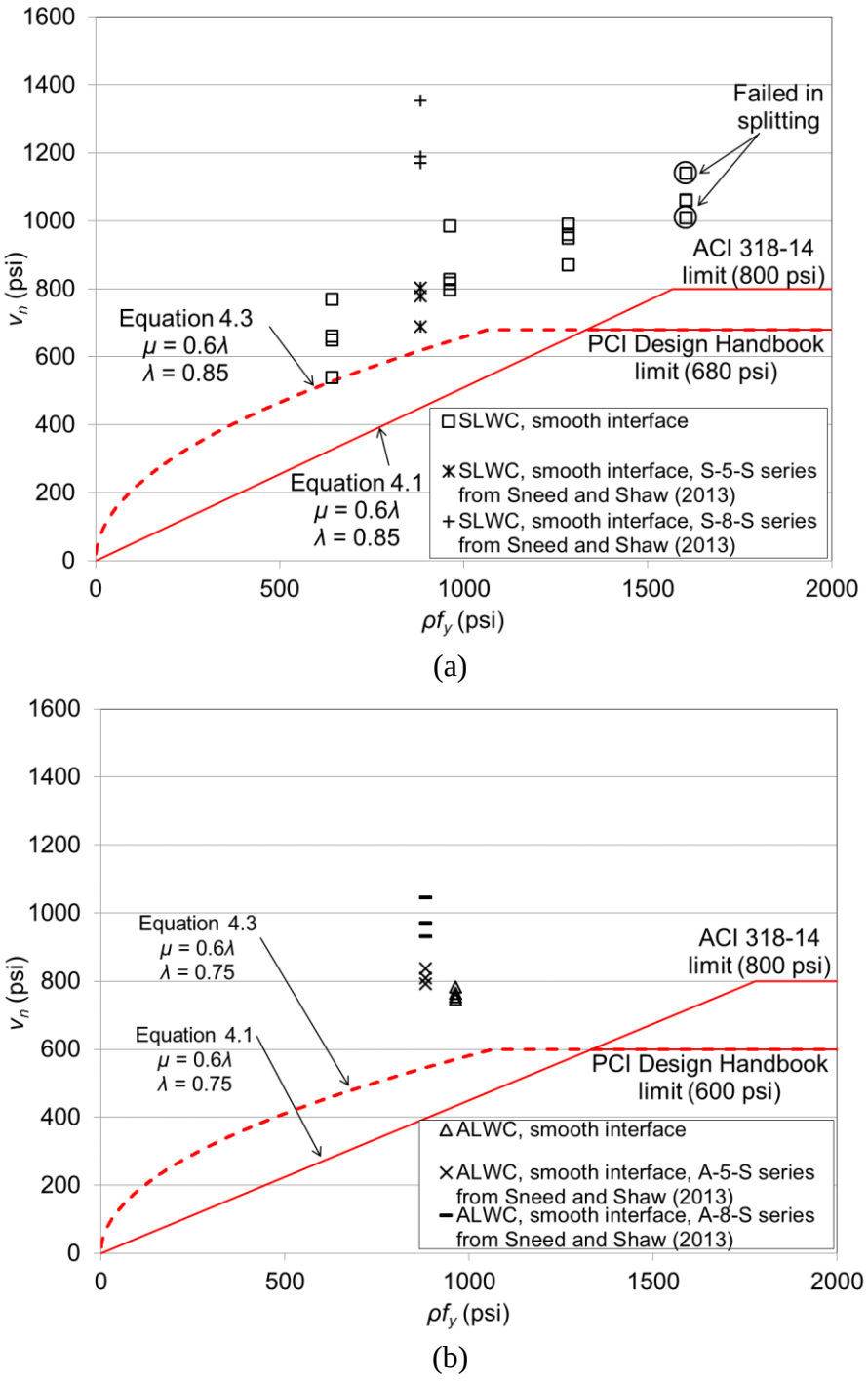

Figure 4.10 Comparison of peak shear stress v_u with Equation 4.1 (μ-approach) and Equation 4.3 (μ_e-approach) for specimens with a smooth interface a) sand-lightweight concrete specimens b) all-lightweight concrete

4.3.3. Effective Coefficient of Friction, μ_e

This section compares the "effective" coefficient of friction associated with the measured shear strength V_u (or v_u) calculated using Equation 4.5, denoted μ_{test}, to the value of μ_e computed using

PCI Equation 5-33 for use in PCI Equation 5-32b for specimens with different interface conditions (monolithic uncracked, monolithic pre-cracked, and cold joint roughened) and different concrete types (normalweight, sand-lightweight, and all-lightweight). As mentioned above, PCI Equation 5-32b is not applicable to cold joint smooth interface conditions, and therefore PCI Equation 5-33 is also not applicable for the cold joint smooth interface case.

$$\mu_{test} = \frac{v_u}{\rho f_{y,limited}} \tag{4.5}$$

As discussed in Section 4.3.1.1, μ_e computed using PCI Equation 5-33 for use in PCI Equation 5-32b is a function of $V_n=V_u/\phi$ (or $v_n=v_u/\phi$), so its value is not constant. Values of μ_{test} are also compared with the coefficient of friction μ specified by the PCI Design Handbook (2010) and the ACI 318 code (2014) (both of which have a constant value, see Table 4.5) and used in PCI Equation 5-32a and ACI Equation 22.9.4.2, respectively.

In this evaluation, μ_{test} is computed with Equation 4.5 using the actual yield stress of the reinforcement f_y, and *not* limited to 60,000 psi per the PCI Design Handbook (2010) and the ACI 318 code (2014). It should be noted that this comparison is different than that in Section 5, which limits the value of f_y to 60,000 psi. The value of μ_e computed using PCI Equation 5-33 is plotted against v_n considering $V_n=V_u/\phi$, where ϕ=1.0, and $v_n=V_n/A_{cr}$. The maximum values of μ, μ_e, and v_n specified by the PCI Design Handbook and ACI 318 code are also indicated in the graphs. Because the maximum value of v_n is a function of the concrete type, normalweight, sand-lightweight, and all-lightweight concrete specimens are presented separately.

4.3.3.1 Normalweight Concrete

Figure 4.11 plots the values of μ_{test} associated with v_u for the normalweight concrete specimens for the monolithic uncracked, monolithic pre-cracked, and roughened interface conditions. Figure 4.11 shows that PCI Equation 5-32b (where μ_e is computed using PCI Equation 5-33) is conservative (all values of μ_{test} plotted to the right and above the equation) for the monolithic uncracked and pre-cracked specimens. PCI Equation 5-32b is also conservative for the roughened interface conditions. Since the coefficient of friction μ is the lower bound of the effective coefficient of friction μ_e, Figure 4.11 shows the value of μ specified by the PCI Design Handbook and the ACI 318 code is conservative with respect to the test results for each concrete type and interface condition when the limit for the maximum shear stress is also considered (Table 4.3). (Note that the value of $v_{n,max}$ varies with f'_c for the ACI 318 code (2014) provisions. For reference, $v_{n,max}$=880 psi for concrete with f'_c=5000 psi, and thus the values of μ_{test} are conservative in this case.)

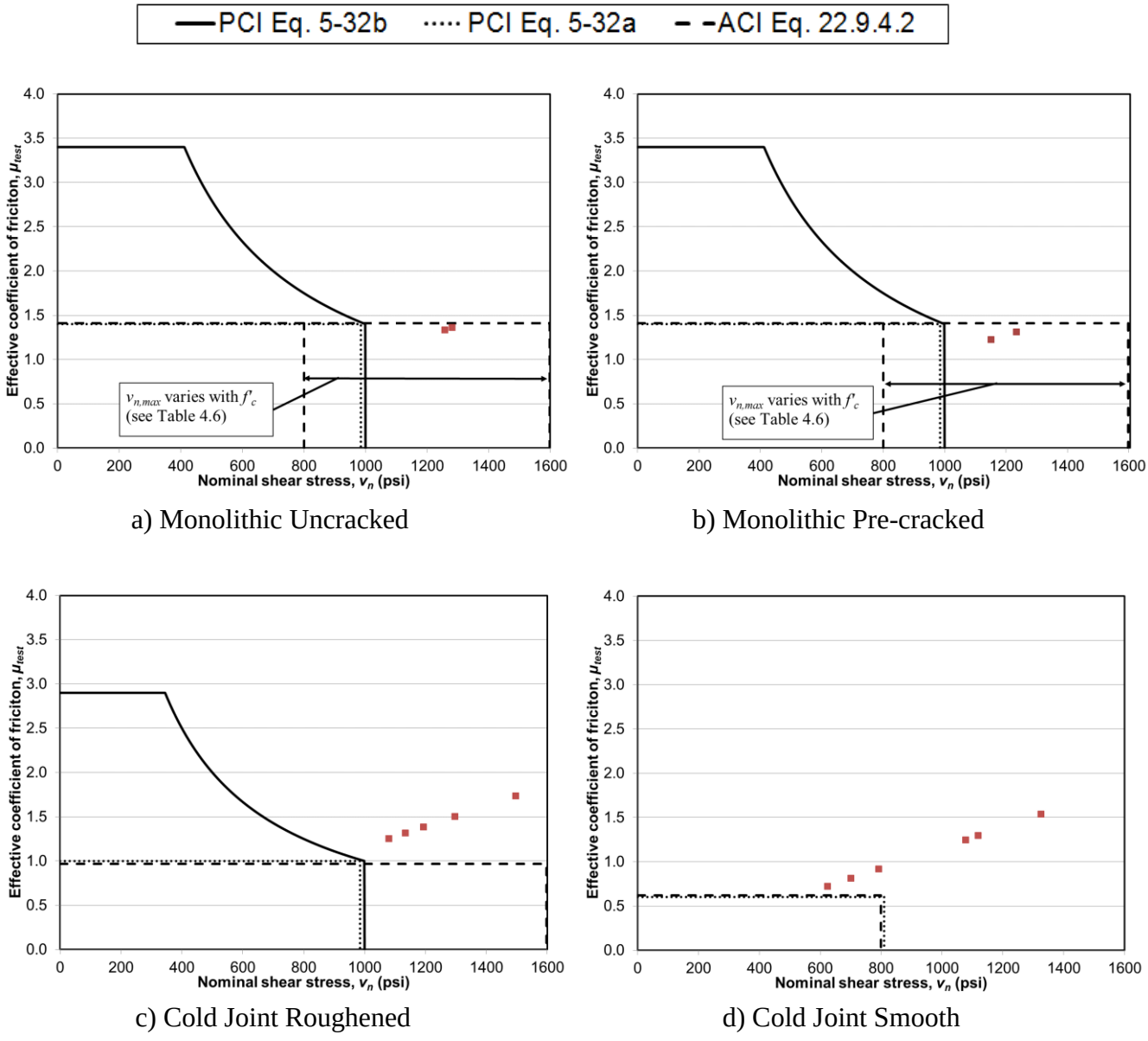

a) Monolithic Uncracked

b) Monolithic Pre-cracked

c) Cold Joint Roughened

d) Cold Joint Smooth

Figure 4.11 Effective coefficient of friction μ_e for normalweight concrete specimens with a a) monolithic uncracked, b) monolithic pre-cracked, c) roughened, and d) smooth interface

4.3.3.2 Sand-lightweight Concrete

Figure 4.12 plots the values of μ_{test} associated with v_u for the sand-lightweight concrete specimens. Specimens that failed in splitting are identified in the graphs. All values of μ_{test} for the monolithic uncracked, monolithic pre-cracked, and roughened interface specimens were conservative compared to PCI Equation 5-32b. Since the coefficient of friction μ is the lower bound of the effective coefficient of friction μ_e, Figure 4.12 shows the value of μ specified by the PCI Design Handbook and the ACI 318 code is generally conservative with respect to the test results for each

concrete type and interface condition, when the limit for the maximum shear stress is also considered (Table 4.3).

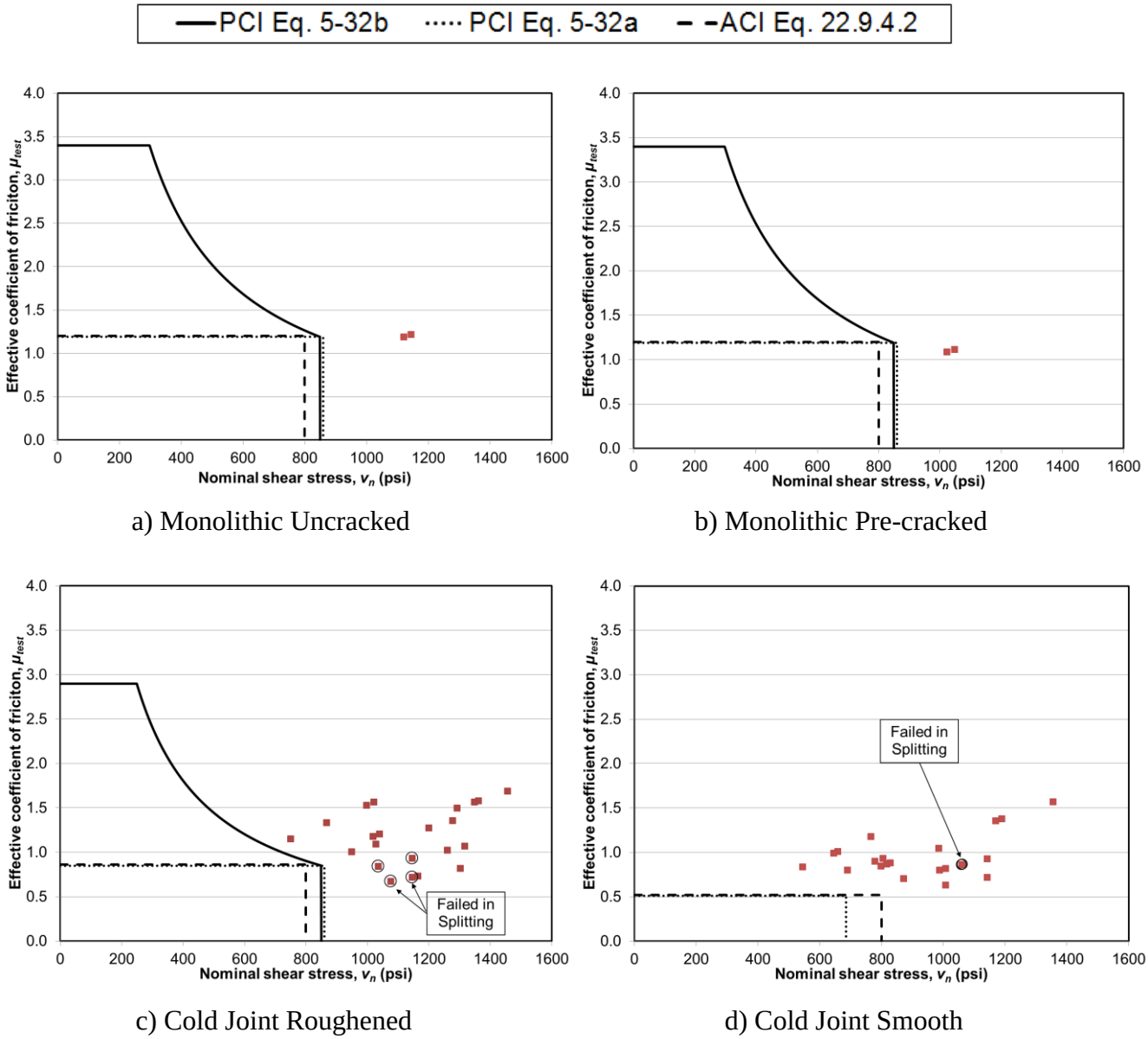

a) Monolithic Uncracked

b) Monolithic Pre-cracked

c) Cold Joint Roughened

d) Cold Joint Smooth

Figure 4.12 Effective coefficient of friction μ_e for sand-lightweight concrete specimens with a) monolithic uncracked, b) monolithic pre-cracked, c) roughened, and d) smooth interface

4.3.3.3 All-lightweight Concrete

Figure 4.13 shows the value of μ_{test} for the all-lightweight concrete specimens. All values of μ_{test} for the monolithic uncracked, monolithic pre-cracked, and roughened interface specimens were conservative compared to PCI Equation 5-32b. Since the coefficient of friction μ is the lower bound of the effective coefficient of friction μ_e, Figure 4.13 shows the value of μ specified by the

PCI Design Handbook and the ACI 318 code is generally conservative with respect to the test results for each concrete type and interface condition, when the limit for the maximum shear stress is also considered (Table 4.3).

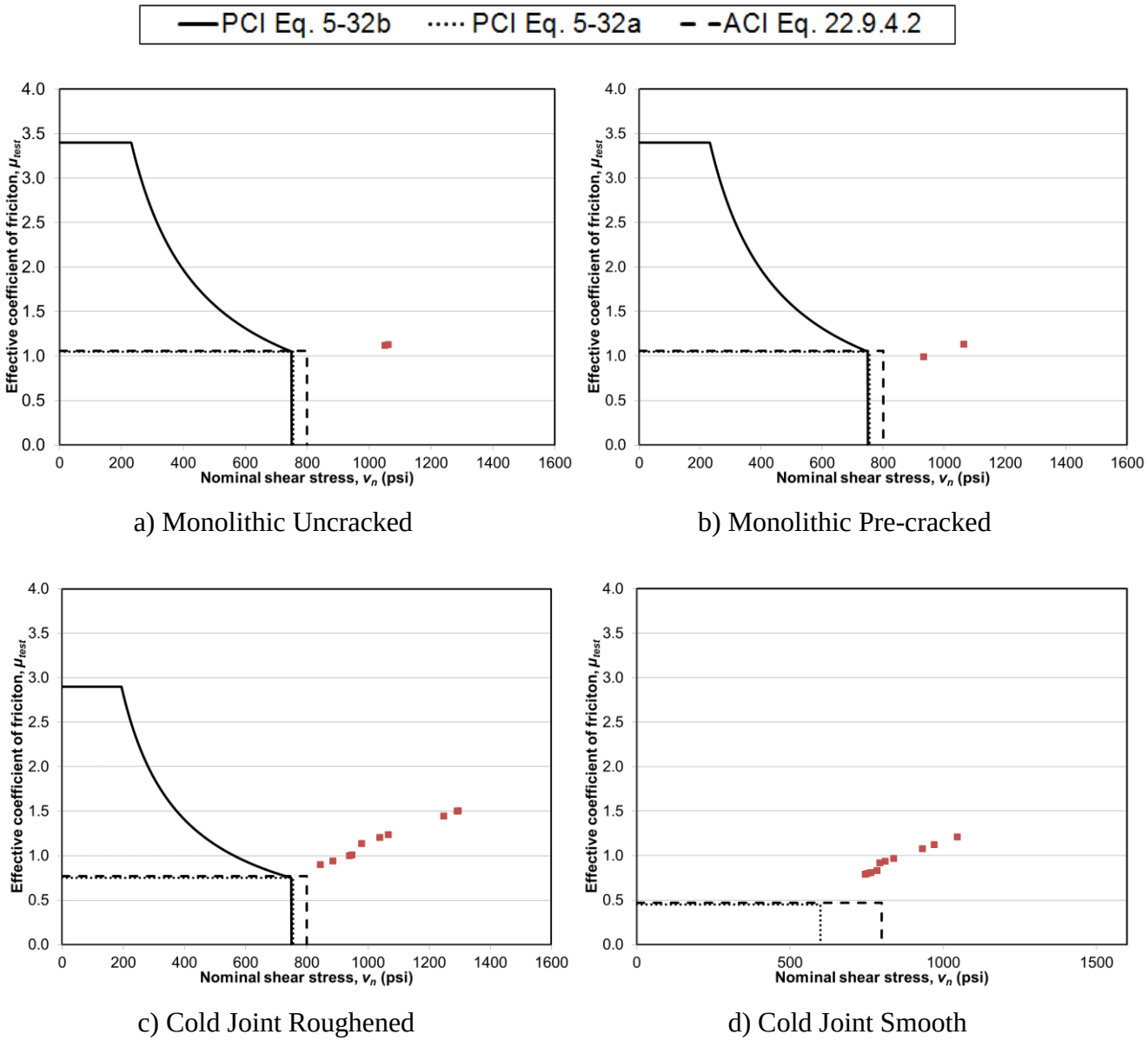

a) Monolithic Uncracked

b) Monolithic Pre-cracked

c) Cold Joint Roughened

d) Cold Joint Smooth

Figure 4.13 Effective coefficient of friction μ_e for all-lightweight concrete specimens with a) monolithic uncracked, b) monolithic pre-cracked, c) roughened, and d) smooth interface

4.3.4. Lightweight Modification Factor, λ

For the coefficient of friction μ-approach, PCI Design Handbook (2010) Equation 5-32a and ACI 318 code (2014) Equation 22.9.4.2 are used along with the appropriate value of the coefficient of friction μ from Table 4.5. For the "concrete placed against hardened concrete not intentionally

roughened" condition (Case 3 in Table 4.5), μ is taken as 0.6λ in the ACI 318 code (2014) and PCI Design Handbook (2010) provisions. In Mattock's 2001 study, this value of μ was validated against experimental data that included normalweight concrete pushoff specimens with a smooth interface that were either pre-cracked or had a broken bond. Accordingly, these test results should represent a lower bound condition of the shear-transfer strength. However, no experimental data were used to compare this coefficient of friction for lightweight aggregate concretes. Mattock pointed out that the shear strength of these specimens were equal to the shear yield strength of the reinforcement perpendicular to the interface (hence the coefficient 0.6 in for the Case 3 interface condition), and that true shear-friction cannot be developed in the absence of interfacial roughness. Given this reasoning, however, it is not clear why the lightweight modification factor λ was included in the ACI 318 code or PCI Design Handbook provisions, especially in the absence of test data on lightweight concretes with a smooth interface condition.

To further examine this issue, Figure 4.14 compares the shear strength v_u of the sand-lightweight and all-lightweight concrete specimens with a smooth interface condition with Equation 4.6 (and 4.13), but with λ taken as 1.0, that is, no influence of concrete type. Data are supplemented with test results on sand-lightweight and all-lightweight concrete cold joint smooth interface specimens from Shaw and Sneed (2013). Results in Figure 4.14 illustrate that the measured shear strengths were larger than values with λ taken as 1.0, for the sand-lightweight and all-lightweight specimens with a smooth interface. These results and the reasoning above question the need for the lightweight modification factor λ in the friction coefficient in the Case 3 interface condition, which is also supported by the results shown in Figure 4.3. Thus, results of this study suggest that the coefficient of friction μ can be taken as 0.6 (not as 0.6λ) for concrete placed against hardened concrete not intentionally roughened in the shear-friction provisions in the ACI 318 code the PCI Design Handbook.

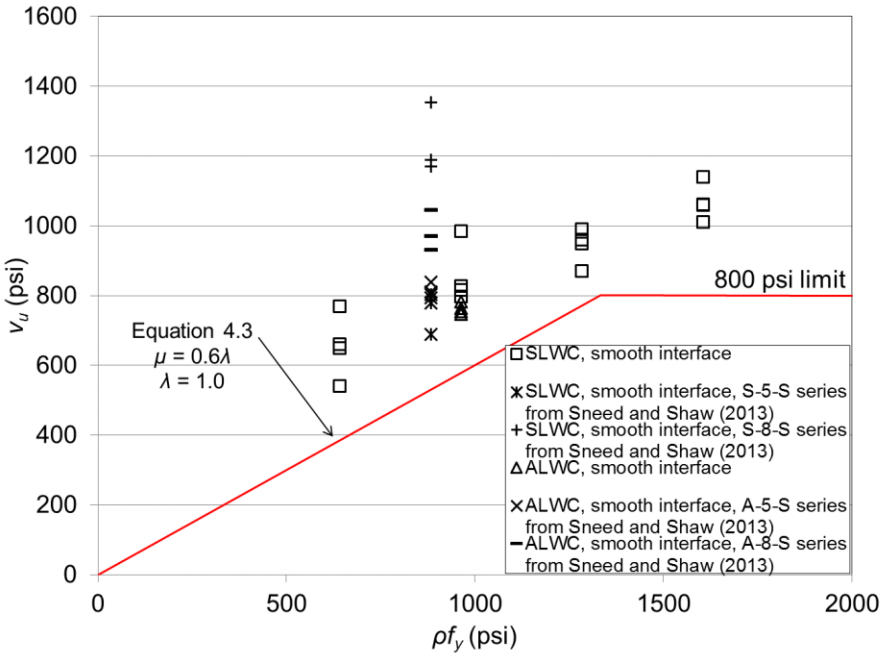

Figure 4.14 Comparison of peak shear stress v_u with Equation 4.1, with λ=1.0, for sand-lightweight and all-lightweight concrete specimens with a smooth interface

4.4. CONCLUDING REMARKS

This section analyzed the results of the experiments conducted in this study. Test results of the 52 pushoff specimens presented in Section 3 were combined with those from the first phase of this study (Sneed and Shaw 2013) to investigate the applicability of the shear-friction concept for lightweight aggregate concretes with different lightweight aggregates and different interface conditions on the shear interface. These results help fill in gaps in the literature with respect to sand-lightweight and all-lightweight concretes and interfaces of concretes cast at different times, that is, cold joint conditions. Analysis of the results led to the following conclusions:

1. The shear strength of specimens with the same reinforcement ratio (ρ=0.013) and a monolithic uncracked or pre-cracked interface increased with increasing unit weight. The shear strength of cold joint specimens with an intentionally roughened interface increased as the unit weight of concrete increased. The shear strength of cold joint specimens with smooth interface appeared to be independent of type or unit weight of concrete.
2. The shear strength of specimens with the same reinforcement ratio (ρ=0.013) and a cold joint roughened interface was higher than the shear strength of corresponding cold joint smooth interface specimens with the same lightweight aggregate material.
3. The sand-lightweight concrete specimens achieved a higher shear strength than the all-lightweight concrete specimens with the same lightweight aggregate material and reinforcement ratio for monolithic and roughened interface conditions.
4. A pre-existing crack reduced the shear strength of normalweight, sand-lightweight, and all-lightweight concrete specimens relative to the corresponding uncracked monolithic specimens.
5. The shear strength of specimens with a roughened interface appeared to be influenced by the type of lightweight aggregate material. The shear strength of lightweight concretes made with expanded slate aggregate was higher than the shear strength of lightweight concretes made with expanded clay aggregate for roughened interface specimens. The shear strength of specimens with a smooth interface appeared to be independent of lightweight aggregate material.
6. Six of the sand-lightweight specimens with clay aggregate and a high reinforcement ratio (ρ =0.017 or 0.022) failed due to concrete splitting prior to shear failure, which was attributed to the low tensile strength of concrete.
7. The shear strength of the sand-lightweight specimens with clay and slate aggregates increased with increasing reinforcement parameter ρf_y; however, particularly for specimens with a roughened interface, the shear strength values leveled off after approximately ρf_y = 1200 psi.
8. Shear strengths computed by the ACI 318 code (2014) (22.9.4.2) and the PCI Design Handbook (2014) (5-32a) using the coefficient of friction μ approach were conservative for the sand-lightweight and all-lightweight monolithic and cold joint specimens in this study. In other words, the use of λ in ACI Equation 22.9.4.2 and PCI Equation 5-32a provided conservative designs for all lightweight aggregates included in this study.
9. Shear strengths computed by the PCI Design Handbook (2014) (5-32a) using the effective coefficient of friction μ_e–approach were conservative for the sand-lightweight and all-lightweight monolithic and cold joint specimens in this study. In other words, the use of λ in PCI Equation 5-32b provided conservative designs for all lightweight aggregates included in this study.

5. EVALUATION OF PCI DESIGN HANDBOOK AND ACI 318 CODE SHEAR-FRICTION DESIGN PROVISIONS

5.1. INTRODUCTION

This section expands on the work in Section 4 of this report and presents an up-to-date database of shear-friction test results collected from the literature and examines the results in terms of the effective coefficient of friction (μ_e) and coefficient of friction (μ) approaches in the PCI Design Handbook (2010) and the ACI 318 code (2014). At this stage, the database is limited to pushoff specimens subjected to monotonic loading and without external normal forces. The evaluation in this section is aimed at providing a global and comprehensive comparison of PCI Design Handbook (2010) and ACI 318 code (2014) shear-friction design provisions with physical test data, examining potential revisions to the design provisions, and identifying gaps in the literature where future work is needed.

This section is written as a stand-alone section to facilitate publication and future work. Background information is presented in Section 5.2. The database is described in Section 5.3 and is presented in Appendix B. Section 5.4 summarizes the analysis of the database. Discussion is provided in Section 5.5, and concluding remarks are presented in Section 5.6.

5.2. BACKGROUND

Since the introduction of the effective coefficient of friction μ_e-approach to the PCI Design Handbook (1978), several studies have been published that expand the database of test results that can be used to compare and validate the shear-friction design provisions. The shear-friction concept has been studied extensively by others, especially for normalweight concrete with various reinforcement ratios, compressive strengths, and interface conditions. Recent studies have focused on the use of high-strength concretes (e.g., Mattock 2001; Kahn and Mitchell 2002; Mansur et al. 2008), lightweight aggregate concretes (e.g., Sneed and Shaw 2013), and non-monolithic (cold joint) interface conditions (Kahn and Mitchell 2002; Harries et al. 2012; Sneed and Shaw 2013).

As discussed in Section 2 of this report, the current PCI Design Handbook (2010) includes two approaches for the design for shear-friction. The first approach, which has existed since the 2nd edition of the handbook (1978), uses the effective coefficient of friction μ_e to compute the required area of shear reinforcement A_{vf} across the shear plane due to factored shear force V_u:

$$A_{vf} = \frac{V_u}{\emptyset f_y \mu_e} \qquad \text{(PCI Design Handbook 7th ed. 5-32b)}$$

where f_y is the yield stress of reinforcement, which has an upper limit of 60,000 psi. In the current edition of the PCI Design Handbook (2010), μ_e is calculated using Equation 5-33:

$$\mu_e = \frac{\phi 1000 \lambda A_{cr} \mu}{V_u} \qquad \text{(PCI Design Handbook 7th ed. 5-33)}$$

in which ϕ is the strength reduction factor (0.75 for shear), A_{cr} is the area of the shear plane, and μ is the coefficient of friction, which is intended to account for friction between the surfaces of the crack interface. The value of μ is a function of the crack interface condition and the concrete type (normalweight, sand-lightweight, or all-lightweight) as summarized in Table 5.1. The modification

factor λ for concrete type is intended to account for different mechanical properties of lightweight aggregate concrete relative to normalweight concrete of the same compressive strength. The value of λ is taken as 1.0 for normalweight concrete, 0.75 for all-lightweight concrete, and may be taken as 0.85 for sand-lightweight concrete (2010). Upper limits on the effective coefficient of friction μ_e are summarized in Table 5.1. Upper limits on the shear strength V_u/ϕ, included in Table 5.1, are also specified by the PCI Design Handbook (2010), which are intended to account for the value at which the shear plane is over-reinforced and the shear transfer strength increases with increasing reinforcement ratios at a reduced rate (Mattock 2001).

Table 5.1 Shear-friction Coefficients and Maximum Shear Strength in PCI Design Handbook (2010) and ACI 318 Code (2014) Shear-Friction Design Provisions

Case	Crack Interface Condition		PCI Design Handbook (2010)		ACI 318 Code (2014)
		μ	Maximum μ_e	Maximum V_u/ϕ	Maximum V_n
1	Concrete to concrete, cast monolithically	1.4λ	3.4	$0.30\lambda f'_c A_{cr} \leq 1000\lambda A_{cr}$	For normalweight concrete: $0.2f'_c A_c \leq (480 + 0.08f'_c)A_c \leq 1600A_c$ For all other cases: $0.2f'_c A_c \leq 800A_c$
2	Concrete to hardened concrete, with roughened surface	1.0λ	2.9	$0.25\lambda f'_c A_{cr} \leq 1000\lambda A_{cr}$	
3	Concrete placed against hardened concrete not intentionally roughened	0.6λ	NA	$0.20\lambda f'_c A_{cr} \leq 800\lambda A_{cr}$	$0.2f'_c A_c \leq 800A_c$
4	Concrete to steel	0.7λ	NA	$0.20\lambda f'_c A_{cr} \leq 800\lambda A_{cr}$	

Substituting V_u/ϕ for the nominal shear strength V_n, PCI Equations 5-32b and 5-33 can be rewritten as Equation 5.1:

$$v_n = 31.62\sqrt{\rho f_y \lambda \mu} \tag{5.1}$$

where ρ is the reinforcement ratio; $\rho = A_{vf}/A_{cr}$, A_{cr} is the area of the shear plane, and $v_n = V_n/A_{cr}$.

PCI Equation 5-32b can be expressed in terms of μ_e associated with the nominal shear stress v_n as shown in Equation 5.2:

$$\mu_e = \frac{v_n}{\rho f_y} \tag{5.2}$$

The second approach to determining the required area of shear-friction reinforcement was introduced in the 7th edition of the PCI Design Handbook (2010) in which the effective coefficient of friction μ_e in Equation 5-32b is replaced with the coefficient of friction μ. This approach, given in Equation 5-32a of the PCI Design Handbook (2010), is applicable for all four crack interface conditions in Table 5.1. Values of the coefficient of friction μ are included in Table 5.1.

$$A_{vf} = \frac{V_u}{\emptyset f_y \mu} \quad \text{(PCI Design Handbook 7th ed. 5-32a)}$$

PCI Equation 5-32a is consistent with the ACI 318 code (2014), although the limits on the shear strength are different. The ACI 318 code (2014) approach is given in Equation 22.9.4.2:

$$V_n = \mu A_{vf} f_y \qquad \text{(ACI 318-14 22.9.4.2)}$$

PCI Equation 5-32a and ACI Equation 22.9.4.2 can be expressed in terms of nominal shear stress v_n as shown in Equation 5.3 (with $V_n = V_u/\phi$, $v_n = V_n/A_{cr}$, and $\rho = A_{vf}/A_{cr}$):

$$\mu = \frac{v_n}{\rho f_y} \qquad (5.3)$$

5.3. DATABASE

The literature was surveyed to collect published test data on direct shear transfer of concrete to concrete (Cases 1-3 in Table 5.1). Works evaluated were limited to those published in English. Various test configurations have been used to evaluate shear-friction, depending on the objective of the particular research study. For the purpose of direct comparison in this section, only the classical pushoff specimens (Hofbeck et al. 1969; Mattock 1976; Mattock et al. 1976; Kahn and Mitchell 2002; Harries et al. 2012; Hoff 1993; Mansur et al 2008) without an external force normal to the shear plane were included. The external force normal to the shear plane criterion excluded studies conducted by Walraven and Reinhardt (1981), Papanicolau and Triantafillou (2002), and Echegaray et al. (2014). Other types of test specimens that were not included in this database were inclined pushoff specimens or those that had inclined reinforcement across the interface such as the specimens in studies conducted by Vangsirirungrang (1971), Mattock and Hawkins (1972), Dulacska (1972), Mattock (1974), and Hawkins and Kuchma (2007). Also excluded were pulloff type specimens such as those studied by Chatterjee (1971) and Mattock and Hawkins (1972), corbel type specimens with moment and tension across the interface such as those studied by Mattock et al. (1975), wall footing type specimens such as those studied by Bass et al. (1989) and Valluvan et al. (1999), and beam-slab connections such as those by Saemann and Washa (1964), Ivey and Buth (1967), Loov and Patnaik (1994), and Gohnert (2000; 2003). Horizontal pushoff specimens studied by Hanson (1960) and Paulay et al. (1974) were not included in this database. The database in this section is limited to specimens subjected to monotonic loading; specimens that were cyclically loaded or specimens with sustained loading were not included. The criteria excluded specimens in the studies by Frenay (1985) and Valluvan et al. (1999). (The database may be expanded to include other conditions as future work.)

The resulting database presented in Appendix B of this report summarizes the reference, specimen ID from the original reference, compressive strength of concrete f'_c, shear interface area A_{cr}, reinforcement ratio ρ, reinforcement yield strength f_y, clamping stress $\rho f_{y,limited}$, peak shear force V_{test}, and peak shear stress v_{test} for each specimen. Compressive strength of concrete f'_c is the value reported at the test date. For cold joint specimens with different concrete strengths on each side of the interface, the lower compressive strength is reported. Reinforcement ratio ρ is computed as A_{vf}/A_{cr}, where A_{vf} is the area of reinforcement crossing the shear plane, and A_{cr} is the area of the shear interface. Only specimens with reinforcing bars of size No. 3 (inch-lb bar size) or 8 mm diameter (SI bar size) and larger were included in this database. f_y is the reported yield strength of the reinforcing bars, while clamping stress $\rho f_{y,limited}$ is computed considering the limitation on the value

of f_y of 60,000 psi per the PCI Design Handbook (2010) and ACI 318 code (2014). While most researchers report the peak shear force using the notation V_u, the peak shear force in the database is denoted V_{test} in this section in order to avoid confusion between it and the ultimate (factored) design shear force, which is also denoted V_u in the PCI Design Handbook (2010) and ACI 318 code (2014) design provisions. The peak shear stress v_{test} is defined as V_{test}/A_{cr}. The tables are organized by interface condition, which is given as concrete to concrete cast monolithically (referred to in this paper as "monolithic uncracked"; Table B.1), concrete to concrete cast monolithically and pre-cracked prior to testing (referred to in this paper as "monolithic pre-cracked"; Table B.2), concrete to hardened concrete with roughened surface (referred to in this paper as "cold joint roughened"; Table B.3), or concrete placed against hardened concrete not intentionally roughened (referred to in this paper as "cold joint smooth"; Table B.4). Within each table, specimens are grouped in terms of concrete type. Concrete type is given as normalweight, sand-lightweight, or all-lightweight, where each type is designated by its aggregate composition. For the purpose of this database, the unit weight of concrete and aggregate source are not included, since most studies did not report these values.

The database includes 302 specimens from 9 studies (Hofbeck et al. 1969; Mattock 1976; Mattock et al. 1976; Kahn and Mitchell 2002; Harries et al. 2012; Hoff 1993; Mansur et al 2008; Sneed and Shaw 2013; present study). Figure 5.1 shows the data distribution in terms of concrete type, interface condition, compressive strength of concrete f'_c, reinforcement ratio ρ, clamping stress $\rho f_{y,limited}$, and area of shear interface A_{cr}. Additional discussion of data distribution is included in the following sections.

5.4. ANALYSIS OF DATABASE

5.4.1. Shear Strength

This section compares the measured shear strength V_{test} to the calculated shear strength V_{calc} computed using the PCI Equation 5-32b (μ_e-approach), PCI Equation 5-32a (μ-approach), and ACI 318 Equation 22.9.4.2 (μ-approach) for specimens with different interface conditions (monolithic uncracked, monolithic pre-cracked, cold joint roughened, and cold joint smooth) and different concrete types (normalweight, sand-lightweight, and all-lightweight). Since PCI Equation 5-32b (μ_e approach) is not applicable for shear-friction design of Case 3 interface conditions (Table 1), it is not compared for cold joint smooth interface specimens. In this evaluation, the shear strength V_{calc} is computed using $f_{y,limited}$, corresponding to the actual reported yield stress of the reinforcement f_y but not taken more than 60,000 psi per the PCI Design Handbook (2010) and the ACI 318 code (2014). The ratio V_{test}/V_{calc} is reported in Tables A.1, A.2, A.3, and A.4 for each test specimen and each of the three design equations (where applicable). Additionally, the mean (Avg), standard deviation (STD), coefficient of variation (COV), and maximum (Max) and minimum (Min) values of V_{test}/V_{calc} are reported in Tables A.1, A.2, A.3, and A.4 for each group of specimens with the same interface condition and concrete type.

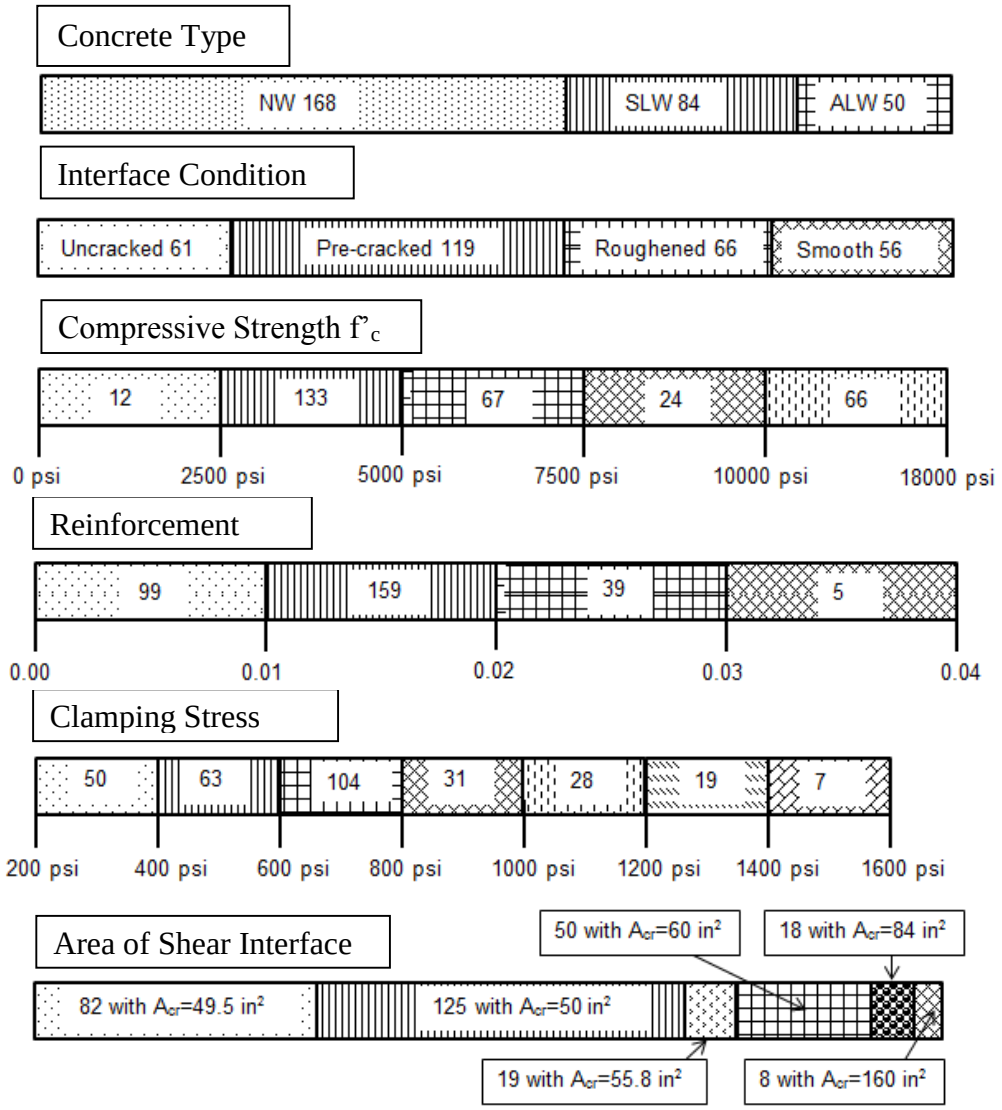

Figure 5.1 Distribution of data in terms of in terms of concrete type, interface condition, compressive strength of concrete f'_c, reinforcement ratio ρ, clamping stress $\rho f_{y,limited}$, and area of shear interface A_{cr}

5.4.1.1 Normalweight Concrete

Figure 5.2 shows the ratio V_{test}/V_{calc} for the normalweight concrete specimens. Monolithic uncracked interface specimens are shown in the first row, monolithic pre-cracked interface specimens are shown in the second row, cold joint roughened interface are shown in the third row, and cold joint smooth interface specimens are shown in the fourth row. The graphs on the left of Figure 5.2 plot V_{test}/V_{calc} versus the compressive strength of concrete f'_c. The graphs on the right of Figure 5.2 plot V_{test}/V_{calc} versus the clamping stress $\rho f_{y,limited}$, where $f_{y,limited}$ is the actual yield stress of the reinforcement (equal to or less than 60,000 psi). Note that the vertical axis of the graphs ranges from 0-4.0 for each of the three equations evaluated. For clarity of presentation in the graphs, values of V_{test}/V_{calc} larger than 4.0 are not plotted, but they are reported in the Appendix Tables B.1-B.4.

For the monolithic uncracked normalweight concrete tests, f'_c ranges from 3840 psi to 17,957 psi, and $\rho f_{y,limited}$ ranges from 211 psi to 1391 psi. All three design provisions produce conservative values of shear strength (i.e., V_{test}/V_{calc} larger than 1.0) for all specimens for the entire ranges of f'_c and $\rho f_{y,limited}$ tested, and especially for large values of f'_c. PCI Equation 5-32b tends to be the most accurate (i.e., mean value closest to 1.0).

For the pre-cracked monolithic normalweight concrete specimens, f'_c ranges from 2385 psi to 16,475 psi, and $\rho f_{y,limited}$ ranges from 223 psi to 1570 psi. All three design provisions produce some V_{test}/V_{calc} values less than 1.0. Figure 2 and Table 2 show that for ACI 318 Equation 22.9.4.2, the values less than 1.0 are associated with specimens made with higher strength concrete, while for PCI Equation 5-32a the values less than 1.0 occur for low values of f'_c (i.e., less than 4000 psi). PCI Equation 5-32b tends to have values less than 1.0 for low values of $\rho f_{y,limited}$. PCI Equation 5-32b tends to be the most accurate.

For cold joint roughened normalweight concrete specimens, f'_c ranges from 2495 psi to 15,218 psi, and $\rho f_{y,limited}$ ranges from 226 psi to 1576 psi. All three design provisions produce conservative values of shear strength for all specimens for the entire ranges of f'_c and $\rho f_{y,limited}$ tested. PCI Equation 5-32b tends to be the most accurate, and PCI Equation 5-32a and ACI Equation 22.9.4.2 are especially conservative for large values of f'_c.

For cold joint smooth normalweight concrete specimens, f'_c ranges from approximately 4860 psi to 14,326 psi, and $\rho f_{y,limited}$ ranges from 224 psi to 1498 psi. ACI Equation 22.9.4.2 and PCI Equation 5-32a produce some V_{test}/V_{calc} values less than 1.0 throughout the range of $\rho f_{y,limited}$. No trends are apparent with respect to compressive strength. Since PCI Equation 5-32b is not applicable for the cold joint smooth condition, it is omitted from the graph.

5.4.1.2 Lightweight Concrete

Figure 5.3 shows the ratio V_{test}/V_{calc} for the combined sand-lightweight and all-lightweight concrete specimens. Monolithic uncracked interface specimens are shown in the top row, monolithic pre-cracked interface specimens are shown in the second row, cold joint roughened interface are shown in the third row, and cold joint smooth interface specimens are shown in the bottom row. The graphs on the left of Figure 5.3 plot V_{test}/V_{calc} versus the compressive strength of concrete f'_c. The graphs on the right of Figure 5.3 plot V_{test}/V_{calc} versus the clamping stress $\rho f_{y,limited}$.

For sand-lightweight concrete specimens with a monolithic uncracked interface, f'_c ranges from approximately 3740 psi to 4770 psi, and $\rho f_{y,limited}$ ranges from 210 psi to 1368 psi. All three design equations produce conservative values of shear strength for all specimens, and PCI Equation 5-32b tends to be the most accurate.

For the pre-cracked monolithic sand-lightweight concrete specimens, f'_c ranges from 2000 psi to 11,020 psi, and $\rho f_{y,limited}$ ranges from 218 psi to 1368 psi. (It should be noted that the Mattock et al. [1969] series C specimens have values of f'_c that are lower than 2500 psi corresponding to the minimum values for structural concrete in accordance with the PCI Design Handbook (2010) and the ACI 318 Code (2014), but they are included in Figure 5.3 for completeness.) All three design equations produce some V_{test}/V_{calc} values less than 1.0. Figure 5.3 and Table B.2 show that PCI

Equation 5-32b tends to have values less than 1.0 for low values of $\rho f_{y,limted}$ and for the entire range of f'_c tested PCI Equation 5-32b tends to be the most accurate.

For cold joint roughened sand-lightweight concrete specimens, f'_c ranges from 4580 psi to 7200 psi, and $\rho f_{y,limited}$ ranges from 540 psi to 1320 psi. All three design provisions produce V_{test}/V_{calc} values larger than 1.0 for all specimens. PCI Equation 5-32b tends to be the most accurate.

For cold joint smooth sand-lightweight concrete specimens, f'_c ranges from approximately 4580 psi to 7200 psi, and $\rho f_{y,limited}$ ranges from 540 psi to 1320 psi. ACI Equation 22.9.4.2 and PCI Equation 5-32a produce V_{test}/V_{calc} values larger than 1.0 throughout the range of $\rho f_{y,limited}$ tested.

For monolithic uncracked all-lightweight concrete specimens, f'_c ranges from approximately 3880 psi to 4700 psi, and $\rho f_{y,limited}$ ranges from 230 psi to 1381 psi. Figure 5.3 shows that all three design equations produce conservative values of shear strength for all monolithic uncracked specimens, and PCI Equation 5-32b tends to be the most accurate.

For pre-cracked monolithic all-lightweight concrete specimens, f'_c ranges from 3880 psi to 4700 psi, and $\rho f_{y,limited}$ ranges from approximately 219 psi to 1404 psi. All three design equations produce some V_{test}/V_{calc} values less than 1.0. Figure 5.3 and Table B.2 show that PCI Equation 5-32b tends to have values less than 1.0 for low values of $\rho f_{y,limited}$. PCI Equation 5-32b tends to be the most accurate.

For cold joint roughened all-lightweight concrete specimens, f'_c ranges from approximately 4380 psi to 7843 psi, and all $\rho f_{y,limited}$ values are 780 psi. All three design equations produce V_{test}/V_{calc} values larger than 1.0 for the ranges of f'_c and $\rho f_{y,limited}$ tested. PCI Equation 5-32b tends to be the most accurate.

For cold joint smooth all-lightweight concrete specimens, f'_c ranges from 4380 psi to 7843 psi, and all $\rho f_{y,limited}$ values are 780 psi. ACI Equation 22.9.4.2 and PCI Equation 5-32a produce V_{test}/V_{calc} values larger than 1.0 for all data, with minimum values equal to or larger than 2.12 for both equations.

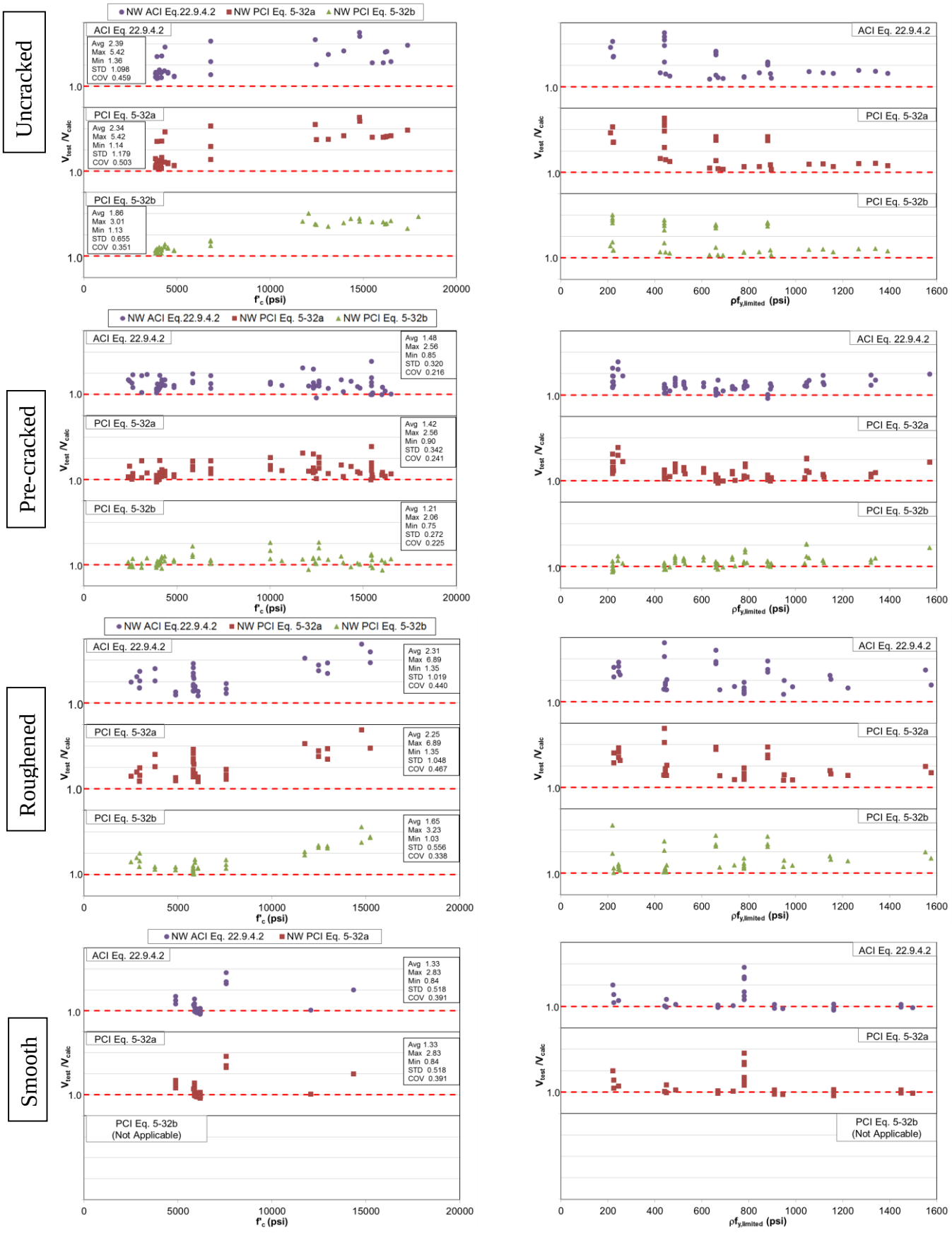

Figure 5.2 Ratio of measured shear strength V_{test} to the shear strength V_{calc} computed using PCI Design Handbook Equation 5-32a, and PCI Design Handbook Equation 5-32b, and ACI 318 Equation 22.9.4.2 versus f'_c and ρf_y for normalweight concrete specimens with different interface conditions: monolithic uncracked (first row), monolithic pre-cracked (second row), cold joint roughened (third row), and cold joint smooth (fourth row). The strength reduction factor ϕ is taken as 1.0 in the figures.

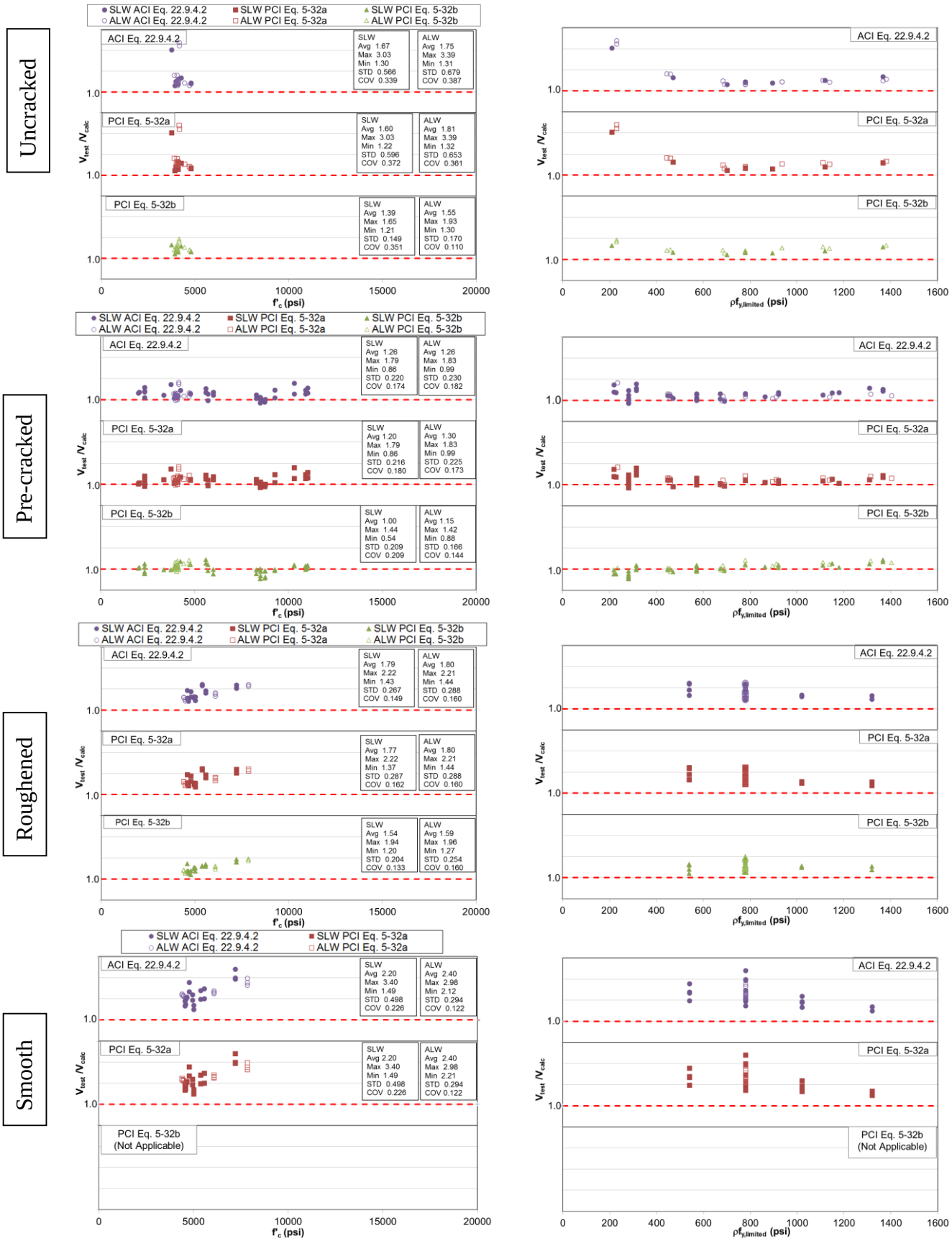

Figure 5.3 Ratio of measured shear strength V_{test} to the shear strength V_{calc} computed using PCI Design Handbook Equation 5-32a, and PCI Design Handbook Equation 5-32b, and ACI 318 Equation 22.9.4.2 versus f'_c and ρf_y for lightweight concrete specimens with different interface conditions: monolithic uncracked (first row), monolithic pre-cracked (second row), cold joint roughened (third row), and cold joint smooth (fourth row). The strength reduction factor ϕ is taken as 1.0 in the figures.

5.4.2. Effective Coefficient of Friction

This section compares the "effective" coefficient of friction μ_{test} associated with the measured shear strength V_{test} (or v_{test}) calculated using Equation 5.4 to the value of μ_e computed using PCI Equation 5-33 for specimens with different interface conditions (monolithic uncracked, monolithic pre-cracked, and cold joint roughened) and different concrete types (normalweight, sand-lightweight, and all-lightweight). As mentioned above, PCI Equation 5-32b is not applicable to cold joint smooth interface conditions, and therefore PCI Equation 5-33 is also not applicable for the cold joint smooth interface case.

$$\mu_{test} = \frac{v_{test}}{\rho f_{y,limited}} \tag{5.4}$$

In this evaluation, μ_{test} is computed with Equation 5.4 using the actual yield stress of the reinforcement taken equal to or less than 60,000 psi per the PCI Design Handbook (2010) and the ACI 318 code (2014), $f_{y,limited}$, for direct comparison with the design provisions. The value of μ_e computed using PCI Equation 5-33 is plotted against v_n considering $V_n=V_u/\phi$, where ϕ=1.0, and $v_n=V_n/A_{cr}$. The maximum values of μ_e and v_n specified by the PCI Design Handbook (2010) are also indicated in the graphs. Because the maximum value of v_n is a function of the concrete type, normalweight, sand-lightweight, and all-lightweight concrete specimens are presented separately.

5.4.2.1 Normalweight Concrete

Figure 5.4 plots the values of μ_{test} associated with v_{test} for the normalweight concrete specimens for the monolithic uncracked, monolithic pre-cracked, and roughened interface conditions (note that smooth interface specimens are discussed later in Section 5.5.3). For the monolithic uncracked and pre-cracked interface conditions, data from Tables A.1 and A.2 with f'_c greater than or equal to 3333 psi are plotted in the figures for consistency with the limits on v_n plotted in the graph (Table 5.1). The only specimens that did not meet this criterion are specimens 2.1 and 2.2 and series 5 by Hofbeck et al. (1969) in Table B.2. For the roughened interface condition, data with f'_c greater than or equal to 4000 psi are plotted in the figure for the same reason, which included all specimens in Table B.3 except for series D by Mattock (1976). Figure 5.4 shows that PCI Equation 5-33 is conservative (all values of μ_{test} plotted to the right and above the equation) for the monolithic uncracked specimens. For the monolithic pre-cracked specimens, there were several unconservative values with respect to PCI Equation 5-33. PCI Equation 5-33 is conservative for the roughened interface conditions.

For comparison, the coefficient of friction μ specified by the PCI Design Handbook (2010) and the ACI 318 code (2014) and used in PCI Equation 5-32a and ACI Equation 22.9.4.2, respectively, is also plotted in Figure 5.4 for the monolithic uncracked, monolithic pre-cracked, and roughened interface conditions, as well as for the cold joint smooth interface condition, using the values in Table 5.1 and including the limitations on v_n (Table 5.1). For the smooth interface condition, data with f'_c greater than or equal to 4000 psi are plotted in the figure, which included all normalweight concrete specimens in Table B.4. Since the coefficient of friction μ is the lower bound of the effective coefficient of friction μ_e, Figure 5.4 shows the value of μ specified by the PCI Design Handbook (2010) and the ACI 318 code (2014) is generally conservative with respect to the test results for each concrete type and interface condition, when the limit for the maximum shear stress is also considered (with the exception of a few normalweight concrete monolithic pre-cracked specimens and some normalweight concrete specimens with a cold joint smooth interface). This

can also be observed from Tables A.1-A.4 where PCI Equation 5-32a and ACI Equation 22.9.4.2 produce values of V_{test}/V_{calc} larger than 1.0 for nearly all specimens, with no value being less than 0.84.

5.4.2.2 Lightweight Concrete

Figure 5.5 plots the values of μ_{test} associated with v_{test} for the sand-lightweight concrete specimens for the monolithic uncracked, monolithic pre-cracked, and roughened interface conditions (note that smooth interface specimens are discussed later in Section 5.5.3). Series C by Mattock et al. (1976) in Table B.2 is omitted from the graph because the values of f'_c were lower than values corresponding to the limits on v_n plotted in the graphs (Table 5.1). All values of μ_{test} for the monolithic uncracked and the roughened interfaces were conservative compared to PCI Equation 5-33. Several of the monolithic pre-cracked specimens, however, were unconservative.

Figure 5.6 shows the value of μ_{test} for the all-lightweight concrete specimens. All values of μ_{test} for the monolithic uncracked and the roughened interfaces were conservative compared to PCI Equation 5-33. Values of μ_{test} for the monolithic pre-cracked specimens were closely predicted by PCI Equation 5-33, however, there were a few unconservative values.

For comparison, the coefficient of friction μ specified by the PCI Design Handbook (2010) and the ACI 318 code (2014) and used in PCI Equation 5-32a and ACI Equation 22.9.4.2, respectively, is also plotted in Figures 5.5 and 5.6 for the monolithic uncracked, monolithic pre-cracked, and roughened interface conditions, as well as for the cold joint smooth interface condition, using the values in Table 5.1 and including the limitations on v_n (Table 5.1). For the smooth interface condition, data with f'_c greater than or equal to 4000 psi are plotted in the figure, which included all lightweight concrete specimens in Table B.4. Since the coefficient of friction μ is the lower bound of the effective coefficient of friction μ_e, Figures 5.5 and 5.6 show the value of μ specified by the PCI Design Handbook (2010) and the ACI 318 code (2014) is generally conservative with respect to the test results for each concrete type and interface condition, when the limit for the maximum shear stress is also considered (with the exception of a few monolithic pre-cracked lightweight concrete specimens). This can also be observed from Tables A.1-A.4 where PCI Equation 5-32a and ACI Equation 22.9.4.2 produce values of V_{test}/V_{calc} larger than 1.0 for nearly all specimens, with no value being less than 0.86.

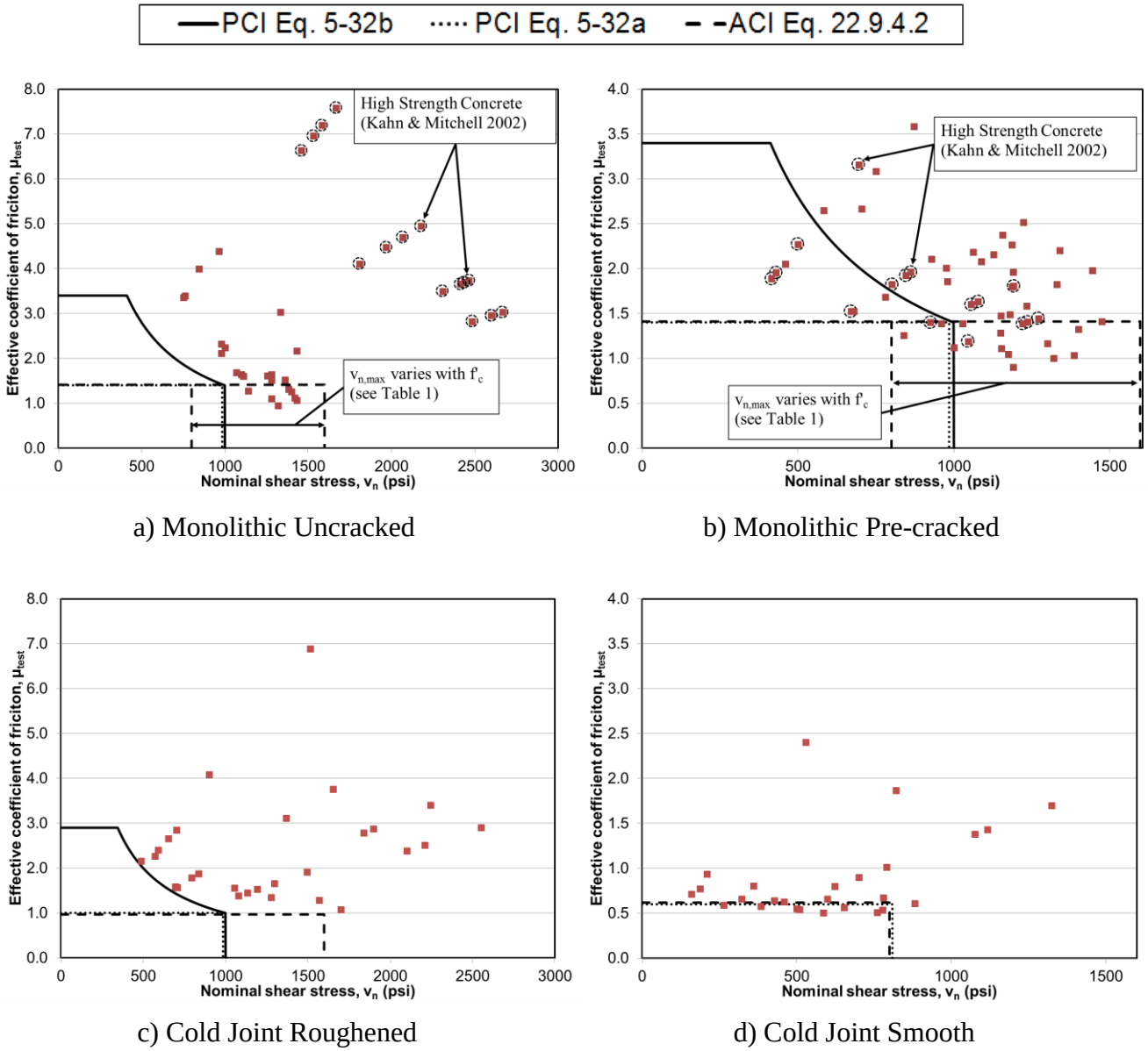

Figure 5.4 Effective coefficient of friction μ_{test} for normalweight concrete specimens with a a) monolithic uncracked, b) monolithic pre-cracked, c) roughened, and d) smooth interface

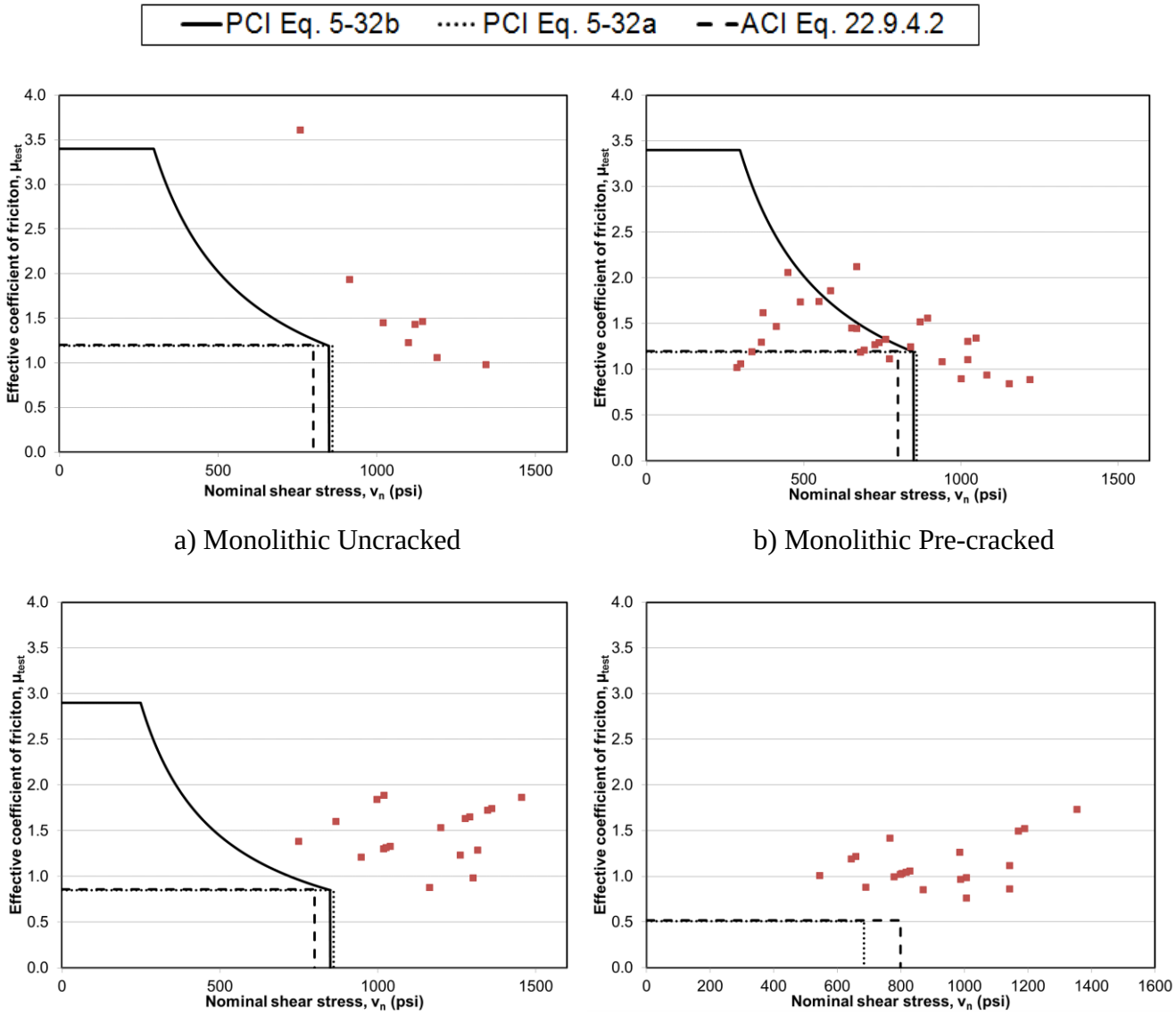

Figure 5.5 Effective coefficient of friction μ_{test} for sand-lightweight concrete specimens with a a) monolithic uncracked, b) monolithic pre-cracked, c) roughened, and d) smooth interface

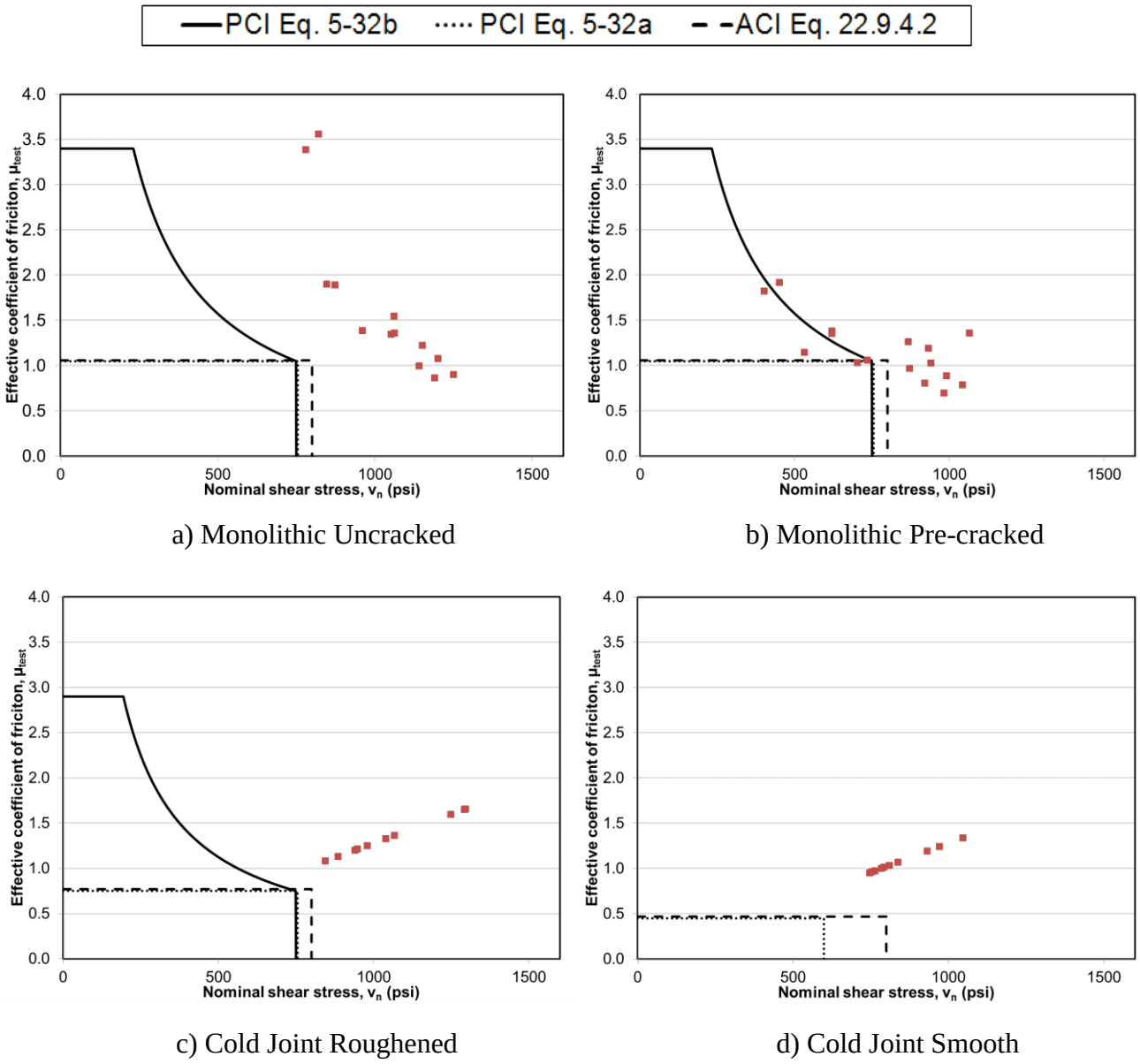

a) Monolithic Uncracked

b) Monolithic Pre-cracked

c) Cold Joint Roughened

d) Cold Joint Smooth

Figure 5.6 Effective coefficient of friction μ_{test} for all-lightweight concrete specimens with a a) monolithic uncracked, b) monolithic pre-cracked, c) roughened, and d) smooth interface

5.5. DISCUSSION

5.5.1. Comparison of Shear-friction Design Equations

Values of V_{test}/V_{calc} summarized in Tables A.1, A.2, and A.3 indicate that PCI Equation 5-32b (μ_e-approach) is more accurate (i.e., mean value closest to 1.0) and has a lower coefficient of variation than both PCI Equation 5-32a and ACI Equation 22.9.4.2 (μ-approach) for normalweight, sand-lightweight, and all-lightweight concrete with monolithic uncracked, monolithic pre-cracked, and cold joint roughened interface conditions. Values of V_{test}/V_{calc} computed using PCI Equation 5-32a and ACI Equation 22.9.4.2 are more conservative (i.e., larger mean value) than values computed using PCI Equation 5-32b. For PCI Equation 5-32a and ACI Equation 22.9.4.2, no values of V_{test}/V_{calc} are lower than 0.75, which is the value of the strength reduction factor ϕ for shear (PCI 2010 and ACI 2014). For PCI Equation 5-32b, the only values of V_{test}/V_{calc} less than 0.75 are pre-cracked sand-lightweight concrete specimens tested by Hoff (1993) with low values of $\rho f_{y,limited}$ (281 psi). However, the shear strength of these specimens exhibited a large degree of scatter, and specimens tested by Mattock et al. (1976) with lower values of $\rho f_{y,limted}$ and lower concrete compressive strength (specimens B1, C1, and D1 in Table B.2) had higher shear strengths. Therefore, the cause of these low values is unknown.

For specimens with a smooth interface condition, Table B.4 shows that average values and coefficients of variation of V_{test}/V_{calc} using PCI Equation 5-32a and ACI Equation 22.9.4.2 are similar for normalweight, sand-lightweight, and all-lightweight concrete. Since PCI Equation 5-32b is not applicable for this case, it is not compared. For both equations, no values of V_{test}/V_{calc} are lower than 0.75.

5.5.2. Distribution of Data

With regard to the distribution of data, Figure 5.2 shows that there is a gap in the data for normalweight concrete specimens with 7000 psi < f'_c <11,000 psi for all interface conditions. Comparison of Figures 5.2 and 5.3 indicates that the available sand-lightweight and all-lightweight concrete test data have a much smaller range of compressive strength than the available normalweight concrete test data for all interface conditions. Figures 5.2 and 5.3 show a consistent range of available test data with respect to clamping stress, with the exception of sand-lightweight and all-lightweight with cold joint roughened and smooth interfaces, where data are lacking for low values of $\rho f_{y,limited}$. With respect to shear interface area, Figure 5.1 shows that most specimens (91%) were of similar size, i.e. A_{cr} of approximately 50 in^2 or 60 in^2; 6% had an A_{cr} of approximately 84 in^2; and 3% had an A_{cr} of approximately 160 in^2.

5.5.3. Use of λ in the Coefficient of Friction μ for a Cold Joint Smooth Interface Condition

For the cold joint smooth interface condition, Figures 5.4, 5.5, and 5.6 bottom right show that the value of the coefficient of friction μ (0.6λ) specified by the PCI Design Handbook (2010) and the ACI 318 code (2014) for normalweight concrete is in good agreement with values determined from the test results using Equation 2, whereas values of μ specified for sand-lightweight and all-lightweight concrete are conservative with respect to the test results. This is in part because the term λ in the coefficient of friction μ (Table 5.1) reduces the value of μ for sand-lightweight and all-lightweight concrete by a factor of 0.85 and 0.75, respectively. In fact, values of μ_{test} determined for the sand-lightweight and all-lightweight concrete specimens with a cold joint smooth interface were higher than those of the normalweight concrete specimens with a smooth interface in most

cases. This can be explained by the fact that the normalweight concrete specimens included in Table B.4 by Mattock (1976) had a broken bond, were pre-cracked, or both, whereas the sand-lightweight and all-lightweight specimens by Sneed and Shaw (2013) and the present study were cast with a smooth cold joint and were not pre-cracked. In his 2001 paper, Mattock pointed out that the shear strength of these normalweight concrete specimens was equal to the shear yield strength of the reinforcement perpendicular to the interface (hence the value of 0.6 in the coefficient of friction μ=0.6λ, Table 5.1), and that true shear-friction across a smooth interface cannot be developed in the absence of interfacial roughness. Additionally, since there is no aggregate crossing the shear interface, the strength of the aggregate should not influence the shear transfer strength. Given this reasoning and the results shown in Figures 5.5 and 5.6 bottom right, there does not appear to be a justification for including the term λ in the coefficient of friction μ for the smooth interface condition in the PCI Design Handbook (2010) and ACI 318 code (2014). Thus, the authors recommend removing the term λ in the coefficient of friction μ for a smooth interface condition (Case 3) to provide more accurate and economical designs.

5.6. CONCLUDING REMARKS

This section presented a database of shear-friction test results collected from the literature and analyzed the results in terms of the effective coefficient of friction μ_e-approach used in the PCI Design Handbook (2010), and the coefficient of friction μ-approach used in the PCI Design Handbook and the ACI 318 code (2014). Gaps in the literature were identified and discussed. Results of the analysis led to the following conclusions:

1. Values of V_{test}/V_{calc} from the database indicate that PCI Equation 5-32b (μ_e–approach) is more accurate and has a lower standard deviation than both PCI Equation 5-32a and ACI Equation 22.9.4.2 (μ-approach) for normalweight, sand-lightweight, and all-lightweight concrete with monolithic uncracked, monolithic pre-cracked, and cold joint roughened interface conditions. For PCI Equation 5-32a and ACI Equation 22.9.4.2, no values of V_{test}/V_{calc} were lower than 0.75. For PCI Equation 5-32b, the only values lower than 0.75 are pre-cracked sand-lightweight concrete specimens tested by Hoff[20] with low values of $\rho f_{y,limted}$ (281 psi). The cause of these low values is unknown.
2. Values of V_{test}/V_{calc} from the database show that PCI Equation 5-32a and ACI Equation 22.9.4.2 provide an accurate estimation of the shear transfer strength for normalweight concrete with a cold joint smooth interface condition. PCI Equation 5-32a and ACI Equation 22.9.4.2 provide conservative estimations of the shear transfer strength for sand-lightweight, and all-lightweight concrete with a cold joint smooth interface condition.
3. There does not appear to be a justification for including the term λ in the coefficient of friction μ=0.6λ for the cold joint smooth (i.e., “concrete placed against hardened concrete not intentionally roughened”) interface condition in the PCI Design Handbook (2010) and ACI 318 code (2014). Therefore it is recommended to remove the term λ in the coefficient of friction μ for a smooth interface condition (Case 3 in Table 5.1) to provide more accurate and economical designs.

6. SUMMARY, CONCLUSIONS, AND RECOMMENDATIONS

6.1 SUMMARY

This study examined the influence of lightweight aggregate concrete on the direct shear transfer across a concrete surface with different interface conditions, including monolithic and cold joints. Cold joint interfaces are common in precast and prestressed concrete elements such as corbels, composite sections, or connections of shear walls to foundations. In these cases, the shear-friction design provisions are used to design for the interface shear. The shear-friction design provisions in the PCI Design Handbook (2010) and the ACI 318 code (2014) are mainly empirical and based on experimental data. Limited data exists with respect to lightweight aggregate concretes. However, increasing use of lightweight concrete motivated this research to determine the validity and conservatism of the current shear-friction design provisions for sand-lightweight and all-lightweight concretes.

The study presented in this report was the second phase of an ongoing investigation of the direct shear transfer across an interface of lightweight aggregate concretes. Results from the first phase of the study were presented in the report by Sneed and Shaw (2013), who studied the shear transfer strength of lightweight aggregate concretes made with expanded shale lightweight aggregate and a cold joint interface condition. In the second phase of the study, the shear transfer strength of lightweight aggregate concretes made with different types of structural lightweight aggregates was investigated. Lightweight aggregate concretes were made with different lightweight aggregate materials (expanded shale, expanded slate, or expanded clay), different interface conditions (monolithic or cold joint), and different reinforcement ratios.

The results of 52 push-off type normalweight and lightweight concrete specimens were evaluated in this phase of the study, and results are summarized in this report. The specimens were cast either monolithically (12 total) or non-monolithically (40 total). Each specimen's target concrete compressive strength was 5000 psi. The unit weight of concretes used ranged between 88 pcf to 148 pcf. For the non-monolithic (cold joint) specimens, the shear plane was either troweled smooth or roughened to an average amplitude of 0.25 in. Lightweight aggregates used to make the lightweight concretes were expanded shale, expanded slate, and expanded clay. The specimens had the shear plane area of 49.5 in^2 that was crossed with closed stirrups constructed using No. 3 deformed steel reinforcing bars. Each monolithic series as well as the slate all-lightweight and clay all-lightweight cold joint series were constructed using three stirrups across the shear plane to create a reinforcement ratio of $\rho = 0.013$. The slate sand-lightweight series and the clay sand-lightweight series contained specimens with varied reinforcement ratios. Either 2, 3, 4, or 5 stirrups were evenly spaced across the shear plane to create reinforcement ratios of 0.009, 0.013, 0.017, or 0.022, respectively.

Data presented for each series was used to analyze the influence of concrete unit weight, lightweight aggregate type, interface condition, and reinforcement ratio on the shear transfer strength of the specimens. Results were compared with the results of previous researchers. Test results were also combined with those from previous research and compared to current design provisions of the PCI Design Handbook (2010) and the ACI 318 code (2014).

6.2. CONCLUSIONS

Based on the results of this study, the following conclusions are made. Conclusions 1-7 summarize the key findings from the experimental work in this study, while Conclusions 8-11 are regarding the PCI and ACI shear friction design provisions:

1. The peak shear stress of the monolithic interface specimens with the same reinforcement ratio (ρ=0.013) increased with increasing unit weight for both monolithic uncracked and pre-cracked specimens. The peak shear stress of cold joint specimens with an intentionally roughened interface increased as the unit weight of concrete increased. The peak shear stress of cold joint specimens with smooth interface appeared to be independent of type or unit weight of concrete.
2. The peak shear stress of roughened interface cold joint specimens was higher than the peak shear stress of smooth interface cold joint specimens with the same reinforcement ratio regardless of lightweight aggregate material.
3. The sand-lightweight concrete specimens achieved a higher peak shear stress than the all-lightweight concrete specimens with the same lightweight aggregate material and reinforcement ratio for all interface conditions.
4. A pre-existing crack reduced the peak shear stress of normalweight, sand-lightweight, and all-lightweight concrete specimens relative to the corresponding uncracked monolithic specimens.
5. The peak shear stress of specimens with a roughened interface appeared to be influenced by lightweight aggregate material. The peak shear stress of lightweight concretes made with expanded slate aggregate was higher than the peak shear stress of lightweight concretes made with expanded clay aggregate for roughened interface specimens. The peak shear stress of specimens with a smooth interface appeared to be independent of lightweight aggregate material.
6. Six of the sand-lightweight specimens with clay aggregate and a high reinforcement ratio (ρ=0.017 or 0.022) failed due to concrete splitting prior to shear failure, which was attributed to the low tensile strength of concrete.
7. The peak shear stress of the sand-lightweight specimens with clay and slate aggregates increased with increasing reinforcement parameter ρf_y; however, particularly for specimens with a roughened interface, the peak shear stress values leveled off after approximately ρf_y = 1200 psi.
8. Shear strengths computed by the ACI 318 (2014) code Equation 22.9.4.2, and the PCI Design Handbook (2010) Equation 5-32a using the coefficient of friction μ-approach were conservative for the sand-lightweight and all-lightweight monolithic and cold joint specimens in this study. Similarly, shear strengths computed by the PCI Design Handbook (2010) Equation 5-32b using the effective coefficient of friction μ_e-approach were conservative for the sand-lightweight and all-lightweight monolithic and cold joint roughened interface specimens in this study. In other words, the use of λ in ACI Equation 22.9.4.4, PCI Equation 5-32a, and PCI Equation 5-32b provided conservative designs for all lightweight aggregates included in this study.
9. Values of V_{test}/V_{calc} from the database presented in Section 5 indicate that PCI Equation 5-32b (μ_e–approach) is more accurate and has a lower standard deviation than both PCI Equation 5-32a and ACI Equation 22.9.4.2 (μ-approach) for normalweight, sand-lightweight, and all-lightweight concrete with monolithic uncracked, monolithic pre-

cracked, and cold joint roughened interface conditions. For PCI Equation 5-32a and ACI Equation 22.9.4.2, no values of V_{test}/V_{calc} were lower than 0.75. For PCI Equation 5-32b, the only values lower than 0.75 are pre-cracked sand-lightweight concrete specimens tested by Hoff (1992) with low values of $\rho f_{y,limted}$ (281 psi). The cause of these low values is unknown.

10. Values of V_{test}/V_{calc} from the database show that PCI Equation 5-32a and ACI Equation 22.9.4.2 provide an accurate estimation of the shear transfer strength for normalweight concrete with a cold joint smooth interface condition. PCI Equation 5-32a and ACI Equation 22.9.4.2 provide conservative estimations of the shear transfer strength for sand-lightweight, and all-lightweight concrete with a cold joint smooth interface condition.
11. There does not appear to be a justification for including the term λ in the coefficient of friction μ=0.6λ for the cold joint smooth (i.e., "concrete placed against hardened concrete not intentionally roughened") interface condition in the PCI Design Handbook (2010) and ACI 318 code (2014). Therefore it is recommended to remove the term λ in the coefficient of friction μ for a smooth interface condition (Case 3 in Table 5.1) to provide more accurate and economical designs.

6.3. RECOMMENDATIONS FOR DESIGN EQUATIONS

The authors recommend that the coefficient of friction μ be taken as 0.6 (not as 0.6λ) for concrete placed against hardened concrete not intentionally roughened in the shear-friction provisions in the PCI Design Handbook (2010) and the ACI 318 code (2014).

6.4. RECOMMENDATIONS FOR FUTURE WORK

The primary recommendation for future work is to expand on the effort initiated in Section 5 of this report. In this study, the influence of lightweight aggregate concrete on the shear transfer strength was investigated. The experimental programs in both phases one and two of this project were designed to isolate specific test variables to examine their influence on the shear strength, and results are presented in Section 4. As discussed in Section 2, several parameters and mechanisms exist that influence the shear transfer strength. In order to properly evaluate existing and proposed shear-friction design provisions, a comprehensive database is needed. The work presented in Section 5 of this report lays the groundwork for a comprehensive evaluation of shear-friction design provisions. At this stage, a database has been developed (Appendix B) and used to evaluate existing shear-friction design provisions in the PCI Design Handbook (2010) and the ACI 318 code (2014) (Section 5). In its current form, the database is limited to pushoff specimens subjected to monotonic loading and without external normal forces. The database presented in this report should be expanded to include other types of loading, specimens with normal forces, etc. As future work, the database could be used to evaluate potential revisions to the shear-friction design provisions in the PCI Design Handbook and ACI 318 code (e.g., values of μ or μ_e, λ, $V_{n,max}$, $\mu_{e,max}$), or to evaluate different shear-friction models (e.g., AASHTO 2014).

Other recommendations for future work include the following:

1. A common industry practice is to make sand-lightweight concrete using lightweight coarse aggregate as a partial substitute for normalweight coarse aggregate. A study to determine the loss of shear strength with certain percentages of normalweight aggregate replaced would determine the validity of ACI 318-14 provision in Table 19.2.4.2. This

provision states that λ may be linearly interpolated between 0.85 and 1.0 on the basis of volumetric fractions, for concrete containing a partial replacement of normalweight coarse aggregate with lightweight coarse aggregate.

2. It would be useful to study the individual contributions of concrete and reinforcing steel to the shear strength of an interface. Decoupling the concrete and steel components could be done in a similar manner as was done by Harries et al. (2012) and would further describe the fundamental mechanisms of shear-friction.
3. The lightweight aggregates used in this study (expanded shale, slate, clay) all had the same maximum nominal size (3/8 in.). Follow-up research is needed to investigate the influence of maximum aggregate size on shear-friction in cold joint specimens.
4. For the purposes of this research the compressive strength of each lightweight aggregate type concrete was nominally the same. Further investigation is needed to determine the effect of various compressive strengths for each lightweight aggregate type concrete.
5. From the distribution of data shown in Figure 5.1, the size of shear plane for the push-off type specimens has not changed much throughout the history of shear-friction investigation. Therefore, potential size effect issues have not been investigated. It is recommended to examine the effect of the shear plane area (keeping the reinforcement ratio constant) on shear transfer capacity.
6. In this study, the casting of the two parts of cold joint specimens was performed with an eight-hour delay to eliminate differences in compressive strength of concretes. This, however, is not the case in the precast prestressed concrete industry. Further research is needed to investigate the influence of longer time period between the casting of the two sections on the shear transfer strength.
7. During the process of this research, it was found that there is no uniform procedure used in pre-cracking monolithic specimens. This may be one of the causes for the relatively large amount of scatter in the data for specimens with a monolithic pre-cracked interface. It would be beneficial for the consistency of data to determine the most efficient and uniform way to pre-crack the push off type specimens.

Appendix A

A. TEST SPECIMEN RESPONSES

A.1 INTRODUCTION

This section presents the shear force-slip relation, shear force-dilation relation, slip-dilation, stress-strain, slip-strain, and dilation-strain relation for each set of test specimens. The values from the two DC-LVDTs measuring slip are averaged for the two faces of the specimen. The values from the DC-LVDTs measuring dilation are averaged also. The strain values, for which noise was an issue, were manually corrected. The strain values were then averaged for all properly functioning strain gages.

A.2 NORMALWEIGHT CONCRETE SPECIMENS

This section presents the results of the normalweight concrete specimens. Specimens presented in this section include series N-MO-U and N-MO-P. These specimens were tested on 2/20/2015. All specimens failed in shear along the shear plane. Horizontal hairline flexural cracks were observed on the side edges of the specimens as shown in Figure A.1. These cracks were typical for all normalweight concrete specimens. The hairline cracks were observed to have no influence on the instrumentation and did not appear to affect the data being recorded. A significant amount of noise was observed in the strain readings during the testing. This can be seen in the figures that follow. The strain gage noise in specimen N-MO-P-1 exceeded values that the strain gage can read according to the manufacturer. For this reason the strain gage readings associated with specimen N-MO-P-1 were deemed unusable and are not displayed in the figures below. Figure A.2 shows the applied shear force versus slip relations for all normalweight concrete specimens. Figure A.3 presents the shear force versus interface dilation relations. Figure A.4 displays slip versus dilation. Figure A.5 shows the applied shear force versus shear reinforcement strain. Figure A.6 shows the slip versus strain relations. And lastly, Figure A.7 shows the dilation versus strain relations.

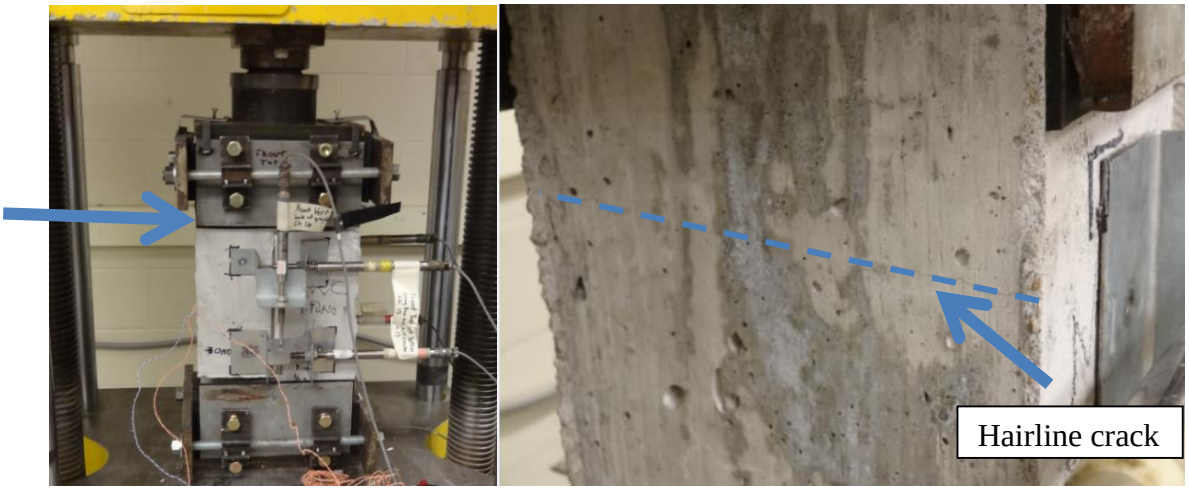

Figure A.1 Location and Example of Hairline Flexural Cracks

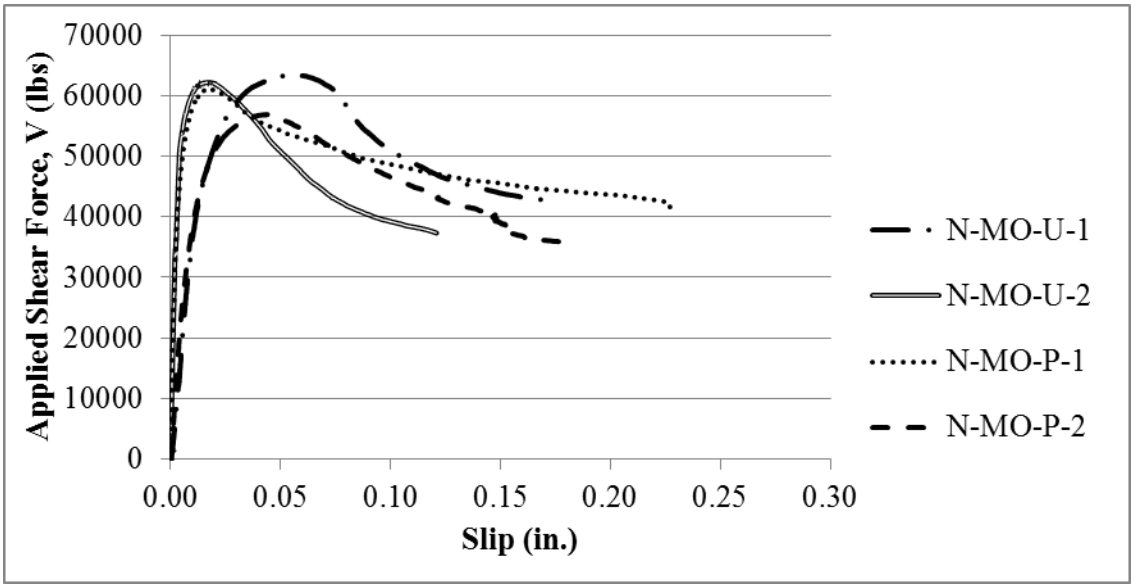

Figure A.2 Applied Shear Force vs. Slip for Normalweight Concrete Monolithic Interface Specimens

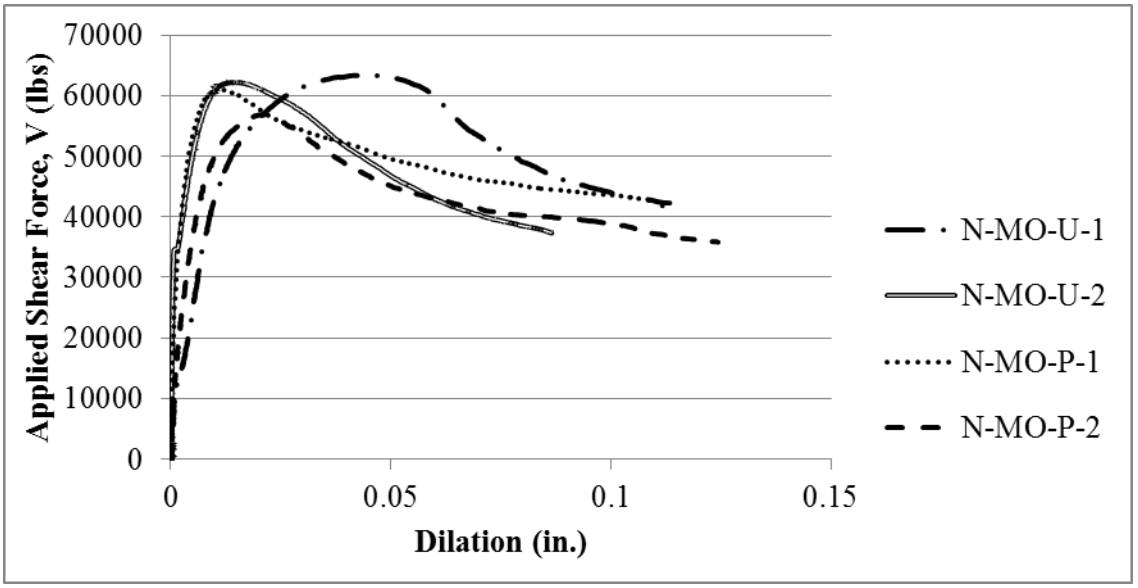

Figure A.3 Applied Shear Force vs. Dilation for Normalweight Concrete Monolithic Interface Specimens

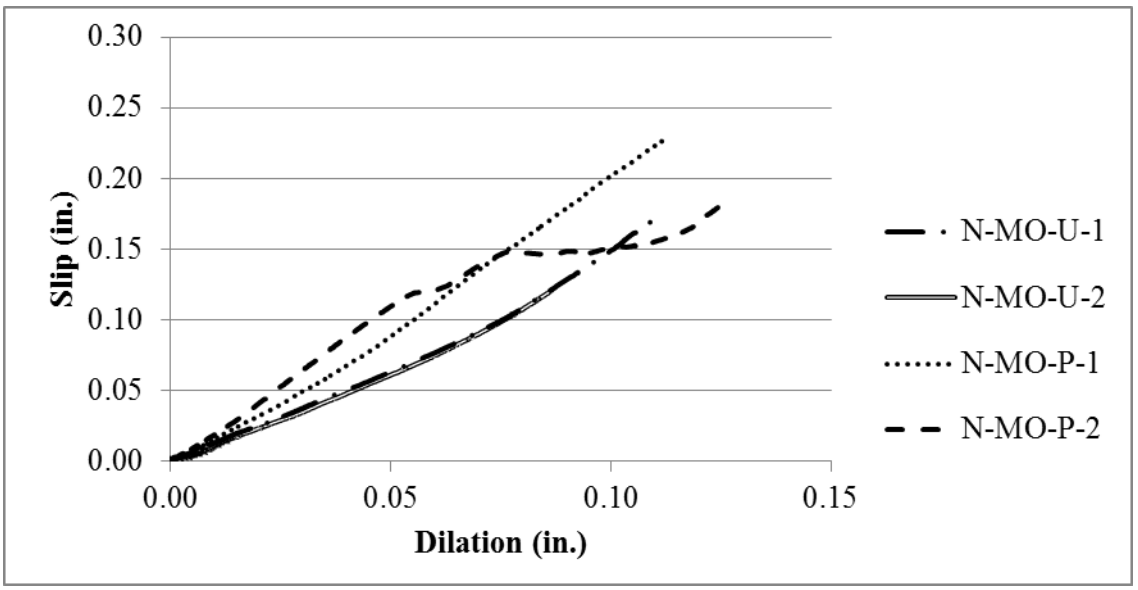

Figure A.4 Slip vs. Dilation for Normalweight Concrete Monolithic Interface Specimens

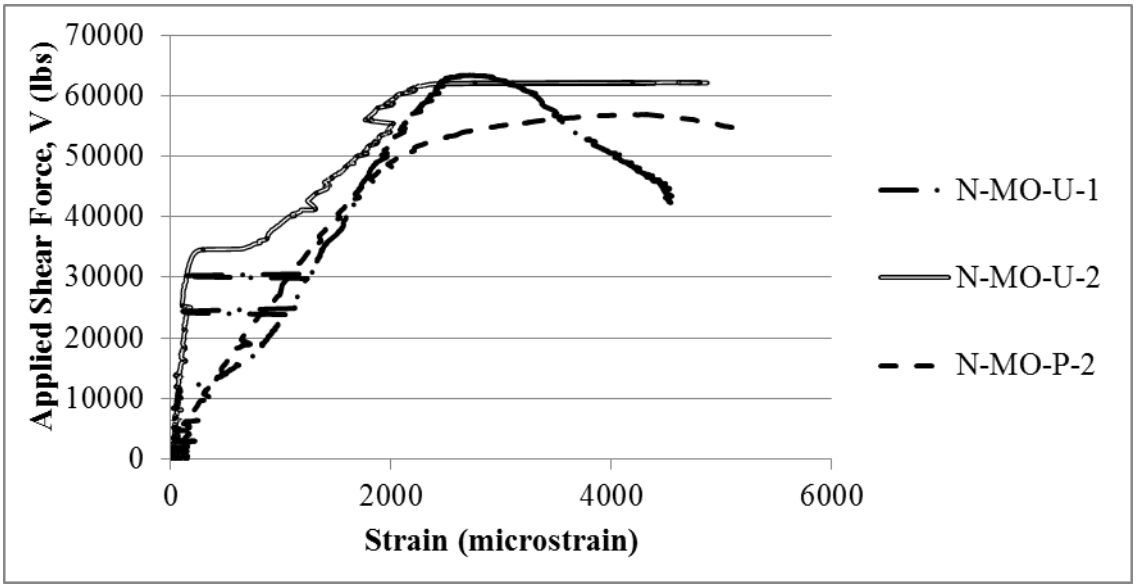

Figure A.5 Applied Shear Force vs. Shear Reinforcement Strain for Normalweight Concrete Monolithic Interface Specimens

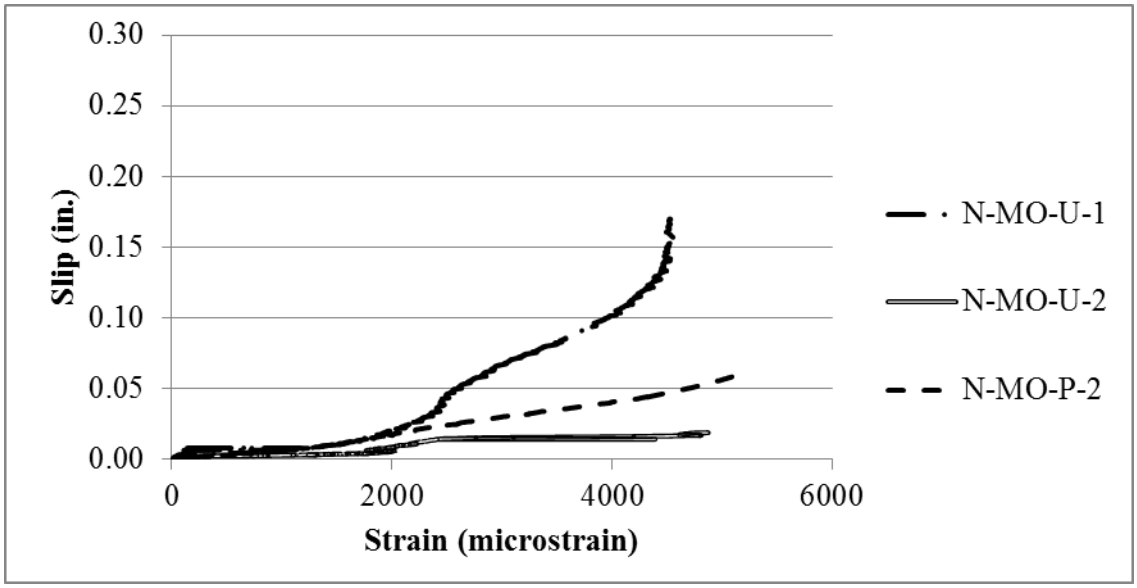

Figure A.6 Slip vs. Shear Reinforcement Strain for Normalweight Concrete Monolithic Interface Specimens

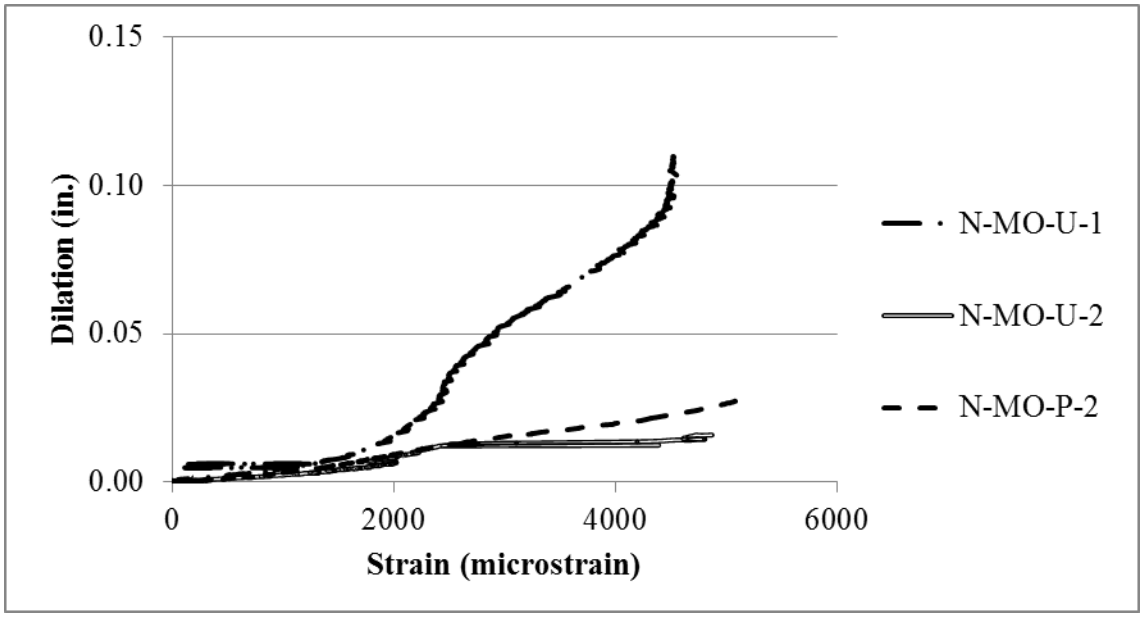

Figure A.7 Dilation vs. Shear Reinforcement Strain for Normalweight Concrete Monolithic Interface Specimens

A.3 SAND-LIGHTWEIGHT CONCRETE SPECIMENS

This section presents the results of the sand-lightweight concrete specimens with a monolithic or cold joint interface. Specimens presented in this section include series S-SH-MO-U, S-SH-MO-P, S-SL-CJ-R, S-SL-CJ-S, S-CL-CJ-R, and S-CL-CJ-S. The testing of expanded shale aggregate sand-lightweight concrete specimens was conducted on 2/25/15. The testing of expanded slate aggregate sand-lightweight concrete specimens was conducted on 2/27/15. The testing of expanded clay aggregate sand-lightweight concrete was conducted on 5/6/15.

A.3.1 Shale aggregate sand-lightweight concrete specimens

All shale aggregate concrete specimens had a monolithic interface. Specimens presented in this section include series S-SH-MO-U and S-SH-MO-P. Hairline flexural cracking was observed in the same location as for the normalweight concrete specimens (Section A.1). A typical crack is shown in Figure A.8. All specimens failed in shear along the shear plane. Figure A.9 shows the applied shear force versus slip relations for the shale sand-lightweight concrete specimens. Figure A.10 presents the shear force versus interface dilation relations. Figure A.11 displays the slip versus dilation relations. Figure A.12 shows the applied shear force versus shear reinforcement strain. Figure A.13 shows the slip versus interface steel strain relations. And finally, Figure A.14 shows dilation versus interface steel strain.

Figure A.8 Typical Hairline Flexural Flange Crack Observed In Shale Aggregate Concrete Specimens

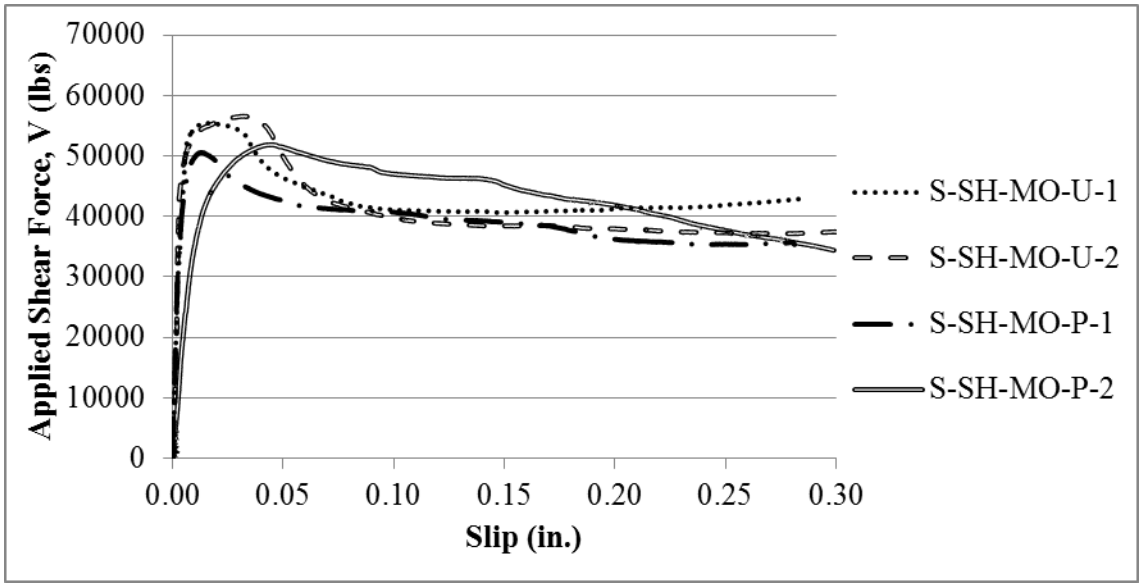

Figure A.9 Applied Shear Force vs. Slip for Shale Sand-Lightweight Concrete Monolithic Interface Specimens; ρ = 0.013

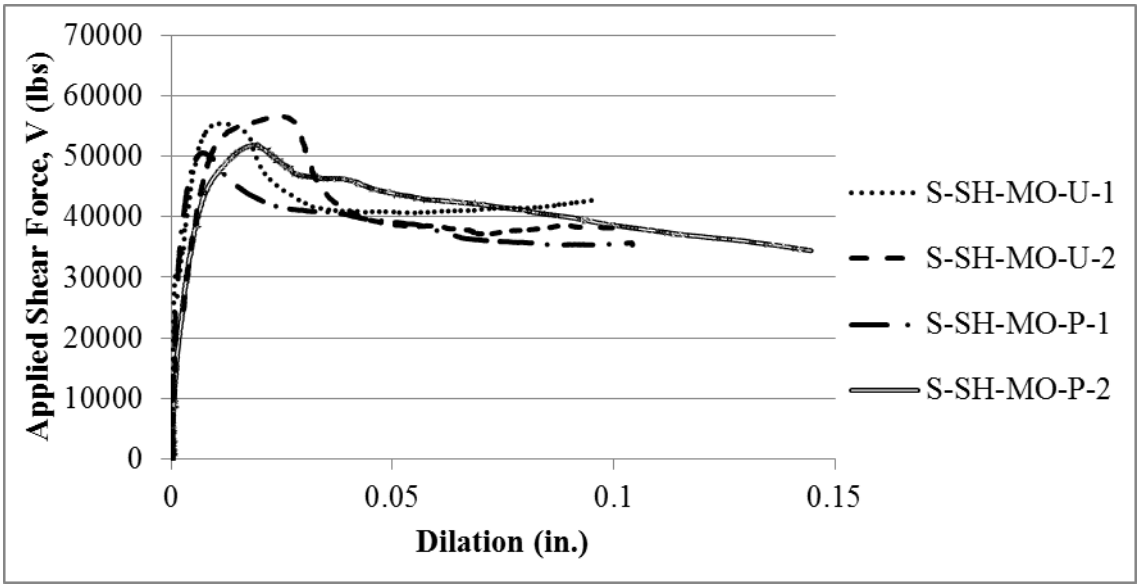

Figure A.10 Applied Shear Force vs. Dilation for Shale Sand-Lightweight Concrete Monolithic Interface Specimens; $\rho = 0.013$

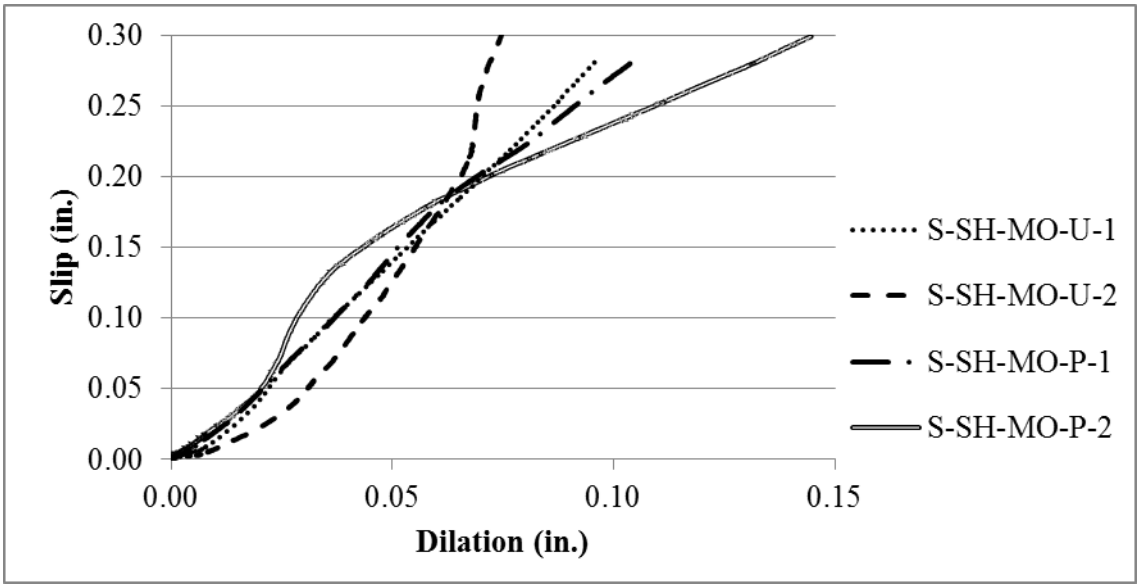

Figure A.11 Slip vs. Dilation for Shale Sand-Lightweight Concrete Monolithic Interface Specimens; $\rho = 0.013$

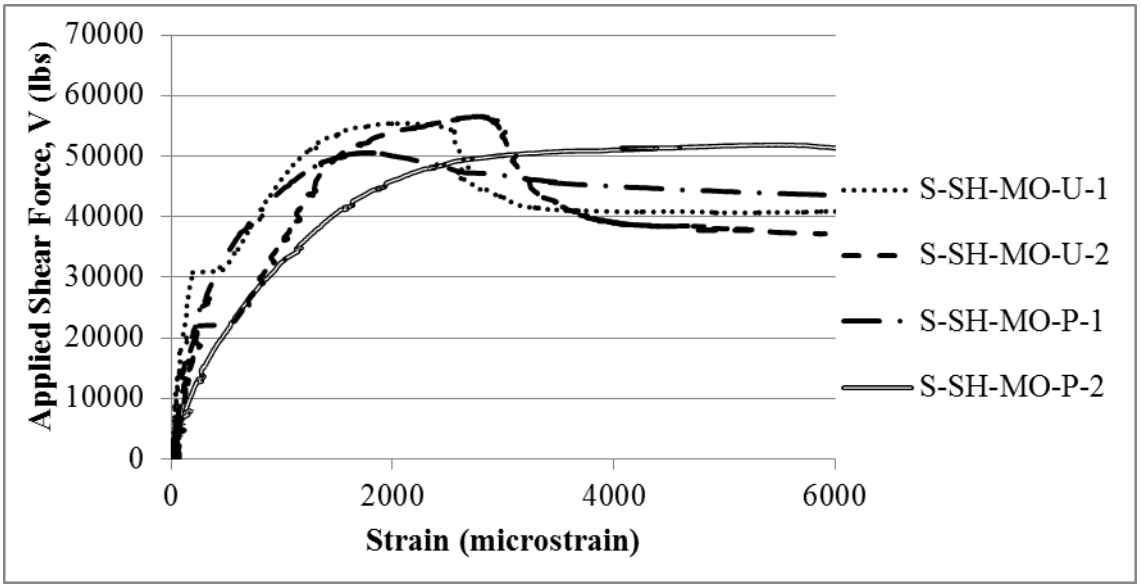

Figure A.12 Applied Shear Force vs. Shear Reinforcement Strain for Shale Sand-Lightweight Concrete Monolithic Interface Specimens; $\rho = 0.013$

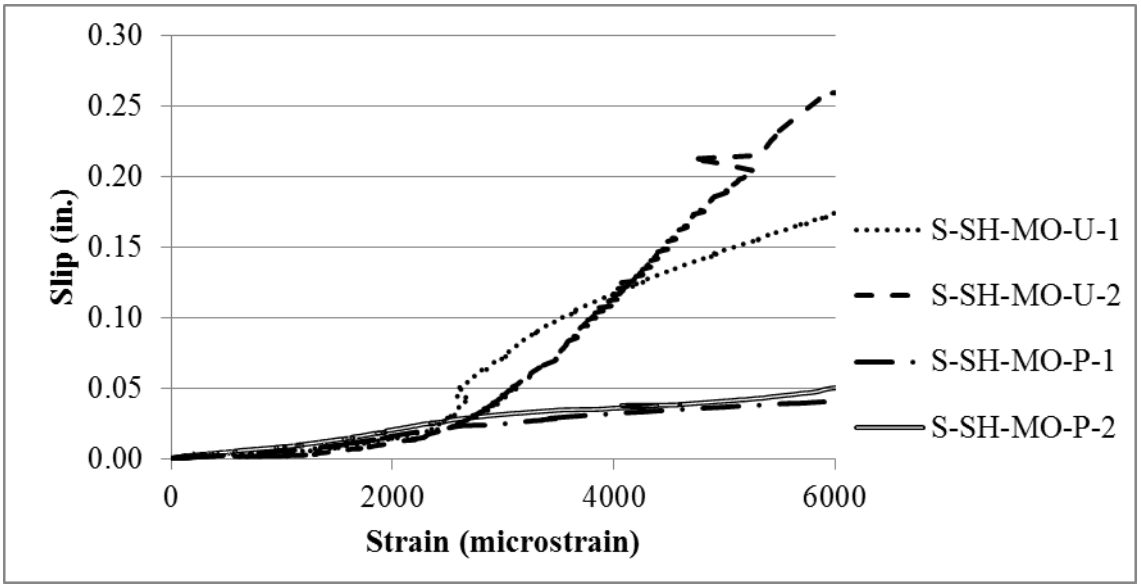

Figure A.13 Slip vs. Shear Reinforcement Strain for Shale Sand-Lightweight Concrete Monolithic Interface Specimens; $\rho = 0.013$

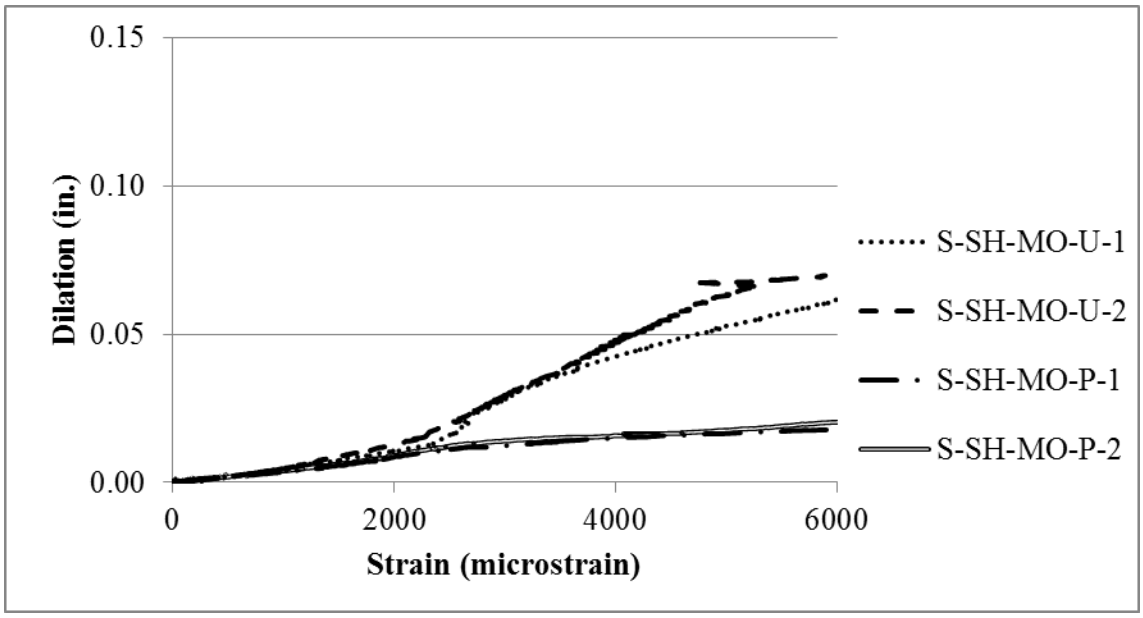

Figure A.14 Dilation vs. Shear Reinforcement Strain for Shale Sand-Lightweight Concrete Monolithic Interface Specimens; ρ = 0.013

A.3.2 Slate aggregate sand-lightweight concrete specimens

A.3.2.1 Specimens with reinforcement ratio of 0.009

The sand-lightweight slate specimens with the lowest reinforcement ratio (ρ = 0.009) were tested on 03/30/2015. Their results are plotted in Figure A.15 through Figure A.19. All specimens failed in shear along the intended shear plane. Another interesting observation is in Figure A.19, the plot of slip vs. interface steel strain. For specimen S-SL-CJ-S-9-1 the figure shows that after the peak applied load (associated with failure) occurs, the slip continues to increase, whereas the axial strain in the bar remains constant. However, the slip vs. interface dilation curve (Figure A.18) shows the crack continuing to widen as slip increases. This could be due to the bar kinking as discussed in Section 2.2.2.

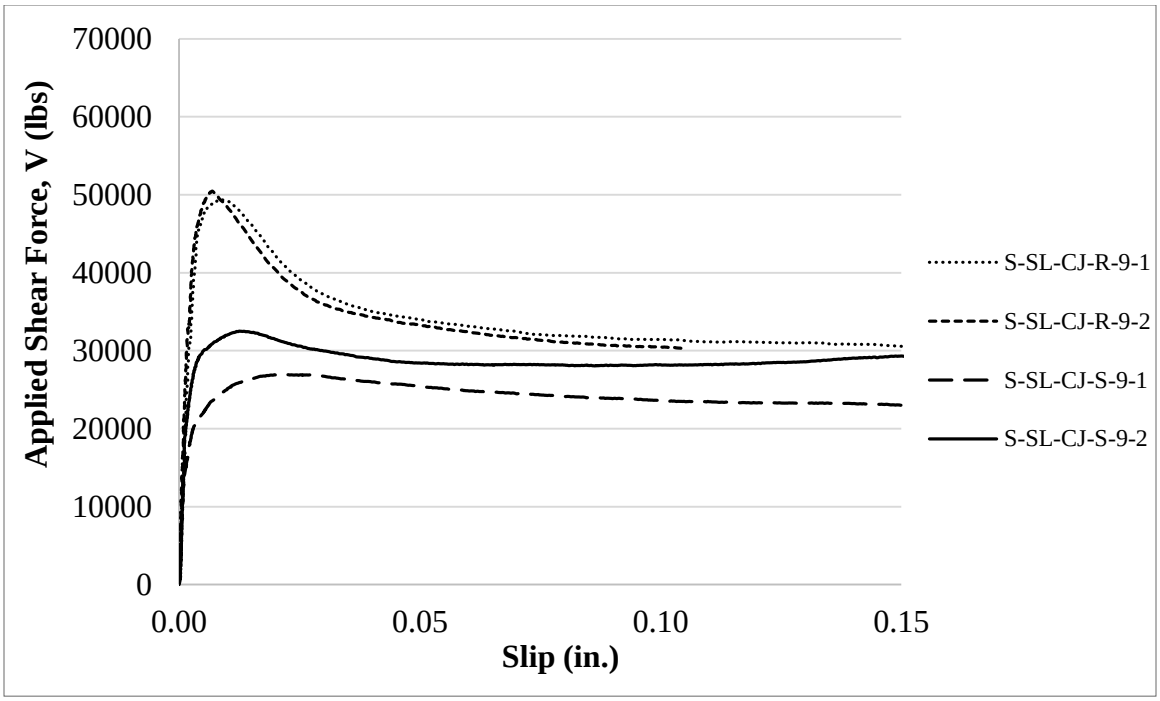

Figure A.15 Applied shear force vs. slip relations for sand-lightweight slate specimens; with ρ = 0.009

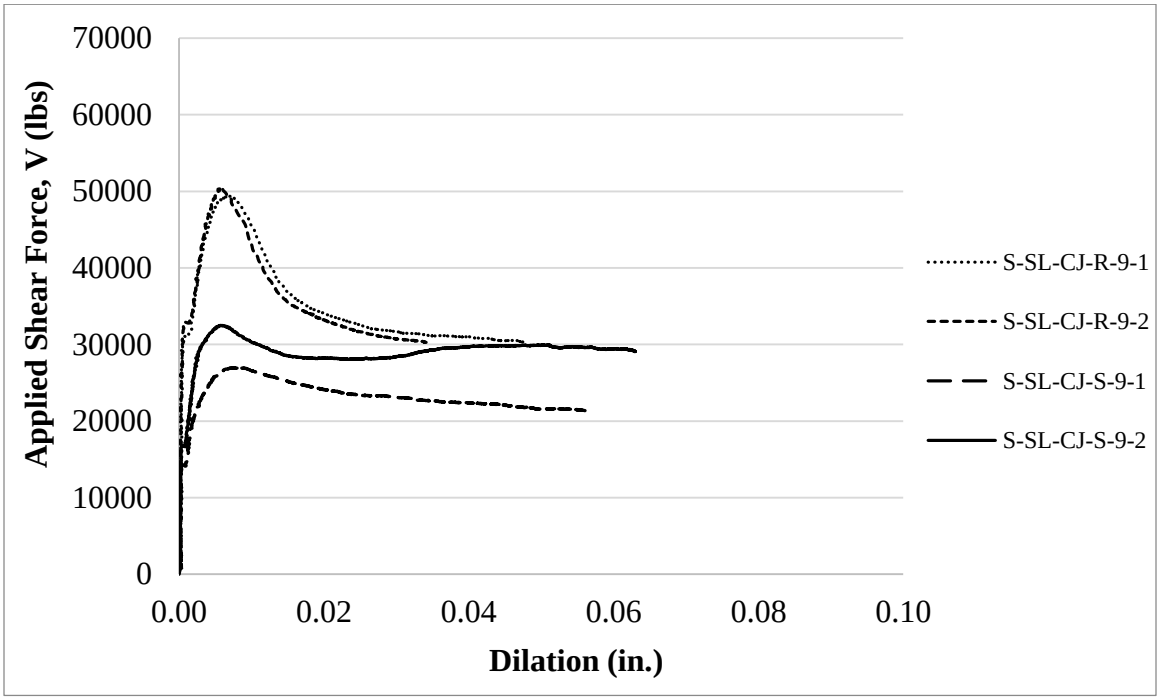

Figure A.16 Applied shear force vs. interface dilation relations for sand-lightweight slate specimens; ρ = 0.009

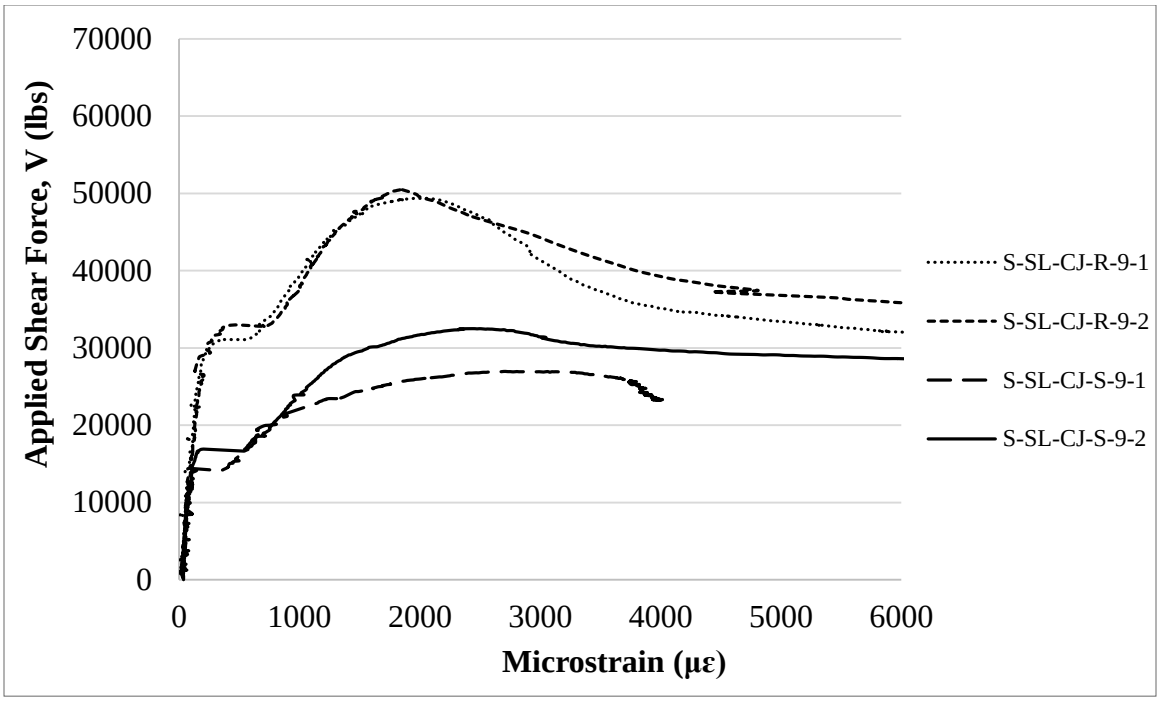

Figure A.17 Applied shear force vs. interface steel strain for sand-lightweight slate specimens; ρ = 0.009

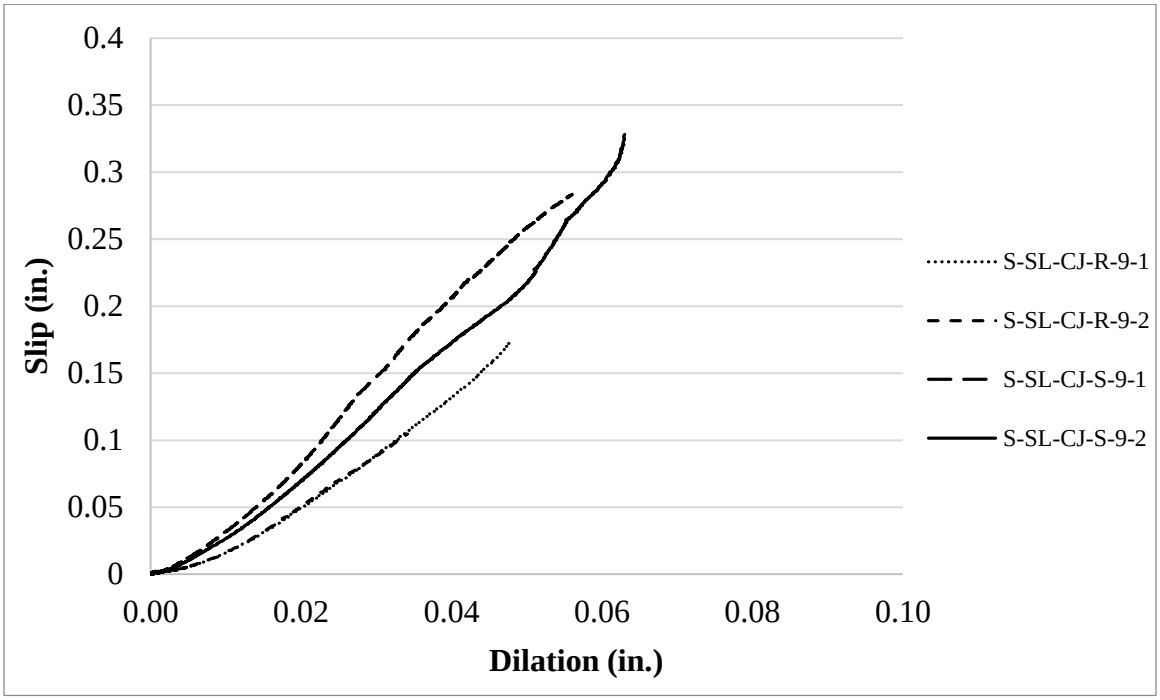

Figure A.18 Slip vs. dilation for sand-lightweight slate specimens; ρ = 0.009

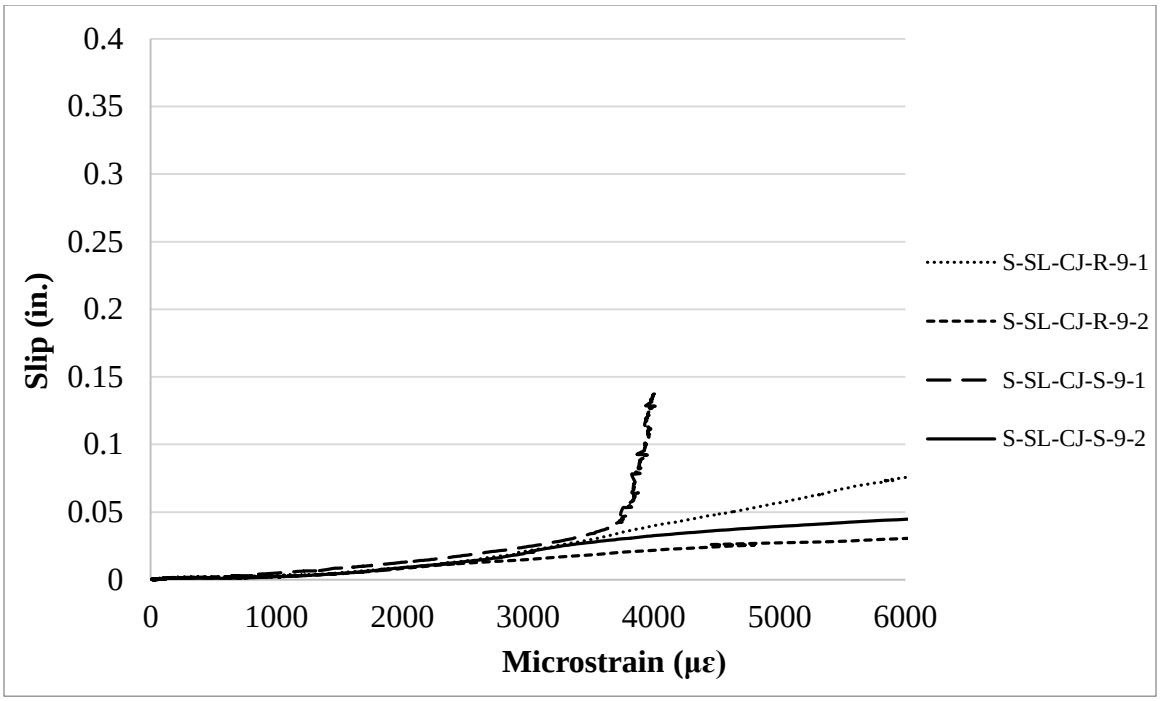

Figure A.19 Slip vs. interface steel strain for sand-lightweight slate specimens; ρ = 0.009

A.3.2.2 Specimens with reinforcement ratio of 0.013

The slate sand-lightweight specimens with reinforcement ratio of 0.013 are presented in this section. Important recorded data are plotted in Figure 3.56 through Figure 3.60.

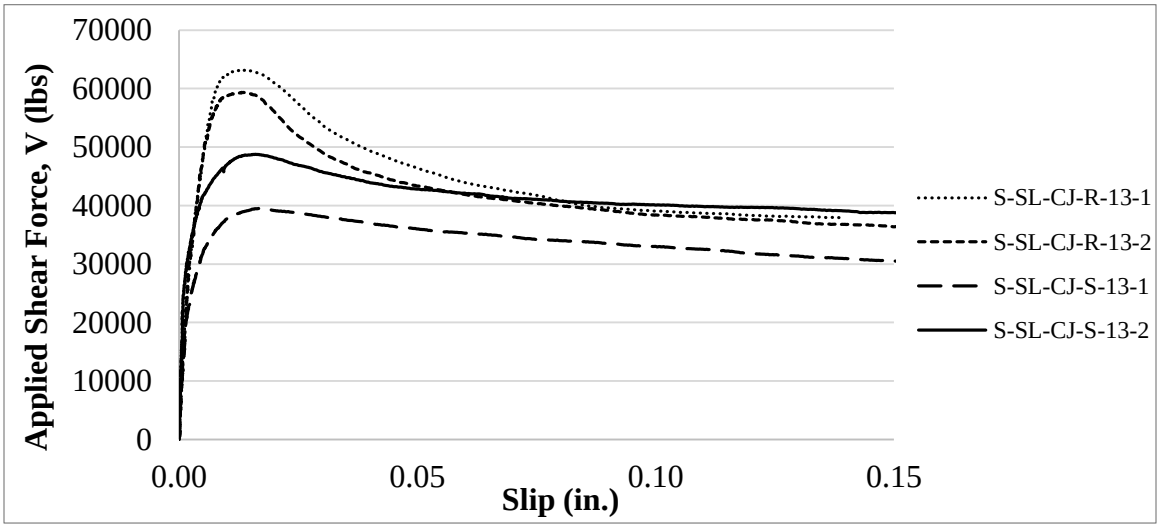

Figure A.20 Applied shear force vs. slip relations for sand-lightweight slate specimens; ρ = 0.013

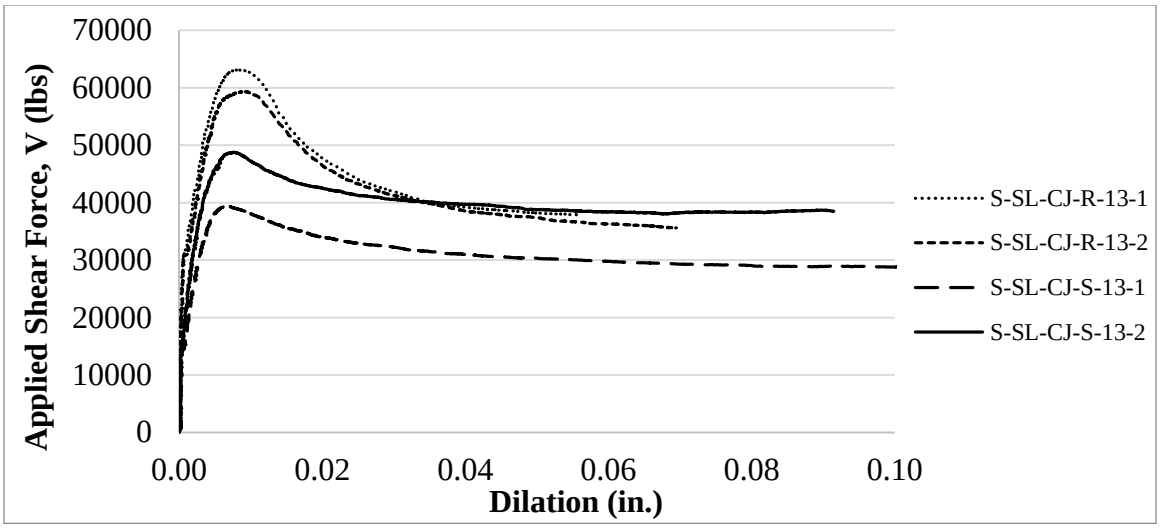

Figure A.21. Applied shear force vs. interface dilation relations for sand-lightweight slate specimens; ρ = 0.013

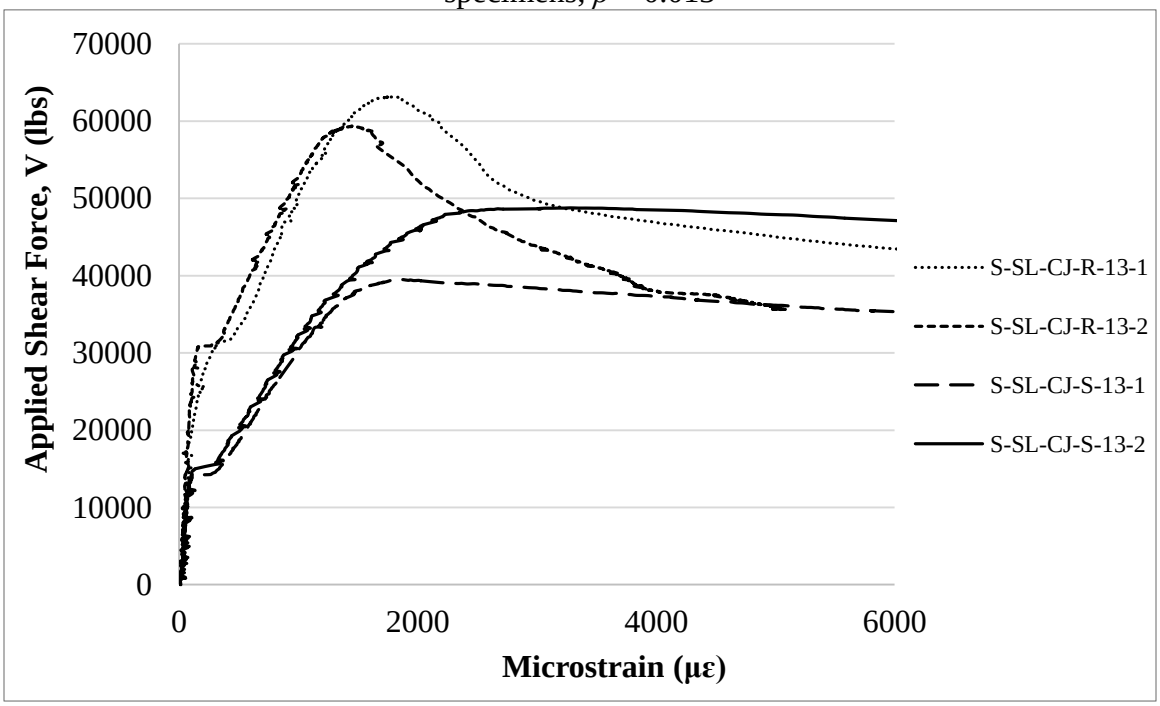

Figure A.22 Applied shear force vs. interface steel strain for sand-lightweight slate specimens; ρ = 0.013

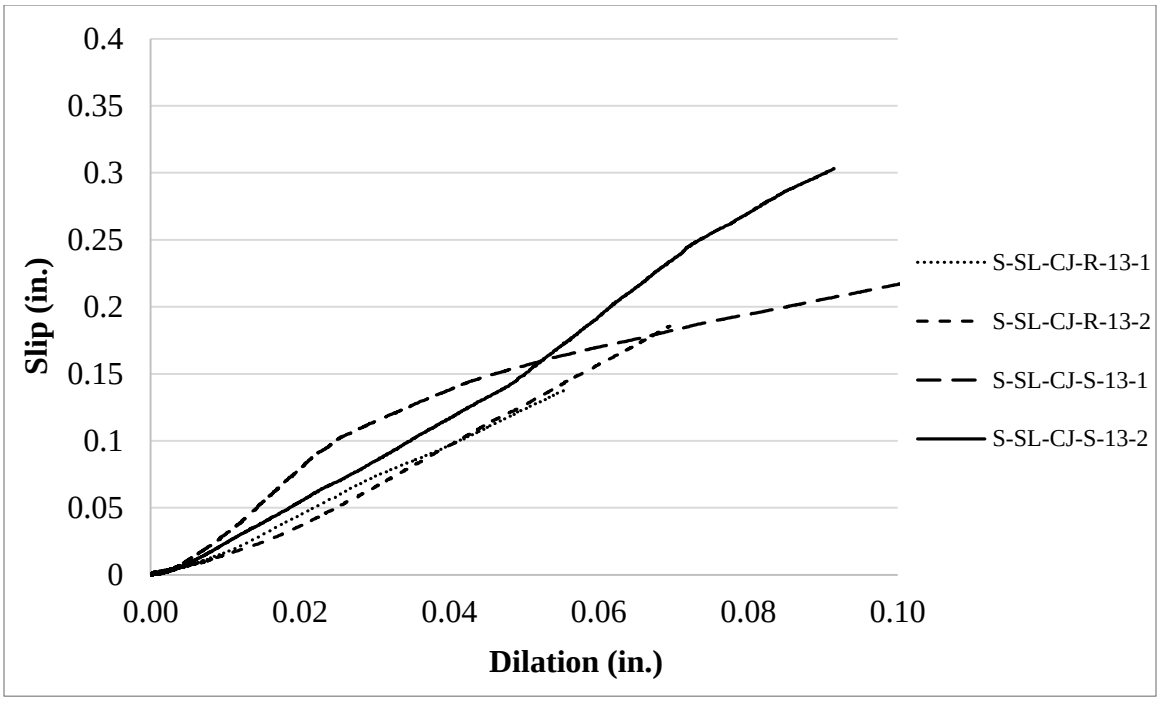

Figure A.23 Slip vs. dilation for sand-lightweight slate specimens; ρ = 0.013

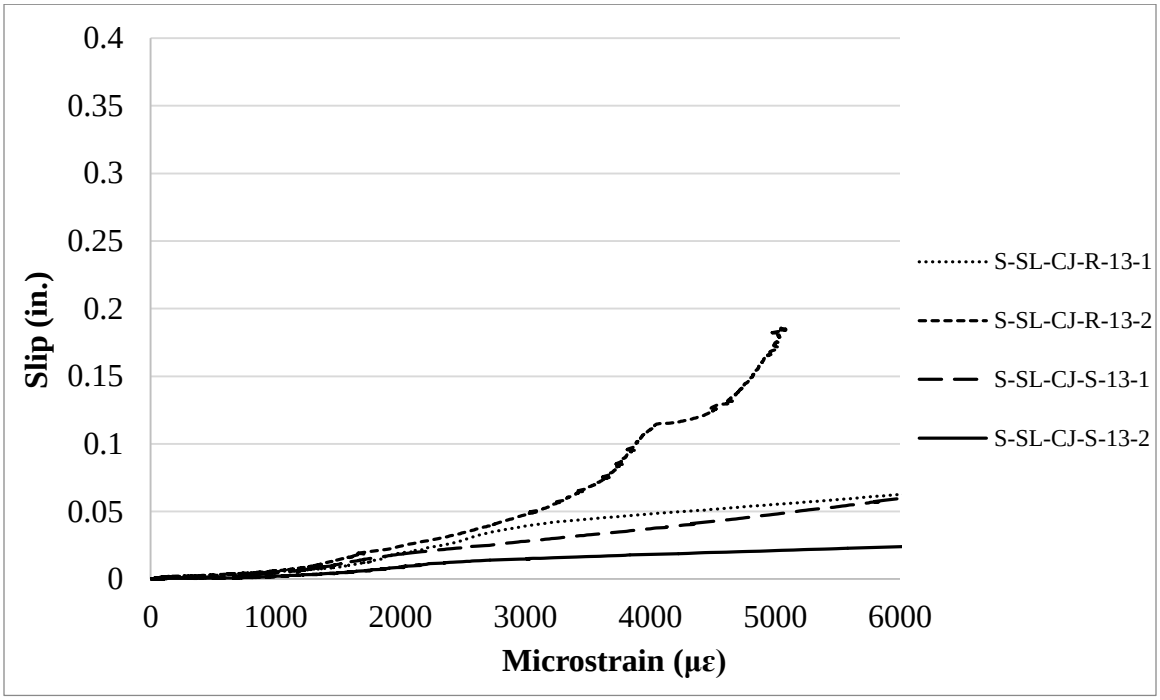

Figure A.24 Slip vs. interface steel strain for sand-lightweight slate specimens; ρ = 0.013

A.3.2.3 Specimens with reinforcement ratio of 0.017

Testing of slate sand-lightweight specimens with reinforcement ratio of 0.017 was performed on 04/06/2015. Results are shown in Figure A.26 through Figure A.30. The only unexpected failure was that of specimen S-SL-CJ-S-17-1. The shear crack did not form at the intended shear plane. Instead, it was about a half inch offset from the vertical centerline of the specimen as shown in Figure A.25. This behavior implies that the bond of one side of the cold-joint interface to the other was very good. Even though the shear plane has a smaller cross-section than the adjacent body of the specimen, as well as a construction joint which was troweled smooth, the crack did not form along the shear plane. In this figure you can also see minor honeycombing of the concrete in the top flange. This occurs when there is inadequate consolidation of the concrete during casting. To avoid honeycombing in other specimens, the construction method was modified. The concrete was vibrated for longer periods of time during specimen construction, especially in the flanges. The concrete was added to the forms in thinner layers and vibrated before the addition of the next layer. Another interesting behavior is observed in Figure A.30, which shows slip vs. strain, after the peak load (associated with failure), the slip continues to increase for Specimen S-CL-CJ-R-17-2, whereas the axial strain in the bar remains relatively constant for that specimen. However, the slip-dilation curve (Figure A.29) shows the crack continuing to widen as slip increases. This could be due to the bar kinking as discussed in Section 2.2.2.

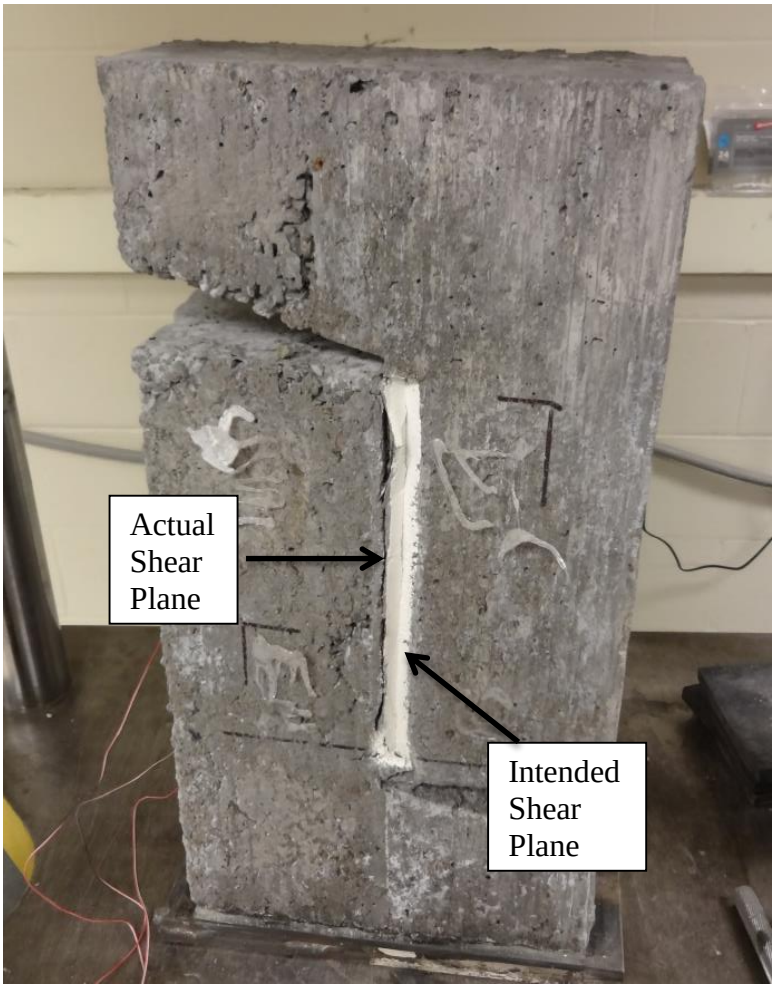

Figure A.25 Shear plane crack of specimen S-SL-CJ-S-17-1

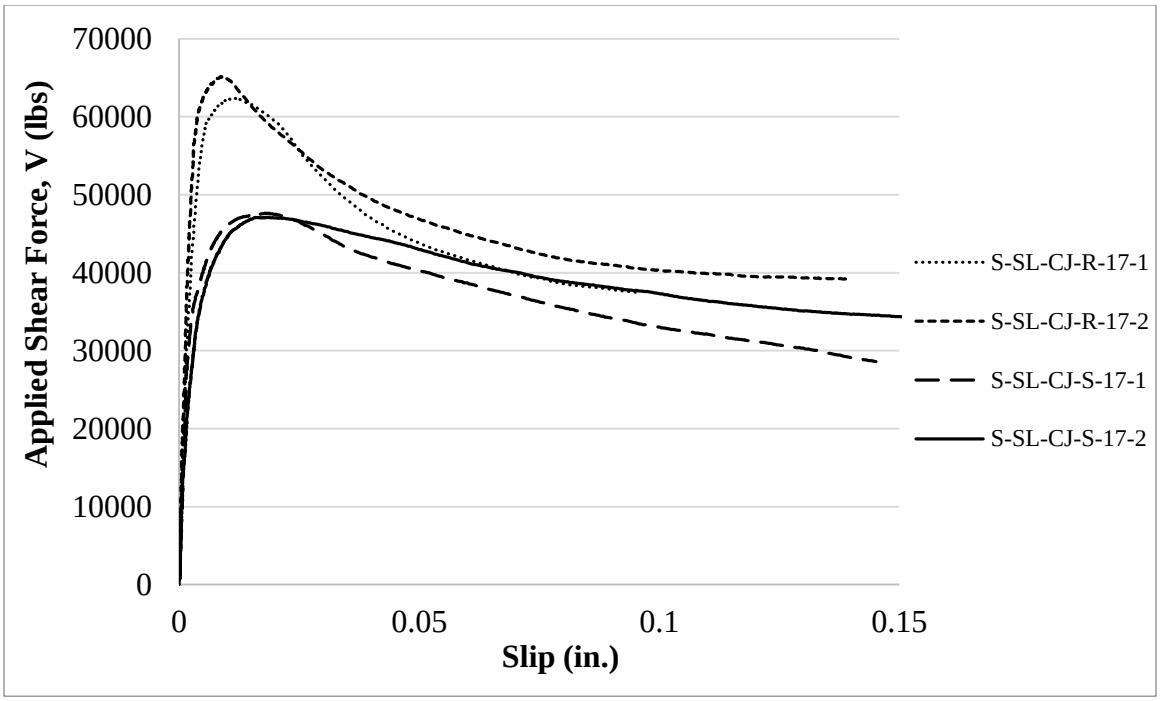

Figure A.26 Applied shear force vs. slip relations for sand-lightweight slate specimens; ρ = 0.017

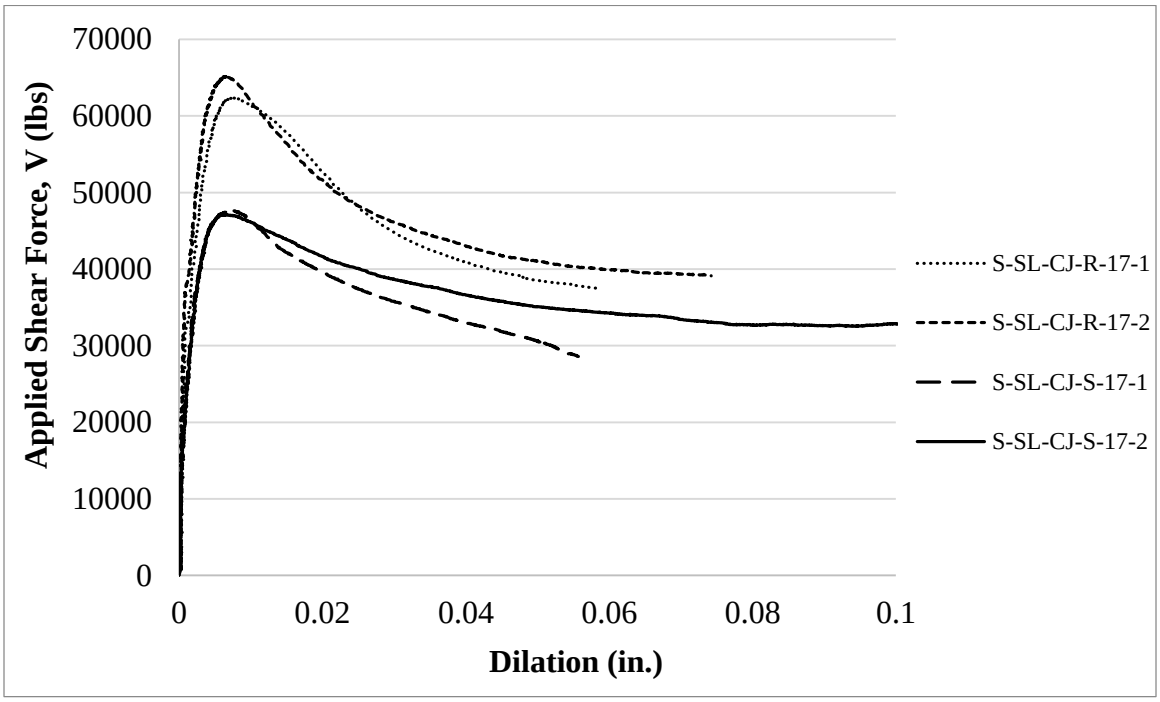

Figure A.27 Applied shear force vs. interface dilation relations for sand-lightweight slate specimens; ρ = 0.017

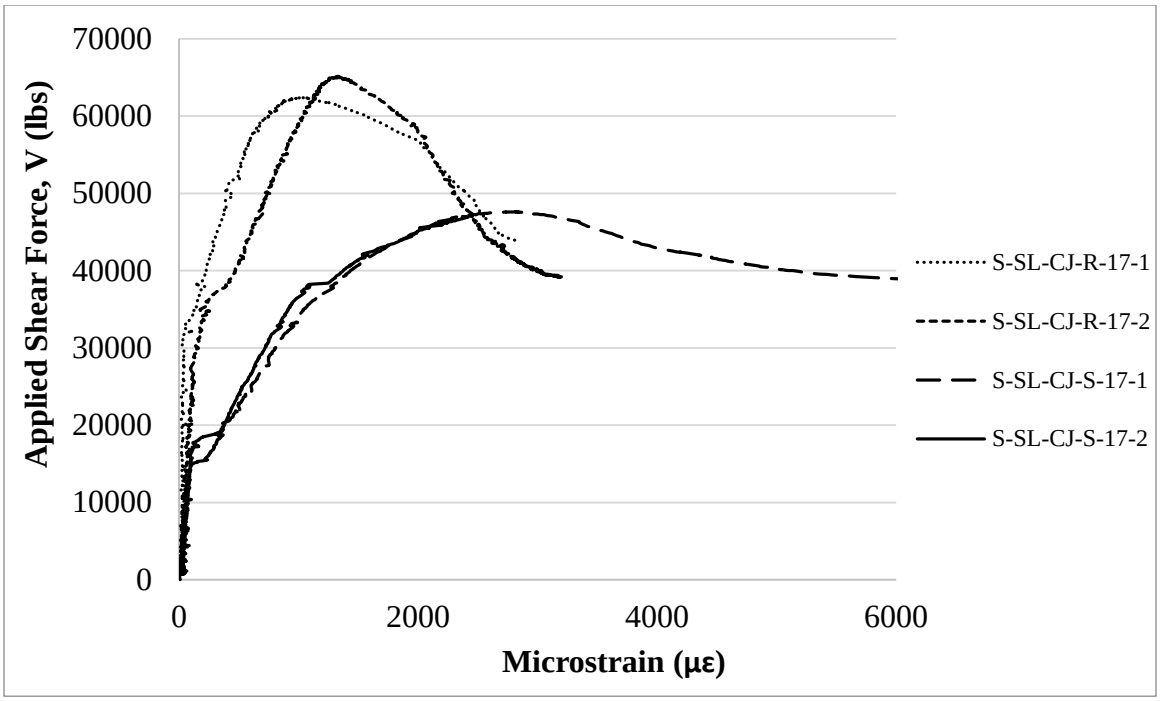

Figure A.28 Applied shear force vs. interface steel strain for sand-lightweight slate specimens; ρ = 0.017

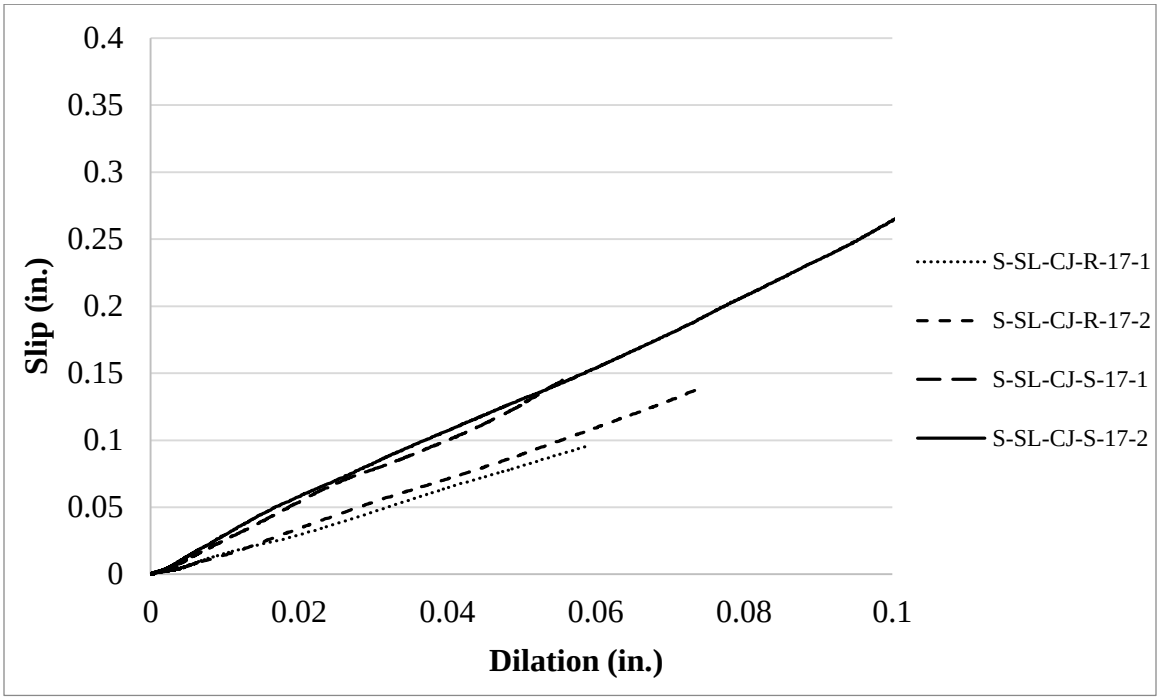

Figure A.29 Slip vs. dilation for sand-lightweight slate specimens; ρ = 0.017

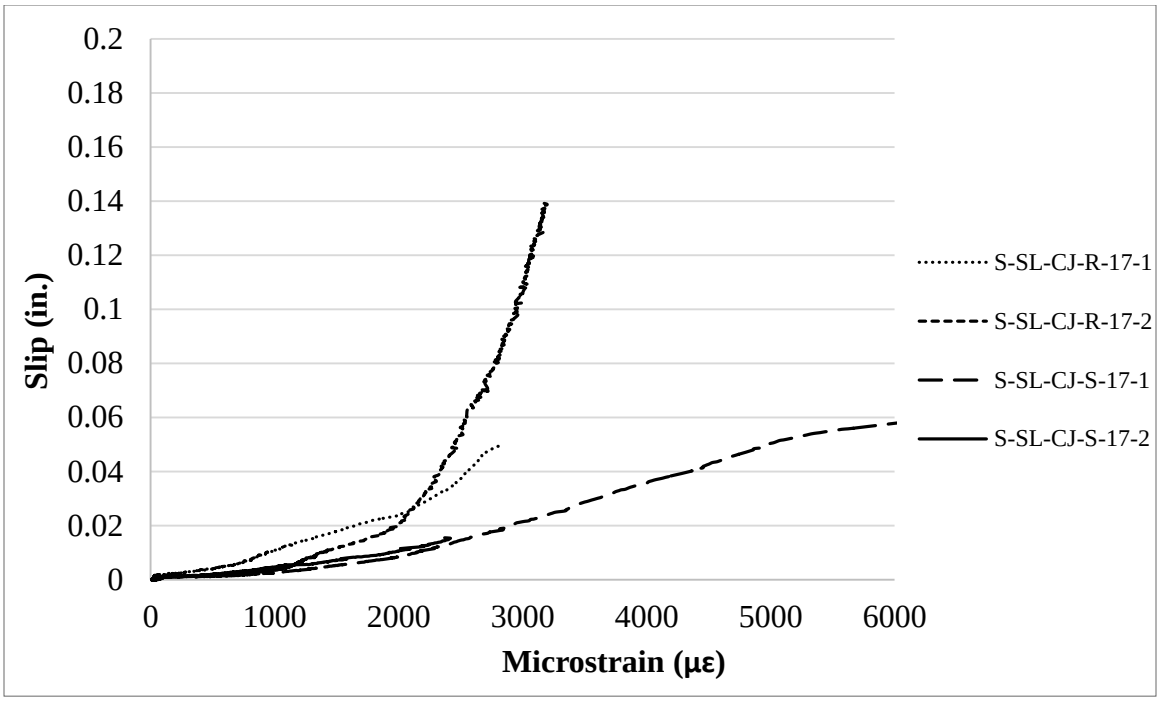

Figure A.30 Slip vs. interface steel strain for sand-lightweight slate specimens; ρ = 0.017

A.3.2.4 Specimens with reinforcement ratio of 0.022

The sand-lightweight slate specimens with the highest reinforcement ratio (0.022) were tested on 03/11/2015. The behaviors of these specimens are plotted in Figure 3.34 through Figure 3.38. Splitting cracks on the side face and flexural cracks on the back face were observed in the roughened specimens of this series (Figure A.31). This behavior was similar to that of the sand-lightweight clay specimens that had splitting failures, with an important exception: when the outer layer of cracked concrete was removed from the slate specimens after testing, a definite shear crack along the shear plane was visible (Figure A.32). This suggests that shear along the shear plane was the principle failure mode. Further investigation of the real-time plots in Figure A.33 show that these two roughened specimens behaved similar to other specimens which failed along the shear plane in that the sharp spikes in slip and dilation correspond to the peak applied shear force. This supports the idea that the failure mode of the roughened specimens of this series was indeed shear along the shear plane.

Another interesting behavior is observed in Figure A.38, which shows slip vs. strain. After the peak load (associated with failure), the slip continues to increase for Specimen S-CL-CJ-R-22-2, whereas the axial strain in the bar remains relatively constant for that specimen. However, the slip-dilation curve (Figure A.37) shows the crack continuing to widen as slip increases. This behavior is similar to Specimen S-CL-CJ-R-17-2 and could be due to the bar kinking. Also, it is worth noting that the interface steel strain did not exceed the steel yield strain for specimen S-SL-CJ-R-22-1 (Figure A.36). Analysis of the raw strain data indicates that the strain gages were damaged prior to reaching the level of strain associated with yield and no further values were able to be recorded past that point. Thus, it is not known if the bars did actually reach yield strain since all three strain gages were damaged early in the test.

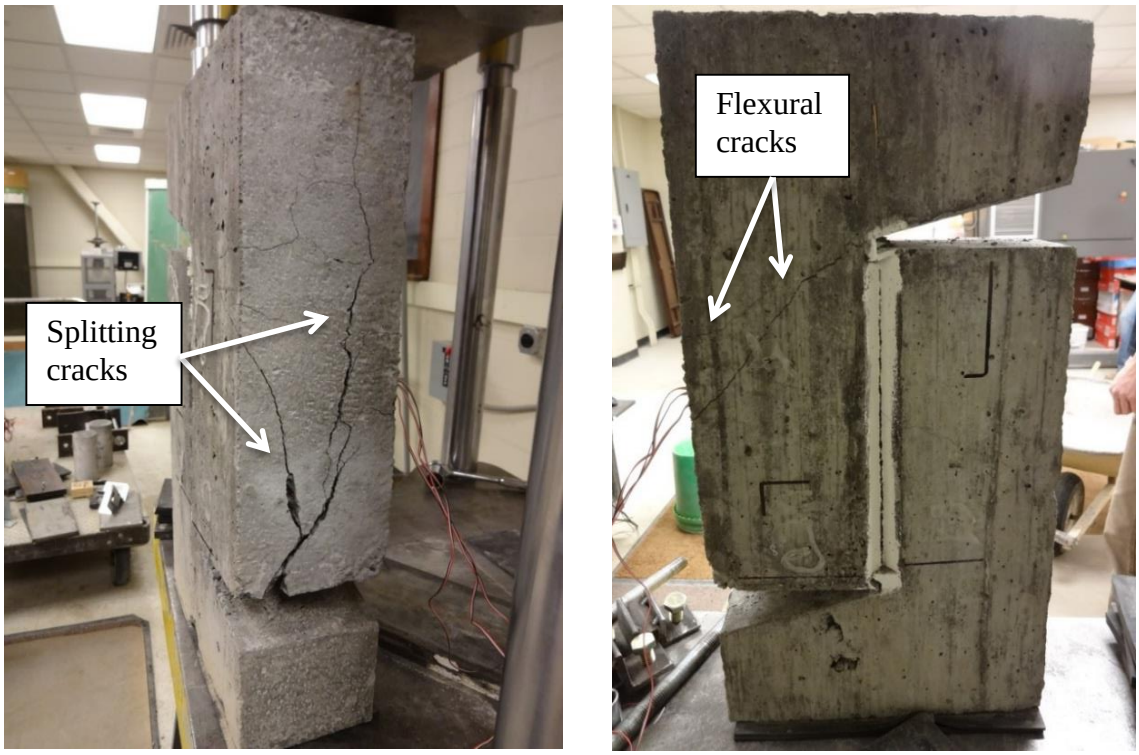

Figure A.31 Specimen S-SL-CJ-R-22-1 shown; splitting cracks on side face (left), and flexural cracks on back face (right)

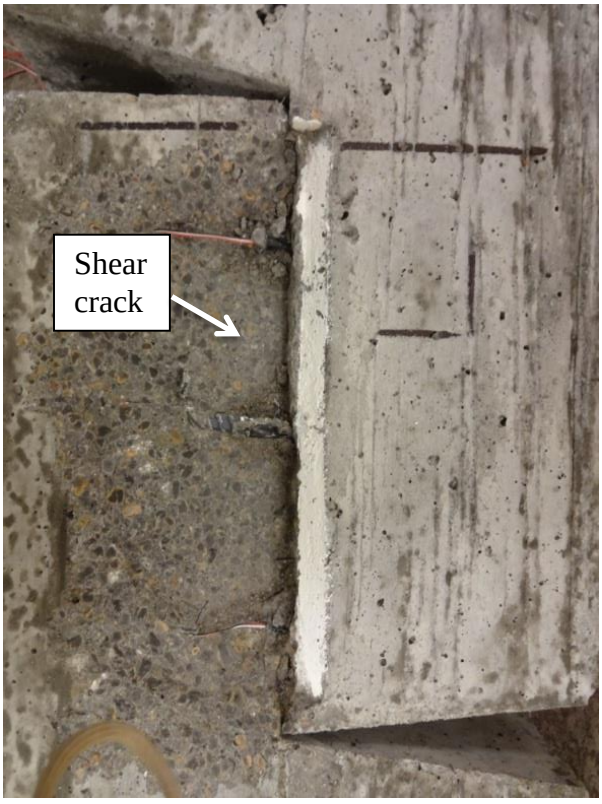

Figure A.32 Specimen S-SL-CJ-R-22-1 with spalled concrete removed and shear plane exposed

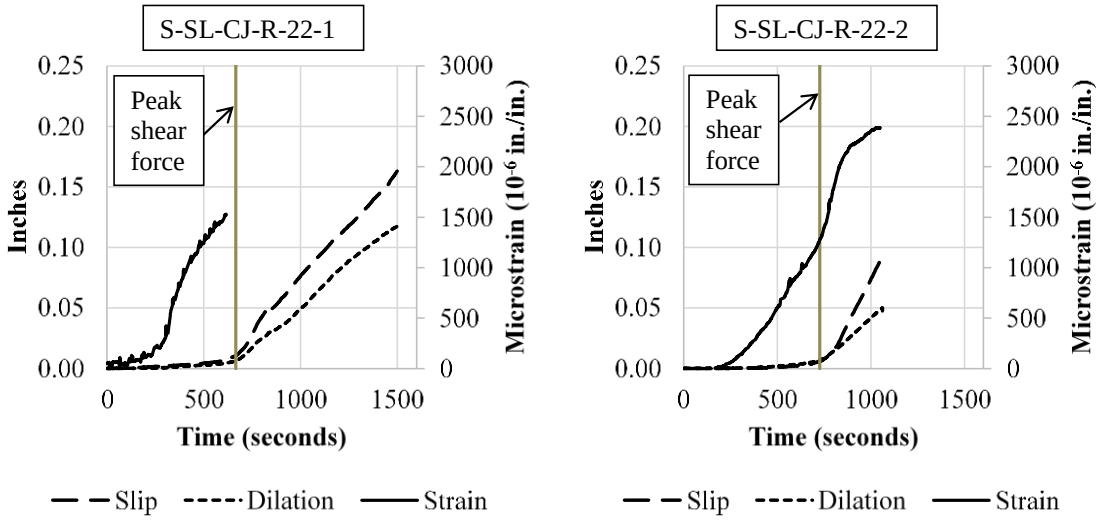

Figure A.33 Real time plots of slip, dilation, and strain for a Specimen S-SL-CJ-R-22-1 (left); and Specimen S-SL-CJ-R-22-1 (right); which both failed due to shear

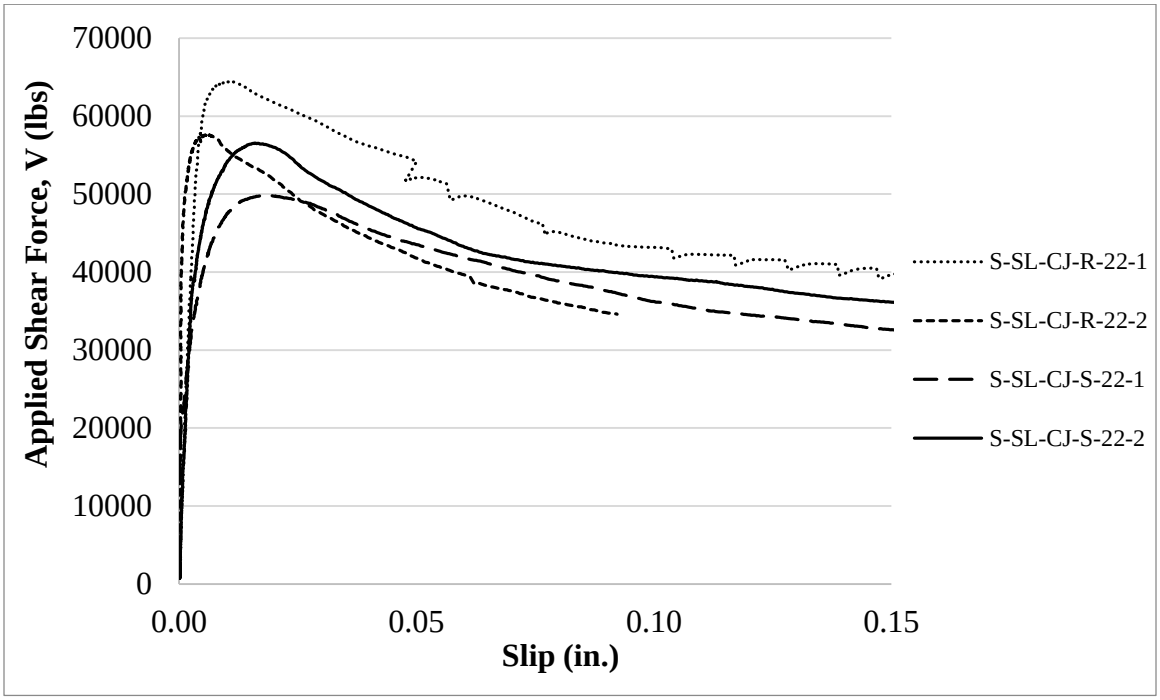

Figure A.34 Applied shear force vs. slip relations for sand-lightweight slate specimens; ρ = 0.022

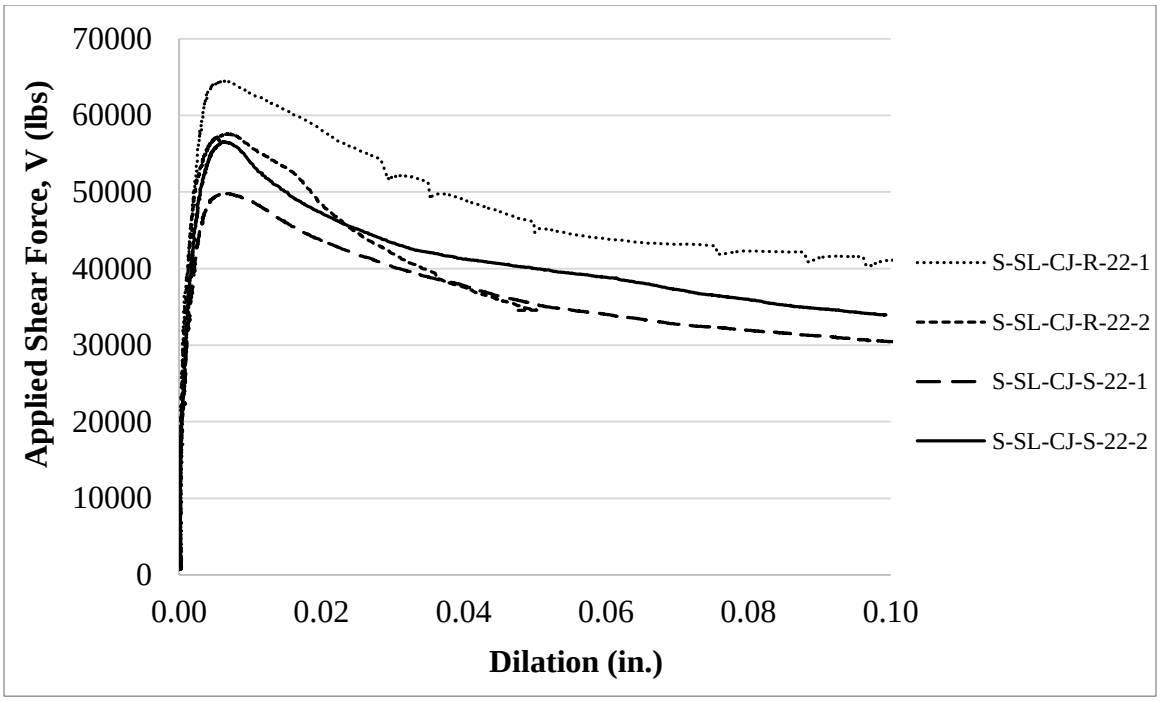

Figure A.35 Applied shear force vs. interface dilation relations for sand-lightweight slate specimens; ρ = 0.022

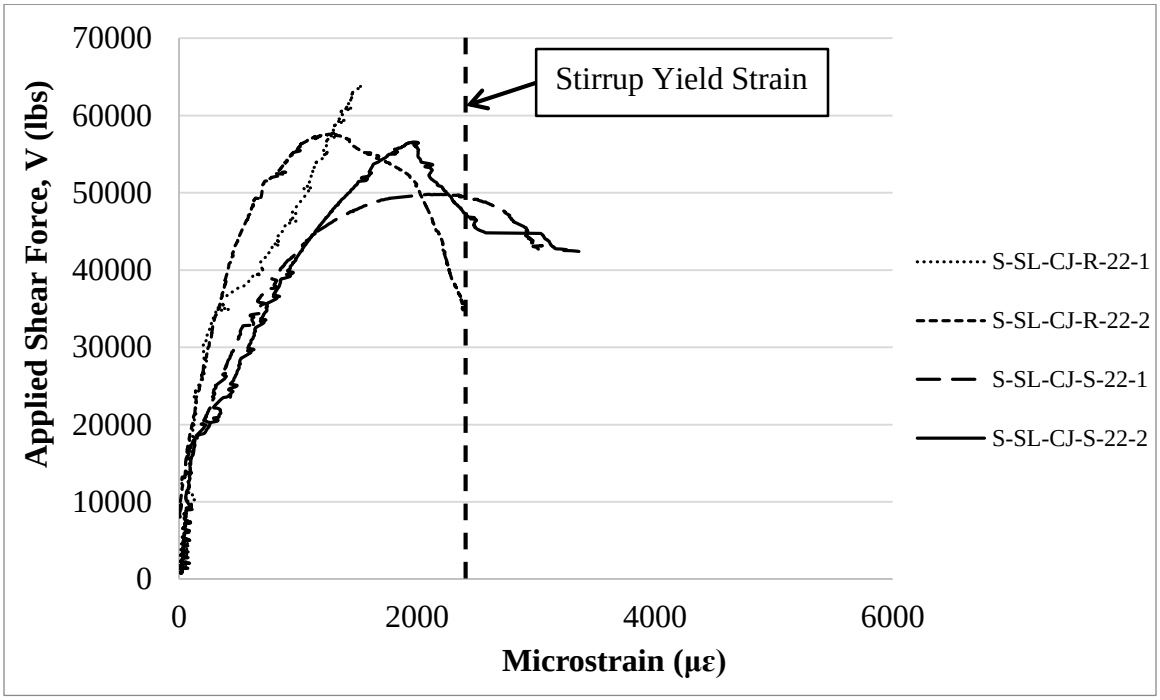

Figure A.36 Applied shear force vs. interface steel strain for sand-lightweight slate specimens; ρ = 0.022

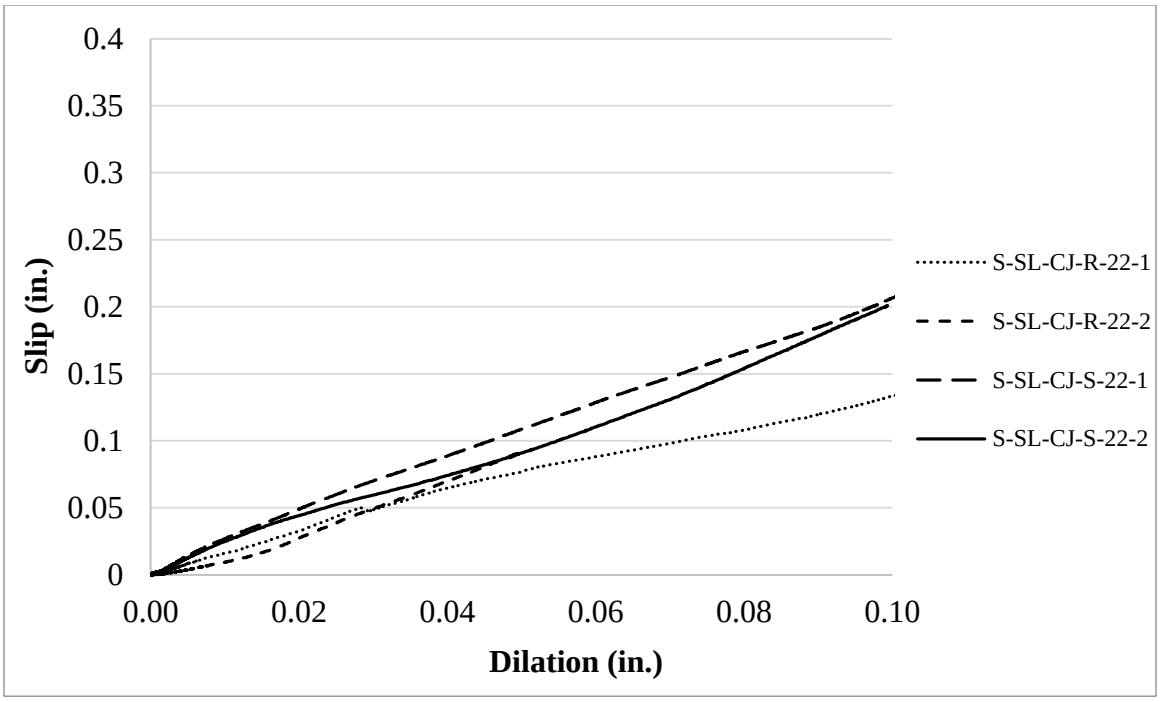

Figure A.37 Slip vs. dilation for sand-lightweight slate specimens; ρ = 0.022

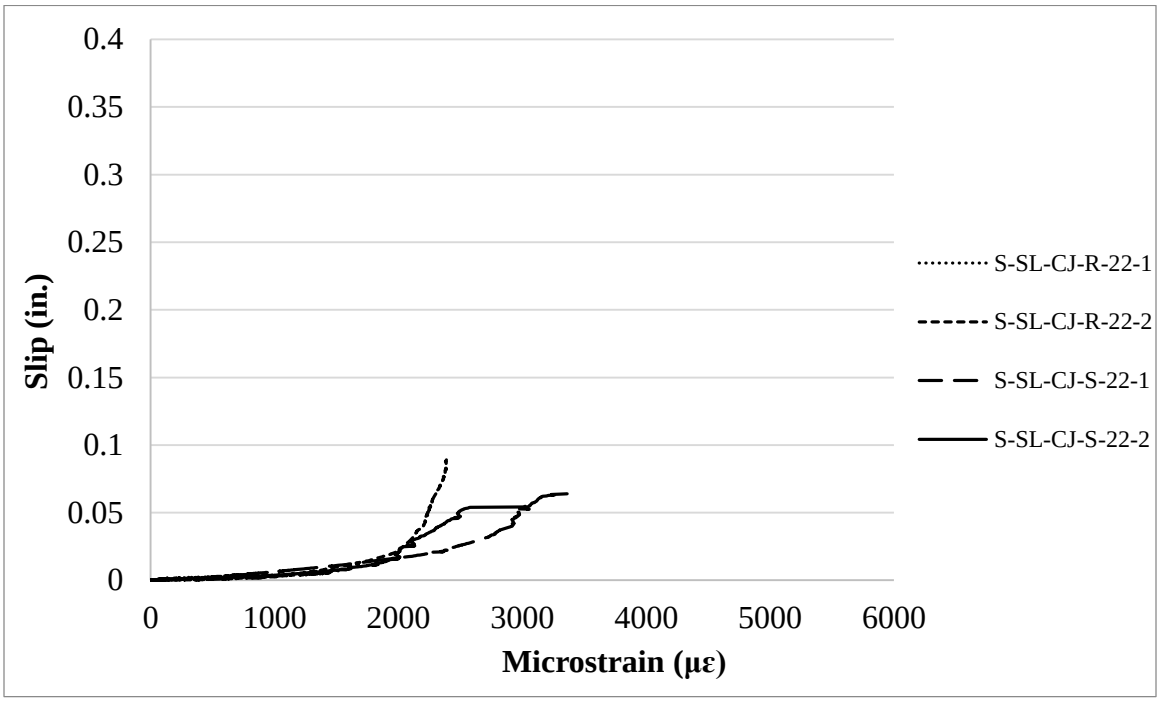

Figure A.38 Slip vs. interface steel strain for sand-lightweight slate specimens; ρ = 0.022

A.3.3 Clay aggregate sand-lightweight concrete specimens

This section presents information regarding the sand-lightweight clay specimens tested in this program. As discussed previously in Section 3.6.1, the sand-lightweight clay specimens with ρ = 0.017 and a roughened interface (two specimens), as well as all four of the sand-lightweight clay specimens with ρ = 0.022 failed due to splitting of the concrete.

A.3.3.1 Specimens with reinforcement ratio of 0.009

Testing of the sand-lightweight clay specimens with a reinforcement ratio of 0.009 occurred on 04/29/15. The results are summarized in Figure A.39 through Figure A.43. All specimens failed along the shear plane as expected.

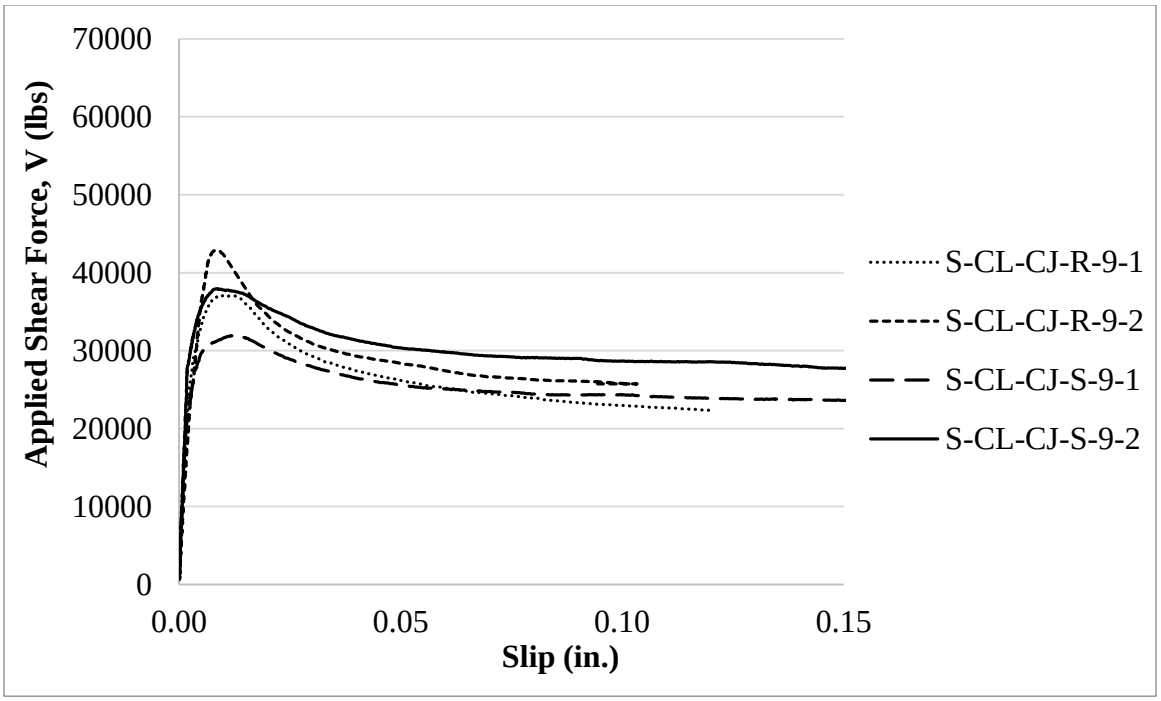

Figure A.39 Applied shear force vs. slip relations for sand-lightweight clay specimens; ρ = 0.009

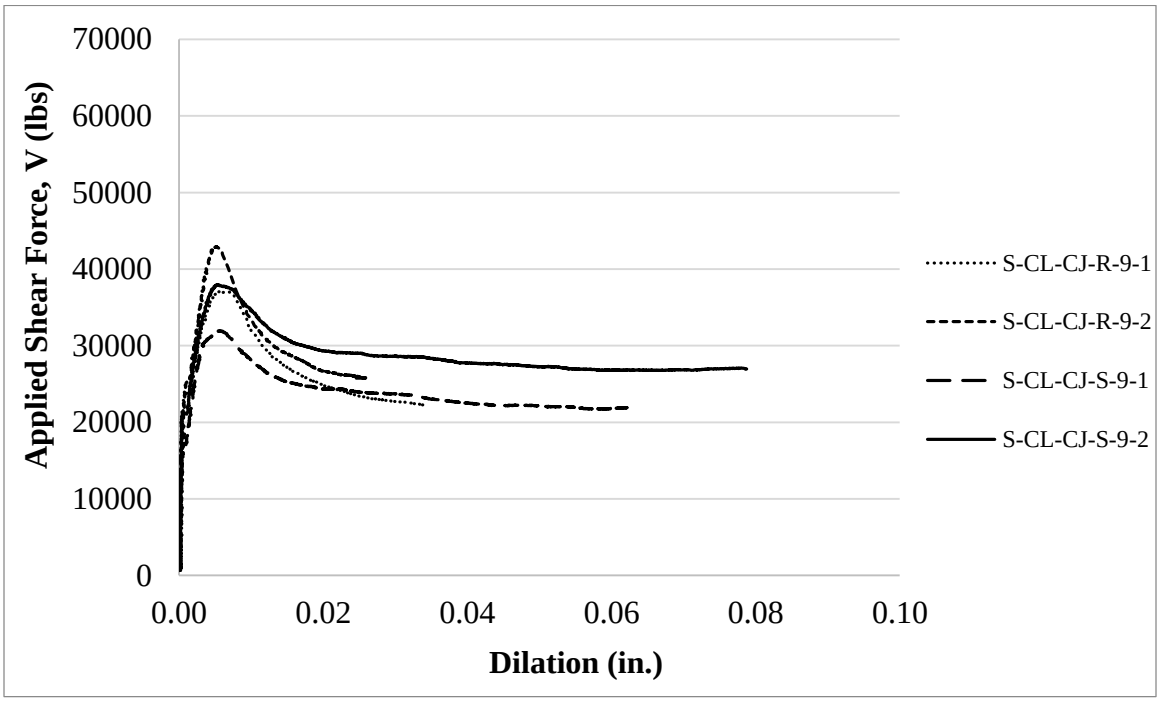

Figure A.40 Applied shear force vs. interface dilation relations for sand-lightweight clay specimens; ρ = 0.009

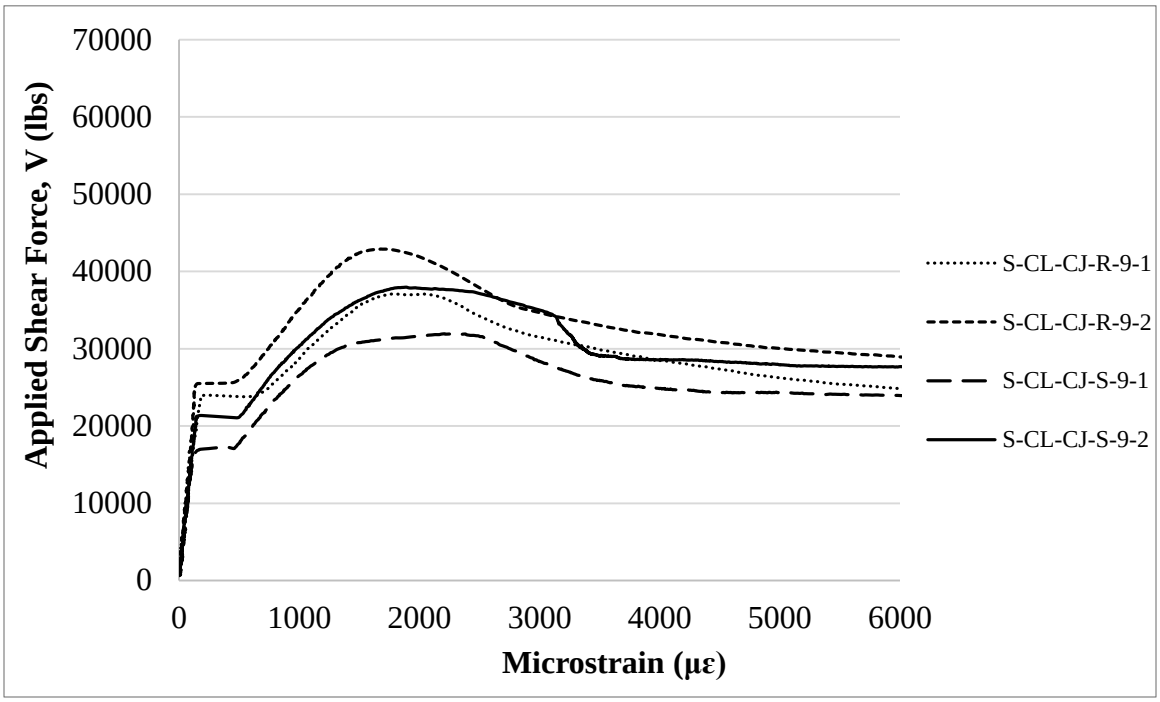

Figure A.41 Applied shear force vs. interface steel strain for sand-lightweight clay specimens; ρ = 0.009

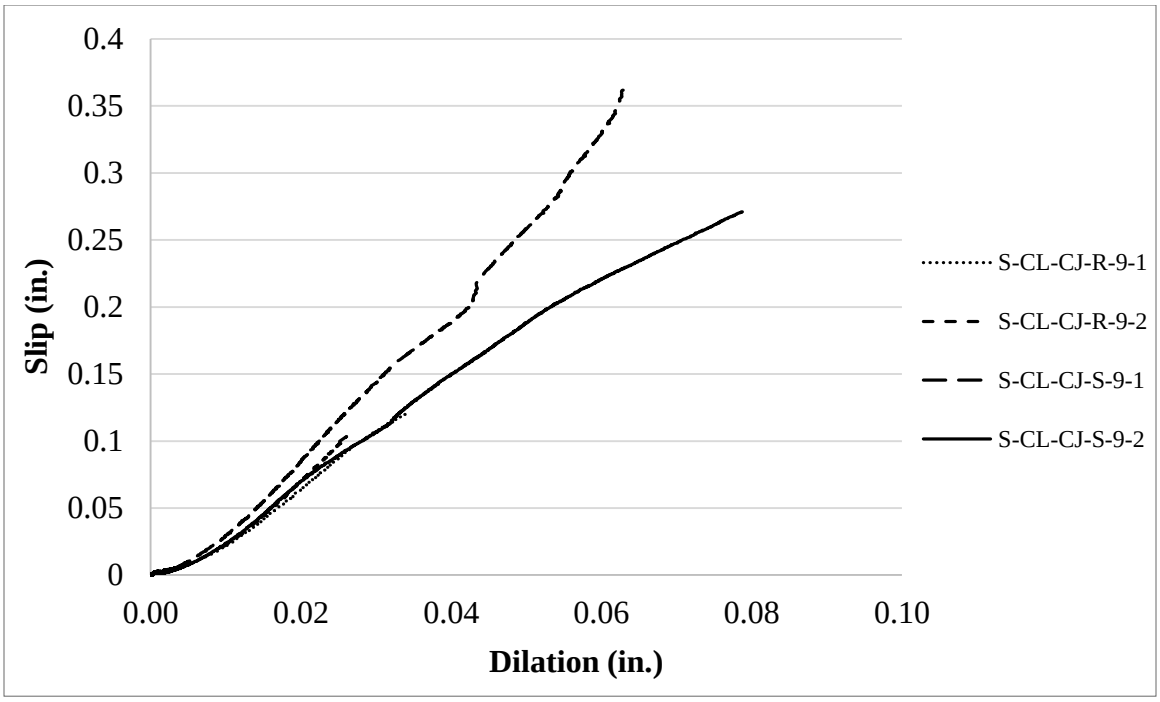

Figure A.42 Slip vs. dilation for sand-lightweight clay specimens; ρ = 0.009

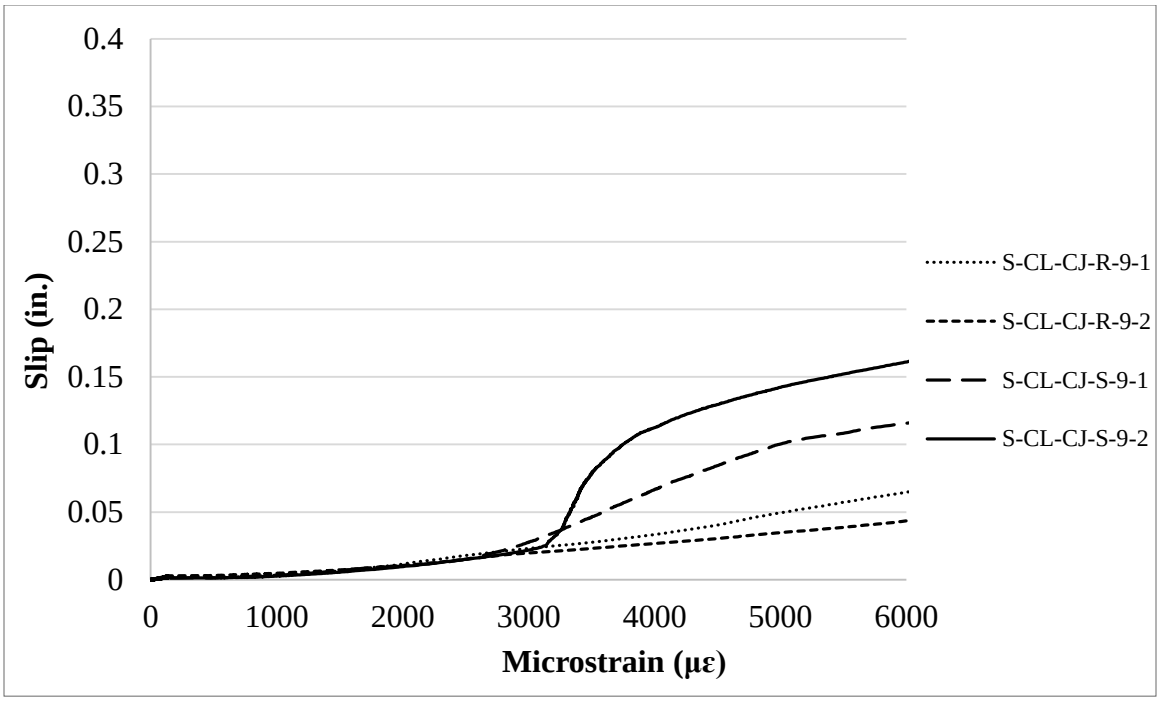

Figure A.43 Slip vs. interface steel strain for sand-lightweight clay specimens; ρ = 0.009

A.3.3.2 Specimens with reinforcement ratio of 0.013

Testing of the sand-lightweight clay specimens with a reinforcement ratio of 0.013 occurred on 05/06/15. The results are summarized in Figure A.44 through Figure A.48.

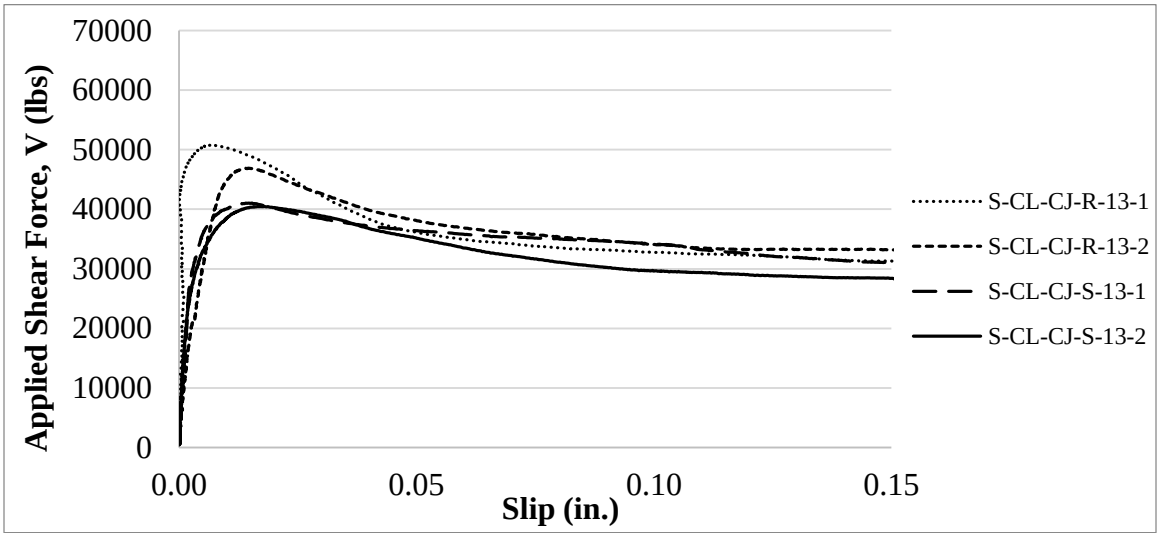

Figure A.44 Applied shear force vs. slip relations for sand-lightweight clay specimens; ρ = 0.013

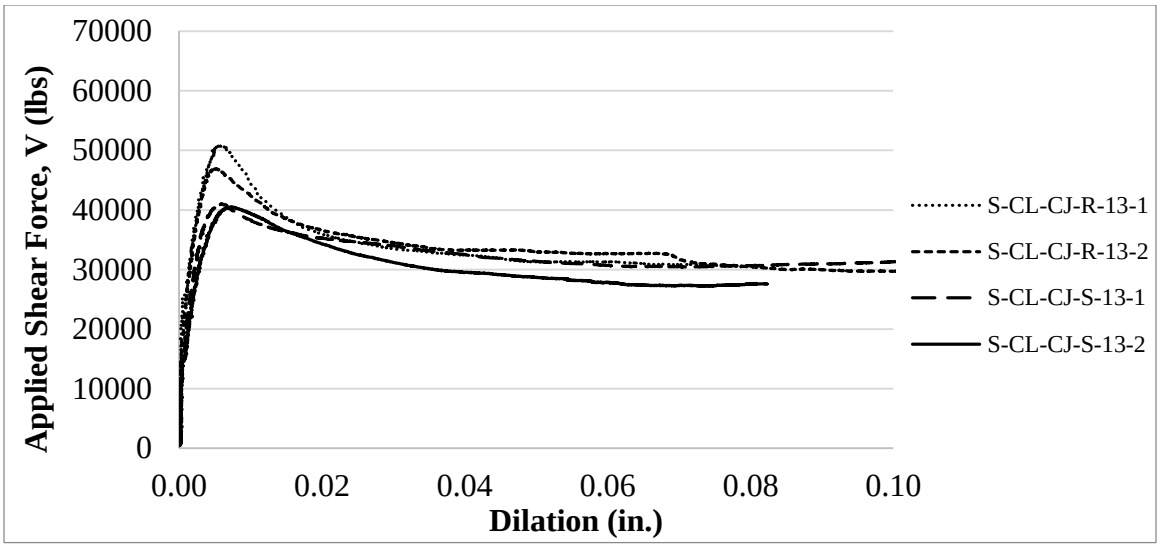

Figure A.45 Applied shear force vs. interface dilation relations for sand-lightweight clay specimens; ρ = 0.013

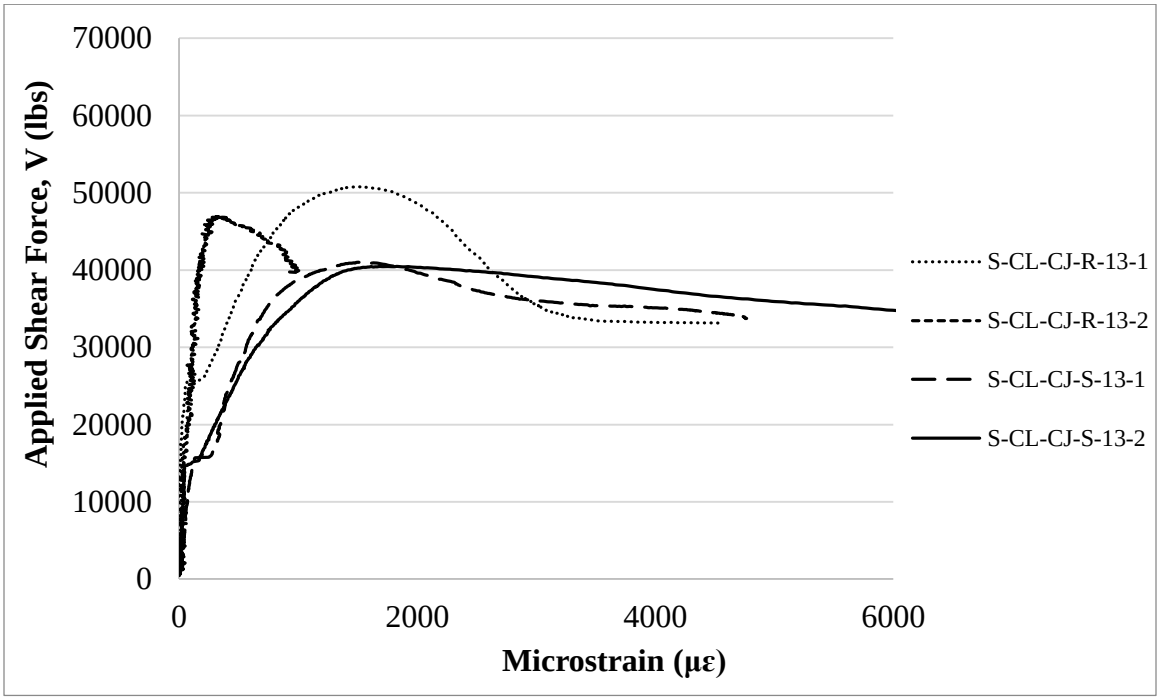

Figure A.46 Applied shear force vs. interface steel strain for sand-lightweight clay specimens; ρ = 0.013

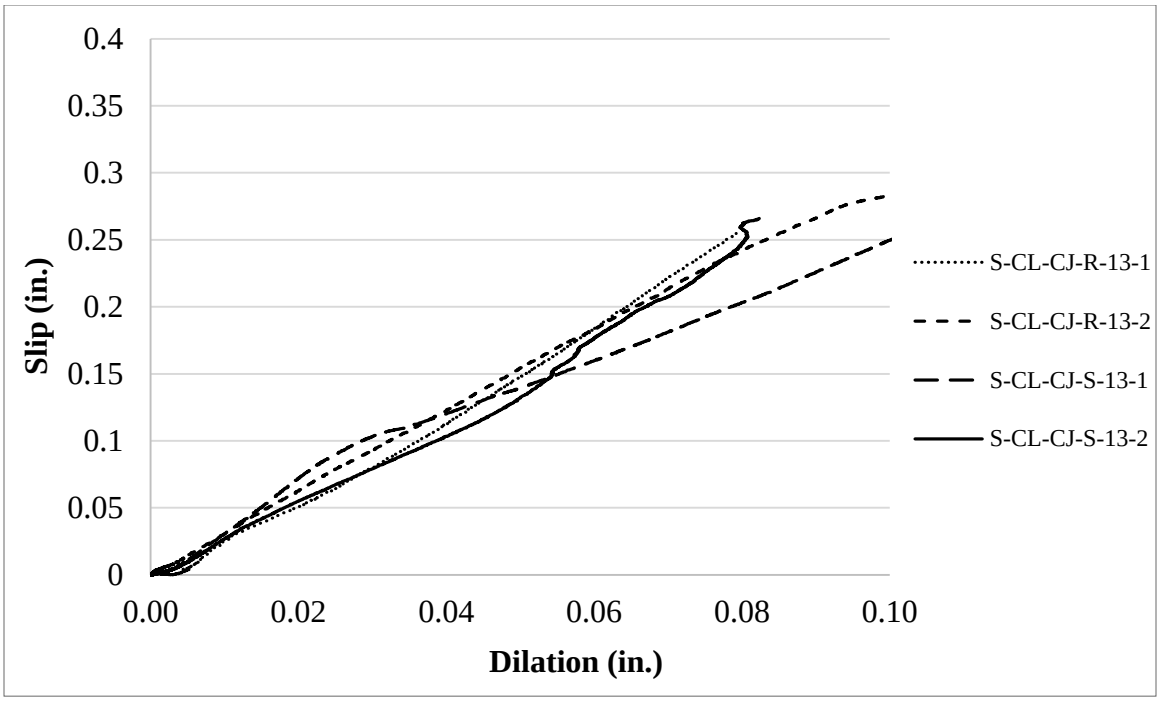

Figure A.47 Slip vs. dilation for sand-lightweight clay specimens; ρ = 0.013

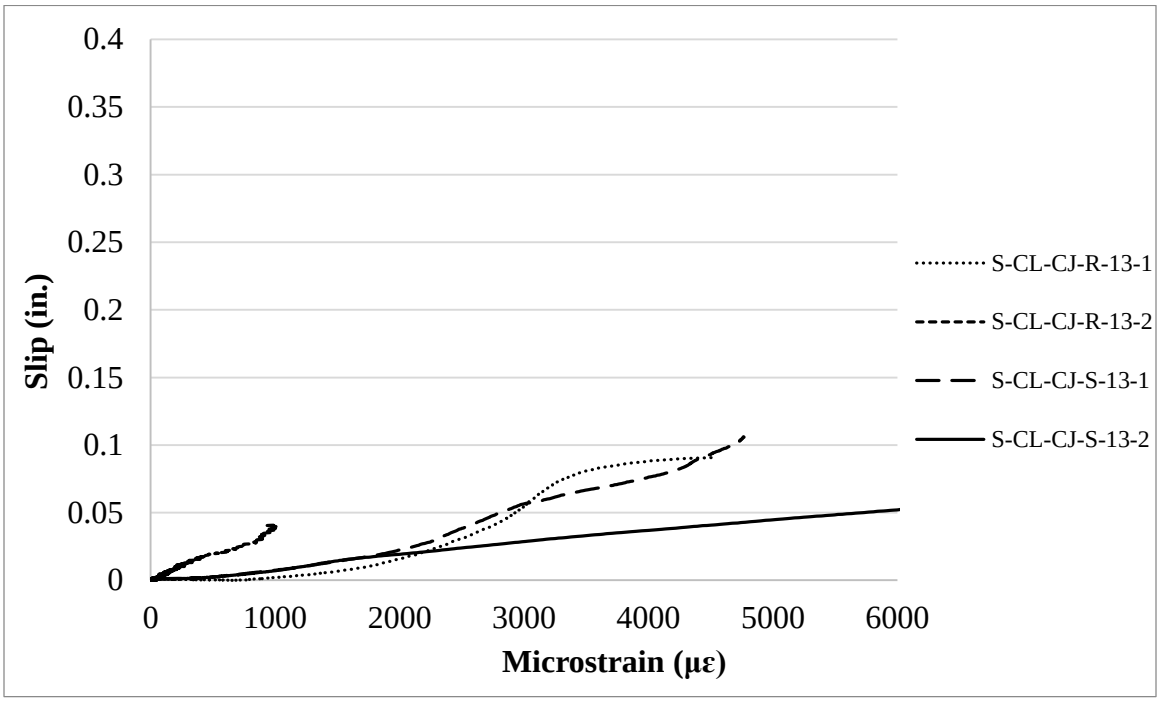

Figure A.48 Slip vs. interface steel strain for sand-lightweight clay specimens; ρ = 0.013

A.3.3.3 Specimens with reinforcement ratio of 0.017

The sand-lightweight clay specimens with a reinforcement ratio of 0.017 were tested on 05/13/15. The results are shown in Figure A.50 through Figure A.54. As mentioned in Section 3.6.1, two of the specimens of this series failed due to splitting rather than shear. These were specimens S-CL-

CJ-R-17-1 and S-CL-CJ-R-17-2, both of which had a roughened interface. It is worth noting that the S-CL-CJ-17 series had the lowest compressive strength on test day of any other series in this study at f'_c = 4,550 psi. Furthermore, this series had the third lowest splitting tensile strength of all the series of the study, having f'_t = 410 psi.

Values were recorded for slip and dilation, but they are not likely valid since they were caused by the front 'panel' of concrete spalling off as the flange flexed. When this section of spalled concrete was removed after testing concluded, it was found that the ‘panel’ only extended to the outer edge of the shear reinforcement and a shear crack could not be seen underneath it (Figure A.49). Therefore, a true shear crack did not form for these two specimens and their load, slip, dilation, and strain data are not truly representative of the shear strength of the specimens. However, it is implied that the true shear strength of these specimens is at least as high as the peak applied shear force from Figures A.50 through A.54. It is also important to note that the interface reinforcing steel did not reach yield strain for specimen S-CL-CJ-R-17-1. The maximum steel strain for this specimen was less than the yield strain.

Figure A.49 Specimen S-CL-CJ-R-17-2 with spalled concrete removed and no shear failure visible

Also worth noting, the shear force vs. interface steel strain graph (Figure A.52) shows roughened specimen behavior much different than smooth interface. The roughened specimens did not have a parabolic peak behavior like the smooth specimens did. This behavior is due to the splitting

failure of the roughened specimens of this series. In addition, Specimen S-CL-CJ-R-17-1 did not exhibit a peak in applied shear force. Another interesting observation is in Figure A.54, the plot of slip vs. interface steel strain. Specimen S-CL-CJ-S-17-1 shows that after the peak applied load (associated with failure) occurs, the slip continues to increase, whereas the axial strain in the bar remains constant. However, the slip vs. interface dilation curve (Figure A.53) shows the crack continuing to widen as slip increases. This could be due to the bar kinking. The bar has been strained, and at this point it is simply rotating. This explains the increases in slip and dilation without an increase in interface steel strain. Another logical explanation is that the strain gage became unattached from the bar, but not damaged to the point where it was unable to take readings.

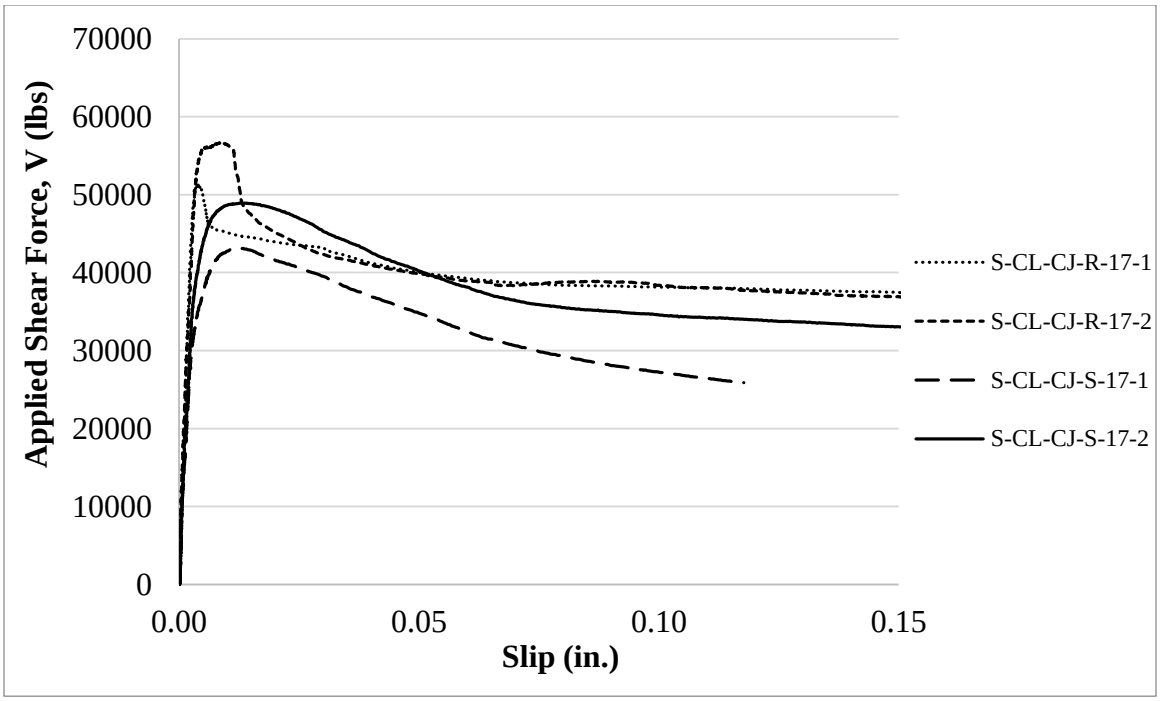

Figure A.50 Applied shear force vs. slip relations for sand-lightweight clay specimens; $\rho = 0.017$

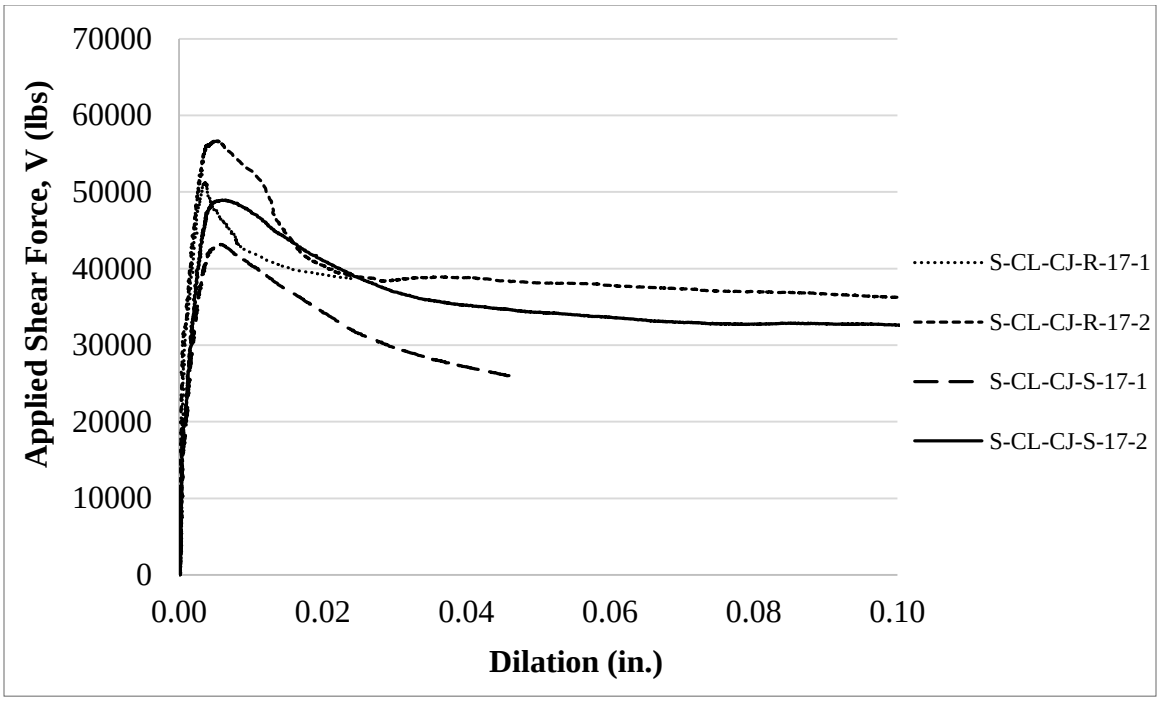

Figure A.51 Applied shear force vs. interface dilation relations for sand-lightweight clay specimens; ρ = 0.017

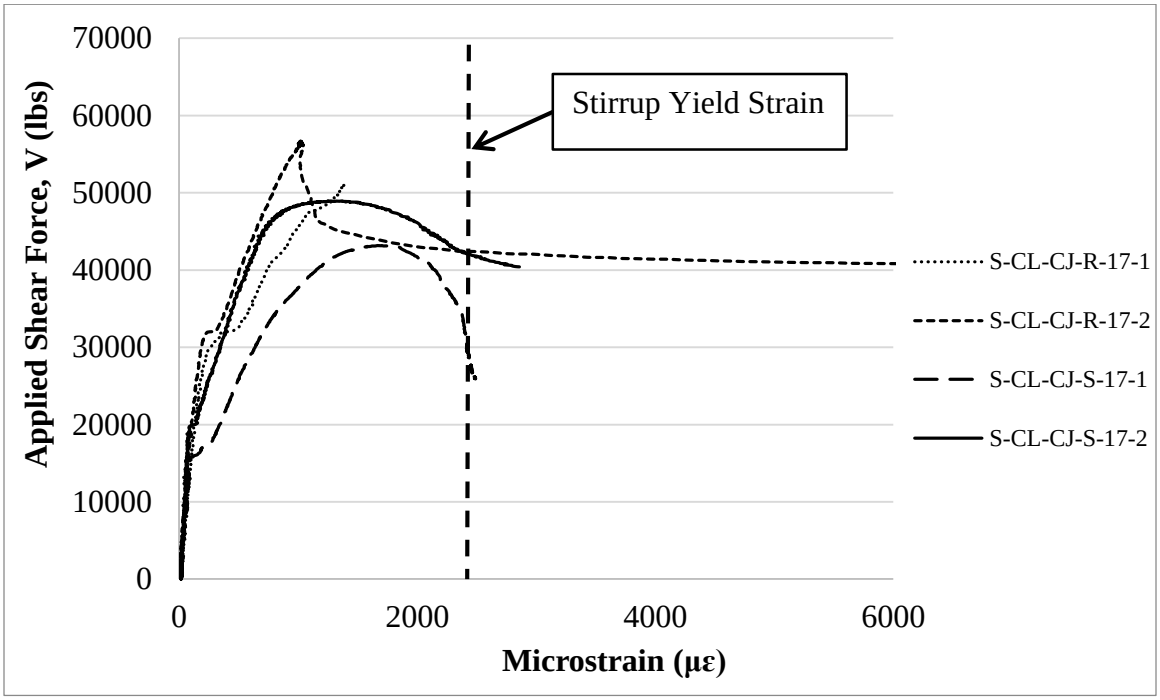

Figure A.52 Applied shear force vs. interface steel strain for sand-lightweight clay specimens; ρ = 0.017

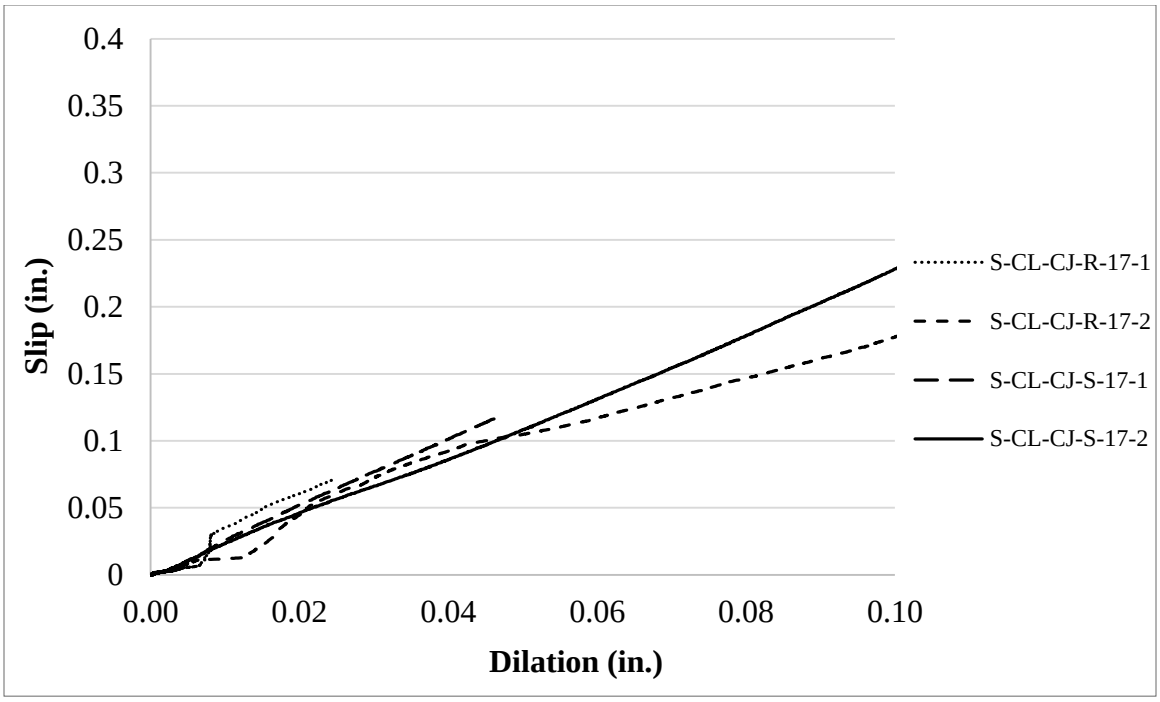

Figure A.53 Slip vs. dilation for sand-lightweight clay specimens; ρ = 0.017

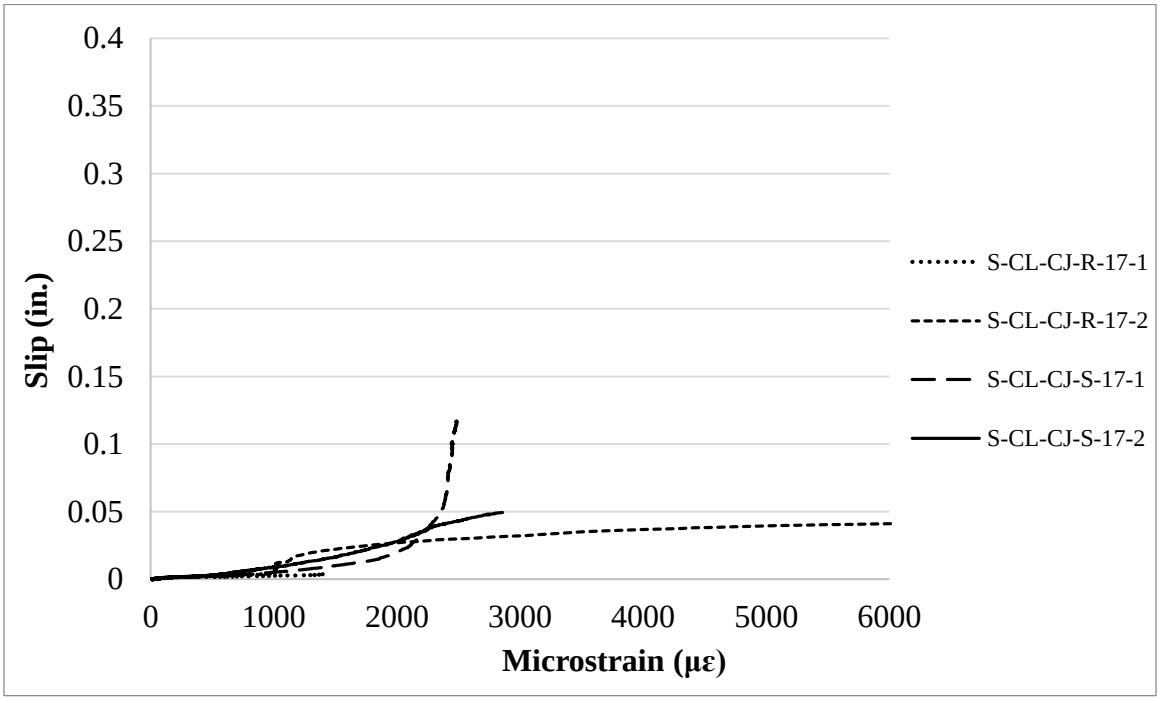

Figure A.54 Slip vs. interface steel strain for sand-lightweight clay specimens; ρ = 0.017

A.3.3.4 Specimens with reinforcement ratio of 0.022

Testing of the sand-lightweight clay specimens with a reinforcement ratio ρ of 0.022 was done on 05/22/15. The results are shown in Figure A.55 through Figure A.59, and as previously discussed, all four specimens of this series failed due to concrete splitting rather than shear.

In the plot of applied shear vs. interface shear strain, Figure A.59, it can be seen that all specimens of this series except S-CL-CJ-R-22-2 failed to reach steel yield strain in the reinforcement stirrups. This means that the level of strain for those shear stirrups stayed below 2,400 $\mu\varepsilon$ and that for this specimen geometry. If there had been more cover on the bars (or no splitting failure), the bars may have been able to yield. Yet, there is no way to determine this other than by redesigning the specimens and re-testing them. A standard cover of ¾ in. was used for the specimens in this study. Increasing the cover to 1.5 in. would possibly prevent this splitting failure issue from occurring.

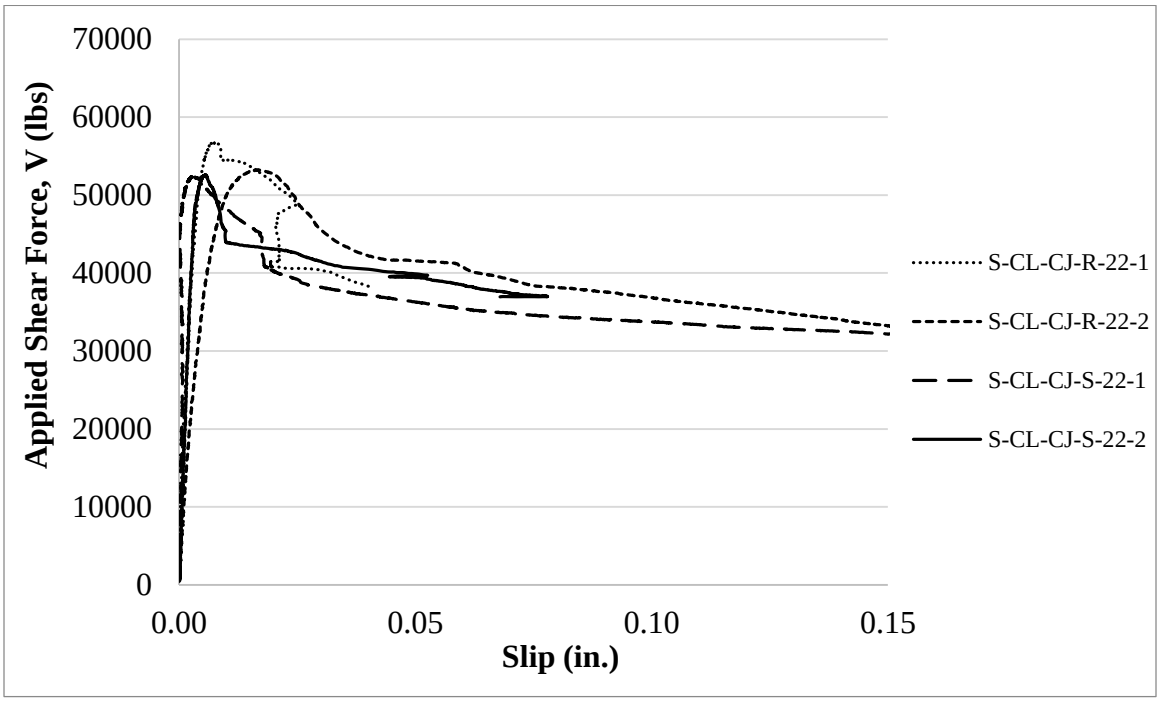

Figure A.55 Applied shear force vs. slip relations for sand-lightweight clay specimens; with ρ = 0.022

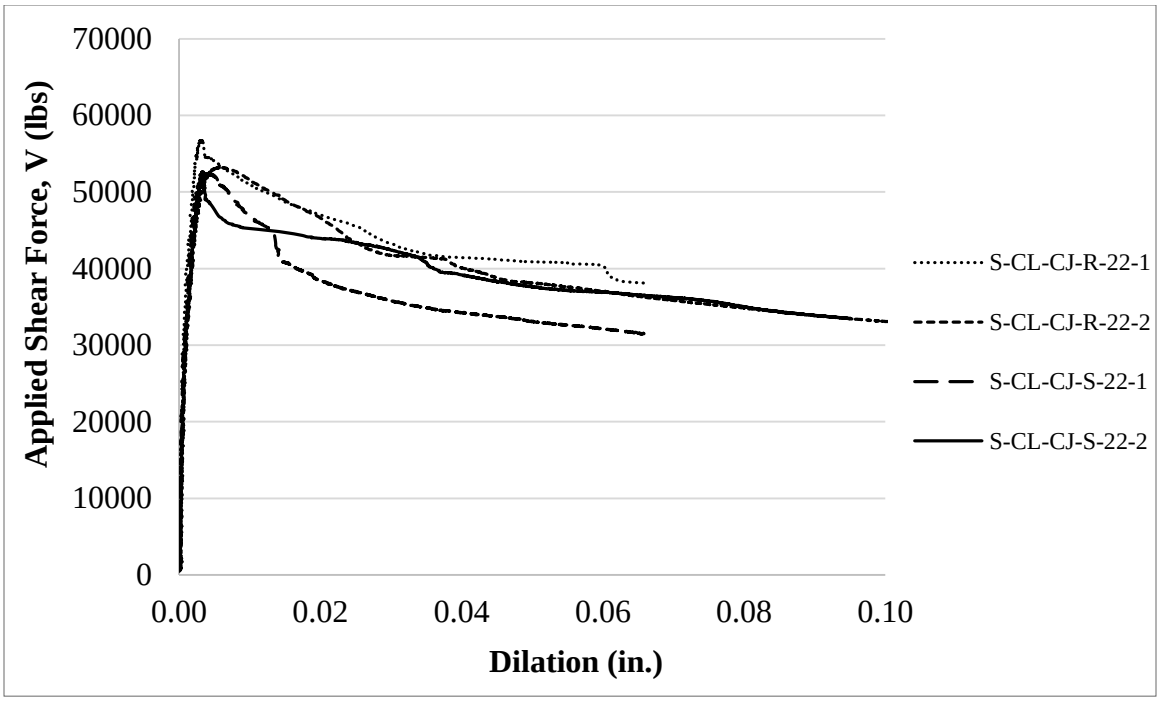

Figure A.56 Applied shear force vs. interface dilation relations for sand-lightweight clay specimens; ρ = 0.022

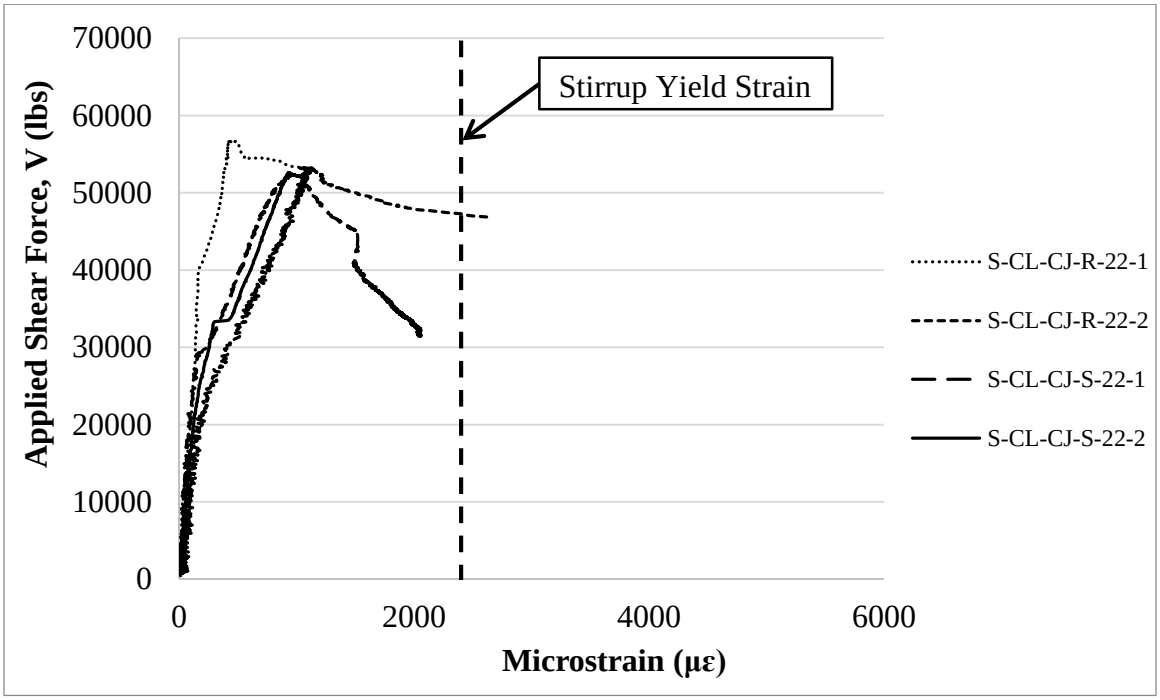

Figure A.57 Applied shear force vs. interface steel strain for sand-lightweight clay specimens; ρ = 0.022

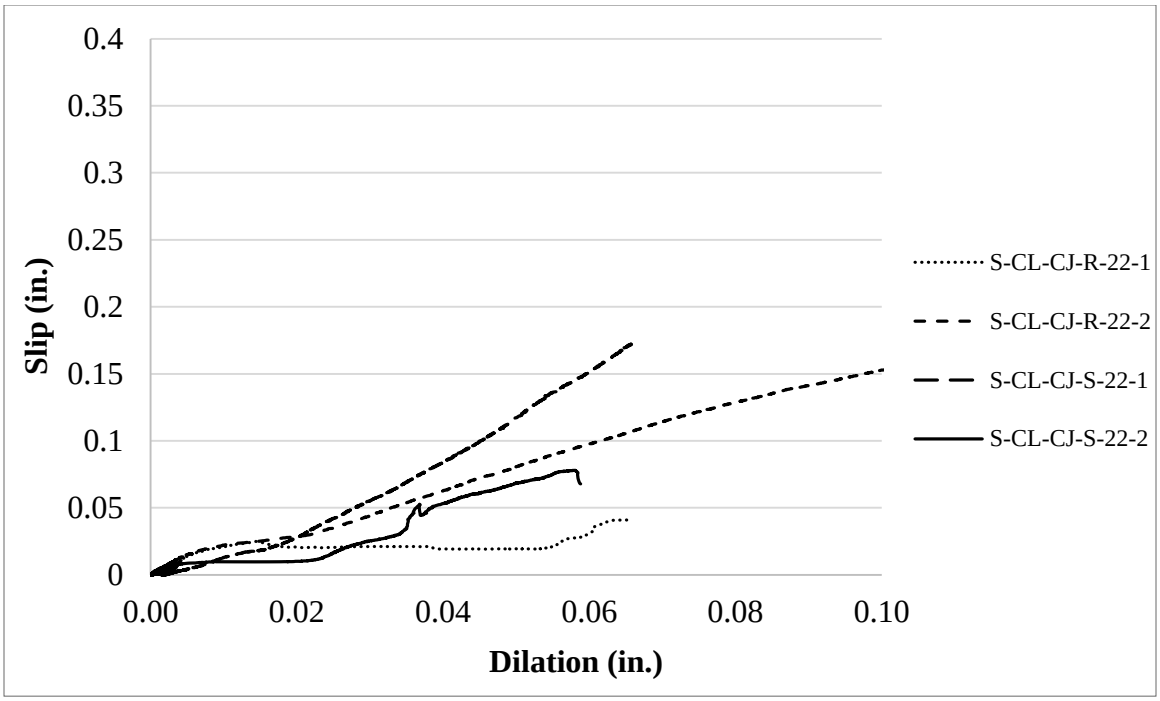

Figure A.58 Slip vs. dilation for sand-lightweight clay specimens; ρ = 0.022

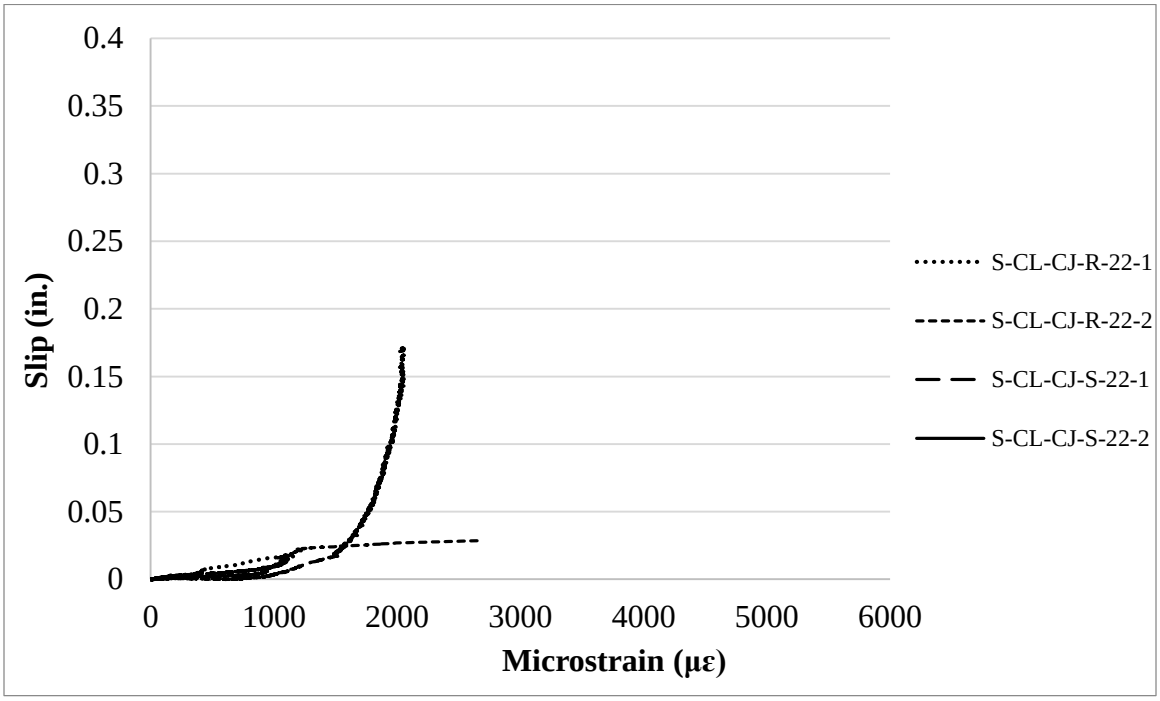

Figure A.59 Slip vs. interface steel strain for sand-lightweight clay specimens; ρ = 0.022

A.4 ALL-LIGHTWEIGHT CONCRETE SPECIMENS

This section presents the results of the all-lightweight concrete specimens with a monolithic or cold joint interface. Specimens presented in the following section include series A-SH-MO-U, A-SH-MO-P, A-SL-CJ-R, A-SL-CJ-S, A-CL-CJ-R, and A-CL-CJ-S. Shale aggregate all-lightweight concrete specimens were tested on 3/6/2015. Slate aggregate all-lightweight concrete specimens were tested on 5/25/2015. Clay aggregate all-lightweight concrete specimens were tested on 4/13/2015.

A.4.1 Shale aggregate all-lightweight concrete specimens

All shale all-lightweight specimens were cast monolithically. All specimens failed in shear along the shear plane. DC-LVDTs measuring back face bottom dilation and back face slip of specimen A-SH-MO-P-2 detached during testing due to concrete cover spalling shown in Figure A.60. During the testing of specimen A-SH-MO-P-1, strain readings exceeding the range of the strain gages were observed. For this reason, the strain data for specimen A-SH-MO-P-1 is not displayed in figures below. The behavior of the shale aggregate all-lightweight concrete specimens is shown in Figure A.61 through Figure A.66. Figure A.61 shows the relations between applied shear force and slip. Figure A.62 shows the applied shear versus dilation relations. Figure A.63 shows the slip versus dilation relations. Figure A.64 shows applied shear force versus strain relations. Figure A.65 shows slip versus strain relations. Lastly, Figure A.66 shows the dilation versus strain relations.

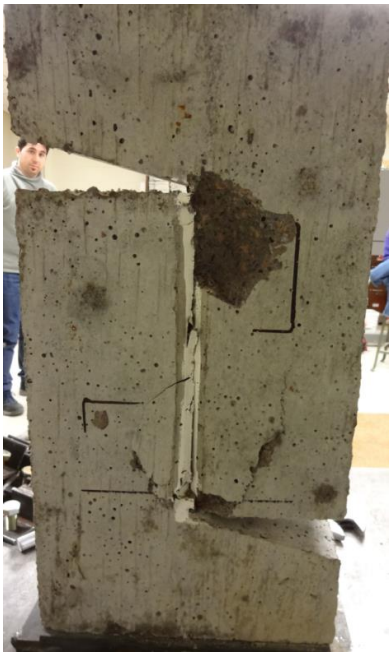

Figure A.60 Concrete Spalling on Specimen A-SH-MO-P-2

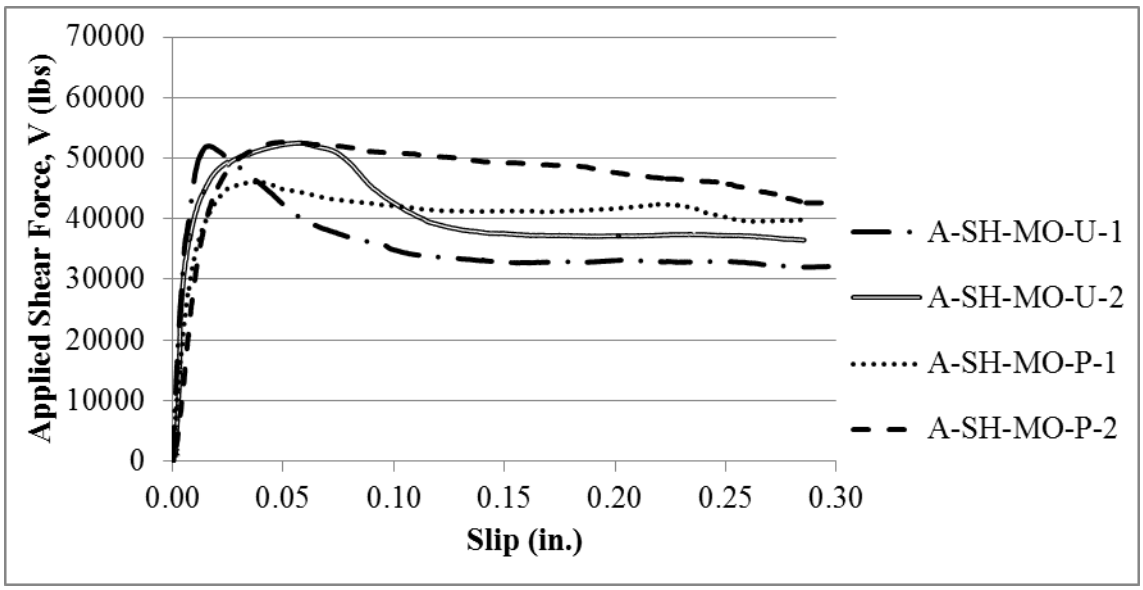

Figure A.61 Applied Shear Force vs. Slip for Shale All-Lightweight Concrete Monolithic Interface Specimens; ρ = 0.013

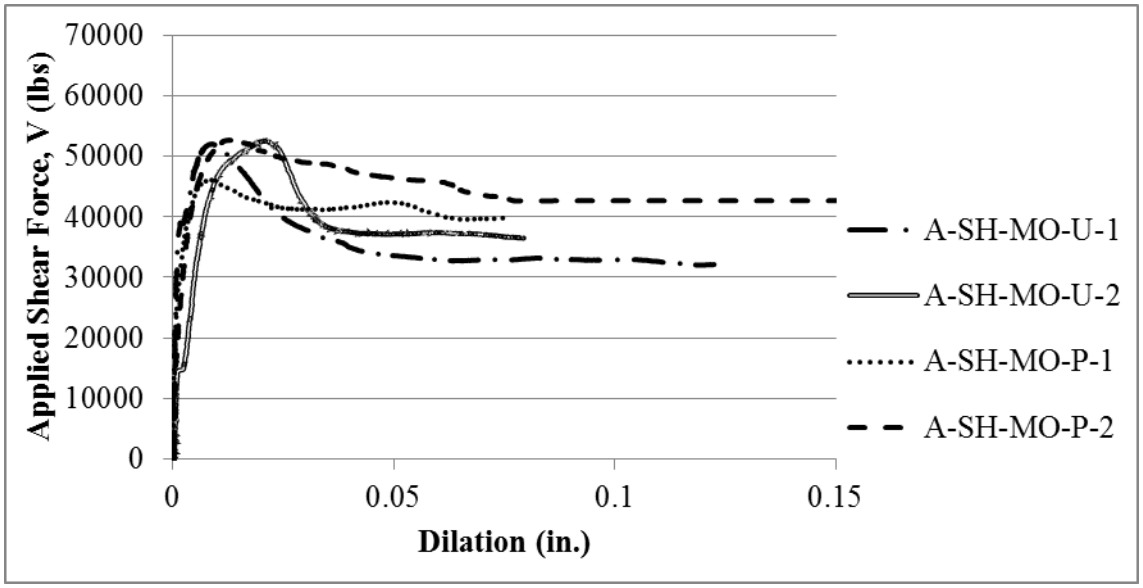

Figure A.62 Applied Shear Force vs. Dilation for Shale All-Lightweight Concrete Monolithic Interface Specimens; ρ = 0.013

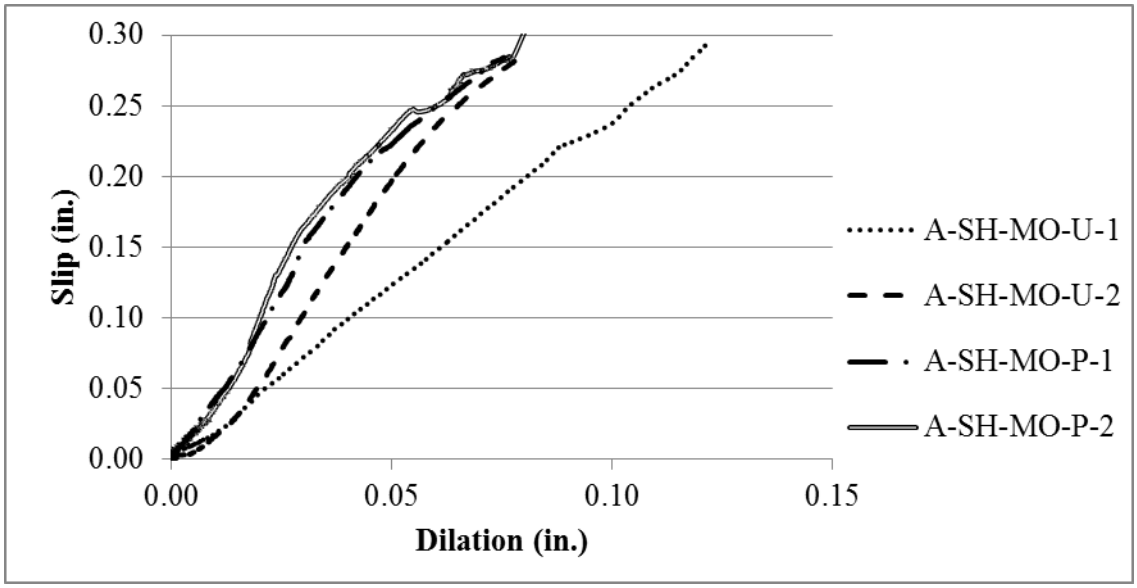

Figure A.63 Slip vs. Dilation for Shale All-Lightweight Concrete Monolithic Interface Specimens; $\rho = 0.013$

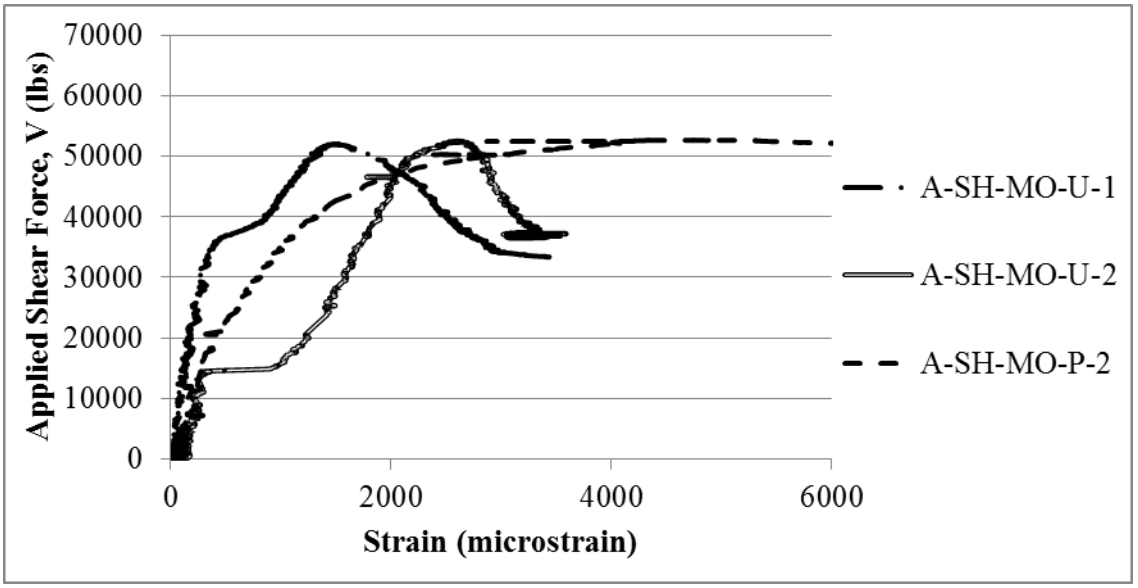

Figure A.64 Applied Shear Force vs. Shear Reinforcement Strain for Shale All-Lightweight Concrete Specimens; $\rho = 0.013$

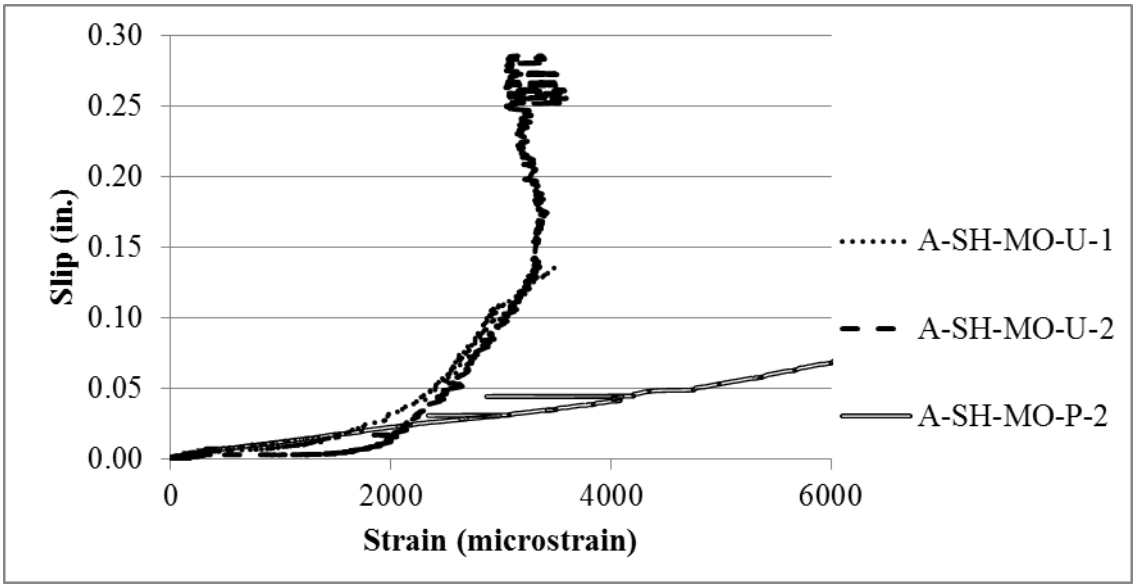

Figure A.65 Slip vs. Shear Reinforcement Strain for Shale All-Lightweight Concrete Monolithic Interface Specimens; ρ = 0.013

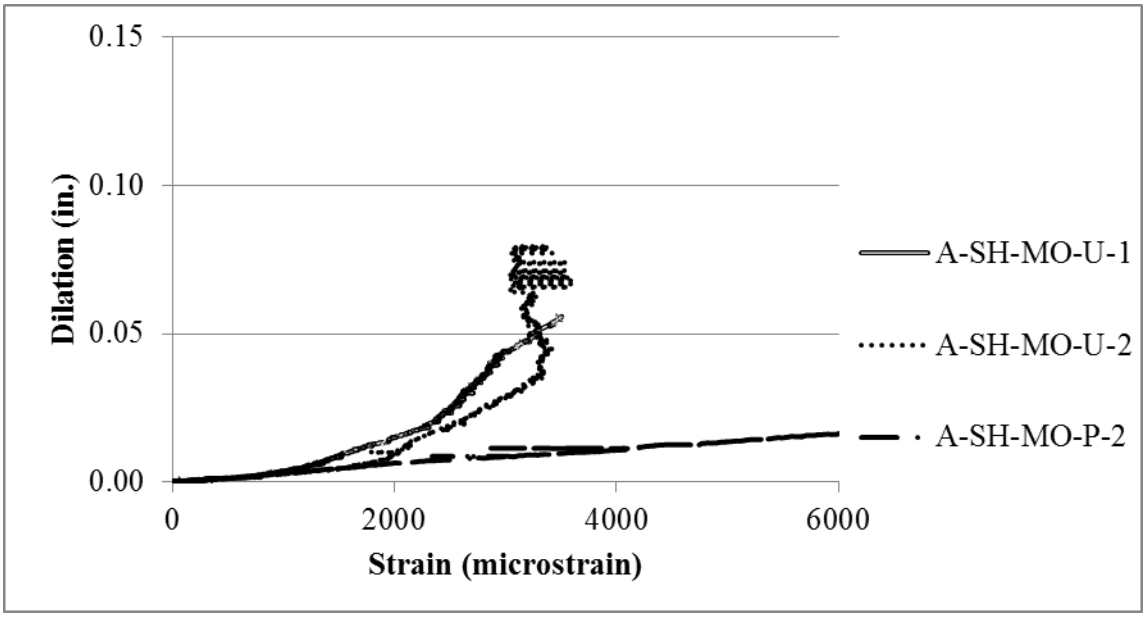

Figure A.66 Dilation vs. Shear Reinforcement Strain for Shale All-Lightweight Concrete Monolithic Interface Specimens; ρ = 0.013

A.4.2 Slate aggregate all-lightweight concrete specimens

All slate aggregate all-lightweight concrete specimens had a cold joint interface. Specimens presented in this section include series A-SL-CJ-R and A-SL-CJ-S. All specimens failed in shear along the shear plane. The behavior of slate aggregate all-lightweight concrete specimens is shown in Figure A.67 through Figure A.72. Figure A.67 shows the relations between applied shear force and slip. Figure A.68 shows the applied shear versus dilation relations. Figure A.69 shows the slip versus dilation relations. Figure A.70 shows the applied shear force versus strain relations. Figure

A.71 shows the slip versus strain relations. Figure A.72 shows the dilation versus shear plane reinforcement strain relations.

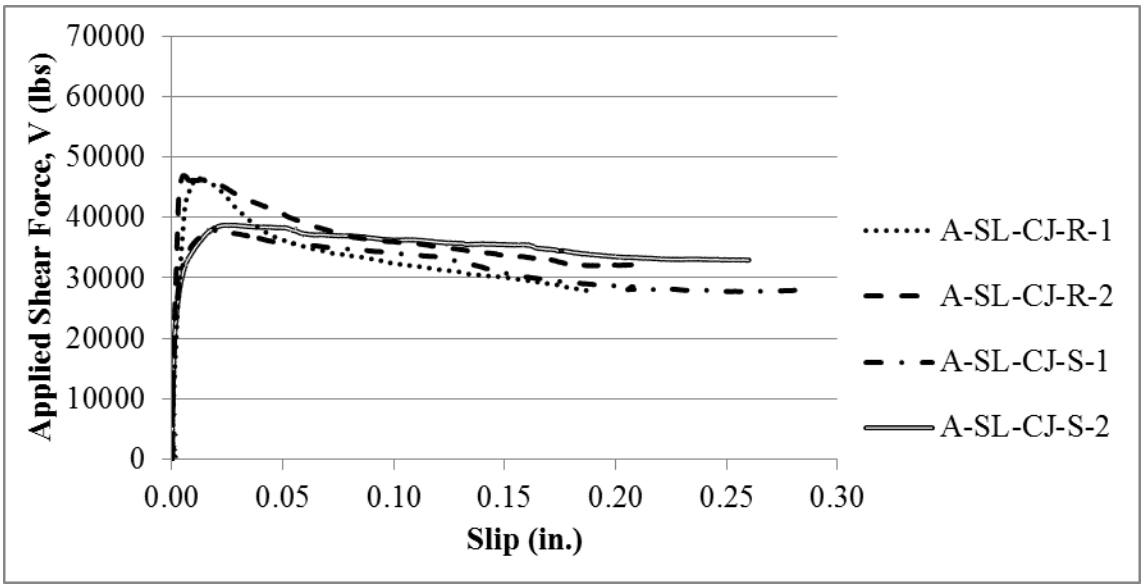

Figure A.67 Applied Shear Force vs. Slip for Slate All-Lightweight Concrete Cold Joint Interface Specimens; $\rho = 0.013$

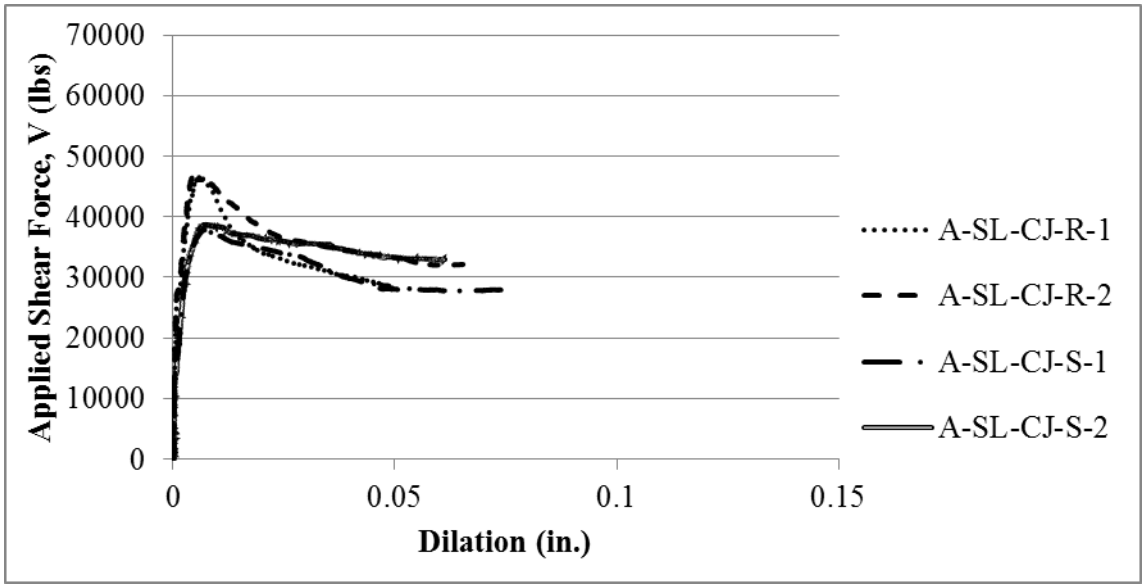

Figure A.68 Applied Shear Force vs. Dilation for Slate All-Lightweight Concrete Cold Joint Interface Specimens; $\rho = 0.013$

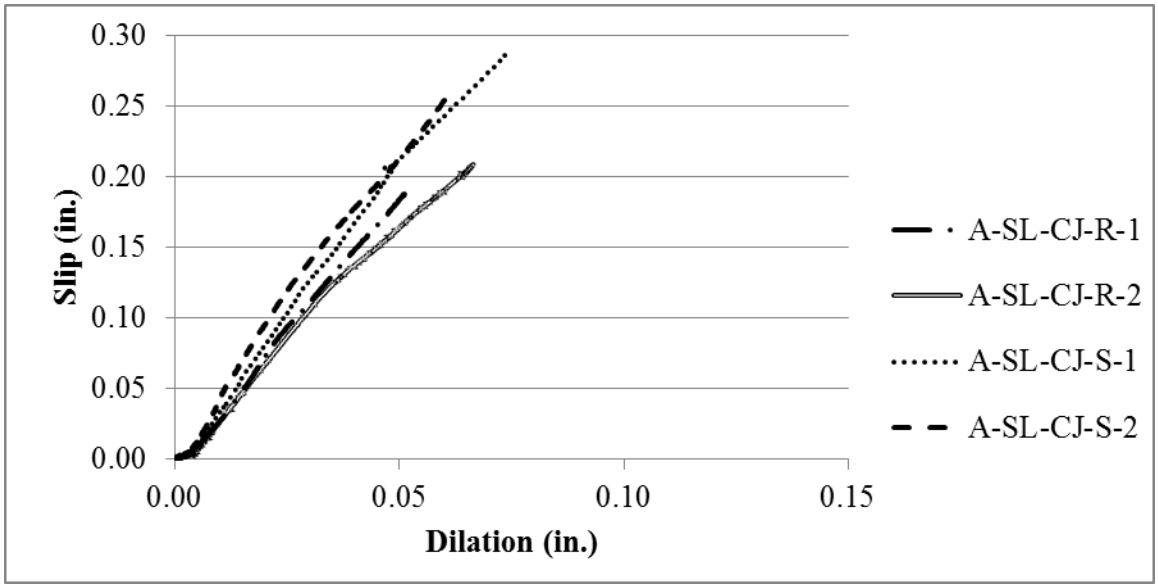

Figure A.69 Slip vs. Dilation for Slate All-Lightweight Concrete Cold Joint Interface Specimens; $\rho = 0.013$

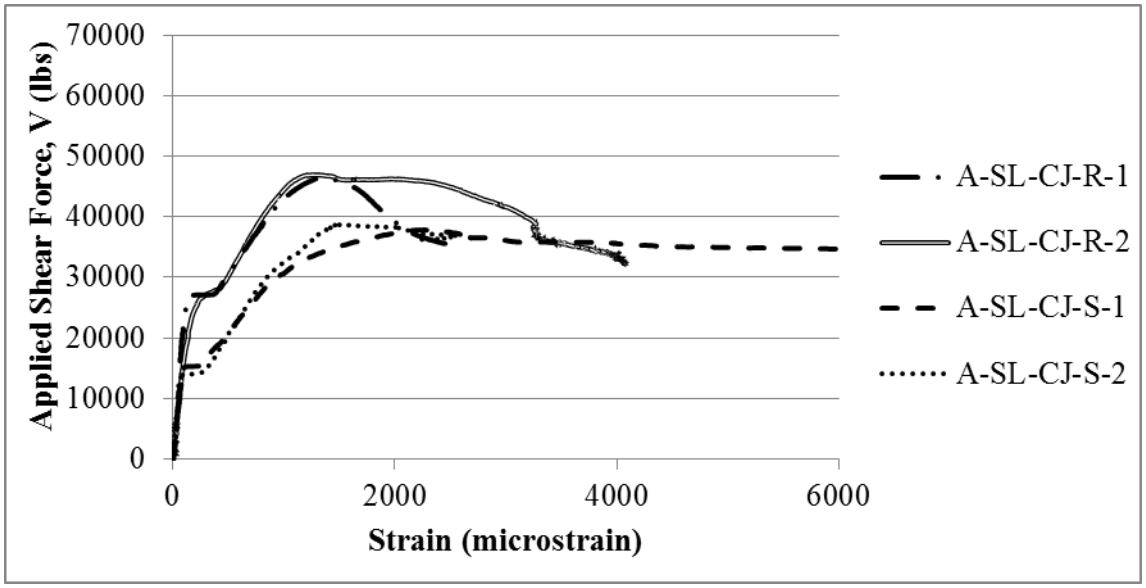

Figure A.70 Applied Shear Force vs. Shear Reinforcement Strain for Slate All-Lightweight Concrete Cold Joint Interface Specimens; $\rho = 0.013$

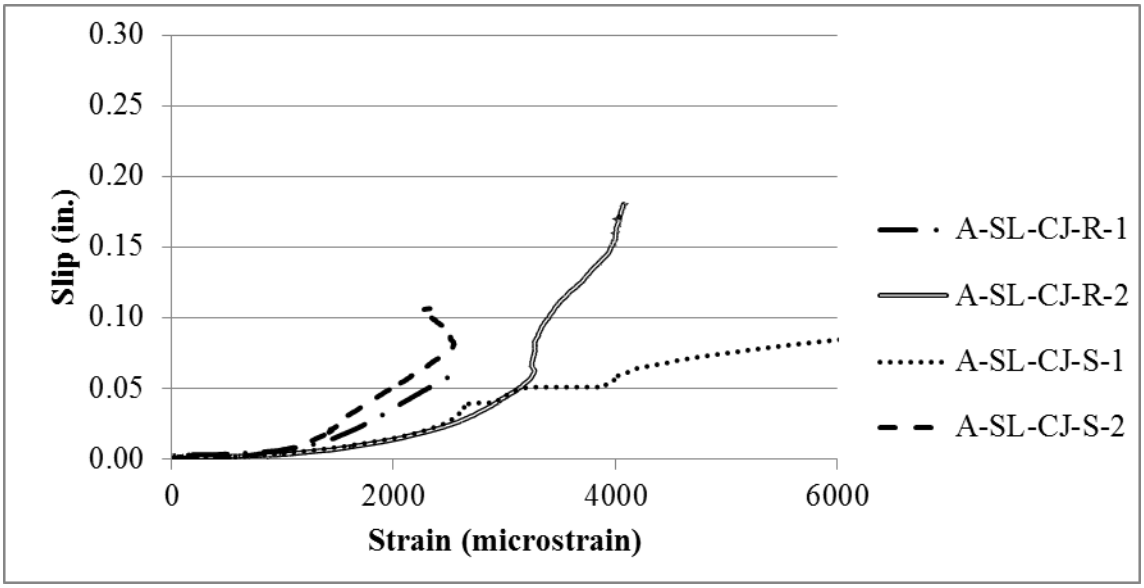

Figure A.71 Slip vs. Shear Reinforcement Strain for Slate All-Lightweight Concrete Cold Joint Interface Specimens

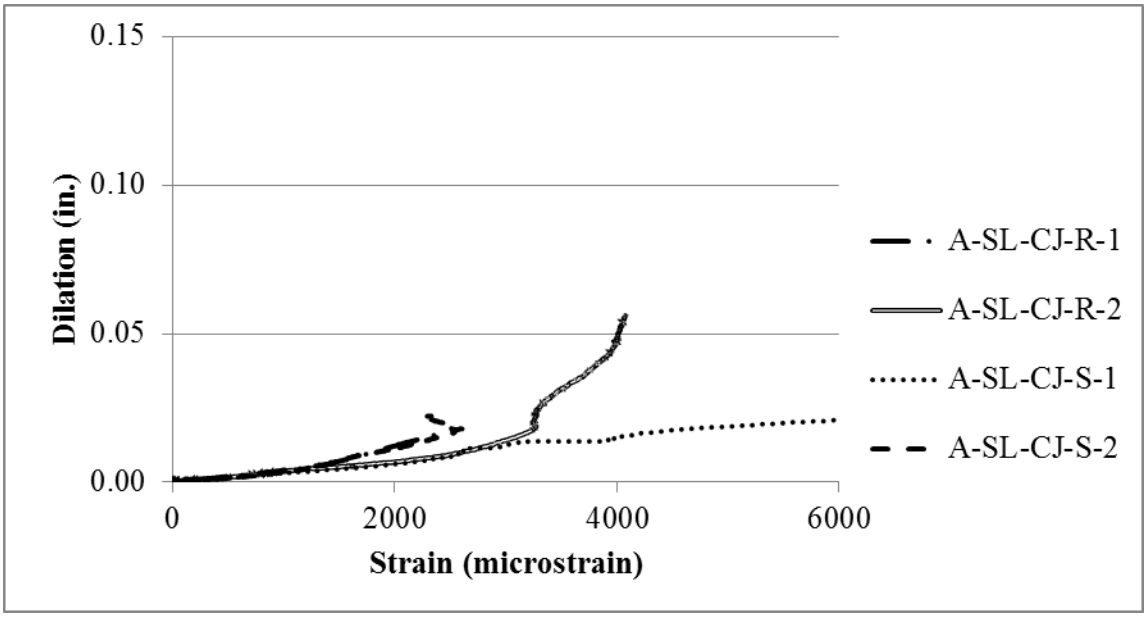

Figure A.72 Dilation vs. Shear Reinforcement Strain for Slate All-Lightweight Concrete Cold Joint Interface Specimens; $\rho = 0.013$

A.4.3 Clay aggregate all-lightweight concrete specimens

All clay all-lightweight concrete specimens had a cold joint interface. Specimens presented in this section include series A-CL-CJ-R and A-CL-CJ-S. All specimens failed in shear along the shear plane. Severe cracking of the concrete cover was observed during testing specimen A-CL-CJ-R-1 prior to reaching the ultimate force. The cracking is shown in Figure A.73a. The cracked concrete cover was physically removed after the test was completed and the result is shown in Figure A.73b. The behavior of the clay aggregate all-lightweight concrete specimens is shown in Figure A.74 through Figure A.79. Figure A.74 shows the relations between applied shear force and slip. Figure

A.75 shows the applied shear versus dilation relations. Figure A.76 shows the slip versus dilation relations. Figure A.77 shows the applied shear force versus strain relations. Figure A.78 shows the slip versus strain relations. Figure A.79 shows the dilation versus strain relations.

Figure A.73 a) Concrete cracking on A-CL-CJ-R-1, b) after the removal of all loose concrete

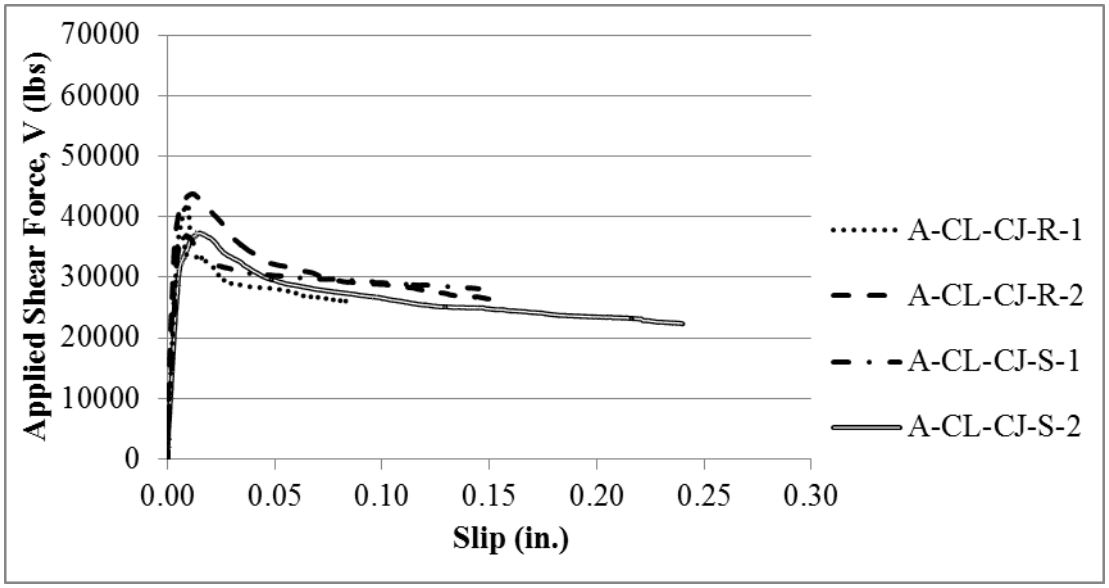

Figure A.74 Applied Shear Force vs. Slip for Clay All-Lightweight Concrete Cold Joint Interface Specimens; $\rho = 0.013$

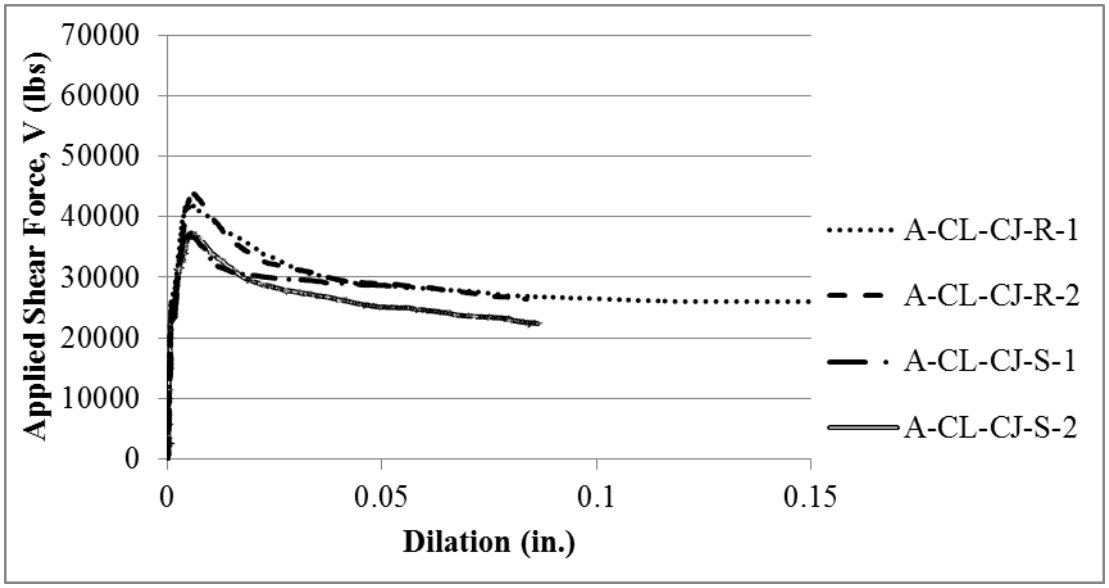

Figure A.75 Applied Shear Force vs. Dilation for Clay All-Lightweight Concrete Cold Joint Interface Specimens; $\rho = 0.013$

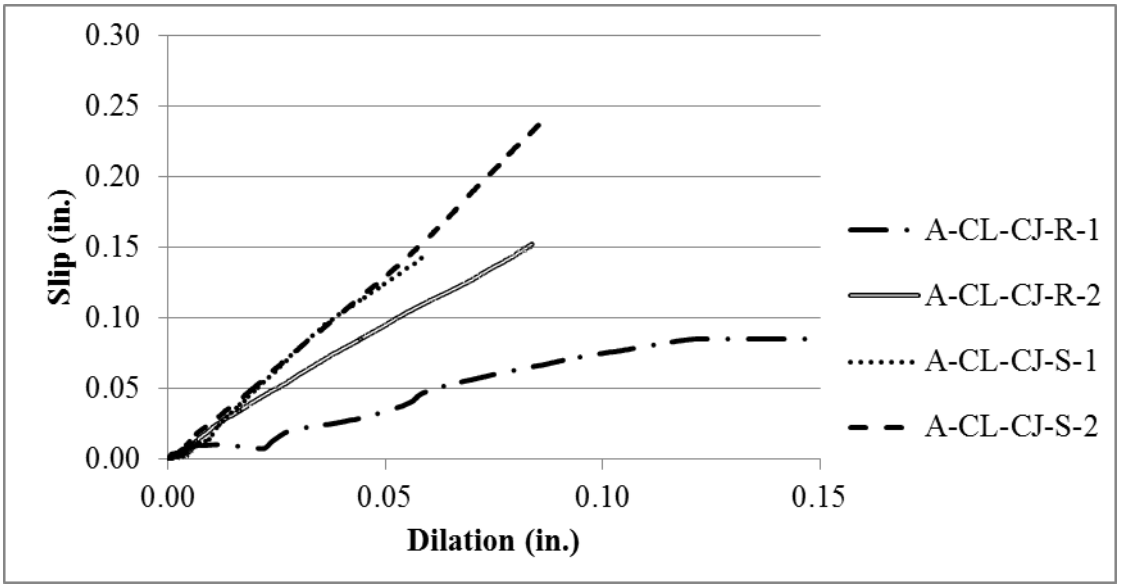

Figure A.76 Slip vs. Dilation for Clay All-Lightweight Concrete Cold Joint Interface Specimens; $\rho = 0.013$

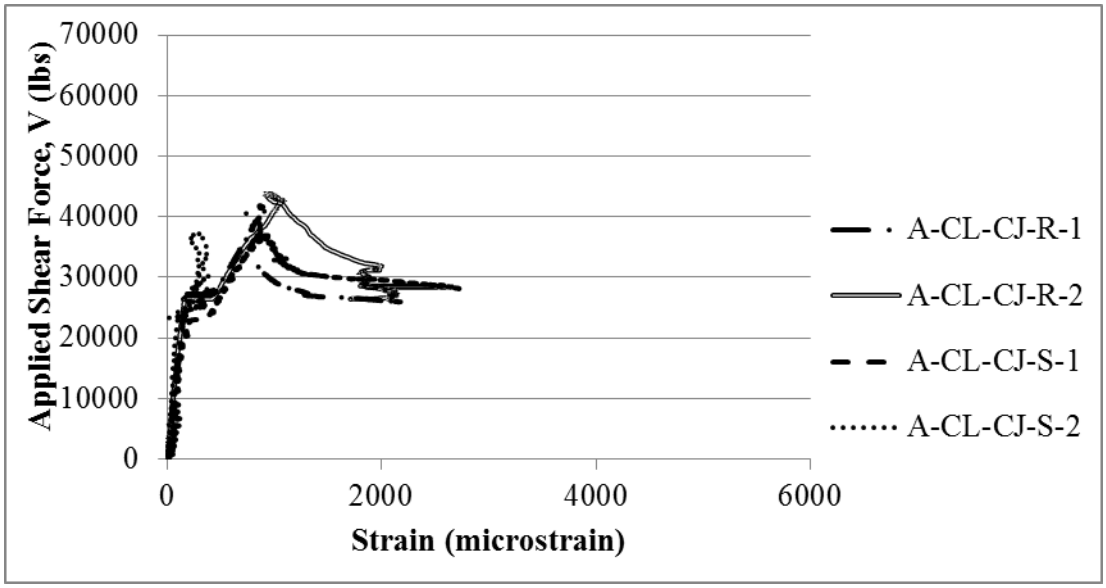

Figure A.77 Applied Shear Force vs. Shear Reinforcement Strain for Clay All-Lightweight Concrete Cold Joint Interface Specimens; ρ = 0.013

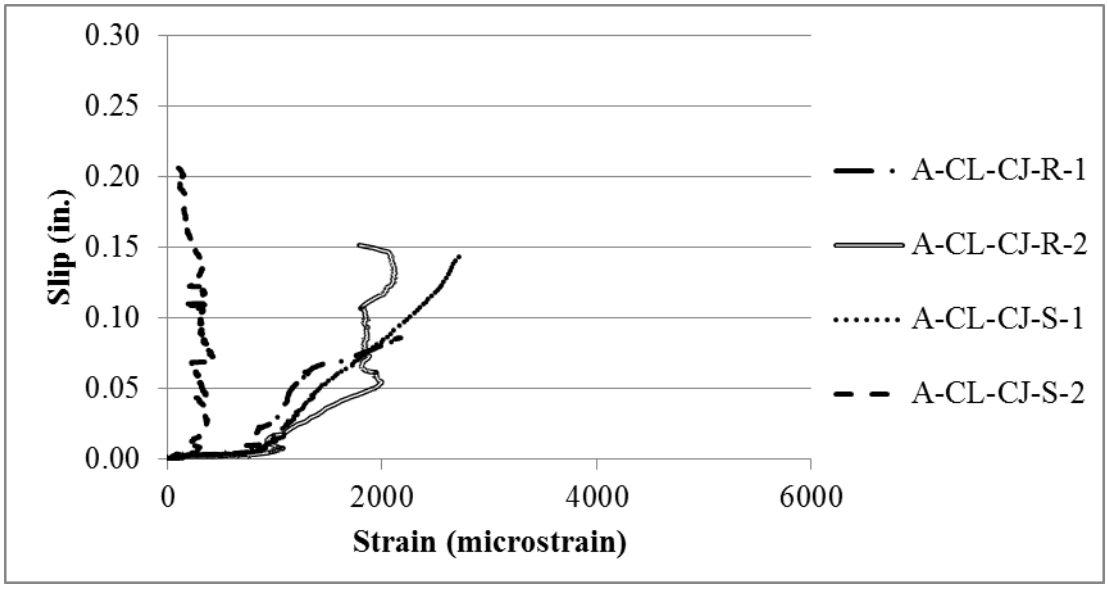

Figure A.78 Slip vs. Shear Reinforcement Strain for Clay All-Lightweight Concrete Cold Joint Interface Specimens; ρ = 0.013

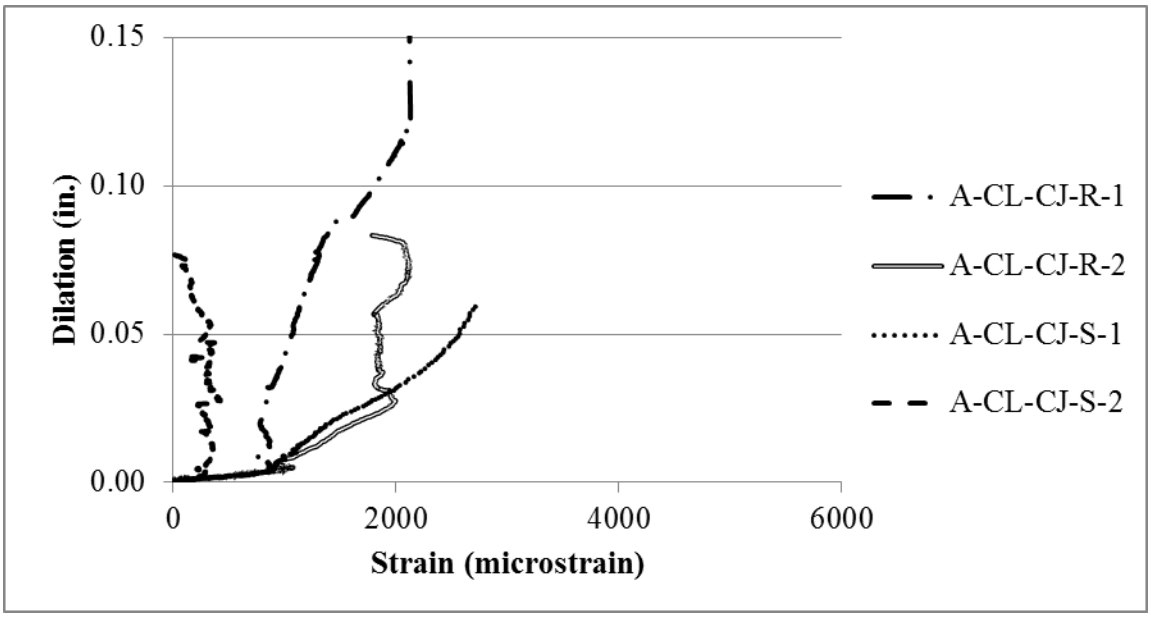

Figure A.79 Dilation vs. Shear Reinforcement Strain for Clay All-Lightweight Concrete Cold Joint Interface Specimens; $\rho = 0.013$

Appendix B

B. SHEAR FRICTION TEST RESULTS

Table B.1 Shear-friction Tests of Pushoff Specimens with Monolithic Uncracked Interface

Researcher(s)	Specimen ID	f'_c (psi)	A_{cr} (in^2)	ρ	f_y (psi)	$\rho f_{y,limited}$ (psi)*	V_{test} (lbs)	v_{test} (psi)	μ_{test}	V_{test}/V_{calc} PCI Eq. 5-32b	V_{test}/V_{calc} PCI Eq. 5-32a	V_{test}/V_{calc} ACI Eq. 22.9.4.2
Normalweight Concrete (λ=1.0)												
Hofbeck, Ibrahim, and Mattock, 1969	1.1A	3920	50	0.004	50700	223	37500	750	3.4	1.34	2.40	2.40
	1.1B	4340	50	0.004	48000	211	42200	844	4.0	1.55	2.85	2.85
	1.2A	3840	50	0.009	50700	446	50000	1000	2.2	1.27	1.60	1.60
	1.2B	4180	50	0.009	48000	422	49000	980	2.3	1.27	1.66	1.66
	1.3A	3840	50	0.013	50700	669	55000	1100	1.6	1.14	1.17	1.43
	1.3B	3920	50	0.013	48000	634	53500	1070	1.7	1.14	1.21	1.36
	1.4A	4510	50	0.018	50700	892	68000	1360	1.5	1.36	1.36	1.62
	1.4B	3855	50	0.018	48000	845	64000	1280	1.5	1.28	1.28	1.66
	1.5A	4510	50	0.022	50700	1115	70000	1400	1.3	1.40	1.40	1.67
	1.5B	4065	50	0.022	48000	1056	69200	1384	1.3	1.38	1.38	1.72
	1.6A	4310	50	0.026	50700	1338	71600	1432	1.1	1.43	1.43	1.74
	1.6B	4050	50	0.026	48000	1267	71000	1420	1.1	1.42	1.42	1.77
Mattock, Li, and Wang, 1976	M1	4180	50	0.004	50900	224	38000	760	3.4	1.36	2.42	2.42
	M2	3900	50	0.009	52700	464	49000	980	2.1	1.22	1.51	1.51
	M3	3995	50	0.013	52300	690	55500	1110	1.6	1.13	1.15	1.39
	M4	4150	50	0.018	50900	896	57000	1140	1.3	1.14	1.14	1.40
	M5	3935	50	0.022	52700	1159	64000	1280	1.1	1.28	1.28	1.63
	M6	4120	50	0.026	52700	1391	66000	1320	0.9	1.32	1.32	1.63
Kahn and Mitchell, 2002	SF-4-1-U	6805	60	0.004	69500	220	57880	965	4.4	1.74	3.13	3.13
	SF4-2-U	6805	60	0.007	69500	440	80080	1335	3.0	1.70	2.17	2.17
	SF-4-3-U	6805	60	0.011	69500	660	85830	1431	2.2	1.49	1.55	1.55
	SF-7-1-U	11734	60	0.004	83000	220	87550	1459	6.6	2.63	4.74	4.74
	SF-7-2-U	12410	60	0.007	83000	440	118110	1969	4.5	2.51	3.20	3.20
	SF-7-3-U	13103	60	0.011	83000	660	138430	2307	3.5	2.40	2.50	2.50
	SF-7-4-U	12471	60	0.015	83000	880	149090	2485	2.8	2.49	2.49	2.02
	SF-10-1-U-a	12053	60	0.004	83000	220	100090	1668	7.6	3.01	5.42	5.42
	SF-10-1-U-b	14326	60	0.004	83000	220	91880	1531	7.0	2.76	4.97	4.97
	SF-10-2-U-a	14776	60	0.007	83000	440	130650	2178	5.0	2.78	3.54	3.54
	SF-10-2-U-b	14804	60	0.007	83000	440	124050	2068	4.7	2.64	3.36	3.36
	SF-10-3-U-a	16170	60	0.011	83000	660	144820	2414	3.7	2.51	2.61	2.61

	SF-10-3-U-b	13934	60	0.011	83000	660	147900	2465	3.7	2.56	2.67	2.67
	SF-10-4-U-a	15468	60	0.015	83000	880	156030	2601	3.0	2.60	2.60	2.11
	SF-10-4-U-b	16476	60	0.015	83000	880	160040	2667	3.0	2.67	2.67	2.16
	SF-14-1-U	17957	60	0.004	83000	220	94950	1583	7.2	2.85	5.14	5.14
	SF-14-2-U	17362	60	0.007	83000	440	108460	1808	4.1	2.30	2.94	2.94
	SF-14-3-U	16255	60	0.011	83000	660	146230	2437	3.7	2.54	2.64	2.64
	SF-14-4-U	16059	60	0.015	83000	880	155970	2600	3.0	2.60	2.60	2.11
Present study	N-MO-U-1	4840	49.5	0.013	72200	780	63410	1281	1.6	1.28	1.28	1.48
	N-MO-U-2	4840	49.5	0.013	72200	780	62200	1257	1.6	1.26	1.26	1.45
								NW	**Avg**	**1.86**	**2.34**	**2.39**
									Max	**3.01**	**5.42**	**5.42**
									Min	**1.13**	**1.14**	**1.36**
									STD	**0.655**	**1.179**	**1.098**
									COV	**0.351**	**0.503**	**0.459**
Sand-lightweight Concrete (λ=0.85)												
Mattock, Li, and Wang, 1976	A1	3740	50	0.004	47700	210	37900	758	3.6	1.65	3.03	3.03
	A2	4095	50	0.009	53600	472	45700	914	1.9	1.32	1.63	1.63
	A3	3910	50	0.013	53200	702	51000	1020	1.5	1.21	1.22	1.30
	A4	4100	50	0.018	50900	896	55000	1100	1.2	1.29	1.29	1.38
	A5	3960	50	0.022	50900	1120	59500	1190	1.1	1.40	1.40	1.50
	A6	4250	50	0.026	51800	1368	67200	1344	1.0	1.58	1.58	1.68
Present study	S-SH-MO-U-1	4770	49.5	0.013	72200	780	55430	1120	1.4	1.32	1.32	1.40
	S-SH-MO-U-2	4770	49.5	0.013	72200	780	56590	1143	1.5	1.34	1.34	1.43
								SLW	**Avg**	**1.39**	**1.60**	**1.67**
									Max	**1.65**	**3.03**	**3.03**
									Min	**1.21**	**1.22**	**1.30**
									STD	**0.149**	**0.596**	**0.566**
									COV	**0.107**	**0.372**	**0.339**
All-lightweight Concrete (λ=0.75)												
Mattock, Li, and Wang, 1976	E1	4150	50	0.004	52300	230	39000	780	3.4	1.83	3.23	3.23
	E2	4030	50	0.009	52300	460	43600	872	1.9	1.45	1.80	1.80
	E3	4065	50	0.013	52300	690	48000	960	1.4	1.30	1.32	1.32
	E4	4040	50	0.018	53200	936	57500	1150	1.2	1.53	1.53	1.44
	E5	4115	50	0.022	50500	1111	60000	1200	1.1	1.60	1.60	1.50
	E6	4050	50	0.026	52300	1381	62500	1250	0.9	1.67	1.67	1.56
	G1	4145	50	0.004	52300	230	41000	820	3.6	1.93	3.39	3.39
	G2	3880	50	0.009	50500	444	42300	846	1.9	1.43	1.81	1.81
	G3	4100	50	0.013	51800	684	53000	1060	1.6	1.44	1.48	1.48

	G4	4420	50	0.018	53200	936	57500	1150	1.2	1.53	1.53	1.44
	G5	4005	50	0.022	51800	1140	57000	1140	1.0	1.52	1.52	1.43
	G6	4005	50	0.026	51800	1368	59500	1190	0.9	1.59	1.59	1.49
Present study	A-SH-MO-U-1	4700	49.5	0.013	72200	780	52030	1051	1.3	1.40	1.40	1.31
	A-SH-MO-U-2	4700	49.5	0.013	72200	780	52550	1062	1.4	1.42	1.42	1.33
								ALW	**Avg**	**1.55**	**1.81**	**1.75**
									Max	**1.93**	**3.39**	**3.39**
									Min	**1.30**	**1.32**	**1.31**
									STD	**0.170**	**0.653**	**0.679**
									COV	**0.110**	**0.361**	**0.387**

Note: * $\boldsymbol{\rho f_{y,\,actual}}$ is computed using the actual yield strength but not greater than 60,000 psi.

Table B.2 Shear-friction Tests of Pushoff Specimens with Monolithic Pre-Cracked Interface

Researcher(s)	Specimen ID	f'_c (psi)	A_{cr} (in^2)	ρ	f_y (psi)	$\rho f_{y,limited}$ (psi)*	V_{test} (lbs)	v_{test} (psi)	μ_{test}	V_{test}/V_{calc} PCI Eq. 5-32b	V_{test}/V_{calc} PCI Eq. 5-32a	V_{test}/V_{calc} ACI Eq. 22.9.4.2
Normalweight Concrete (λ=1.0)												
Hofbeck, Ibrahim, and Mattock, 1969	2.1	3100	50	0.004	50700	223	29500	590	2.6	1.06	1.89	1.89
	2.2	3100	50	0.009	50700	446	34000	680	1.5	0.86	1.09	1.10
	2.3	3900	50	0.013	50700	669	42000	840	1.3	0.87	0.90	1.08
	2.4	3900	50	0.018	50700	892	50000	1000	1.1	1.00	1.00	1.28
	2.5	4180	50	0.022	50700	1115	65000	1300	1.2	1.30	1.30	1.60
	2.6	4180	50	0.026	50700	1338	69250	1385	1.0	1.39	1.39	1.70
	3.3	3100	50	0.009	50700	446	34000	680	1.5	0.86	1.09	1.10
	3.4	4040	50	0.016	47200	741	51400	1028	1.4	1.03	1.03	1.28
	3.5	4040	50	0.025	42400	1039	57600	1152	1.1	1.15	1.15	1.43
	4.1	4070	50	0.004	66100	264	35200	704	2.7	1.16	1.90	1.90
	4.2	4070	50	0.009	66100	528	49000	980	1.9	1.14	1.33	1.33
	4.3	4340	50	0.013	66100	792	59000	1180	1.5	1.18	1.18	1.43
	4.4	4340	50	0.018	66100	1056	70000	1400	1.3	1.40	1.40	1.69
	4.5	3390	50	0.022	66100	1320	66000	1320	1.0	1.32	1.32	1.95
	5.1	2450	50	0.004	50700	223	25500	510	2.3	0.91	1.63	1.63
	5.2	2620	50	0.009	50700	446	35000	700	1.6	0.89	1.12	1.34
	5.3	2385	50	0.013	50700	669	40500	810	1.2	1.13	1.13	1.70
	5.4	2580	50	0.018	50700	892	39750	795	0.9	1.03	1.03	1.54
	5.5	2620	50	0.022	50700	1115	50500	1010	0.9	1.28	1.28	1.93
Mattock, Li, and Wang, 1976	N1	4180	50	0.004	50900	224	23000	460	2.1	0.82	1.47	1.47
	N2	3900	50	0.009	52700	464	39000	780	1.7	0.97	1.20	1.20
	N3	3995	50	0.013	52300	690	48000	960	1.4	0.98	0.99	1.20
	N4	4150	50	0.018	50900	896	57500	1150	1.3	1.15	1.15	1.42
	N5	3935	50	0.022	50900	1120	58750	1175	1.0	1.18	1.18	1.49
	N6	4120	50	0.026	50000	1320	59500	1190	0.9	1.19	1.19	1.47
Kahn and Mitchell, 2002	SF-4-1-C	6805	60	0.004	69500	220	35000	583	2.7	1.05	1.89	1.89
	SF-4-2-C	6805	60	0.007	69500	440	55690	928	2.1	1.18	1.51	1.51
	SF-4-3-C	6805	60	0.011	69500	660	71130	1186	1.8	1.23	1.28	1.28
	SF-7-1-C	11734	60	0.004	83000	220	41680	695	3.2	1.25	2.26	2.26
	SF-7-2-C	12410	60	0.007	83000	440	51730	862	2.0	1.10	1.40	1.40
	SF-7-3-C	13103	60	0.011	83000	660	71510	1192	1.8	1.24	1.29	1.29

	SF-7-4-C	12471	60	0.015	83000	880	62730	1046	1.2	1.05	1.05	0.85
	SF-10-1-C-a	12053	60	0.004	83000	220	25780	430	2.0	0.77	1.40	1.40
	SF-10-1-C-b	14326	60	0.004	83000	220	29970	500	2.3	0.90	1.62	1.62
	SF-10-2-C-a	14676	60	0.007	83000	440	50780	846	1.9	1.08	1.37	1.37
	SF-10-2-C-b	14804	60	0.007	83000	440	48110	802	1.8	1.02	1.30	1.30
	SF-10-3-C-a	16170	60	0.011	83000	660	64650	1078	1.6	1.12	1.17	1.17
	SF-10-3-C-b	13924	60	0.011	83000	660	63360	1056	1.6	1.10	1.14	1.14
	SF-10-4-C-a	15468	60	0.015	83000	880	74160	1236	1.4	1.24	1.24	1.00
	SF-10-4-C-b	16476	60	0.015	83000	880	76280	1271	1.4	1.27	1.27	1.03
	SF-14-1-C	16015	60	0.004	83000	220	24880	415	1.9	0.75	1.35	1.35
	SF-14-2-C	15496	60	0.007	83000	440	40180	670	1.5	0.85	1.09	1.09
	SF-14-3-C	15392	60	0.011	83000	660	55500	925	1.4	0.96	1.00	1.00
	SF-14-4-C	15982	60	0.015	83000	880	73270	1221	1.4	1.22	1.22	0.99
Mansur et al., 2008	AN-2	5831	55.8	0.009	76870	523	66180	1186	2.3	1.39	1.62	1.62
	AN-4	5831	55.8	0.017	76870	1046	82305	1475	1.4	1.48	1.48	1.56
	AN-6	5831	55.8	0.026	76870	1570	104570	1874	1.2	1.87	1.87	1.98
	AM-2	10008	55.8	0.009	76870	523	60710	1088	2.1	1.27	1.49	1.49
	AM-3	10008	55.8	0.013	76870	785	93075	1668	2.1	1.67	1.67	1.52
	AM-4	10008	55.8	0.017	76870	1046	113555	2035	1.9	2.04	2.04	1.59
	AH-2	12618	55.8	0.009	76870	523	62940	1128	2.2	1.32	1.54	1.54
	AH-3	12618	55.8	0.013	76870	785	100050	1793	2.3	1.79	1.79	1.63
	AH-4	12618	55.8	0.017	76870	1046	114670	2055	2.0	2.06	2.06	1.40
	B1-4	10618	55.8	0.011	43511	486	54460	976	2.0	1.18	1.43	1.43
	B2-2	12314	55.8	0.006	43511	243	41850	750	3.1	1.29	2.20	2.20
	B2-4	12314	55.8	0.011	43511	486	59260	1062	2.2	1.29	1.56	1.56
	B2-5	12314	55.8	0.014	43511	608	66460	1191	2.0	1.29	1.40	1.40
	B2-6	12314	55.8	0.017	43511	730	74215	1330	1.8	1.33	1.33	1.30
	B3-4	13808	55.8	0.011	43511	486	64505	1156	2.4	1.40	1.70	1.70
	B4-2	15432	55.8	0.006	43511	243	48660	872	3.6	1.49	2.56	2.56
	B4-4	15432	55.8	0.011	43511	486	68245	1223	2.5	1.48	1.80	1.80
	B4-5	15432	55.8	0.014	43511	608	74770	1340	2.2	1.45	1.57	1.57
	B4-6	15432	55.8	0.017	43511	730	80630	1445	2.0	1.45	1.45	1.41
Present study	N-MO-P-1	4840	49.5	0.013	72200	780	61070	1234	1.6	1.23	1.23	1.42
	N-MO-P-2	4840	49.5	0.013	72200	780	56970	1151	1.5	1.15	1.15	1.33
								NW	**Avg**	**1.21**	**1.42**	**1.48**
									Max	**2.06**	**2.56**	**2.56**
									Min	**0.75**	**0.90**	**0.85**

									STD	**0.272**	**0.342**	**0.320**
									COV	**0.225**	**0.241**	**0.216**
Sand-lightweight Concrete (λ=0.85)												
Mattock, Li, and Wang, 1976	B1	3740	50	0.004	49600	218	22500	450	2.1	0.96	1.73	1.73
	B2	3360	50	0.009	50900	448	32600	652	1.5	0.97	1.22	1.22
	B3	3910	50	0.013	50900	672	42000	840	1.3	1.02	1.05	1.07
	B4	4100	50	0.018	49100	864	47000	940	1.1	1.11	1.11	1.18
	B5	3960	50	0.022	50500	1111	50000	1000	0.9	1.18	1.18	1.26
	B6	4250	50	0.026	51800	1368	57700	1154	0.8	1.36	1.36	1.44
	C1	2330	50	0.004	49600	218	18200	364	1.7	0.77	1.40	1.40
	C2	2330	50	0.009	53600	472	25700	514	1.1	0.87	0.92	1.10
	C3	2000	50	0.013	50900	672	26300	526	0.8	1.03	1.03	1.32
	C4	2050	50	0.018	52300	920	28000	560	0.6	1.07	1.07	1.37
	C5	2330	50	0.022	53600	1179	32000	640	0.5	1.08	1.08	1.37
	C6	2330	50	0.026	49600	1309	37000	740	0.6	1.25	1.25	1.59
	D1	5995	50	0.004	51800	228	18500	370	1.6	0.77	1.36	1.36
	D2	5995	50	0.009	52300	460	33400	668	1.5	0.98	1.22	1.22
	D3	5710	50	0.013	52300	690	38600	772	1.1	0.92	0.94	0.97
	D4	5710	50	0.018	52300	920	51100	1022	1.1	1.20	1.20	1.28
	D5	5600	50	0.022	52300	1151	54100	1082	0.9	1.27	1.27	1.35
	D6	5600	50	0.026	51800	1368	61000	1220	0.9	1.44	1.44	1.53
Hoff, 1993	1 LWC1	8490	84	0.005	53600	281	24108	287	1.0	0.54	0.86	0.86
	2 LWC1	8510	84	0.005	53600	281	30660	365	1.3	0.68	1.09	1.09
	3 LWC1	8290	84	0.005	53600	281	34692	413	1.5	0.78	1.24	1.24
	4 LWC1	8490	84	0.010	68000	571	63924	761	1.3	1.00	1.12	1.12
	5 LWC1	8510	84	0.010	69000	571	57120	680	1.2	0.89	1.00	1.00
	6 LWC1	8290	84	0.010	68000	571	61068	727	1.3	0.96	1.07	1.07
	1 LWC2	9270	84	0.005	53600	281	41076	489	1.7	0.92	1.46	1.46
	2 LWC2	8760	84	0.005	53600	281	28140	335	1.2	0.63	1.00	1.00
	3 LWC2	8730	84	0.005	53600	281	25116	299	1.1	0.56	0.89	0.89
	4 LWC2	9270	84	0.010	68000	571	62076	739	1.3	0.97	1.09	1.09
	5 LWC2	8760	84	0.010	68500	571	58128	692	1.2	0.91	1.02	1.02
	6 LWC2	8730	84	0.010	68500	571	57120	680	1.2	0.89	1.00	1.00
	1 HSLWC	10310	84	0.005	72100	314	56112	668	2.1	1.18	1.79	1.79
	2 HSLWC	10910	84	0.005	72100	314	46032	548	1.7	0.97	1.47	1.47
	3 HSLWC	11020	84	0.005	72100	314	49140	585	1.9	1.04	1.56	1.56
	4 HSLWC	10310	84	0.010	66800	571	73080	870	1.5	1.14	1.28	1.28

	5 HSLWC	10910	84	0.010	66800	571	73080	870	1.5	1.14	1.28	1.28
	6 HSLWC	11020	84	0.010	66800	571	75096	894	1.6	1.18	1.31	1.31
Present study	S-SH-MO-P-1	4770	49.5	0.013	72200	780	50593	1022	1.3	1.20	1.20	1.28
	S-SH-MO-P-2	4770	49.5	0.013	72200	780	51880	1048	1.3	1.23	1.23	1.31
								SLW	**Avg**	**1.00**	**1.20**	**1.26**
									Max	**1.44**	**1.79**	**1.79**
									Min	**0.54**	**0.86**	**0.86**
									STD	**0.209**	**0.216**	**0.220**
									COV	**0.209**	**0.180**	**0.174**
All-lightweight Concrete (λ=0.75)												
Mattock, Li, and Wang, 1976	F1	4150	50	0.004	53200	234	22500	450	1.9	1.05	1.83	1.83
	F2	4030	50	0.009	52300	460	26500	530	1.2	0.88	1.10	1.10
	F2A	3970	50	0.009	50900	448	31000	620	1.4	1.04	1.32	1.32
	F3	4065	50	0.013	52300	690	36700	734	1.1	1.00	1.01	1.01
	F3A	3970	50	0.013	51400	678	35100	702	1.0	0.96	0.99	0.99
	F4	4040	50	0.018	50900	896	43500	870	1.0	1.16	1.16	1.09
	F5	4115	50	0.022	51800	1140	46000	920	0.8	1.23	1.23	1.15
	F6	4050	50	0.026	53200	1404	49100	982	0.7	1.31	1.31	1.23
	H1	4145	50	0.004	49800	219	20000	400	1.8	0.96	1.74	1.74
	H2	3880	50	0.009	51800	456	31000	620	1.4	1.03	1.30	1.30
	H3	4100	50	0.013	51800	684	43300	866	1.3	1.18	1.21	1.21
	H4	4420	50	0.018	51800	912	47000	940	1.0	1.25	1.25	1.18
	H5	3950	50	0.022	50500	1111	49500	990	0.9	1.32	1.32	1.25
	H6	4080	50	0.026	49800	1315	52100	1042	0.8	1.39	1.39	1.30
Present study	A-SH-MO-P-1	4700	49.5	0.013	72200	780	46120	932	1.2	1.24	1.24	1.16
	A-SH-MO-P-2	4700	49.5	0.013	72200	780	52690	1064	1.4	1.42	1.42	1.33
								ALW	**Avg**	**1.15**	**1.30**	**1.26**
									Max	**1.42**	**1.83**	**1.83**
									Min	**0.88**	**0.99**	**0.99**
									STD	**0.166**	**0.225**	**0.230**
									COV	**0.144**	**0.173**	**0.182**

Note: * $\rho f_{y,\,actual}$ is computed using the actual yield strength but not greater than 60,000 psi.

Table B.3 Shear-friction Tests of Pushoff Specimens with Roughened Interface

Researcher(s)	Specimen ID	f'_c (psi)	A_{cr} (in^2)	ρ	f_y (psi)	$\rho f_{y,limited}$ (psi)*	V_{test} (lbs)	v_{test} (psi)	μ_{test}	V_{test}/V_{calc} PCI Eq. 5-32b	V_{test}/V_{calc} PCI Eq. 5-32a	V_{test}/V_{calc} ACI Eq. 22.9.4.2
Normalweight Concrete (λ=1.0)												
Mattock, 1976	B1	5840	50	0.004	51270	226	24350	487	2.2	1.03	2.16	2.16
	B2	5840	50	0.009	50550	445	35000	700	1.6	1.05	1.57	1.57
	B3	6055	50	0.013	51270	677	52700	1054	1.6	1.28	1.56	1.56
	B4	6055	50	0.018	53820	947	63800	1276	1.3	1.31	1.35	1.35
	B5	5895	50	0.025	49250	1262	78500	1570	1.3	1.57	1.57	1.65
	B6	5895	50	0.032	49250	1576	85000	1700	1.1	1.70	1.70	1.79
	D1	3770	50	0.004	51270	226	29500	590	2.6	1.24	2.62	2.62
	D2	3770	50	0.009	51270	451	46000	920	2.0	1.37	2.04	2.04
	D3	2940	50	0.013	56000	739	50500	1010	1.4	1.37	1.37	1.72
	D4	2940	50	0.018	56000	986	50100	1002	1.0	1.36	1.36	1.70
	D4A	2495	50	0.018	54000	950	49700	994	1.0	1.59	1.59	1.99
	D5	2955	50	0.025	46360	1150	60500	1210	1.1	1.64	1.64	2.05
	D5A	2795	50	0.025	46200	1146	62500	1250	1.1	1.79	1.79	2.24
	D6	2955	50	0.032	48500	1552	73500	1470	0.9	1.99	1.99	2.49
Kahn and Mitchell, 2002	SF-7-1-CJ	11734	60	0.004	83000	220	54000	900	4.1	1.92	4.09	4.09
	SF-7-2-CJ	11734	60	0.007	83000	440	82100	1368	3.1	2.06	3.11	3.11
	SF-7-3-CJ	12471	60	0.011	83000	660	110300	1838	2.8	2.26	2.78	2.78
	SF-7-4-CJ	12471	60	0.015	83000	880	132680	2211	2.5	2.36	2.51	2.51
	SF-10-3-CJ	12953	60	0.011	83000	660	113910	1899	2.9	2.34	2.88	2.88
	SF-10-4-CJ	12953	60	0.015	83000	880	126040	2101	2.4	2.24	2.39	2.39
	SF-14-1-CJ	14756	60	0.004	83000	220	90910	1515	6.9	3.23	6.89	6.89
	SF-14-2-CJ	14756	60	0.007	83000	440	99190	1653	3.8	2.49	3.76	3.76
	SF-14-3-CJ	15218	60	0.011	83000	660	134710	2245	3.4	2.76	3.40	3.40
	SF-14-4-CJ	15218	60	0.015	83000	880	153120	2552	2.9	2.72	2.90	2.90
Harries, Zeno, Shahrooz 2012	615-3A	5800	160	0.004	67300	246	112500	701	2.9	1.41	2.85	2.85
	615-3B	5800	160	0.004	67300	246	96500	591	2.4	1.19	2.40	2.40
	615-4A	5800	160	0.007	61500	438	114500	694	1.6	1.05	1.58	1.58
	615-4B	5800	160	0.007	61500	444	129000	794	1.8	1.19	1.79	1.79
	1035-3A	5800	160	0.004	130000	252	90000	571	2.3	1.14	2.27	2.27
	1035-3B	5800	160	0.004	126000	246	105000	653	2.7	1.32	2.66	2.66
	1035-4A	5800	160	0.007	140000	444	135700	835	1.9	1.25	1.88	1.88
	1035-4B	5800	160	0.008	131300	450	113500	706	1.6	1.05	1.57	1.57
Sneed and Shaw, 2013	N-5-R-4	4860	49.5	0.013	66200	780	59060	1193	1.5	1.35	1.53	1.53
	N-5-R-5	4860	49.5	0.013	66200	780	53420	1079	1.4	1.22	1.38	1.38
	N-5-R-6	4860	49.5	0.013	66200	780	53440	1080	1.4	1.22	1.38	1.38

	N-8-R-1	7550	49.5	0.013	66200	780	74040	1496	1.9	1.69	1.92	1.92
	N-8-R-2	7550	49.5	0.013	66200	780	56090	1133	1.5	1.28	1.45	1.45
	N-8-R-3	7550	49.5	0.013	66200	780	64140	1296	1.7	1.47	1.66	1.66
								NW	**Avg**	**1.65**	**2.25**	**2.31**
									Max	**3.23**	**6.89**	**6.89**
									Min	**1.03**	**1.35**	**1.35**
									STD	**0.556**	**1.048**	**1.019**
									COV	**0.338**	**0.467**	**0.440**
Sand-lightweight Concrete (λ=0.85)												
Sneed and Shaw, 2013	S-5-R-1	4580	49.5	0.013	66200	780	51430	1039	1.3	1.38	1.57	1.57
	S-5-R-2	4580	49.5	0.013	66200	780	50400	1018	1.3	1.36	1.54	1.54
	S-5-R-3	4580	49.5	0.013	66200	780	63900	1291	1.7	1.72	1.95	1.95
	S-8-R-1	7200	49.5	0.013	66200	780	72040	1455	1.9	1.94	2.20	2.20
	S-8-R-2	7200	49.5	0.013	66200	780	67380	1361	1.7	1.81	2.05	2.05
	S-8-R-3	7200	49.5	0.013	66200	780	66720	1348	1.7	1.80	2.03	2.03
Present study	S-SL-CJ-09-R-1	5380	49.5	0.009	72200	540	49340	997	1.8	1.60	2.17	2.17
	S-SL-CJ-09-R-2	5380	49.5	0.009	72200	540	50480	1020	1.9	1.63	2.22	2.22
	S-SL-CJ-13-R-1	5570	49.5	0.013	72200	780	63170	1276	1.6	1.70	1.92	1.92
	S-SL-CJ-13-R-2	5570	49.5	0.013	72200	780	59370	1199	1.5	1.60	1.81	1.81
	S-SL-CJ-17-R-1	4950	49.5	0.017	72200	1020	62380	1260	1.2	1.48	1.48	1.58
	S-SL-CJ-17-R-2	4950	49.5	0.017	72200	1020	65150	1316	1.3	1.55	1.55	1.65
	S-SL-CJ-22-R-1	5000	49.5	0.022	72200	1320	64460	1302	1.0	1.53	1.53	1.63
	S-SL-CJ-22-R-2	5000	49.5	0.022	72200	1320	57590	1163	0.9	1.37	1.37	1.45
	S-CL-CJ-9-R-1	4770	49.5	0.009	72200	540	37100	749	1.4	1.20	1.63	1.63
	S-CL-CJ-9-R-2	4770	49.5	0.009	72200	540	42900	867	1.6	1.39	1.89	1.89
	S-CL-CJ-13-R-1	4640	49.5	0.013	72200	780	50800	1026	1.3	1.37	1.55	1.55
	S-CL-CJ-13-R-2	4640	49.5	0.013	72200	780	46900	947	1.2	1.26	1.43	1.43
								SLW	**Avg**	**1.54**	**1.77**	**1.79**
									Max	**1.94**	**2.22**	**2.22**
									Min	**1.20**	**1.37**	**1.43**
									STD	**0.204**	**0.287**	**0.267**
									COV	**0.133**	**0.162**	**0.149**
All-lightweight Concrete (λ=0.75)												
Sneed and Shaw, 2013	A-5-R-1	6080	49.5	0.013	66200	780	48440	979	1.3	1.48	1.67	1.67
	A-5-R-2	6080	49.5	0.013	66200	780	52800	1067	1.4	1.61	1.82	1.82
	A-5-R-3	6080	49.5	0.013	66200	780	51410	1039	1.3	1.57	1.78	1.78
	A-8-R-1	7843	49.5	0.013	66200	780	61770	1248	1.6	1.88	2.13	2.13
	A-8-R-2	7843	49.5	0.013	66200	780	63940	1292	1.7	1.95	2.21	2.21
	A-8-R-3	7843	49.5	0.013	66200	780	64130	1295	1.7	1.96	2.21	2.21
Present study	A-SL-CJ-13-R-1	4380	49.5	0.013	72200	780	46500	939	1.2	1.42	1.61	1.61
	A-SL-CJ-13-R-2	4380	49.5	0.013	72200	780	46900	947	1.2	1.43	1.62	1.62
	A-CL-CJ-13-R-1	4460	49.5	0.013	72200	780	41800	844	1.1	1.27	1.44	1.44

	A-CL-CJ-13-R-2	4460	49.5	0.013	72200	780	43800	885	1.1	1.34	1.51	1.51
									Avg	**1.59**	**1.80**	**1.80**
									Max	**1.96**	**2.21**	**2.21**
								ALW	**Min**	**1.27**	**1.44**	**1.44**
									STD	**0.254**	**0.288**	**0.288**
									COV	**0.160**	**0.160**	**0.160**

Note: * $\rho f_{y,\,actual}$ is computed using the actual yield strength but not greater than 60,000 psi.

Table B.4 Shear-friction Tests of Pushoff Specimens with Smooth Interface

Researcher(s)	Specimen ID	f'_c (psi)	A_{cr} (in^2)	ρ	f_y (psi)	$\rho f_{y,limited}$ (psi)*	V_{test} (lbs)	v_{test} (psi)	μ_{test}	V_{test}/V_{calc} PCI Eq. 5-32b	V_{test}/V_{calc} PCI Eq. 5-32a	V_{test}/V_{calc} ACI Eq. 22.9.4.2
Normalweight Concrete (λ=1.0)												
Mattock, 1976	C1	5870	50	0.004	50910	224	10500	210	0.9	N/A	1.56	1.56
	C2	5870	50	0.009	50910	448	18000	360	0.8	N/A	1.34	1.34
	C3	5980	50	0.013	50550	667	21400	428	0.6	N/A	1.07	1.07
	C4	5980	50	0.018	51640	909	30000	600	0.7	N/A	1.10	1.10
	C5	6165	50	0.022	52730	1160	39000	780	0.7	N/A	1.12	1.12
	C6	6165	50	0.032	45250	1448	44100	882	0.6	N/A	1.10	1.10
	G1	5870	50	0.004	50910	224	8000	160	0.7	N/A	1.19	1.19
	G2	5870	50	0.009	50910	488	13200	264	0.6	N/A	0.98	0.98
	G3	5980	50	0.013	50550	732	19200	384	0.6	N/A	0.96	0.96
	G4	5980	50	0.018	51640	944	25000	500	0.6	N/A	0.92	0.92
	G5	6165	50	0.022	52730	1216	29300	586	0.5	N/A	0.84	0.84
	G6	6165	50	0.032	45250	1498	38900	778	0.5	N/A	0.97	0.97
	H1	5825	50	0.004	55450	210	9400	188	0.8	N/A	1.28	1.28
	H2	6080	50	0.009	55450	480	16100	322	0.7	N/A	1.10	1.10
	H3	6080	50	0.013	55450	720	23000	460	0.6	N/A	1.05	1.05
	H4	6075	50	0.018	53640	960	25500	510	0.5	N/A	0.90	0.90
	H5	6180	50	0.025	46800	1157	32700	654	0.6	N/A	0.94	0.94
	H6	5900	50	0.032	46800	1488	38000	760	0.5	N/A	0.95	0.95
Kahn and Mitchell, 2002	SF-10-1-CJ	14326	60	0.004	83000	220	31730	529	2.4	N/A	2.00	2.00
	SF-10-2-CJ	12053	60	0.007	83000	440	49290	822	1.9	N/A	1.04	1.04
Sneed and Shaw, 2013	N-5-S-4	4860	49.5	0.013	66200	780	30850	623	0.8	N/A	1.33	1.33
	N-5-S-5	4860	49.5	0.013	66200	780	34680	701	0.9	N/A	1.50	1.50
	N-5-S-6	4860	49.5	0.013	66200	780	39150	791	1.0	N/A	1.69	1.69
	N-8-S-1	7550	49.5	0.013	66200	780	65560	1324	1.7	N/A	2.83	2.83
	N-8-S-2	7550	49.5	0.013	66200	780	53300	1077	1.4	N/A	2.30	2.30
	N-8-S-3	7550	49.5	0.013	66200	780	55330	1118	1.4	N/A	2.39	2.39
								NW	**Avg**	**N/A**	**1.33**	**1.33**
									Max	**N/A**	**2.83**	**2.83**
									Min	**N/A**	**0.84**	**0.84**
									STD	**N/A**	**0.518**	**0.518**
									COV	**N/A**	**0.391**	**0.391**

Sand-lightweight Concrete (λ=0.85)												
Sneed and Shaw, 2013	S-5-S-1	4580	49.5	0.013	66200	780	38530	778	1.0	N/A	1.96	1.96
	S-5-S-2	4580	49.5	0.013	66200	780	34110	689	0.9	N/A	1.73	1.73
	S-5-S-3	4580	49.5	0.013	66200	780	39800	804	1.0	N/A	2.02	2.02
	S-8-S-1	7200	49.5	0.013	66200	780	67030	1354	1.7	N/A	3.40	3.40
	S-8-S-2	7200	49.5	0.013	66200	780	57880	1169	1.5	N/A	2.94	2.94
	S-8-S-3	7200	49.5	0.013	66200	780	58860	1189	1.5	N/A	2.99	2.99
Present study	S-SL-CJ-09-S-1	5380	49.5	0.009	72200	540	26950	544	1.0	N/A	1.98	1.98
	S-SL-CJ-09-S-2	5380	49.5	0.009	72200	540	32590	658	1.2	N/A	2.39	2.39
	S-SL-CJ-13-S-1	5570	49.5	0.013	72200	780	39490	798	1.0	N/A	2.01	2.01
	S-SL-CJ-13-S-2	5570	49.5	0.013	72200	780	48770	985	1.3	N/A	2.48	2.48
	S-SL-CJ-17-S-1	4950	49.5	0.017	72200	1020	49810	1006	1.0	N/A	1.93	1.93
	S-SL-CJ-17-S-2	4950	49.5	0.017	72200	1020	56530	1142	1.1	N/A	2.20	2.20
	S-SL-CJ-22-S-1	5000	49.5	0.022	72200	1320	49810	1006	0.8	N/A	1.49	1.49
	S-SL-CJ-22-S-2	5000	49.5	0.022	72200	1320	56530	1142	0.9	N/A	1.70	1.70
	S-CL-CJ-9-S-1	4770	49.5	0.009	72200	540	31900	644	1.2	N/A	2.34	2.34
	S-CL-CJ-9-S-2	4770	49.5	0.009	72200	540	37900	766	1.4	N/A	2.78	2.78
	S-CL-CJ-13-S-1	4640	49.5	0.013	72200	780	41000	828	1.1	N/A	2.08	2.08
	S-CL-CJ-13-S-2	4640	49.5	0.013	72200	780	40400	816	1.0	N/A	2.05	2.05
	S-CL-CJ-17-S-1	4550	49.5	0.017	72200	1020	43100	871	0.9	N/A	1.67	1.67
	S-CL-CJ-17-S-2	4550	49.5	0.017	72200	1020	48900	988	1.0	N/A	1.90	1.90
								SLW	**Avg**	**N/A**	**2.20**	**2.20**
									Max	**N/A**	**3.40**	**3.40**
									Min	**N/A**	**1.49**	**1.49**
									STD	**N/A**	**0.498**	**0.498**
									COV	**N/A**	**0.226**	**0.226**
All-lightweight Concrete (λ=0.75)												
Sneed and Shaw, 2013	A-5-S-1	6080	49.5	0.013	66200	780	41470	838	1.1	N/A	2.39	2.39
	A-5-S-2	6080	49.5	0.013	66200	780	40080	810	1.0	N/A	2.31	2.31
	A-5-S-3	6080	49.5	0.013	66200	780	39250	793	1.0	N/A	2.26	2.26
	A-8-S-1	7843	49.5	0.013	66200	780	46090	931	1.2	N/A	2.65	2.65
	A-8-S-2	7843	49.5	0.013	66200	780	48040	970	1.2	N/A	2.76	2.76
	A-8-S-3	7843	49.5	0.013	66200	780	51740	1045	1.3	N/A	2.98	2.98
Present study	A-SL-CJ-13-S-1	4380	49.5	0.013	72200	780	37800	764	1.0	N/A	2.18	2.18
	A-SL-CJ-13-S-2	4380	49.5	0.013	72200	780	38800	784	1.0	N/A	2.23	2.23
	A-CL-CJ-13-S-1	4460	49.5	0.013	72200	780	36900	745	1.0	N/A	2.12	2.12
	A-CL-CJ-13-S-2	4460	49.5	0.013	72200	780	37300	754	1.0	N/A	2.15	2.15

	ALW	Avg	N/A	2.40	2.40
		Max	N/A	2.98	2.98
		Min	N/A	2.12	2.12
		STD	N/A	0.294	0.294
		COV	N/A	0.122	0.122

Note: * $\rho f_{y,\,actual}$ is computed using the actual yield strength but not greater than 60,000 psi.

**Specimens were reported as having a smooth interface, so they are included in this table.

REFERENCES

AASHTO (2014). "AASHTO LRFD Bridge Design Specifications," Seventh edition, American Association of State Highway and Transportation Officials (AASHTO), Washington, DC.

ACI Committee 318 (2014). "Building Code Requirements for Structural Concrete and Commentary (ACI 318R-14)," Farmington Hills, MI: American Concrete Institute.

Anderson, A. R., "Composite Designs in Precast and Cast-in-Place Concrete," *Progressive Architecture, Vol.* 41, No. 9, September 1960, pp. 172-179.

ASTM A370 (2015). "Standard Test Methods and Definitions for Mechanical Testing of Steel Products." Annual book of ASTM standards, ASTM, West Conshohocken, Pennsylvania.

ASTM A615 (2012). "Standard Specification for Deformed and Plain Carbon-Steel Bars for Concrete Reinforcement." Annual book of ASTM standards, ASTM, West Conshohocken, Pennsylvania.

ASTM C29 (2009). "Standard Test Method for Bulk Density (Unit Weight) and Voids in Aggregate." Annual book of ASTM standards, ASTM, West Conshohocken, Pennsylvania.

ASTM C33 (2013). "Standard Specification for Concrete Aggregates" Annual book of ASTM standards, ASTM, West Conshohocken, Pennsylvania.

ASTM C39 (2015). "Standard Test Method for Compressive Strength of Cylindrical Concrete Specimens" Annual book of ASTM standards, ASTM, West Conshohocken, Pennsylvania.

ASTM C127 (2015). "Standard Test Method for Density, Relative Density (Specific Gravity), and Absorption of Coarse Aggregate." Annual book of ASTM standards, ASTM, West Conshohocken, Pennsylvania.

ASTM C128 (2015). "Standard Test Method for Density, Relative Density (Specific Gravity), and Absorption of Fine Aggregate." Annual book of ASTM standards, ASTM, West Conshohocken, Pennsylvania.

ASTM C136 (2006). "Standard Test Method for Sieve Analysis of Fine and Coarse Aggregates." Annual book of ASTM standards, ASTM, West Conshohocken, Pennsylvania.

ASTM C138 (2014). "Standard Test Method for Density (Unit Weight), Yield, and Air Content (Gravimetric) of Concrete." Annual book of ASTM standards, ASTM, West Conshohocken, Pennsylvania.

ASTM Cl43 (2015). "Standard Test Method for Slump of Hydraulic-Cement Concrete." Annual book of ASTM standards, ASTM, West Conshohocken, Pennsylvania.

ASTM Cl73 (2014). “Standard Test Method for Air Content of Freshly Mixed Concrete by the Volumetric Method.” Annual book of ASTM standards, ASTM, West Conshohocken, Pennsylvania.

ASTM C 330 (2014). “Standard Specification for Lightweight Aggregates for Structural Concrete.” Annual book of ASTM standards, ASTM, West Conshohocken, Pennsylvania.

ASTM C469 (2014). “Standard Test Method for Static Modulus of Elasticity and Poisson's Ratio of Concrete in Compression.” Annual book of ASTM standards, ASTM, West Conshohocken, Pennsylvania.

ASTM C496 (2011). “Standard Test Method for Splitting Tensile Strength of Cylindrical Concrete Specimens.” Annual book of ASTM standards, ASTM, West Conshohocken, Pennsylvania.

ASTM C1231 (2014). “Standard Practice for Use of Unbonded Caps in Determination of Compressive Strength of Concrete Cylinders.” Annual book of ASTM standards, ASTM, West Conshohocken, Pennsylvania.

Bass, R.A., Carrasquillo, R.L., and Jirsa, J.O. (1989). “Shear Transfer Across New and Existing Concrete Interfaces,” *ACI Structural Journal*, Vol. 84, No. 4, pp. 383-393.

Birkeland, H.W. (1969), Class Notes for Course on “Precast and Prestressed Concrete,” University of British Columbia, Spring 1968.

Birkeland, P.W. and Birkeland, H.W. (1966). “Connections in Precast Concrete Construction,” ACI Journal, *Proceedings*, Vol. 63, No. 3, pp. 345-368.

Chatterjee, P. “Shear Transfer in Reinforced Concrete”, University of Washington, 1971.

Dulacska, H. (1972). “Dowel action of reinforcement crossing cracks in concrete.” *ACI Journal Proceedings*, Vol. 69, No. 12.

Echegaray-Oviedo, J., Cuenca, E., Navarro-Gregori, J., and Serna, P. “Influence of the Fiber Reinforcement in Concrete under Direct Shear.”

Frénay, J. W. (1985). "Shear transfer across a single crack in reinforced concrete under sustained loading. Part I: Experiments". *Delft University of Technology, Faculty Civil Engineering and Geosciences*.

Gohnert, M. (2000). "Proposed theory to determine the horizontal shear between composite precast and in situ concrete". *Cement and Concrete Composites*, 22(6), 469–476.

Gohnert, M. (2003). "Horizontal shear transfer across a roughened surface". *Cement and Concrete Composites*, 25(3), 379–385.

Hanson, N.W., (1960). "Precast-Prestressed Concrete Bridges 2: Horizontal Shear Connections," *PCA – Journal of the Research and Development Division*, Vol. 2, No. 2, pp. 38-58.

Harries, K.A., Zeno, G., and Shahrooz, B. (2012). "Toward an Improved Understanding of Shear-Friction Behavior," *ACI Structural Journal*, Vol. 109, No. 6, pp. 835-844.

Hawkins, N. M., & Kuchma, D. A. (2007). NCHRP Report 579–Application of LFRD Bridge Design Specifications to High-strength Structural Concrete: Shear Provisions. *National Cooperative Highway Research Program*.

Hofbeck, J. A., Ibrahim, I.O., and Mattock, A. H. (1969). "Shear Transfer in Reinforced Concrete," ACI Journal, *Proceedings*, V. 66, No. 2, pp. 119-128.

Hoff, G.C. (1993). "High Strength Lightweight Aggregate Concrete for Arctic Applications--Part 3: Structural Parameters," *American Concrete Institute Special Publication*, SP-136, pp. 175-246.

Hsu, T.T.C., Mau, S.T., and Chen, B. (1987). "Theory of Shear Transfer Strength of Reinforced Concrete," *ACI Structural Journal*, Vol. 84, No. 2, pp. 149-160.

Ivey, D.L. and Buth, E. (1967) "Shear Capacity of Lightweight Concrete Beams." *ACI Journal Proceedings*, Vol. 64, No. 10. pp. 634-43.

Kahn, L.F. and Mitchell, A.D. (2002). "Shear-friction Tests with High-Strength Concrete," *ACI Structural Journal*, Vol. 99, No. 1, pp. 98-103.

Krc, K. (2015). "An Investigation of Shear-Friction of Lightweight Aggregate Concretes." MS Thesis. Missouri University of Science and Technology, Rolla, MO, 167 pp.

Loov, R.E. and Patnaik, A.K. (1994). "Horizontal Shear Strength of Composite Beams with a Rough Interface," *PCI Journal*, Vol. 39, No. 1, pp. 48-58.

Mansur, M.T., Vinayagam, T., and Tan, K-H. (2008). "Shear Transfer Across a Crack in Reinforced High-Strength Concrete," *ASCE Journal of Materials in Civil Engineering*, Vol. 20, No. 4, pp. 294-302.

Mast, R.F. (1968). "Auxiliary Reinforcement in Concrete Connections," *ASCE Journal of the Structural Division Proceedings*, Vol. 94, No. ST6, pp. 1485-1504.

Mattock, A.H. (1974). "Shear Transfer in Concrete Having Reinforcement at an Angle to the Shear Plane," American Concrete Institute Publication SP-42, *Shear in Reinforced Concrete*, pp. 17-42.

Mattock, A. H., Li, W. K., and Wang, T. C. (1976). "Shear Transfer in Lightweight Reinforced Concrete." *PCI Journal*, Vol. 21, No. 1, pp. 20-39.

Mattock, A.H. (1976). "Shear Transfer Under Monotonic Loading Across and Interface Between Concretes Cast at Different Times," *University of Washington Department of Civil Engineering Report SM 76-3*.

Mattock, A.H. (2001). "Shear-friction and High-Strength Concrete," *ACI Structural Journal*, Vol. 98, No. 1, pp. 50-59.

Mattock, A. H., Johal, L, and Chow, C. H. (1975). "Shear Transfer in Reinforced Concrete with Moment or Tension Acting Across the Shear Plane." *PCI Journal*, Vol. 20, No. 4, pp. 76-93.

Mattock, A.H. and Hawkins, N.M. (1972). "Shear Transfer in Reinforced Concrete – Recent Research," *PCI Journal*, Vol. 17, No. 2, pp. 55-75.

Papanicolaou, C. G., and Triantafillou, T. C. (2002). "Shear transfer capacity along pumice aggregate concrete and high-performance concrete interfaces." *Materials and Structures*, 35(4), 237–245.

Paulay, T., R. Park, and Phillips, M.H. (1974). "Horizontal Construction Joints In Cast-In-Place Reinforced Concrete," *American Concrete Institute Special Publications*, SP-42, pp. 599-616.

Precast/Prestressed Concrete Institute (1978). *PCI Design Handbook: Precast and Prestressed Concrete Institute*. 2th ed. Chicago: Precast/Prestressed Concrete Institute.

Precast/Prestressed Concrete Institute (2004). *PCI Design Handbook: Precast and Prestressed Concrete Institute*. 6th ed. Chicago: Precast/Prestressed Concrete Institute.

Precast/Prestressed Concrete Institute (2010). *PCI Design Handbook: Precast and Prestressed Concrete Institute*. 7th ed. Chicago: Precast/Prestressed Concrete Institute.

Raths, C. H. (1977). "Reader Comments: Design Proposals for Reinforced Concrete Corbels." *PCI Journal*, Vol. 21, No. 3, pp 93–98.

Saemann, J. and Washa, G.W. (1964). "Horizontal Shear Connections Between Precast Beams and Cast-In Place Slabs," *ACI Journal Proceedings*, Vol 61, No. 11, pp. 1383-1408.

Shaikh, F.A. (1978). "Proposed Revisions to Shear-friction Provisions." *PCI Journal*, Vol. 23, No. 2, pp. 12-21.

Shaw, D. (2013). "Direct Shear Transfer of Lightweight Aggregate Concretes with Non-Monolithic Interface Conditions." MS Thesis. Missouri University of Science and Technology.

Sneed, L.H. and Shaw, D. (2013). "Lightweight Modification Factor for Shear Friction Influence of Unit Weight on the Shear Transfer of Concretes Cast at Different Times," Report NUTC

R276/R317, Center for Transportation Infrastructure and Safety/NUTC Program, Missouri University of Science and Technology, 117 pp.

Shaw, D. and Sneed, L. (2014). "Interface Shear Transfer of Lightweight Aggregate Concretes Cast at Different Times," *PCI Journal*, V. 59, No. 3, pp. 130-144.

Sneed, L.H., Krc, K., Wermager, S., and Meinheit, D., (*in press, 2016*) "Interface Shear Transfer of Lightweight Aggregate Concretes," PCI Journal.

Tanner, John A. (2008). "Calculating Shear-friction Using Effective Coefficient of Friction." *PCI Journal*, Vol. 53, No. 3, pp. 114-20.

Valluvan, R., Kreger, M. E., and Jirsa, J. O. (1999). "Evaluation of ACI 318-95 Shear-Friction Provisions." *ACI Structural Journal*, 96(4).

Vangsirirungruang, K. "Effect of Normal Compressive Stresses on Shear Transfer in reinforced Concrete", University of Washington, 1971.

Walraven, J. C.; Frenay, J.; and Pruijssers, A. (1987). "Influence of Concrete Strength and Load History on the Shear-friction Capacity of Concrete Members," *PCI Journal*, Vol. 32, No. 1, pp. 66-84.

Walraven, J. C., and Reinhardt, H. W. (1981). "Theory and experiments on the mechanical behaviour of cracks in plain and reinforced concrete subjected to shear loading." HERON, 26 (1A), 1981.

Walraven, J. and Stroband. J. (1994). "Shear-friction in High-Strength Concrete," *American Concrete Institute Special Publication*, SP-42, pp. 311-330.

Wermager, S. (2015). "Shear-Friction of Sand-lightweight Clay and Slate Aggregate Concretes with Varied Reinforcement Ratios." MS Thesis. Missouri University of Science and Technology, Rolla, MO, 182 pp.